on the dynamics of high-concentrated mud suspensions

over het gedrag van hooggeconcentreerde slibsuspensies

On the dynamics of high-concentrated mud suspensions

PROEFSCHRIFT

ter verkrijging van de graad van doctor
aan de Technische Universiteit Delft,
op gezag van de Rector Magnificus prof. ir. K.F. Wakker,
in het openbaar te verdedigen ten overstaan van een commissie,
door het College voor Promoties aangewezen,
op donderdag 7 oktober 1999 te 13:30 uur

door Johan Christian WINTERWERP
vliegtuigbouwkundig ingenieur
geboren te den Haag

Dit proefschrift is goedgekeurd door de promotor:
Prof. dr. ir. J.A. Battjes

Samenstelling promotiecommissie:

Rector Magnificus, voorzitter	
Prof. dr. ir. J.A. Battjes,	Technische Universiteit Delft, promotor
Dr. ir. C. Kranenburg,	Technische Universiteit Delft, toegevoegd promotor
Prof. dr. ir. J.E. Berlamont,	Katholieke Universiteit Leuven (België)
Prof. dr. J. Dronkers,	Universiteit Utrecht
Prof. dr. K.R. Dyer,	Plymouth University (UK)
Prof. dr. ir. L.C. van Rijn,	Universiteit Utrecht
Prof. dr. ir. H.J. de Vriend,	Technische Universiteit Delft

The studies described in this thesis have been financed by Rijkswaterstaat (The Netherlands Ministry of Transport, Public Works and Water Management) through their SILTMAN project, by the European Union in the framework of the 2nd and 3rd MAST-programmes (the G8M Morphodynamics project and the COSINUS project), and through WL|DELFT HYDRAULICS' corporation research funds.

Front cover: aerial photograph of the Port of Zeebrugge, kindly made available by HAECON, Belgium.

Reproduced by Judels Brinkman & Ammerlaan, Delft, from a camera-ready copy supplied by the author.

This thesis is also published as Report No 99-3 in the series "Communications on Hydraulic and Geotechnical Engineering" of Delft University of Technology, Faculty of Civil Engineering and Geosciences, ISSN 0169-6548.

I promise to listen attentively, Theaetetus, so long as you spare me the details of your achievements in the theory of numbers, and speak a language which I, an ordinary man, can understand.

Socrates (469-399 BC)

Abstract

Many harbour basins and navigation channels suffer from rapid siltation, forcing managing authorities to carry out expensive maintenance programmes to safeguard navigation. This rapid siltation is often attributed to the occurrence of high concentrations of suspended cohesive sediment and/or fluid mud observed in the turbidity maxima of estuaries or during episodic events in coastal areas. The present study is dedicated to the transport and fate of such High-Concentrated Mud Suspensions (HCMS) with emphasis on the processes in the vertical.

HCMS is defined as a suspension with Newtonian fluid properties, that measurably affects the turbulent mixing processes in the water column. From an extensive literature review it is concluded that HCMS is encountered all over the world under a large variety of hydrodynamic and meteorological conditions. Its occurrence may vary largely with time and in space, however. Abundant availability of mobilisable mud seems to be a sufficient condition for such occurrences.

The behaviour of HCMS in the water column is governed by vertical mixing processes, and by (hindered) settling processes. These mixing processes are affected by sediment-induced buoyancy effects and are a function of the mass concentration of the suspended sediment, whereas a proper description of the (hindered) settling processes requires both the mass and volumetric sediment concentrations.

The relation between mass and volumetric concentrations is provided by a fractal description of the mud flocs, implying a power law behaviour of various mud properties. From this description a new formulation for the settling velocity as a function of floc size is derived, which is consistent with Stokes' law in the case of massive particles with a fractal dimension 3 (e.g. sand), and which agrees well with empirical data from the literature. The hindered settling formula by Richardson and Zaki, derived for fairly large, massive particles, does not account for the floc structure typical for cohesive sediment, and a new formula is proposed. This formula also compares well with empirical data from the literature.

The evolution of floc size, hence settling velocity, in a turbulent environment is described through a new flocculation model in a Eulerean framework, that includes the effects of turbulence-induced aggregation and floc breakup. This model predicts that the growth of flocs in open water systems can seriously be limited by a limited residence time of these flocs in the water column, as a result of small water depth and/or of long flocculation times. The model also predicts gelling concentrations in estuaries of the right order of magnitude; gelling values in coastal areas under storm conditions are grossly underpredicted at present. Though this flocculation model compares well with the scarcely available empirical data and yields qualitatively sound results, extensive further validation against comprehensive data sets is required before the model can be deployed with confidence for practical applications.

The sediment-induced buoyancy effects, mentioned in the third paragraph, already become manifest at moderate suspended sediment concentrations, for non-cohesive as well as cohesive sediments. An important implication of these buoyancy effects is the existence of a saturation concentration C_s, which is a measure for the maximal sediment load that can be carried in suspension by a turbulent flow. At concentrations

beyond C_s, the flow becomes super-saturated and both the turbulence field and the concentration profile collapse.

For steady flow conditions, a simple scaling law for C_s can be derived on the basis of a critical flux Richardson number, which value is known from stratified flow experiments reported in the literature. For tidal flow conditions, scaling laws for C_s are derived from an integral entrainment model. As these are fairly complicated, these scaling laws are not easy to apply in practice.

The saturation concentration for mud can be compared with the equilibrium concentration which is well-known for sand suspensions. A major difference with sandy suspensions, though, is that sand immediately forms a rigid bed upon deposition, whereas cohesive sediment generates a fluid mud layer, the initial concentration of which is determined by the gel point of the mud. At the fluid mud - water interface little turbulence can be generated, which explains the above mentioned collapse. The fluid mud can become rigid by consolidation processes, after which the production of turbulent energy at the water-mud interface becomes possible again, so that mixing is restored.

This consolidation process is described with a new consolidation model in a Eulerean reference frame, that includes both the effects of consolidation and hindered settling, using a fractal description of the material functions. The consolidation model compares excellently with a numerical benchmark experiment described in the literature, and the combined model gives a reasonable description of a hindered settling - consolidation experiment. However, in combination with the simple Bingham model used in this study, this consolidation model largely overpredicts the strength evolution of a consolidating mud layer.

The various process formulations have been implemented in a one-dimensional vertical numerical model, referred to as the 1DV POINT MODEL in this thesis, which allows the simulation of the effects of flocculation and gellation, settling, hindered settling and lutocline formation, consolidation, remixing, and sediment-induced buoyancy effects on the turbulence field of HCMS in estuarine and coastal environments. The various formulations also provide the relevant scaling parameters of the processes which govern the dynamics and appearances of HCMS under a wide variety of conditions.

This model concept is validated through application to well-documented laboratory experiments and field measurements, i.e. flume experiments with sand to study the velocity profile in sediment-laden flow, consolidation and entrainment experiments with cohesive sediment in an annular flume, measurements in and upstream of the turbidity maximum in the Ems Estuary, and measurements during storm conditions in the Maasmond area, the entrance to the Port of Rotterdam. In general, the measurements and model simulations agree well.

The suspended sediment concentration profiles in general and the rapid settling around slack water in particular, as observed in the Ems River, can only be simulated properly if the effects of both flocculation and sediment-induced buoyancy are accounted for in the 1DV POINT MODEL. These simulations also indicate that the floc size may vary by an order of magnitude over the tidal cycle; computed floc sizes and settling velocities agree reasonably with in situ measurements.

The measured time series of suspended sediment concentration at 0.15 and 0.55 m above the sea bed in the Maasmond area can only be simulated properly if the effects of hindered settling, sediment-induced buoyancy effects, salinity-induced buoyancy effects and augmented mixing by waves are all accounted for in the 1DV POINT MODEL. A temporary fluid mud layer of about 1 dm appears to be formed on the North Sea sea bed around slack water, which is mixed rapidly during accelerating tide. The simulations also indicate that the flow in the Maasgeul, the access channel to the Port of Rotterdam, is not able to keep the available sediment in suspension.

From a series of sensitivity analyses it is concluded that under stormy conditions, auto-saturation can occur, i.e. the flow can erode so much sediment that it becomes super-saturated. This is probably the explanation for the occurrence of mud banks observed at several locations in the world.

This study revealed the important role of the aforementioned processes in the rapid siltation phenomena described in the first paragraph. Implementation of appropriate models of these processes in a full three-dimensional model is required to help the managing authorities to control their maintenance problems and to improve the economic exploitation of their port.

Samenvatting

In veel havenbassins en -geulen treedt grote aanslibbing op, waardoor de verantwoordelijke havenautoriteiten kostbaar baggeronderhoud dienen uit te voeren om een veilige vaarweg te kunnen garanderen. Deze grote aanslibbing wordt met name gevonden in het troebelingsmaximum van estuaria of tijdens stormomstandigheden in kustgebieden, waarbij hooggeconcentreerde slibsuspensies en/of vloeibare sliblagen worden aangetroffen. De voorliggende studie behandelt het transport van zulke Hooggeconcentreerde Slibsuspensies (HCMS), met name het gedrag in de verticaal.

HCMS is gedefinieerd als een slibsuspensie met Newtonse vloeistofeigenschappen, waarbij een meetbare interactie optreedt met de turbulente waterbeweging. Uit literatuuronderzoek blijkt dat HCMS over de gehele wereld wordt aangetroffen onder een grote verscheidenheid aan hydrodynamische en meteorologische omstandigheden. Een voldoende voorwaarde hiervoor lijkt een overvloedige beschikbaarheid van mobiliseerbaar slib te zijn. Voorkomens van HCMS variëren echter sterk over de ruimte en met de tijd.

Het gedrag van HCMS over de verticaal wordt bepaald door de verticale mengingsprocessen, welke op hun beurt beïnvloed worden door de door slib geïnduceerde stratificatie-effecten, en door het depositiegedrag van slib, waaronder de zogenaamde "gehinderde bezinking". Deze mengingsprocessen hangen samen met de massaconcentratie van het slib, terwijl het depositiegedrag wordt bepaald door zowel de massa- als de volumeconcentratie van het slib.

De relatie tussen de massa- en de volumeconcentratie van slib wordt gegeven door een fractale beschrijving van de slibvlokken, hetgeen impliceert dat diverse slibeigenschappen in de vorm van machtswetten weergegeven kunnen worden. Met behulp van deze beschrijving is een nieuwe formulering afgeleid voor de relatie tussen de valsnelheid van de slibvlokken en hun diameter. Deze relatie is consistent met de wet van Stokes in geval van massieve deeltjes met een fractale dimensie 3, zoals zand; zij blijkt ook goed met in de literatuur beschreven waarnemingen overeen te komen. De vaak gebruikte formulering van Richardson en Zaki voor gehinderde bezinking is opgesteld voor tamelijk grote, massieve deeltjes en houdt geen rekening met de typische vlokstructuur van slibdeeltjes. Daarom wordt een nieuwe gehinderde-bezinkingformule voorgesteld, welke goed overeenkomt met in de literatuur beschreven data.

De grootte van de slibvlokken, en daarmee van de valsnelheid, in een turbulente stroming wordt beschreven met een nieuw flokkulatiemodel in een Eulers coördinatenstelsel. In dit model worden de effecten van aggregatie en vlokafbraak beide meegenomen. Het model voorspelt dat de vlokgroei in open watersystemen fors beperkt kan worden door een beperkte verblijftijd van de slibvlokken in de turbulente waterkolom, bijvoorbeeld in geval van een geringe waterdiepte, dan wel van lange flokkulatietijden. Met het model kan ook de grootte van de gelconcentratie bepaald worden. Deze concentratie blijkt voor estuarine omstandigheden redelijk voorspeld te kunnen worden; onder stormomstandigheden blijkt zij echter fors onderschat te worden. De resultaten verkregen met het flokkulatiemodel blijken goed overeen te komen met meetgegevens, welke echter slechts in zeer beperkte mate beschikbaar

zijn. Verdere validatie aan de hand van een uitgebreider meetbestand is noodzakelijk voordat het model met vertrouwen kan worden toegepast onder praktijkomstandigheden.

De bovengenoemde, door sediment-geïnduceerde stratificatie-effecten treden, zowel voor zand als voor slib, reeds bij vrij lage sedimentconcentraties op. Als gevolg van deze stratificatie blijkt er een verzadigingsconcentratie C_s te bestaan, welke een maat is voor de maximale hoeveelheid slib die door een turbulente stroming als suspensie getransporteerd kan worden. Bij concentraties groter dan C_s raakt de stroming oververzadigd en storten zowel de turbulente menging als het verticale concentratieprofiel in elkaar.

Voor stationaire stromingsomstandigheden blijkt een eenvoudige schaalregel voor C_s te kunnen worden afgeleid, waarbij gebruik gemaakt wordt van een kritiek flux Richardsongetal, waarvan de waarde uit de literatuur bekend is. Voor getij-omstandigheden blijken schaalregels afgeleid te kunnen worden met een zogenaamd integraal entrainmentmodel. Aangezien deze schaalregels tamelijk complex zijn, zijn deze echter niet eenvoudig toepasbaar.

De verzadigingsconcentratie voor slib kan vergeleken worden met de evenwichtsconcentratie voor zandsuspensies. Een groot verschil is echter dat zandkorrels na depositie direct een vaste bodem vormen, alwaar turbulentieproductie mogelijk is, terwijl vallende slibvlokken een vloeibare sliblaag vormen, waarvan de concentratie bepaald wordt door de gelconcentratie. Aan het grensvlak tussen de waterkolom en de vloeibare sliblaag kan nauwelijks turbulentie geproduceerd worden, hetgeen het ineenstorten van de turbulentie en het concentratieprofiel verklaart. Pas als de vloeibare sliblagen door consolidatie een zekere sterkte hebben ontwikkeld, ontstaat een steviger grensvlak en is turbulentieproductie aldaar weer mogelijk, waardoor de mengingscapaciteit van de stroming hersteld wordt.

Om dit proces te kunnen beschrijven is een nieuw consolidatiemodel in een Eulers coördinatensysteem ontwikkeld dat de effecten van consolidatie onder eigen gewicht en gehinderde bezinking verdisconteert, en waarbij gebruik gemaakt wordt van een fractale formulering van de materiaalparameters. Het nieuwe model blijkt een in de literatuur beschreven numeriek consolidatie-experiment goed te kunnen simuleren; ook de simulatie van een in het laboratorium uitgevoerd gehinderde bezinking - consolidatie-experiment is redelijk. De sterkte-ontwikkeling van zo'n consoliderende sliblaag, beschreven met het eenvoudige Bingham model gebruikt in deze studie, wordt echter sterk overschat.

De verschillende procesformuleringen zijn geïmplementeerd in een eendimensionaal verticaal numeriek model, dat in dit proefschrift het 1DV POINT MODEL wordt genoemd. Hiermee kunnen de effecten van flokkulatie, gelvorming, gehinderde bezinking, grensvlakvorming, consolidatie, verticale menging en de invloed van het slib op het turbulentieveld voor Hooggeconcentreerde Slibsuspensies in estuaria en kustgebieden gesimuleerd worden. Met behulp van deze formuleringen zijn ook de diverse schaalregels afgeleid die het gedrag en het voorkomen van HCMS onder een verscheidenheid van omstandigheden beschrijven.

Het modelconcept is gevalideerd met behulp van goed gedocumenteerde laboratoriumexperimenten en veldmetingen, namelijk gootexperimenten met zand om de invloed van dat zand op het verticale snelheidsprofiel te bestuderen, consolidatie-

en entrainmentexperimenten met cohesief sediment in een carrousel, metingen in en bovenstrooms van het troebelingsmaximum in het Eemsestuarium, en metingen tijdens stormomstandigheden in het Maasmondgebied. Over het algemeen blijken de metingen goed met het model gereproduceerd te kunnen worden.

De verticale slibconcentratieprofielen en de snelle bezinking rondom kentering, welke in de Eems zijn waargenomen, kunnen slechts bevredigend worden gesimuleerd indien zowel de effecten van flokkulatie als van sediment-geïnduceerde stratificatie-effecten in het 1DV POINT MODEL worden meegenomen. Uit deze simulatie blijkt ook dat de vlokgrootte sterk varieert over de getijperiode; de berekende waarden voor deze vlokgrootte en de bijbehorende valsnelheid komen redelijk overeen met de in de werkelijkheid gemeten waarden.

De in het Maasmondgebied op 0.15 m en 0.55 m boven de zeebodem gemeten tijdreeksen van de zwevend slibconcentratie kunnen slechts bevredigend gesimuleerd worden, indien zowel de effecten van gehinderde bezinking, van sediment-geïnduceerde stratificatie-effecten, van zout-zoet-geïnduceerde stratificatie-effecten, als van de door golven vergrote verticale menging in het 1DV POINT MODEL worden meegenomen. Uit de simulaties blijkt dat rondom stroomkentering een dunne, ca. 1 dm dikke vloeibare sliblaag ontstaat, welke tijdens versnellende getijstroming weer over de waterdiepte wordt gemengd, en dat de stroming in de Maasgeul zelf niet in staat is het opgewoelde slib in suspensie te houden.

Ook is een aantal gevoeligheidsanalyses met het model uitgevoerd. Hieruit blijkt ondermeer dat onder stormomstandigheden golven tot verzadiging van de slibverticaal kunnen leiden, hetgeen waarschijnlijk het bestaan van modderbanken voor diverse kusten verklaart.

Uit deze studie blijkt de belangrijke invloed van de diverse, hierboven beschreven processen op de snelle aanslibbing in havenbassins en -geulen. Implementatie van deze processen in een driedimensionaal slibtransportmodel is noodzakelijk om havenautoriteiten van adequaat advies te kunnen voorzien voor het onderhoud van hun vaarwegen.

Table of contents

1. Introduction

1.1 General

The front cover of this thesis shows an aerial photograph of a concentrated suspension of cohesive sediment in the turbid waters around the entrance to the Port of Zeebrugge, Belgium. The sediment concentration within this turbid zone is estimated at several hundreds of mg/l (Bastin et al., 1982). Following the flood tide, this sediment will enter the harbour basin, where it can settle, accumulating at a mean rate of about 2 m per year. This necessitates frequent dredging operations, removing annually about 10^7 m^3 of sediment, to safeguard navigation. Such concentrated mud suspensions are observed frequently all over the world in estuaries and at coastal sites under a large variety of conditions. For instance, the ports along the Dutch coast suffer from similar siltation rates: the annual accumulation in the silt traps in the Caland-/Beerkanaal of Rotterdam Port ("Bufferput, vak E and F") and in the harbour basins of IJmuiden amounts to about 4 m, whereas about 2 m of siltation is observed in the Port of Scheveningen. The existence of pronounced fresh-saline water induced density currents is probably the cause of the higher siltation rates at Rotterdam and IJmuiden. The siltation in these channels and harbour basins results in deposits of soft sediment, often referred to as fluid mud, and mainly occurs as a result of episodic events (storm conditions, e.g. Verlaan and Spanhof, 1994, and Merckelbach, 1996).

1.2 Definition of High-Concentrated Mud Suspensions

The expression "fluid mud" was probably first introduced by Inglis and Allen (1957) in their publication on the sediment dynamics in the Thames estuary. Since then, sediment appearances with a wide variety of concentrations are called fluid mud. In the literature also the terms "creme de vase" (Migniot, 1968) and "sling mud" (NEDECO, 1968) are used. Kirby and Parker (1983) have tried to order the terminology a bit. They distinguish between:

- a settled bed with a density of 1300 to 1700 g/l,
- a stationary suspension with a sediment concentration between about 0.1 and 200 g/l, and
- a mobile suspension with a sediment concentration between about 1 and 150 g/l.

These definitions are not unambiguous because of the large overlap in concentration range. Recently, Parker and Hooper (1994) propose the term Hyperconcentrated Benthic Layers instead of fluid mud, as the latter term is most often related to the detection with a high-frequency echo-sounder. It is well known that the reflections of such echo-sounders are caused by the gradients in the sediment density, rather than by the density itself. This is one of the causes of the ambiguity of the definitions above.

In this study we use slightly different definitions and we distinguish between three regimes of cohesive sediment suspensions:

1. **Fluid mud** is a suspension of cohesive sediment at a concentration beyond the gelling point (e.g. Section 2.4), i.e. of the order of several 10 to 100 g/l. This

suspension exhibits profound non-Newtonian behaviour, and it is either stationary or moving. In the latter case the fluid mud flow may be laminar or turbulent and its dynamics will be fairly independent of the flow in the water column above.

2. A **High-Concentrated Mud Suspension (HCMS)** is a suspension of cohesive sediment at a concentration of a few 100 to a few 1,000 mg/l. This suspension behaves Newtonian, though possibly with a somewhat increased viscosity, and is transported with the main flow. An important feature of HCMS is its interaction with the turbulent flow field.
3. A **Low-Concentrated Mud Suspension** is a suspension of cohesive sediment at a concentration of the order of several 10 to maybe a few 100 mg/l. This suspension behaves Newtonian and does not significantly affect the turbulent flow field.

Concentrations between those typical for fluid mud and HCMS do occur in practice, but they are transient and the suspension cannot be stable (Winterwerp, 1996). As such, no intermediate category is required.

In this study we show that the occurrence of HCMS is entirely related to the availability of sediment and the hydro-meteo conditions prevailing. As a result, classification of the sediment dynamics at a particular site may vary with time, e.g. over a spring-neap tidal cycle, or over the year (seasonal variations in river flow and/or wave activity). Moreover, HCMS occurrences are generally confined in space as well. Yet they are important as they form the key in our understanding and modelling of the rapid siltation in many harbour basins and navigational channels, and of the behaviour of the turbidity maximum in estuaries.

1.3 Aim of this study

The research presented in this thesis is aimed at enhancing our understanding of the behaviour of HCMS under a variety of hydro-meteo conditions. We focus on the influence of suspensions of cohesive sediment on the turbulent flow structure and related vertical mixing and the interactions with the volumetric effects of the sediment. We derive scaling parameters that govern the dynamics of HCMS from an analysis of the relevant mathematical-physical formulations. In the end, the results of this study should contribute to the development of a full three-dimensional mathematical model that can be used to simulate the transport and fate of High-Concentrated Mud Suspensions in estuaries and coastal sites.

1.4 Problem analysis

Mud is a mixture of clay particles (lutum), organic matter, water, sand and sometimes gas. It exhibits cohesive properties because of the first three components, as a result of which mud behaves basically different from non-cohesive sediment, e.g. sand. Moreover, these properties enable organic and inorganic contaminants to adhere to the mud, in which case dredging operations may become very costly because of the need to neutralise the environmental impact of the polluted sediment.

The description of the horizontal transport processes of a given amount of mud, suspended by the main flow, is fairly straightforward and well understood. However, the amount of sediment that can be transported is governed by several properties of the suspended matter and processes in the water column:

- Flocculation: because of the cohesive nature of mud, flocs are formed, affecting the settling velocity and the bed structure,
- Settling and mixing: the mud particles are bound to fall through the water column by gravity effects, opposed by mixing processes generated by the turbulent water movement,
- Deposition: settling mud particles may become part of the bed under specific conditions,
- Re-entrainment: during accelerating flow the particles from the bed may be re-entrained into the water column by the turbulent flow,
- Gelling: deposited mud particles, when left still for sufficient time, will form a structure, causing the build-up of strength that can resist re-entrainment,
- Consolidation: another step in bed formation is self-weight consolidation, when pore water is squeezed out of the bed, and the strength of the bed increases further,
- Liquefaction: when subject to cyclical loading, the bonds between the particles can be broken gradually, reversing the consolidation process, and
- Erosion: even when the bed has achieved a considerable strength, it can still be eroded again by turbulent flow or by waves.

These processes may act simultaneously or successively. Often, though, just some of these play a role, depending on the conditions prevailing. In the case of concentrated mud suspensions, however, several of these processes become a function of the mud concentration itself, and a complicated interactive picture emerges. It is shown in this study that the dynamics in the water column, i.e. the cycle of mixing and settling over the vertical as a function of the driving tidal forces, are of vital importance to understand the behaviour of these concentrated mud suspensions. Because of their interactive nature, an analysis of these processes is therefore only possible if a series of restricting assumptions are made.

We limit ourselves to situations where horizontal gradients in flow velocity and sediment concentration are of minor importance; this does not necessarily imply that horizontal advection effects are absent. However, we require that typical length scales of a HCMS-occurrence, such as the length of the turbidity maximum in an estuary, is large compared typical length scales of the advecting flow, such as the tidal excursion. Thus we assume that the volume of sediment in the water column is either constant and determined by processes far away from our site of observation, so that we do not have to worry about its source, or is determined by local water-bed exchange processes. In the first case, all sediment particles remain part of the water-sediment mixture, i.e. they will remain within the water column. In the latter case, the volume of sediment is governed by the local flow conditions and the bed structure.

We study the behaviour of HCMS in estuarine and coastal waters. These are shallow in general, and we apply the shallow water approximation to describe the (tidal) flow. This implies that the momentum equation in vertical direction reduces to the hydrostatic pressure condition. In line with this approach, we assume a nearly horizontal bed, which simplifies the boundary conditions to the three-dimensional

equations for HCMS considerably. Moreover, we also neglect the effects of converging and diverging flows and of secondary currents, so that the vertical flow velocity is zero everywhere.

We treat the water-sediment mixture as a single-phase fluid in which all particles follow the turbulence movements, but for their settling velocity. Uittenbogaard (1994) argues that this is a correct assumption if $w_s << w'_{rms}$, where w_s is the settling velocity of the sediment and w'_{rms} a measure for the vertical turbulent velocity fluctuations. Because w_s is of the order of 0.1 - 1 mm/s for mud and $w'_{rms} \approx u_*$ in open-channel flow (Nezu and Nakagawa, 1993), where u_* is the shear velocity with typical values of several cm/s, this condition is generally met for cohesive sediments in estuarine and coastal waters. It is noted that the Rouse number $\beta = w_s/\kappa u_*$ appears to be a proper parameter to establish whether a sediment suspension may be treated as a single phase fluid.

Uittenbogaard (1994) showed theoretically that even sand particles with a diameter up to 200 μm can properly follow the turbulent movements, occurring in typical tidal flows, allowing for a single-phase description. This is sustained by Muste and Patel (1995) who measured the fluctuating velocity components of suspended sand particles of 250 μm median diameter in a turbulent flow and conclude that their rms-value is only about 15 to 20 % smaller than the rms-values of the fluctuating fluid velocity components.

A third important restriction is that in the major part of our analyses we treat the suspension as a Newtonian fluid, though with an increased viscosity, if necessary. Non-Newtonian effects will enter our analyses only when gelling and consolidation effects are treated. However, we do so without a thorough derivation or analysis of the underlying mathematical-physical formulations: we will merely apply those reported in the literature.

We also assume that apparent viscous effects by grain-grain interactions are not important. Bagnold (1954) showed that such effects can indeed be neglected for massive, elastic, non-cohesive particles (sand) if a characteristic parameter, presently known as the Bagnold number B, which is the ratio of the shear stresses induced by grain-grain collisions and the turbulent stresses, does not exceed the critical value $B_{crit} = 40$. For sand particles with a typical diameter $D = 100$ μm, transported in turbulent open channel flow, $B \approx 1$. As collisions between particles of cohesive sediment are not elastic, but result in either aggregation or floc breakup, our assumption is certainly valid for concentrated mud suspensions.

These assumptions lead to a description of the suspension as a single-phase fluid. The flow of the fluid can be described by the classical Reynolds-averaged Navier-Stokes equations, taking into account the effects of the turbulence and sediment on the stress tensor. The sediment balance is classically given by (see also Section 3.2):

$$\frac{\partial c}{\partial t} + \frac{\partial}{\partial x_i}\left(\left(u_i - \delta_{i3} w_{s,eff}\right)c\right) - \frac{\partial}{\partial x_j}\left(\Gamma_{ij}\left(\frac{\partial c}{\partial x_i}\right)\right) = 0 \qquad (1.1)$$

where c is the sediment concentration, either by mass or by volume[1)], u_i is the fluid velocity, $w_{s,eff}$ is the effective settling velocity of the sediment particles, Γ_{ij} is the eddy diffusivity tensor, t is time, x_i is a Cartesian co-ordinate (x_3 is the vertical co-ordinate, positive upward; see page 23) and δ_{ij} is the Kronecker delta.

In general, the concentration of suspended sediment in the water column increases towards the river or sea bed. Because of hindered settling effects (e.g. Section 4.4) the effective settling velocity of the sediment lower in the water column is smaller than in the upper part, as a result of which a distinct interface develops, commonly referred to as the lutocline. Such lutoclines have been observed many times in the laboratory (e.g. Been and Sills, 1983) and in the field (e.g. Kirby and Parker, 1983), and they are of great importance because of their role in the (damping of) vertical turbulent mixing processes. The process of lutocline formation was first studied by Kynch (1952). From a rigorous analysis of the Kynch-equations, Kranenburg (1992) showed that lutoclines are always formed under natural conditions in estuaries and coastal regions. Hence, we conclude that hindered settling and lutocline formation are important. Note that these processes are governed by the volumetric effects of the suspended sediment.

We assume that turbulent mixing processes of the suspended sediment over the water column can be described properly with the so-called k-ε model, where k is the turbulent kinetic energy and ε the dissipation rate per unit mass. This turbulence closure model is applicable for stratified conditions (Rodi, 1984, Uittenbogaard, 1995); some further comments are given in Section 3.3. The effects of non-breaking surface waves on the bed shear stresses and vertical mixing are accounted for. This limits the analyses and formulations in this study to mud occurrences outside breaker-zones, which can occur in coastal areas and on intertidal mud flats. We exclude all influence of the suspended sediment particles on the turbulence field itself, except for the buoyancy effects of the sediment suspension on the vertical mixing processes, which particularly occur near the aforementioned lutoclines (see also Chapter 2). These buoyancy effects are known to depend on the gradients in the mass concentration c of the suspended sediment.

Hence we conclude that the settling term in (1.1) requires a description of the sediment concentration in mass and volumetric units, whereas the diffusion term requires a description using concentration by mass. This implies that a complete analysis of the sediment dynamics necessitates a functional relation between the volumetric and mass concentrations of the sediment. This is particularly relevant at high sediment concentrations, as hindered settling and buoyancy effects become increasingly important. Such a relationship is conveniently provided by fractal geometry, which is used throughout this thesis. Section 4.2 summarises a short description of this approach and its advantages and limitations for cohesive sediment.

Furthermore, we assume that sand and organic matter content are so low that they do not significantly affect the behaviour of the suspension, except maybe for the value of the empirical coefficients in physico-chemical formulations required to describe the mud kinetics.

[1)] Elsewhere in this thesis c will exclusively be used for the sediment concentration by mass, whereas the volumetric concentration of the mud flocs will be represented by ϕ.

These assumptions allow us to apply a single-phase, one-dimensional vertical mathematical description of the relevant processes. This description is implemented in a one-dimensional numerical model, referred to as the 1DV POINT MODEL throughout this thesis, which is used in our analysis of the behaviour of High-Concentrated Mud Suspensions.

1.5 Set-up of this thesis

A summary of the literature on HCMS and their frequency of occurrence is presented in Chapter 2. This chapter also discusses studies on the influence of sediment-laden flow on the turbulence properties, carried out both in the laboratory and in the field. The various issues discussed in Section 1.4 are further elaborated in the next chapters. Chapter 3, 4 and 5 present the governing equations; the details of their implementation in the 1DV POINT MODEL are given in Appendix B. Chapter 3 is dedicated to the description of the (turbulent) water movement and the mass balance, including the effects of waves. This merely summarises earlier work carried out by others at WL|delft hydraulics in a series of studies on turbulence modelling in stratified flows (e.g. Section 3.3), and the extensions especially implemented for application to suspended sediment. Chapter 4 describes the kinetics of cohesive sediment particles: it includes an explanation of the fractal description of flocs of cohesive sediment, a formula for the settling velocity of cohesive sediment, including the effects of hindered settling, summarises literature on hindered settling and proposes a simple formula for turbulence-induced flocculation effects. Chapter 5 contains the well-known Gibson equation for self-weight consolidation, but in a Eulerian reference frame and adopting a fractal description of the material functions. In Section 6 the concept of saturation is explained and elaborated and scaling parameters for HCMS-behaviour are derived. Deployment of the 1DV POINT MODEL to practical cases to validate the modelling concepts derived in the preceding chapters is presented in Chapter 7. These cases comprise an analysis and discussion of measurements both in the laboratory and in the field. Chapter 8 summarises the theoretical developments in the preceding sections and elaborates on the consequences of the various parameters and scaling parameters of the dynamics of High-Concentrated Mud Suspensions. Special attention is paid to the various time scales that characterise the behaviour of HCMS in a tidal environment. Conclusions and recommendations are presented in Chapter 9.

2. Sediment-fluid interactions: a literature survey

2.1 General

The literature contains an overwhelming amount of publications on sediment-flow interactions. However, many questions have not yet been resolved definitely, amongst which the effect of suspended sediment particles on the micro-structure of the turbulent flow and how this affects the turbulent energy cascade. We therefore do not present a complete discussion of all possible effects, but limit ourselves to those phenomena which seem important in understanding the behaviour of HCMS. Yet, we pay thorough attention to the influence of loose granular sediment (sand) on the turbulent velocity field, as the many studies published on this subject can be used to validate some of our premises and of our modelling abilities - see Section 2.2.

This chapter further discusses literature on drag reduction at low mud concentrations in Section 2.3 and on the gellation of hyper-concentrated mud suspensions in Section 2.4. This implies that only some aspects of mud rheology are treated. The major part of this chapter contains a summary on HCMS-occurrences and behaviour, as reported in the literature, and on observed interactions with the hydrodynamics - see Section 2.5. A summary of relevant numerical modelling studies reported in the literature is presented in Section 2.6. Finally, Section 2.7 contains a brief discussion on the implications of the various findings with respect to the description of HCMS-dynamics.

The effective settling velocity (including the effects of flocculation) of sediment particles, hindered settling effects and consolidation are also manifestations of sediment-fluid interactions. The description of these processes, however, is so closely linked to the mathematical-physical formulations for the evolution of the settling velocity and bed formation, that the discussion of relevant literature is postponed to Chapters 4 and 5.

2.2 Effect of non-cohesive sediment suspensions

Many (experimental) studies have been published on the effect of suspended sand on the vertical velocity profile in turbulent open-channel flow. The two classical papers by Vanoni (1946) and by Einstein and Chien (1955) are generally referred to. Vanoni executed experiments for hydraulically rough flow in a flume of 18 m length, 0.85 m width and 0.15 m water depth with sand of 90, 120 and 147 μm median diameter. During the experiments, no sand was allowed to settle on the bed. Vanoni established the effective Von Kármàn constant κ_s for sediment-laden flow from the slope of the flow velocity profile in the lower 50 % of the water column from plots on semi-logarithmic axes and concluded that κ_s decreases with increasing suspended sediment concentration c. Vanoni hypothesised that this decrease is caused by buoyancy effects, i.e. the damping of turbulence by the suspended sediment. Almost 10 years later, Einstein and Chien reported on their experiments for hydraulically rough flow in a flume of 13.3 m length, 0.3 m width and 0.12 m water depth with sand of 94, 274 and

150 μm median diameter. The suspended sediment concentrations were much larger than Vanoni's. Again no sediment is allowed to settle on the bed. Also Einstein and Chien found decreasing κ_s-values with increasing c. They reasoned that part of the available stream power P_f is required to keep the sediment in suspension and they plotted the variation of κ_s as a function of the ratio of this required power P_s to the available power, defined as:

$$\frac{P_s}{P_f} = \frac{\Delta w_s c}{\rho_w U S} \tag{2.1}$$

where Δ is the relative sediment density: $\Delta = (\rho_s - \rho_w)/\rho_s$, ρ_s is the sediment density, ρ_w is the water density, S is the energy slope and U the mean flow velocity. This graph is also presented by Vanoni (1977) and is given in Fig. 2.1. Lyn (1984) argued that the power ratio P_s/P_f can be regarded as a suspension Richardson number, suggesting indeed a contribution of turbulent damping to the decrease in κ_s.

Winterwerp et al. (1990) found a similar decrease at relatively low sediment concentrations, but at higher concentrations a reverse trend was observed. This result was attributed to the effects of hindered settling, which decreases the power required to keep the sediment in suspension. This reverse trend was predicted earlier by Arai and Takahashi (1986) in a model that accounts explicitly for the effects of grain-grain interactions in keeping the sediment in suspension.

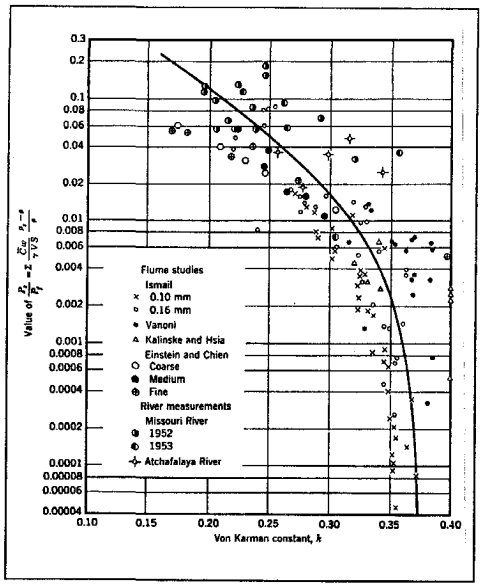

Fig. 2.1: Variation of effective Von Kármàn constant κ_s with suspended sediment concentration (after Vanoni, 1977).

The decrease in κ_s-values with increasing c was well accepted in sedimentology until it was challenged by Coleman (1981 and 1986). Coleman argued that the logarithmic part of the velocity profile in open channel flow is limited to the lower 10 to 20 % of the water column. Higher in the water column the velocity profile is governed by the law of the wake. The analyses by Vanoni (1946) and Einstein and Chien (1955) would

therefore not be correct: the velocity distribution should be plotted in defect-form. Coleman carried out a new series of experiments in a flume with a smooth bottom of 15 m length, 0.35 m width and 0.17 m depth with sand of 105, 210 and 420 μm median diameter. He also re-analysed the data of Vanoni and Einstein-Chien, using the velocity defect law:

$$\frac{U_m - u}{u_*} = \left(-\frac{2.3}{\kappa} \log \frac{z}{z_m} + 2\frac{\Pi}{\kappa} \right) - \frac{\Pi}{\kappa} \omega \left(\frac{z}{z_m} \right) \tag{2.2}$$

where U_m is the maximal velocity in the water column at depth z_m, Π is the wake strength coefficient and ω is a wake function. From his experiments, Coleman established a relationship between Π and the bulk Richardson number Ri_* for the flow, defined as $Ri_* = gh(\rho_{z=h}-\rho_{z=0})/\rho_m u_*^2$, where ρ_m is the depth-mean density, and found that Π increases from about 0.2 for clear water flow to more than 0.8 for sediment-laden flow at the highest Ri_*-values in his experiments. Relevant velocity profiles are represented in Fig. 2.2, which is directly copied from Coleman's paper.

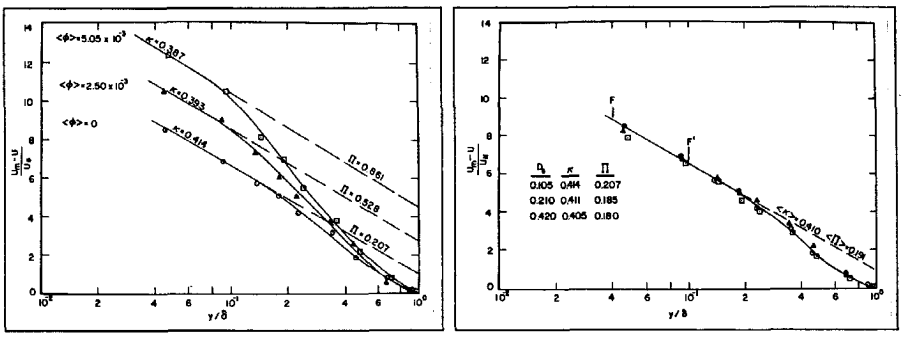

Fig. 2.2: Velocity profiles for clear water and sediment-laden flow (Coleman, 1981).

Note that δ in Fig. 2.2 represents z_m of (2.2). Gust (1984) pointed out in a fierce discussion of Coleman's work, that his analysis for sediment-laden flow is based on one data point only. Later, Valiani (1988) also questioned the correctness of Coleman's conclusion on the basis of an error analysis of the data. Another problem is that the velocity profile in flumes is affected by secondary currents, resulting in a decreasing velocity near the water surface. This certainly affects the parameters in the velocity defect law (see also Section 7.1).

Itakura and Kishi (1980) also re-analysed the experimental data by Vanoni, Einstein-Chien and some others. They applied the Monin-Obukhov theory to establish a length scale for sediment-laden flows. This resulted in a log-linear velocity-defect profile, which may be viewed as a formulation with a linear wake profile. Their approach is therefore conceptually similar to Coleman's. This led Lyn (1986) to remark that *"whether the velocity profile is best represented by a pure log-law with $\kappa_s < \kappa$, or with a log-wake law with a variable wake coefficient is still being debated. In spite of some qualitative similarity such as the idea of turbulence damping, the first and second approach ultimately diverge. The use of a pure log-law with variable κ_s implies a view in which the structure of turbulence is changed radically throughout the flow. In*

using the log-wake law, the suspension primarily affects the outer flow, in such a way that near the bed the structure of turbulence remains essentially unchanged from that of clear-water flow."

This analysis inspired Lyn (1986, 1988) to approach the sediment-flow interaction from a different angle. He studied this interaction on the basis of "similarity theory", in which he assigned characteristic length, velocity and concentration scales to the inner and outer part of the flow. According to his experimental data and theoretical analysis, the effect of the suspended sediment on the velocity profile is confined to about the lower 20 % of the water column. Note however, that the coefficients in his similarity model were tuned with the measurements. Hence, theory and data predict the same behaviour by definition. Another problem with this approach is that Lyn's analysis is difficult to compare with the more classical theories.

A more theoretical approach of the sediment-flow interaction is presented by Hino (1963) and more recently by Zhou and Ni (1995). Hino's work was aimed at explaining the reduction in κ_s as a function of the suspended sediment concentration in turbulent flow, including observations by Elata and Ippen (1961) that a suspension of non-buoyant particles also causes a reduction in κ_s together with an increase in turbulent intensities. His analysis started from the turbulent energy equation for clear water flows. The effect of sediment would be the addition of a buoyancy term to account for the energy required to keep the particles in suspension, and a decrease in the dissipation term, as "*the volume of liquid phase contributing to the turbulent dissipation is decreased by the existence of the solid particles*". After some tuning of the various coefficients in the model, Hino was able to reproduce the velocity profiles measured by Vanoni and by Elata and Ippen. However, we note that the experiments by Elata and Ippen were **not** carried out with non-buoyant particles, but with 100 to 150 μm dylene polystylene particles with a specific density of 1.05 and a settling velocity of about 0.1 cm/s. Though specific density and settling velocity are much smaller than for common sand, this does not imply that buoyancy effects are negligible for the polystylene particles. In fact it is expected that they are as important as for cohesive sediment, which is the subject of the present study.

The increase in turbulence intensity, measured by Elata and Ippen, may be explained from local sediment-flow interactions. The flow around the particles generates a wake that generates small scale turbulence. The size of the largest eddies within this wake is of the order of the particle diameter. Hence, though these eddies may contribute to the turbulence intensities, their scale is so small that they do not affect the mixing of these particles, and as such can be neglected in our analysis. However, no experimental data are available to verify this hypothesis.

Zhou and Ni (1995) carried out a perturbation analysis for the mean flow components of the Reynolds stress equations and the continuity equations for the fluid and the sediment; it was assumed that the turbulent flow fluctuations are not affected by the presence of sediment. The sediment-flow interaction was accounted for by an additional force term in the Reynolds stress equations. They showed that the zeroth order approximations of the perturbation equation for the flow yields a logarithmic velocity distribution. The zeroth and first order approximation of the perturbation equation for the concentration distribution yield a Rousean profile, and the profile found by Itakura and Kishi, respectively. The effect of the sediment on the flow

profile to first order appears to be a parabolic mean flow profile to be superposed on the turbulent flow profile. This would result in a more laminar-flow-like velocity profile with a subsequent decrease in effective κ. They compared a linearised form of their perturbation equations with experimental data reported in the literature (Coleman, 1981 and Einstein-Chien, 1955) and found good agreement after tuning two coefficients in the linearised equation. It is noted that these coefficients do vary considerably for the various experiments; hence no generic model has been obtained. Moreover, this linearised equation is nothing more than the defect law described above with a quadratic wake function. Zhou and Ni finally noted that their equations show that the available kinetic energy of the flow is redistributed, but they cannot indicate in which way: this would vary for different experimental conditions.

It is remarkable that in their analyses only few authors refer to studies on heat- and/or salinity-induced stratification effects; see for instance Turner (1973). Probably Barenblatt (1953) was the first to elaborate on this analogy. Barenblatt introduced the Monin-Obukhov length scale $\ell \equiv \rho u_*^3 / \kappa g \overline{\rho' w'}$ to establish a damping function for the eddy viscosity, resulting in a log-linear velocity profile:

$$\frac{u}{u_*} = \frac{1}{\kappa}\left[\ln\left(\frac{z}{z_0}\right) + \beta\frac{z}{\ell}\right] \tag{2.3}$$

where β is a constant; $\beta \approx 4.7$. This work was further elaborated by Taylor and Dyer (1977) to establish the effect of various flow and sediment properties on the velocity profile.

Further work was presented by Soulsby and Wainwright (1987) in the form of a stability diagram based on the Monin-Obukhov stability parameter $M_\zeta = z/\ell$: stratification effects are negligible if $M_\zeta < 0.03$. In constructing their stability diagram, Soulsby and Wainwright assumed the log-lin-velocity profile (2.3), local equilibrium, i.e. $\overline{\rho' w'} = \Delta w_s c$, a linear eddy viscosity profile and a semi-empirical pick-up function to establish the reference concentration c_a in the Rouse concentration profile. M_ζ is established as a function of u_*, θ_c (critical Shields parameter), w_s and z in an u_*-D diagram, in which the values of the grain diameter D range from fine silt to coarse gravel. From this diagram it was concluded that for fine sediments stratification always occurs in the upper part of the water column. The diagram was more or less validated with a few field data from the Thames and the North Sea for suspended sediment concentrations ranging from about 10 to 10,000 mg/l.

The discussions above are restricted to the effect of suspended sediment on the mean velocity profile with some indirect deduction on the turbulent flow properties. Only Muste and Patel (1997) carried out detailed measurements of the turbulent velocity intensities as a function of suspended sediment concentration. Their experiments were carried out for hydraulically rough flow in a flume with a concrete bottom of 30 m length, 0.91 m width and 0.13 m water depth. Various amounts of sand, sieved to a 210 to 250 μm diameter interval, were injected into the flume; no deposition on the bed was allowed. Though no data on the suspended sediment concentrations are given in their paper, depth-averaged values for three series of

experiments are estimated at about 100, 200 and 400 mg/l. Detailed laser-Doppler velocity measurements revealed no significant effect of the suspended sediment on the rms-values of the horizontal and vertical velocity fluctuations of the fluid. The measured velocity fluctuations of the sediment particles themselves, however, were some 15-20 % lower throughout the depth. Muste and Patel concluded that these experiments do not provide evidence for sediment-induced turbulent damping effects, as this would also affect the turbulent flow properties. Apparently, the major effect in their experiments is the inability of the dense particles to follow the turbulent flow fluctuations completely.

Lyn (1986, 1988) carried out experiments in a 13 m long, 0.267 m wide tilting flume at about 6 cm water depth and super-critical flow conditions. Various grain sizes are used; his experiments with a clean flume bottom ("starved bed experiments") are all carried out with 190 μm sand. No detailed data on the suspended sediment concentration are given, but for the starved bed experiments these concentrations were well below equilibrium values. The effects of the sediment appeared to be confined to a thin layer close to the bed, affecting the mean flow profile locally and causing an increase in bed friction. Lyn also did not measure any significant effect of the sediment on the turbulence intensities and he concluded from this that buoyancy effects on the flow profile will be small.

A very elegant experiment was performed by Lau and Chu (1987) in a tilting flume of 22 m length and 0.67 m width, at a water depth of 0.16 m and flow a velocity of about 1 m/s. They measured the vertical mixing rate of a passive tracer (10 ppt salt, made non-buoyant with methanol) in clear water and sediment-laden flow, at a sediment concentration of 1 and 5 g/l. From these measurements they deduced a reduction in vertical eddy diffusivity by 57 and 73 % for the tests with sediment and attributed this reduction to turbulence damping by sediment-induced buoyancy effects.

The results of the various turbulence measurements are difficult to interpret, as they do not include data on the turbulent energy spectrum. Hence, no analysis can be performed as to whether suspended sediment does or does not affect the overall turbulent flow structure: an increase in turbulent energy at the scale of the grains could be balanced by a decrease in energy of the larger, grain-carrying eddies. In that case, the total turbulent intensity would remain constant, but the effective eddy diffusivity would decrease. As long as no experimental evidence on the effect of suspended sediment on the energy spectrum becomes available, the results and conclusions by Lau and Chu (1987) are more convincing than those by Muste and Patel (1997) and by Lyn (1986).

Unfortunately, empirical evidence of the effect of suspended sediment on the hydraulic resistance (bed friction) of the flow is even more confusing. This is shown in Table 2.1, summarising the effect of suspended sediment on the bed friction coefficient, as presented by various authors:

author	effect on bed friction
Vanoni (1946)	decrease
Einstein-Chien (1955)	?
Taylor-Dyer (1977)	decrease
Itakura-Kishi (1980)	decrease (theoretical. analysis)
Coleman (1981, 1986)	almost no effect
Soulsby-Wainwright (1987)	decrease
Lyn (1986, 1988)	increase by 30 - 50 %
Winterwerp et al. (1990)	increase by 30 - 50 %
Villaret-Trowbridge (1991)	decrease
Muste and Patel (1997)	increase by 3 - 5 %

Table 2.1: Effect of suspended sediment on bed friction with respect to clear water.

Van Rijn (1993) attributed this confusion to different regimes for the various experiments: several experiments may have been executed at Reynolds numbers in the transitional regime. One would expect that, if buoyancy-induced turbulence damping were a major agent, the overall hydraulic resistance would decrease. Moreover, Lau (1982) showed theoretically also that the observed modifications of the velocity profiles as a function of suspended sediment concentration should result in a decrease in overall hydraulic resistance.

2.3 Effect of dilute clay additives

It has been known for several decades that the addition of a small amount of polymer to a fluid reduces its hydraulic resistance considerably (e.g. Lumley, 1969). Gust (1976) studied the effect of dilute clay suspensions ($\phi_p < 1$ ppt) on the velocity profiles of saline water-clay suspensions in a small flume of 8 cm width and 6 cm water depth for hydraulically smooth conditions at a variety of free-stream Reynolds numbers. He observed drag reductions up to 40 %, which he attributed to a thickening of the viscous sublayer by a factor of 2 to 5; the turbulence structure further away from the wall does not alter, and the universal logarithmic law appears still applicable with a standard value for the Von Kármàn constant (i.e. $\kappa = 0.4$, e.g. Fig. 2.3).

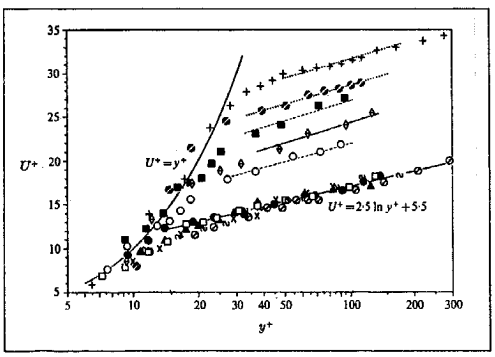

Fig. 2.3: Velocity profiles measured by Gust (1976) for various clay concentrations and Reynolds numbers.

This thickening of the viscous sublayer was predicted by Lumley (1969) on the basis of dimensional reasoning assuming a virtual slip at the wall, as observed in several experimental studies. Gust hypothesised that the physical mechanism behind drag reduction is the streamlining of deformable mud flocs; this process would resemble the mechanisms acting in polymer suspensions.

Wang et al. (1998) reported considerable drag reduction during experiments in a flume with much higher clay suspensions (up to ϕ_p = 7 %) in fresh water. They suggested that, apart form the effects mentioned above, turbulence is damped by the high viscosity of the fluid and the formation of a network at high concentrations. Indeed, a concentration beyond 5 % probably implies gelling, even at fresh water conditions, with a plug-like flow.

Some further analysis of the data reported by Gust is carried out through simulations with the 1DV POINT MODEL (Appendix B). From this analysis it is concluded that the observed drag reduction cannot be explained by sediment-induced buoyancy effects alone: the computed concentration profiles are more or less Rousean, and gradient Richardson numbers remain well under the critical value. In fact, the simulations for identical conditions with and without suspended sediment show a decrease in shear velocity by only about 3 %, i.e. one tenth of the reductions reported by Gust and by Wang et al.

2.4 Hyper-concentrated suspensions - gellation

We have defined HCMS as a Newtonian fluid. However, its dynamics, and especially the interaction with fluid-mud appearances, are affected by some non-Newtonian effects, as explained in this section. In the Introduction it is argued that for cohesive sediment non-Newtonian effects by particle-particle collisions can be neglected. However, collisions result in aggregation of the particles, forming large clusters or flocs, which is one of the important phenomena in cohesive sediment dynamics. When these flocs become space-filling they form a network structure, called a gel, and a measurable strength builds up. This takes some time though (Toorman, 1997, amongst many others). The ratio of the time scale for gelling and the time scale of the driving forces (the tide) therefore becomes an important parameter (e.g. Chapter 4). At concentrations beyond the gelling point (hindered) settling processes do no longer occur and a further compaction of the sediment-water mixture is caused by self-weight consolidation processes. Hence, also the time scale for consolidation enters our analyses (see Section 8.1).

The tide-driven erosion-deposition cycle is an important process in HCMS-dynamics. During the depositional phase a pronounced interface is formed, often with temporary fluid mud appearances. Under quiet conditions, a network can develop within the fluid mud layer. The subsequent increase in viscosity augments the momentum transfer between the fluid mud layer and the overlying low-concentrated water column. As a result, the fluid mud layer may be dragged with the main flow, in which case the vertical mixing (entrainment) is expected to decrease. Also the strength build-up within the mud layer opposes the interfacial exchange processes. On the other hand, the interface becomes more rigid and local turbulence production is again

stimulated. De Wit (1995), for instance, measured a decrease in turbulence intensities by about 20 % after the fluidization of a fluid mud layer by waves. Turbulent pressure fluctuations are probably damped by the visco-elastic fluid mud in the same manner as the damping of surface waves over muddy beds (e.g. De Wit, 1995, or Dalrymple and Liu, 1978).

The present thesis is not focused on the strength evolution of (consolidating) fluid mud layers. However, we need a realistic description of this process to complete the description of HCMS-dynamics. This description is given in Section 5.3 in our formulation of the stress tensor of consolidating HCMS-suspensions.

In this section we limit ourselves to a global description of the gelling process. For cohesive sediment, gelling starts at fairly low concentrations, the exact value depending on the sediment and pore water characteristics (Van Olphen, 1977). Table 2.2 gives a summary of the solid-phase volumetric gelling concentrations ϕ_{gel} reported in the literature, together with the corresponding mass concentration c_{gel} and bulk density ρ_{gel}, assuming saline water and $\rho_s = 2650$ kg/m^3. It follows that typical values for the gelling concentration amount to $\phi_{gel} = 0.03$ - 0.04, corresponding to a bulk density of about 1080 kg/m^3. This seems a reasonable value for fluid mud appearances. In this study we therefore apply these values, if no more detailed data are available.

	ϕ_{gel} [-]	c_{gel} [kg/m^3]	ρ_{gel} [kg/m^3]
Buscall et al. (1988)	0.02-0.05	50-130	1050-1100
Odd and Cooper (1989)	0.03	80	1070
Toorman (1992)	0.05	130	1100
Williams and Williams (1989)	0.01-0.07	30-180	1040-1130

Table 2.2: Summary of gelling values reported in the literature.

2.5 HCMS occurrences and behaviour

In The Netherlands, appearances of High-Concentrated Mud Suspensions are fairly common. Van Leussen and Van Velzen (1989) reported on sediment suspensions with (temporary) high concentrations near the river bed in the turbidity maximum of the Rotterdam Waterway, i.e. near the Botlek harbour basin, in the Borndiep (the tidal channel between Terschelling and Ameland in the Waddensea), and in the turbidity maximum in the Ems estuary. Data from the Ems estuary are further elaborated upon in Section 7.3. Recent measurements, carried out in the framework of the SILTMAN-project by Rijkswaterstaat (Netherlands Ministry of Transport and Public Works) in the North Sea around the entrance to Rotterdam Port (i.e. the "Maasmond-area"), also revealed HCMS during storm conditions. The analysis of these data is elaborated in detail in Section 7.4.

Van der Ham (1999) and Van der Ham et al. (1998) carried out detailed turbulence measurements in the major channel of the Dollard estuary (the "Grote Gat"). They measured the mean values and turbulent fluctuations of flow velocity and suspended sediment concentrations at various heights at concentrations of a few 100 to a few

1,000 mg/l, and found that the vertical turbulence structure (i.e. the turbulent stresses, the vertical transport and the flux-Richardson number) is affected significantly by the suspended sediment.

Note that all these sites in The Netherlands can be classified as meso-tidal with a tidal range between 3 and 4 m.

Adams et al. (1990) reported on a series of observations on the vertical sediment structure in a drainage channel in the Namyang Bay tidal flats, on the west coast of South Korea. This area is characterised by strong tidal effects with a tidal range of 4.9 to 7.7 m for neap and spring tide, respectively, with peak spring values up to 9 m. The observations were made during ebb tide at a water depth of the order of 4 m. Continuous measurements of current speed and turbidity revealed a depth-averaged velocity of about 0.6 m/s with a strong gradient around a lutocline of 1 m thickness, and suspended sediment concentrations of the order of 1 g/l in the highly turbulent layer below the lutocline. Only little sediment was found in the upper layer. This highly stratified structure is characterised by a gradient Richardson number $Ri_g \approx 0.33$, and by pronounced interfacial waves with higher frequency Kelvin-Helmholz billows filling the entire water depth.

Faas and Wartel (1985) reported concentrations of several 100 mg/l in the turbidity maximum of the Scheldt River near Antwerp, Belgium. Also off the Belgian coast, around the entrance of Zeebrugge Port, high concentrations up to a few g/l have been monitored frequently (Bastin et al., 1982).

Probably the first publication on HCMS is by Inglis and Allen (1957) describing the sediment dynamics in the Thames, UK (called fluid mud though in their paper). The Thames is a meso-tidal river with a distinct turbidity maximum, called the Mud-Reaches. During a 13-hour campaign, the sediment concentration at 60 % of the water depth was measured to vary between about 50 and 1,000 mg/l. Later, even larger concentrations up to a few g/l have been measured near the bed (Odd, 1988).

West and Oduyemi (1989) measured mean and fluctuating velocity components and sediment concentrations in the Tamar (1984) and Conway (1984) estuaries at neap, intermediate and spring tide conditions with water depths varying between 1 and 5 m and suspended sediment concentrations ranging from 50 to 4,000 mg/l. From these measurements they deduced a reduction in the vertical turbulent momentum flux by about 80 % at Richardson numbers beyond 0.3 to 0.5 and a reduction in the vertical turbulent sediment flux up to 90 % at Richardson numbers up to unity. The difference in damping between the vertical fluctuating momentum and sediment flux was attributed to the role of internal waves, which contribute to the velocity fluctuations, but not to vertical mixing (see also Uittenbogaard, 1995).

The UK counts many sedimentologically dynamic estuaries and numerous studies have been published. The estuaries along the east coast in general have meso-tidal conditions, and HCMS-concentrations are reported for Brisbane River (Odd, 1988), and the Tamar and Trent estuaries (Arundale et al., 1997). Along the south and west coast macro-tidal conditions prevail. Many studies have been reported on the Severn estuary which has a tidal range of about 14.5 m at spring tide and 6.5 m at neap tide (e.g. IOS, 1977, Kirby and Parker, 1980, Hydraulics Research Station, 1980, and Odd and Cooper, 1989). This estuary is notorious for its fluid mud appearances. The various data show a strong influence of the spring-neap tidal cycle: during spring tide

the vast, but loosely consolidated fluid mud layers in the estuary, deposited during neap tide, are eroded slowly. On top of these fluid mud layers, the suspension in the water column can reach concentrations of a few g/l, with several distinct lutoclines around slack water. The various studies are all dedicated to the behaviour of the fluid mud layers themselves, their formation, mobility and detectability.

Also the macro-tidal Loire (Teisson and Fritsch, 1988, Le Hir, 1997) and Gironde estuaries (e.g. du Penhoat and Salomon, 1979) in France are renowned for their fluid mud occurrences. Allen et al. (1980) studied the influence of the tide on maintaining the turbidity maximum at a concentration of the order of 1 g/l. They concluded that the tidal erosion-deposition cycle is the major mechanism in maintaining this turbidity maximum and that the effects of fresh-saline water induced gravitational circulation is of minor importance. However, the latter process may be responsible for the supply of sediment through long-term residual transports. The processes within the Loire estuary strongly resemble those in the Severn (Le Hir, 1997). The spring-neap tidal cycle drives an erosion-deposition-consolidation cycle generating and re-entraining vast layers of fluid mud yielding a high concentrated suspension of a few g/l in the overlying water column.

Wolanski et al. reported on the sediment dynamics in the macro-tidal South Alligator River (Wolanski et al., 1988) and the meso-tidal Normanby estuary (Wolanski et al., 1992) in Australia. Both rivers show high concentrations, varying between 1 and 6 g/l. In their analysis, Wolanski et al. focused on the vertical exchange processes and stressed the important role of sediment-induced buoyancy effects on the vertical turbulence structure. Hence, these appearances are in line with our HCMS-definition.

Several studies on HCMS-appearances in East-Asia have been published. Wolanski et al. (1996) reported HCMS in the Mekong river (Vietnam), both in the upstream fresh water part and in the salinity-affected downstream estuary. HCMS in China was reported by Shen et al. (1993) in the Yangtze estuary, by Dong et al. (1997) and Guan et al. (1998) in the macro-tidal Jiaojiang River and by Wright et al. (1990) in the Yellow River. Note that the latter river even can be considered as hyper-concentrated with depth-mean concentrations up to 200 g/l. Still, in the river mouth HCMS at a few 100 mg/l (locally up to a few g/l) can occur in the water column when fresh deposits are eroded by either the tidal current and/or waves. A thorough study on the sediment dynamics in Ariake Bay, Japan, dedicated to the extension of Kumamoto Port (Kihara et al., 1994) revealed HCMS-occurrences when the soft mud on the sea bed is mobilised by wave activity.

Wells (1983) described HCMS-occurrences (called fluid mud in his paper) at a variety of coastal sites: South Louisiana (Atchafalaya Bay), the north coast of South America (Guyana and Surinam) and the west coast of Korea (Yellow Sea, near the Kum River). Though the tidal and wave conditions for these sites are very different (micro-, meso- and macro-tidal, moderate and high wave energy), the sediment dynamics are qualitatively very similar. Wells analyses mainly focused on the attenuation of wave energy by the fluid mud and the mobility of the soft and mobilised mud. Unfortunately, no analysis on the sediment processes in the water column was presented.

The results of the two-year AMASEDS-campaign, covering low, rising, high and falling river flow on the Amazon continental shelf, including a part of the Amazon mouth, have been reported recently (Kineke, 1993, Kineke and Sternberg, 1995 and Kineke et al., 1996). Detailed measurements over the water depth at numerous locations of suspended sediment, flow velocity, salinity and temperature were carried out; unfortunately, no data were collected on settling velocity or wave activity.

This study revealed the importance of fresh-saline water induced gravitational circulations on the horizontal sediment transport processes and the accumulation of the sediments in the turbidity zone, and of the role of the spring-neap tidal cycle in establishing the settling and mixing processes in the water column. Huge patches of fluid mud were observed, and almost the entire survey area, covering about 300 by 500 km^2, revealed suspended sediment concentrations of the order of many 100 mg/l to a few g/l, hence in our HCMS-range.

In their analysis, Kineke et al. stress the role of the vertical stratification, induced both by the river flow and the sediment suspension, and of the hindered settling processes on the sediment dynamics. This is further elaborated upon in the next section.

Contrary to the situation with non-cohesive sediment, no contradicting data on the effect of HCMS on the effective hydrodynamic drag have been reported in the literature. Dong et al. (1997) and Guan et al. (1998) reported a decrease of 30 % in the Manning roughness coefficient $n = 0.015$ $sm^{-1/3}$ in the Jiaojiang estuary in China (mean effective Chézy value of $C \approx 90$ $m^{1/2}/s$). Wang et al. (1998) reported values of the Manning roughness coefficient of $n = 0.035$ $sm^{-1/3}$ in a canal diverting clean water from the Yellow River, and of $n = 0.025$ $sm^{-1/3}$ for hyper-concentrated suspensions in the same canal. In the lower reaches of the Yellow River even lower values were found of about $n = 0.01$ $sm^{-1/3}$. From a detailed analysis of the data from a large series of tidal stations and numerical simulations of the tidal propagation on the Amazon shelf, Beardsley et al. (1995) deduced an overall decrease in hydraulic roughness of 50 %, which they explicitly attributed to huge fluid mud appearances in the Amazon mouth. The analyses and simulations revealed a mean effective Chézy value on the outer shelf of $C \approx 60$ $m^{1/2}/s$, a mean effective Chézy value on the inner shelf of about $C \approx 90$ $m^{1/2}/s$, and locally in the areas of fluid mud appearances of $C \approx 110$ $m^{1/2}/s$. A Chézy value of $C = 110$ $m^{1/2}/s$ was also found from similar simulations of the tidal propagation in the Yangtze River by PDC (1996).

Wolanski et al. (1992) emphasised the influence of high suspended sediment concentrations on the sediment-induced anisotropy of the turbulence. They refer to field observations on the limited vertical mixing of turbidity currents with ambient water and on the apparent total collapse of turbulence in laboratory experiments with sediment-laden flow.

2.6 Numerical modelling studies

We are aware of only a few studies, reported in the literature, in which the turbulent water movement is explicitly coupled to the sediment dynamics through a sediment-induced buoyancy term in the turbulence closure equation(s). These models are briefly

discussed in this section so as to provide a reference for the modelling studies presented in this thesis.

The first such model that has been published is probably by Adams et al. (1981a, 1981b). They applied a simple three-dimensional model of flow and suspended sediment concentration, neglecting horizontal advection and diffusion effects. The modelled flow velocities can be regarded as perturbations on the geostrophic components. The vertical eddy viscosity is modelled with the so-called Mellor-Yamada level II turbulence closure scheme, which is essentially a k-l turbulence model, where l is the mixing length. This scheme accounts for buoyancy effects induced by vertical gradients in suspended sediment concentration and water temperature. The mass balance accounted for a multi-disperse (non-cohesive) sediment, in which the horizontal transport gradients were neglected as well. The effects of hindered settling were not included.

The model was applied in a sensitivity analysis for Florida Strait (i.e. deep sea) conditions by studying the effect of various amounts of suspended sediment of various grain size on the turbulent kinetic energy, the eddy diffusivity, and the effective hydraulic resistance. Their results are discussed elsewhere in this chapter. No comparison with field data was presented however, which may be the reason that this work has been ignored for a long time.

Recently, a thorough diagnostic modelling study was set up at Laboratoire National d'Hydraulique in France. Teisson et al. (1992) presented a 1DV Reynolds stress model in which the flow is driven by a horizontal pressure gradient (water surface slope). The vertical stress equations include a sediment-induced buoyancy term. The sediment balance equation however does not account for the effects of hindered settling. This model was applied to analyse the sediment - turbulent flow interaction, and the first ideas on the existence of a saturation concentration for cohesive sediment (see Section 6.1) were announced in this paper.

Teisson et al. also presented some preliminary analyses with a two-phase flow model, applying a standard k-ε turbulence model, including buoyancy effects. The flow-sediment interaction is modelled as a drag force on the sediment particles, thus implicitly accounting for the effects of hindered settling. They showed that this model concept allows a continuous simulation of sediment dynamics in the entire water column, including part of the bed.

Later this model was extended by Villaret et al. (1996) to include a description for the evolution of floc size with some heuristic aggregation and floc breakup formulations. The latter formulation contains a description with a user-defined maximal attainable floc size. The model was used to carry out some sensitivity analyses establishing the floc size distribution over the water column as a function of various model parameters. No experimental data for the validation of these descriptions are available though.

Galland (1996) and Galland et al. (1997) published work on an extension of the Reynolds stress model including low-Reynolds number effects. Galland et al. carried out a detailed validation of the model against data published by Coleman (1981, 1986) showing good agreement between the numerical simulations and the experiments. Next, the model was used to study the sediment-induced buoyancy effects on the velocity and sediment concentration profile and to verify the similarity relations

derived by Teisson et al. (1992). Finally this model was applied to establish the coefficients in a Munk-Anderson like damping function in a simple 1DV-code with buoyancy-corrected eddy viscosity and diffusivity.

The most comprehensive studies were conducted by Le Hir (1997) and Le Hir et al. (1998) who developed and applied a 2DV and a 3D two-phase model. In the momentum equation advection and Coriolis effects are neglected. The sediment-flow interaction is modelled through a force accounting for gravity, interfacial drag forces and effective (particle-particle) and turbulent stresses. A mixing length concept with a Richardson-number-dependent damping function was applied. In a later phase of the studies also a visco-plastic formulation for the behaviour of fluid mud was implemented.

In Le Hir (1997) a series of sensitivity analyses, carried out with a 1DV-version of the code, was presented on the effects of buoyancy-induced turbulence damping and of the various sediment-dependent parameters. Next, schematic simulations of the behaviour of the turbidity maximum and fluid mud dynamics in the Loire estuary were carried out and qualitatively compared with observations.

Recently Le Hir et al. (1998) presented results of simulations with the model of the fluid mud dynamics and the turbidity maximum in the Gironde estuary. Again a series of sensitivity analyses was carried out with the aim of establishing the relative importance of a proper formulation of the various processes. The settling velocity was modelled as a function of the sediment concentration, accounting for the effects of flocculation and hindered settling, and a visco-plastic rheological model was used to describe the stress-strain relations. These formulations limit the vertical concentration gradients, and appeared to be necessary to obtain reasonable vertical profiles of suspended sediment concentration.

Guan et al. (1998) reported on their simulations of the mud dynamics in the Jiaojiang River with a width-averaged two-dimensional model (2DV). This model includes the effects of salinity and sediment on the fluid density, a Prandtl's mixing length concept with a Richardson-number-dependent damping formulation for the vertical eddy viscosity and eddy diffusivity, and the common Partheniades and Krone formulations for the water-bed exchange processes. They distinguished between consolidated mud deposits, that cannot be eroded within one tidal cycle, and limited fresh mud deposits, which can be eroded during accelerating tide only. In this way they prescribe the amount of sediment within the system explicitly. The settling velocity was kept constant and no hindered settling effects were accounted for. From a comparison between their numerical results and the field data, Guan et al. inferred that at a concentration beyond 20 g/l the turbulence mixing collapses. This process was not implicitly included in their turbulence model but it was explicitly accounted for by arbitrarily reducing the vertical eddy diffusivity when $c > 20$ g/l. As a result, a fair agreement between numerical results and field data was obtained.

Simulations without sediment-induced buoyancy effects were carried out to demonstrate the influence of the sediment on the velocity and concentration profiles. A fairly low value of the Manning roughness coefficient was required to achieve the proper tidal propagation (see Section 2.5).

2.7 Discussion

All studies reported in the literature show an appreciable effect of suspended sediment on the turbulence properties of open-channel flow at already moderate sediment concentrations. For non-cohesive sediment an ongoing debate exists as to whether this effect is primarily limited to the outer part of the flow through a modification of the defect law, or whether the entire flow structure is affected through a decrease of the effective von Kármàn constant κ_s. Surprisingly, not much attention is paid in these discussions to the underlying physical processes, such as the damping of the vertical turbulence structure by buoyancy effects, as suggested by Vanoni (1946), and elaborated upon by Barenblatt (1953) and others. From these latter analyses we conclude that it depends on the specific flow and sediment characteristics, whether the major effect of the sediment on the velocity profile is found near the bed, or higher in the water column. Moreover, the deviation from the logarithmic law of the wall, including the decrease in flow velocity near the water surface, observed during flume experiments by many researchers is, at least partly, caused by the effects of side wall friction and secondary currents - this is further elaborated in Section 7.1. It is hypothesised that in sediment-laden flows in open channels these side wall effects become relatively more important, when the contribution of near-bed produced turbulence is decreased because of buoyancy effects, which would explain the results by Coleman (see Section 2.2), for instance.

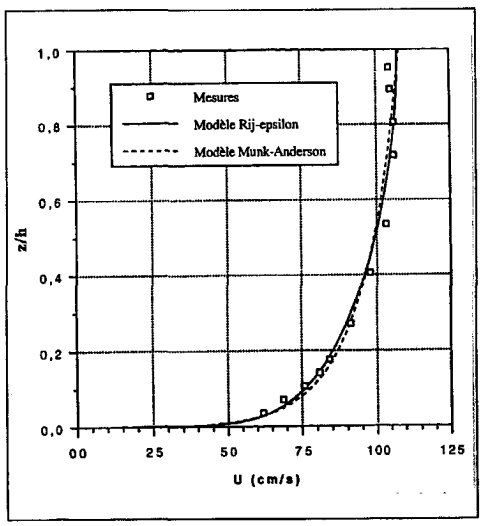

Fig. 2.4: Simulation by Galland (1996) of velocity profile in sediment-laden flow (data by Coleman, 1981) with a Reynolds stress model.

The numerical simulations of the measurements presented by Coleman (1981), as published by Galland (1996) and presented in Fig. 2.4, are therefore interesting. These experiments were carried out in a 15 m long flume of 35.6 cm width and a water depth of about 17 cm. The median diameter of the sand used amounts to 105 μm, and no sediment was allowed to settle on the bed. The simulations were carried out with the 1DV Reynolds-stress model described in Section 2.6, including buoyancy terms in the vertical stress equations. No other fluid-sediment interaction processes were

accounted for. Fig. 2.4 shows that the reproduction of the velocity profile is satisfactory. The overprediction of the flow velocity near the water surface is caused by secondary flow effects in the flume. The near-bed concentration amounts to about 50 g/l. In Section 7.1 we will discuss the influence of the buoyancy effects on the slope of the logarithmic velocity profile in some further detail.

The literature on field observations all report strong stratification effects. A considerable damping of the vertical turbulent transport was actually measured by West and Oduyemi (1989) and Van der Ham (1998), and Adams et al. (1990) reported on highly stratified conditions with internal waves riding on the interface. This agrees with the analysis of the tidal propagation over extended muddy areas, such as the Amazon Delta and the Yangtze River, yielding a substantial decrease in effective hydraulic resistance. The important role of turbulence damping is further confirmed by the various numerical analyses reported in the literature, showing strong effects of suspended sediment on the flow structure and the vertical sediment concentration profile.

Laboratory studies show that small amounts of clay particles may substantially decrease the effective hydraulic resistance of turbulent flow, probably by an increase in the thickness of the viscous sub-layer. However, these studies were conducted at hydraulically smooth flow conditions. In nature, hydraulically rough conditions are more common, and we therefore will neglect this effect in the present study.

In summary we can conclude that HCMS-appearances, though confined in space, occur frequently under a wide variety of hydro-meteo conditions all over the world. The interaction between the suspended sediment and the turbulent water movement, at least for fine-grained sediment, for which the particles can follow the turbulent eddy movements properly, is confined to sediment-induced buoyancy effects. Moreover, the interaction with fluid mud appearances appears to be important. Fluid mud can be formed from HCMS's and vice versa, fluid mud may act as a source for the generation of HCMS.

The summary of numerical modelling studies, reported in the literature, shows that at present the modelling of sediment-induced buoyancy effects relevant for HCMS-dynamics is feasible with the current state-of-the-art in turbulent flow modelling. Little attention though is paid to the effects of even higher sediment concentrations, generating highly stratified conditions and to the volumetric aspects of HCMS-dynamics, such as flocculation, gellation and hindered settling, and their interaction with the turbulent flow field. This is therefore one of the major subjects in this thesis. The relevant mathematical-physical equations are presented and discussed in the three following chapters.

3. Equations for the mean flow and turbulence

This chapter presents the relevant equations for the turbulent water movement and transport of suspended sediment in three dimensions. A one-dimensional version of the relevant set of equations is obtained by neglecting all horizontal gradients, except for the pressure term; this 1D-version has been implemented in the 1DV POINT MODEL (see Appendix B) and is used to study the dynamics of HCMS.

3.1 The mean water movement

The present study is dedicated to the behaviour of High-Concentrated Mud Suspensions in shallow water, hence the hydrostatic pressure approximation is valid, and we assume that the bed is horizontal. We have shown that the water-sediment mixture can be treated as a single-phase fluid. The fluid is incompressible and we assume that the Boussinesq approximation is allowed, i.e. variations in the fluid density ρ can be neglected, except in the gravitational terms. Using Einstein's summation convention, the three-dimensional continuity equation reads:

$$\frac{\partial u_i}{\partial x_i} = 0 \tag{3.1}$$

The three-dimensional momentum equation reads:

$$\frac{\partial u_i}{\partial t} + \frac{\partial u_i u_j}{\partial x_j} - e_{ijk} f_k u_j = \frac{1}{\rho}\frac{\partial \sigma_{ij}}{\partial x_j} - \delta_{i3} g \tag{3.2}$$

The equation of state, $\rho = \rho(S,c)$, will be specified in Section 3.2. In (3.1), (3.2) and the equation of state we have used the following notation:

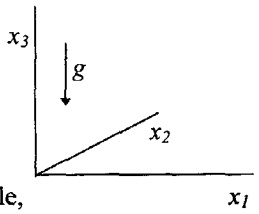

c = suspended sediment concentration by mass,
f = Coriolis parameter,
g = acceleration of gravity,
S = salinity,
t = time,
u_i = flow velocity, averaged over the turbulent time scale,
x_i = Cartesian co-ordinate (x_3 is positive upward - see sketch),
ρ = bulk density of water-sediment mixture, and
σ_{ij} = stress tensor.

We have used the Kronecker delta δ_{ij} ($\delta = 1$ for i = j, and $\delta = 0$ for $i \neq j$) and the permutator e_{ijk} (e = 1 for cyclical i, j and k, e = -1 for anti-cyclical i, j and k; otherwise e = 0).

The stress tensor σ_{ij} consists of a part induced by fluid stresses and a part induced by inter-particle stresses. In the water column at suspended sediment concentrations up to the gelling point, the latter part is negligible. Also stresses induced by particle-particle interaction are very small in the water column (see Chapter 1). We assume that the first two stresses may be superimposed according to the Kelvin-Voigt theory:

$$\sigma_{ij} = \sigma_{ij}^{f} + \sigma_{ij}^{s} \tag{3.3}$$

where superscript ^{f} refers to the water phase and ^{s} to the interparticle stresses caused by the solids structure in the bed. Both stresses can be separated into a deviatoric part τ_{ij} and an isotropic part p:

$$\sigma_{ij} = \tau_{ij} - \delta_{ij} p\,, \quad \text{where } p = -\tfrac{1}{3}\sigma_{ii} \tag{3.4}$$

According to (3.3) the isotropic pressure can be written as:

$$p = p^{f} + p^{s} \tag{3.5}$$

In soil mechanics (3.5) is also known as the effective stress concept. This decomposition allows us to include contributions to the stress tensor resulting from the following processes:

1. Molecular effects (viscosity), possibly affected by (weak) non-Newtonian effects,
2. Turbulence - we assume that the eddy viscosity and eddy diffusivity are isotropic by applying the k-ε turbulence closure model (e.g. Section 3.3), and
3. Interparticle stresses - we elaborate on this topic in Chapter 5 when deriving a simple consolidation and strength evolution model.

Thus, after applying the Reynolds averaging procedure for turbulent flow, the stress tensor becomes (Malvern, 1969):

$$\sigma_{ij} = \tau_{m,ij}^{f} - \delta_{ij} p^{f} + \sigma_{T,ij} + \tau_{ij}^{s} - \delta_{ij} p^{s} \tag{3.6}$$

in which $\tau_{m,ij}^{f}$ are the molecular stresses and $\sigma_{T,ij}$ the turbulent stresses (see (3.8)). The molecular stress is modelled with Fick's law (Malvern, 1969, Hinze, 1975):

$$\tau_{m,ij}^{f} = \mu\left(\frac{\partial u_i}{\partial x_j} + \frac{\partial u_j}{\partial x_i}\right) \tag{3.7}$$

in which μ is the dynamic viscosity of the (Newtonian) fluid. The turbulent stress tensor is modelled with the Boussinesq eddy viscosity concept (e.g. Hinze, 1975, Rodi, 1984):

$$\sigma_{T,ij} = \rho\nu_T\left(\frac{\partial u_i}{\partial x_j} + \frac{\partial u_j}{\partial x_i}\right) - \frac{2}{3}\delta_{ij}\rho k \tag{3.8}$$

in which ν_T is a scalar quantity, representing the turbulent eddy viscosity and k the turbulent kinetic energy, to be defined in Section 3.3.

In the remainder of this chapter we drop the superscript ^{f} and use the symbol p exclusively for the water pressure. Because of the hydrostatic pressure assumption, the momentum equation in the vertical direction x_3 simplifies to:

$$\frac{\partial p}{\partial x_3} = -\rho g \tag{3.9}$$

We consider water systems with a free surface only, which may vary with time, though, as a result of which the pressure term can be written as:

$$p(x_3) = p_{atm} + g\int_{x_3}^{Z_s} \rho dx_3' \tag{3.10}$$

where p_{atm} is the pressure at the water surface $x_3 = Z_s(t)$, i.e. $p(Z_s) = p_{atm}$. The inter-particle stress σ_{ij}^s is elaborated in Section 5.4; it is zero, unless stated otherwise.

The boundary conditions at the water level $x_3 = Z_s(t)$ and at the horizontal (rigid) bed $x_3 = Z_b$ for the continuity equation and the momentum equation read:

$$u_3 = 0\Big|_{x_3=Z_b} \quad ; \quad u_3 = \frac{\partial Z_s}{\partial t}\Big|_{x_3=Z_s} \qquad i = 1,2 \tag{3.11}$$

$$\tau_{b,i} = \rho(\nu + \nu_T)\frac{\partial u_i}{\partial x_3}\Big|_{x_3=Z_b} \quad ; \quad \tau_{s,i} = \rho(\nu + \nu_T)\frac{\partial u_i}{\partial x_3}\Big|_{x_3=Z_s} \qquad i = 1,2 \tag{3.12}$$

The kinematic boundary conditions express that the bed and the water surface are material surfaces; this water surface can be a function of time. Because we assume that the bed is (almost) horizontal and that the slope in water surface is small, these kinematic conditions reduce to (3.11). Under tidal flow conditions the velocity profile is logarithmic over the major part of the water depth and over the major part of the tidal cycle, as is shown recently once more by Lueck and Lu (1997) from a series of velocity measurements with an ADCP in the 30 m deep Cordova channel (Canada). Therefore, at the bed, the logarithmic law of the wall is applied to compute the bed shear stress τ_b, i.e. we exclude the low-Reynolds and sediment affected sub-layer, but include possible wave effects (see Section 3.4). Also the shear stress at the water surface τ_s caused by wind action, for instance, can be specified. Such effects, though, are not elaborated upon in this study.

Also in horizontal direction, boundary conditions have to be specified. However, various possibilities exist, depending on the characteristics of the flow (Vreugdenhil, 1994). For more details, the reader is referred to Uittenbogaard et al. (1992), where the entire procedure to set the boundary conditions in a numerical three-dimensional model is outlined in detail.

3.2 The mass balance equation for suspended sediment

We have reasoned in Chapter 1 that suspensions of cohesive sediment can be treated as a single-phase fluid, the particles following the turbulent water movements properly, except for their settling velocity. The mass balance for fine-grained suspended sediment in three dimensions can therefore be described with the well-known advection-diffusion equation, which reads:

$$\frac{\partial c^{(i)}}{\partial t} + \frac{\partial}{\partial x_i}\left(\left(u_i - \delta_{i3}w_s^{(i)}\right)c^{(i)}\right) - \frac{\partial}{\partial x_i}\left(\left(D_s + \Gamma_T\right)\frac{\partial c^{(i)}}{\partial x_i}\right) - \frac{\partial}{\partial x_i}\left(\delta_{i3}\overline{w_s'c'^{(i)}}\right) = 0 \tag{3.13}$$

where $c^{(i)}$ is the ensemble averaged sediment concentration by mass of fraction (i)[1], D_s the molecular diffusion coefficient, Γ_T the eddy diffusivity defined as $\Gamma_T = \nu_T/\sigma_T$ (see Section 3.3) - we assume that D_s and Γ_T are the same for all sediment fractions, which is correct for small particles ($w_s << u_3'$) in dilute suspensions (Felderhof and Ooms, 1990) - and $w_s^{(i)}$ is the effective settling velocity of the (i)-th sediment fraction. The settling velocity is further elaborated upon in the Chapter 4. The last term in (3.13) stems from a correlation between the turbulent fluctuations in c and $w_s^{(i)}$ (see also Section 4.5.1). We have shown in Chapter 1 for HCMS that $w_s << w'$. Because the turbulent fluctuations of the settling velocity are much smaller than its mean value, we can certainly neglect the last term in (3.13) with respect to the turbulent diffusion term, as this term represents the correlation $\overline{w'c'}$.

We note that the settling velocity w_s is small in general. This implies that small vertical flow velocities, such as occurring in converging flow, as a result of bed level variations, can significantly affect the settling behaviour of the sediment. This will impose a limitation in the application of a 1DV-model.

The total transport through the water surface is zero. At the horizontal bed the total transport balances possible sources or sinks[2]. Hence the boundary conditions read:

$$\left\{\left(u_3 - w_s^{(i)}\right)c^{(i)} - \left(D_s + \Gamma_T\right)\frac{\partial c^{(i)}}{\partial x_3}\right\}\Bigg|_{x_3=Z_s} = 0 \quad \text{and}$$
$$\left\{\left(u_3 - w_s^{(i)}\right)c^{(i)} - \left(D_s + \Gamma_T\right)\frac{\partial c^{(i)}}{\partial x_3}\right\}\Bigg|_{x_3=Z_b} = E_{b,c} \tag{3.14}$$

At the rigid bed Z_b we apply the classical formulae of Partheniades and Krone:

$$E_{b,c} = -w_s^{(i)}\, c^{(i)} \mathrm{S}\left(1 - \theta_d^{(i)}\right) + M^{(i)} \mathrm{S}\left(\theta_e^{(i)} - 1\right) \quad \text{at} \quad x_3 = Z_b \tag{3.15}$$

in which M is a positive empirical erosion parameter, θ_e is a non-dimensional threshold shear stress for erosion, $\theta_e = \tau_b/\tau_e$, τ_e is the critical shear stress for erosion, θ_d is a non-dimensional threshold shear stress for deposition, $\theta_d = \tau_b/\tau_d$, τ_d a threshold shear stress for deposition (N.B. in general $\tau_d < \tau_e$), and S(x) is a ramp function: for $x > 0$, S = x and for $x \leq 0$, S = 0.

The molecular diffusion term D_s is given by the Stokes-Einstein equation:

$$D_s = \frac{kT}{6\pi\mu D} \tag{3.16}$$

in which

D = particle size,

---

[1] Note that the superscript (i) is only an identifier for the sediment fraction and does not obey Einstein's summation convention.

[2] Note that both at the water surface and at the bed, diffusive transports are zero, hence both the settling and diffusion terms in (3.14) are zero. This is implemented in the 1DV POINT MODEL - see Appendix B.

k = Boltzman constant (= $1.38 \cdot 10^{-23}$ J/K), and
T = absolute water temperature.

The influence of the suspended sediment concentration on the bulk fluid density is given by the equation of state:

$$\rho\left(S, c^{(i)}\right) = \rho_w(S) + \sum_i \left\{ \left(1 - \frac{\rho_w(S)}{\rho_s^{(i)}} \right) c^{(i)} \right\} \tag{3.17}$$

with $\rho_w(S)$ the density of the water as a function of salinity only.

3.3 The k-ε turbulence model

We limit ourselves to turbulent flow at high Reynolds numbers, i.e. $Re_T > 100$. This so-called turbulence Reynolds number Re_T is defined as:

$$Re_T \equiv \frac{\sqrt{k}\,\ell}{\nu} \approx \frac{2\nu_T}{\nu} \tag{3.18}$$

in which k is the turbulent kinetic energy, to be defined in (3.19), ℓ is a typical length scale of the turbulence (mixing length) and ν is the kinematic molecular viscosity, i.e. $\nu = \mu/\rho$. For $Re_T < 100$ the kinematic viscosity becomes important at all turbulent length scales, and a so-called low-Reynolds-number turbulent closure model has to be applied. We recognise that in HCMS low Reynolds number effects may occur, for instance near lutoclines and near the bed. Yet, we neglect such effects in the present study, as they are probably small with respect to buoyancy effects; they are subject of an ongoing study within another framework of research.

Recent studies reveal that, for the conditions treated in the present study, a decrease in turbulent energy of the order of 20 % may occur as a result of the influence of the individual sediment particles on the turbulence properties (e.g. Felderhof and Ooms, 1990 and Ooms and Schinkel, 1998 - see also Section 2.2). Yet we also neglect this effect, as buoyancy effects on the turbulence structure, induced by the suspended sediment, become dominant at the conditions at which the influence of the individual sediment particles on the turbulence starts to play a role.

In shallow waters, turbulence mixing is not exactly isotropic. Hinze (1975) and Nezu and Nakagawa (1993), amongst others, reported on experimental data in open channel flow showing that rms-values of turbulent fluctuations in the transverse velocity component are about 30 % smaller than those of the fluctuations in the direction of the mean flow velocity, whereas the turbulent fluctuations in the vertical direction are even about 45 % smaller. However, at length scales of the order of the water depth, the differences in the turbulent velocity components are smaller, as was shown for instance by Nezu and Rodi (1986) from a series of detailed turbulence measurements with an LDA-system in a 65 cm wide tilting flume at a water depth of 10 cm and flow velocities ranging from 0.07 to 1.2 m/s. Also recent ADCP-measurements by Sukhodolov et al. (1998) in the Spree river (Germany) revealed

fairly isotropic turbulence properties at length scales of the same order of and smaller than the water depth.

We are concerned with shallow water flows where a boundary layer approximation is valid. In that case isotropic turbulence models, such as the k-ε model, are well suited to establish the mixing properties perpendicular to the wall and the main shear flow. Such models are applied with great success, as shown from comparisons with experimental data, e.g. Launder and Spaulding (1974), Rodi (1984), Uittenbogaard et al. (1992). We recognise that horizontal mixing is underestimated by such isotropic models, but this is not relevant as we focus on the processes across the water depth. Hence, we can ignore anisotropic effects in the horizontal plane and apply the isotropic k-ε turbulence closure model. Rodi (1984) and Uittenbogaard (1995) have shown that this model applies to fairly stratified flow conditions. For highly stratified flow conditions, however, the buoyancy effects are overestimated, resulting in too much damping of the vertical exchange of momentum (Simonin et al., 1989). This is attributed to internal waves which may augment the vertical transport of momentum, but the effects of which are not included in the standard k-ε model. Uittenbogaard (1995) therefore advocates the implementation of additional source and sink terms in the k-ε model, the descriptions of which are determined from internal wave properties. We have carried out several tests with this extended k-ε model (e.g. Winterwerp and Uittenbogaard, 1997 and Winterwerp, 1998) and concluded that it has only little effect on the cases addressed in this thesis. We will therefore apply the standard k-ε model only (e.g. Launder and Spaulding, 1974 and Rodi, 1984).

The turbulent kinetic energy k and the turbulent dissipation rate ε per unit mass are defined by (see Tennekes and Lumley, 1994):

$$k \equiv \frac{1}{2}\overline{(u_i' u_i')} \quad \text{and} \quad \varepsilon = \frac{1}{2}\nu \overline{\left(\frac{\partial u_i'}{\partial x_j} + \frac{\partial u_j'}{\partial x_i}\right)^2} \tag{3.19}$$

where u_i' is the fluctuating part of the instantaneous velocity component. The eddy viscosity in the turbulent stress tensor (3.8) becomes:

$$\nu_T = c_\mu \frac{k^2}{\varepsilon} \tag{3.20}$$

The standard k-ε model reads:

$$\frac{\partial k}{\partial t} + \frac{\partial u_i k}{\partial x_i} - \frac{\partial}{\partial x_i}\left(\nu + \frac{\nu_T}{\sigma_k}\right)\frac{\partial k}{\partial x_i} = \nu_T \left(\frac{\partial u_i}{\partial x_j} + \frac{\partial u_j}{\partial x_i}\right)\frac{\partial u_i}{\partial x_j} + \delta_{i3}\frac{g}{\rho}\frac{\nu_T}{\sigma_T}\frac{\partial \rho}{\partial x_i} - \varepsilon \tag{3.21a}$$

$$\begin{aligned} &\frac{\partial \varepsilon}{\partial t} + \frac{\partial u_i \varepsilon}{\partial x_i} - \frac{\partial}{\partial x_i}\left(\nu + \frac{\nu_T}{\sigma_\varepsilon}\right)\frac{\partial \varepsilon}{\partial x_i} = \\ &\quad = c_{1\varepsilon}\nu_T \frac{\varepsilon}{k}\left(\frac{\partial u_i}{\partial x_j} + \frac{\partial u_j}{\partial x_i}\right)\frac{\partial u_i}{\partial x_j} + \delta_{i3}(1 - c_{3\varepsilon})\frac{\varepsilon}{k}\frac{g}{\rho}\frac{\nu_T}{\sigma_T}\frac{\partial \rho}{\partial x_i} - c_{2\varepsilon}\frac{\varepsilon^2}{k} \end{aligned} \tag{3.21b}$$

The first term in (3.21) gives the rate of change of either k or ε, the second term represents advection, the third term represents diffusion, the fourth term is the turbulence production term, the fifth term represents destruction by buoyancy effects and the last term represents dissipation. We have used the Reynolds analogy, that is that also the diffusive transport of the turbulence parameters can be modelled as a gradient-type transport, using the turbulent Prandtl-Schmidt numbers σ_k and σ_ε. The values of most of the coefficients have been obtained from calibration of the model against grid-generated turbulence and matching with the logarithmic law of the wall, and they are well established in the literature (e.g. Spaulding and Launder, 1974 and Rodi, 1984).

The values of the Prandtl-Schmidt number σ_T and the coefficient $c_{3\varepsilon}$ are less well established. Here we follow Uittenbogaard (1995)[3)]. He showed conclusively that in free turbulence, $\sigma_T = 0.7$, even under highly stratified conditions. Experimental data deviating from this value are explained in terms of the effects of internal waves, which do transfer momentum, but not mass. This effect is generally accounted for by a modification of σ_T, which is often modelled as a function of the Richardson number itself. Uittenbogaard (1995) instead, promotes the use of additional terms in the k-ε model through which the effects of internal waves can be described explicitly. He also argues why $\sigma_T < 1$. In turbulent flow, packages of fluid are deformed continuously by the turbulent stresses in the fluid. The deformation of these packages, however, is restricted by the requirements of continuity: if the deformation in two directions is given at any instant, then the deformation in the third direction follows from continuity. In other words, if $\partial u_1'/\partial x_1$ and $\partial u_2'/\partial x_2$ are given, $\partial u_3'/\partial x_3$ is set. This affects the value of the correlation between the turbulent velocity components. This restriction does not apply to a solute, as a solute can diffuse freely through the fluid. Hence the correlation between c' and u_i' has more degrees of freedom than the correlation between the turbulent velocity components themselves. As we have concluded that the particles of fine-grained sediment can be treated as a passive tracer (apart from its settling velocity) in a single-phase description, the argument above is also valid for the turbulent diffusion of the fine sediment in the present study.

From an analysis of the experiments in stratified flow by Lienhard and Van Atta (1990), Uittenbogaard (1995) also concluded that for stable stratified flows, the buoyancy term in the ε-equation vanishes ($c_{3\varepsilon} = 1$). For unstable stratified flow conditions $c_{3\varepsilon} = 0$ is fair, which represents ε-production, i.e. small-scale turbulence production by Rayleigh-Taylor instabilities.

The various coefficients in the standard k-ε model are summarised in Table 3.1:

			Prandtl-Schmidt numbers				stable stratification	unstable stratification
c_μ	$c_{1\varepsilon}$	$c_{2\varepsilon}$	σ_k	σ_ε	σ_T	κ	$c_{3\varepsilon}$	$c_{3\varepsilon}$
0.09	1.44	1.92	1.0	1.3	0.7	0.41	1	0

Table 3.1: Coefficients in standard k-ε turbulence model.

[3)] In the Introduction we concluded that HCMS can be described as single-phase fluid; Uittenbogaard's analyses for salinity- or temperature induced stratification effects therefore also apply to HCMS.

We apply Dirichlet boundary conditions to the model:

$$k|_{x_3=Z_b} = \frac{u_*^2}{\sqrt{c_\mu}}, \quad \varepsilon|_{x_3=Z_b} = \frac{u_*^3}{\kappa z_{wc}}, \quad k|_{x_3=Z_s} = 0, \quad \varepsilon|_{x_3=Z_s} = 0 \tag{3.22}$$

in which the effects of waves may be included in the shear velocity u_* and where the roughness length z_{wc} for current and waves is elaborated in Section 3.4; when no waves are present $z_{wc} = z_0$, which is the well-known roughness length for flow only. We appreciate that the boundary condition at $x_3 = Z_s$ does not agree entirely with experimental data, and that a Neuman-condition may be preferable. However, this is the standard condition applied in the DELFT3D-software at present, which is the basis for our 1DV POINT MODEL. It is noted that the eddy viscosity ν_T is determined by the ratio of k^2 and ε, which is zero at the water surface.

We are particularly concerned with the dynamics of fine-grained sediment suspensions. One of the major agents in these dynamics is the vertical mixing; hence the time scale at which the mixing processes respond to variations in driving forces is of importance. Therefore we present an estimate of the time scales for the turbulence parameters.

Karelse and Van Kester (1995) carried out numerical simulations with a three-dimensional model with a k-ε turbulence module of an extensive series of turbulence measurements under tidal conditions in the Delft Tidal Flume. A similar study was carried out by Baumert and Radach (1992) on data reported in the literature, including field data from the River Elbe. Both studies showed that the measured hysteresis effects in flow and turbulence properties during accelerating and decelerating tides are properly described by the k-ε turbulence model.

Therefore, we can establish the relevant time scale conveniently from the balance equation (3.21a) for the turbulent kinetic energy. The turbulence time scale T_T (for homogeneous conditions) is obtained by setting diffusion, production and buoyancy in (3.21a) to zero:

$$T_T \propto \frac{k}{\varepsilon} = c_\mu \frac{\nu_T}{k} \approx c_\mu \frac{0.1 h u_*}{1.7 u_*^2} \approx 0.06 \frac{h}{u_*} \tag{3.23}$$

where the coefficient 1.7 stems from the mean value of $k(Z_b)$ and $k(Z_s)$ in (3.22). From (3.23) it follows that T_T amounts to a few minutes at most for open-channel flow. This conclusion is consistent with Baumert and Radach (1992) who showed that in shallow water the Strouhal number St ($St \equiv u_* T/h$, where T = tidal period) is large, and consequently phase shifts between turbulent parameters and flow velocity are small. Hence, we may assume that with respect to the other relevant time scales (e.g. Chapter 8), the turbulence field responds instantaneously to variations in the driving forces.

3.4 The effect of surface waves

We do not study the effect of surface waves on the flow field, except through their influence on the bed shear stress. We are mainly concerned with the influence of the waves on the vertical mixing (of sediment). The wave effect is modelled with the approach of Grant and Madsen (1979) in the form of an additional bed boundary condition to the flow model, applying linear wave theory to relate wave length and period, and orbital excursion and water velocity. This approach gives good results for larger wave-activity, but for smaller waves, the wave-effect is overestimated by about 20 % (e.g. Soulsby et al., 1993). We prefer this method though above other, more accurate methods (e.g. Soulsby et al., 1993) because of its simplicity and physical transparency.

The rms-value of the wave-induced bed shear stress vector is defined by:

$$\tau_w = \left\langle \tilde{\tau}_w^2 \right\rangle^{1/2} = \rho u_{*w}^2 \;\; ; \;\; u_{*w}^2 = \tfrac{1}{2} f_w \hat{u}_{orb}^2 \tag{3.24}$$

in which the amplitude $\hat{u}_{orb}$ of the near-bed horizontal orbital velocity vector is determined from the rms wave height H_{rms}. The friction coefficient f_w follows from Swart's formula (e.g. Soulsby et al., 1993):

$$\begin{aligned} &\text{for } \frac{A}{k_s} > \frac{\pi}{2}: \; f_w = 0.00251 \cdot \exp\left\{ 5.21 \left(\frac{A}{k_s} \right)^{-0.19} \right\}, \text{ and} \\ &\text{for } \frac{A}{k_s} \le \frac{\pi}{2}: \; f_w = 0.3 \end{aligned} \tag{3.25}$$

where k_s is the Nikuradse roughness height related to the roughness length z_0 through $k_s \approx 30\, z_0$ and $A \equiv \hat{u}_{orb}/\omega$, with ω = wave frequency. The wave-affected boundary layer thickness δ_w is given by (Grant and Madsen, 1979):

$$\delta_w = \frac{2\kappa}{\omega} \left| u_{*fw} \right| = \frac{2\kappa}{\omega} \sqrt{u_{*f}^2 + u_{*w}^2} \tag{3.26}$$

where the subscript $._w$ reflects wave-related parameters, $._f$ flow-related parameters and $._{fw}$ the effects of current-wave interaction. It is noted that in our study we assume that flow and waves have the same direction; if this is not the case, the reader is referred to Grant and Madsen to accommodate for the non-linear effects that govern the interaction between waves and currents. Within the turbulent wave-boundary layer the (mean) eddy viscosity ν_T reads:

$$z_0 \le (x_3 - Z_b) \le \delta_w : \;\; \nu_T = \kappa \left| u_{*fw} \right| (x_3 - Z_b) = \kappa \sqrt{u_{*f}^2 + u_{*w}^2} \, (x_3 - Z_b) \tag{3.27}$$

Note that the near-bed shear stress $\tau_b = \rho_w u_{*f}^2$ is constant throughout the wave-boundary, but as yet unknown, and yields a logarithmic velocity profile based on $|u_{*fw}|$. Above the wave-boundary layer, wave-induced turbulence is not notable and Grant and Madsen assume:

$$(x_3 - Z_b) > \delta_w : \;\; \nu_T = \kappa \left| u_{*f} \right| (x_3 - Z_b) \tag{3.28}$$

which yields the usual logarithmic velocity profile with $|u_{*f}|$ as a parameter. The two velocity profiles are matched at $(x_3 - Z_b) = \delta_w$. The wave-induced turbulence contributes to the mean flow above the wave-boundary through an increase in effective roughness z_{wc}:

$$\delta_w \geq z_0 : \quad \frac{z_{wc}}{z_0} = \left(\frac{\delta_w}{z_0}\right)^{\beta} ; \quad \beta = 1 - \left(1 + \left(\frac{u_{*w}}{u_{*f}}\right)^2\right)^{-1/2} \tag{3.29}$$

The effective bed shear stress τ_b and shear velocity u_*, as applied in the preceding sections, follow from applying the logarithmic law of the wall using z_{wc} instead of z_0. No other effects of wave-current interactions are accounted for.

4. A model for flocculation and settling velocity

4.1 Introduction

The evolution of the effective settling velocity of cohesive sediment is the result of aggregation and floc breakup processes, as a consequence of which the settling velocity of mud flocs can be a few orders of magnitude larger than that of the primary particles. Aggregation is caused by mutual collisions of and the subsequent adherence between the particles, and breakup is caused by turbulent stresses and mutual collisions. The effects of the latter are assumed to be small for cohesive sediment (e.g. Section 4.5.3). The flocculation process is governed by three agents:

1. Brownian motions cause the particles to collide to form aggregates,
2. Particles with a large settling velocity will overtake particles with a small settling velocity: collisions between these particles may result in aggregation (generally referred to as differential settling), and
3. Turbulent motions will cause particles, carried by the eddies, to collide and form flocs; turbulent shear on the other hand may disrupt the flocs again, causing floc breakup (generally referred to as shear effects).

In this study we will use the term "flocculation" explicitly to describe the combined processes of aggregation and floc breakup, and the term "flocs" for aggregates of fine-grained cohesive sediment.

Many studies have been reported on the effects of flocculation on the particle size distribution of suspended matter. Mathematical-physical formulations for the collision frequency by the three agents in the first paragraph are well known and are reported in many papers and reviews, e.g. McCave (1984) and Van Leussen (1994). From the studies by O'Melia (1980), McCave (1984) and Van Leussen (1994) it can be concluded that aggregation due to Brownian motion is negligible in estuaries and coastal regions.

Casamitjana and Schladow (1991 and 1993) solved the vertical mass balance equations for a discrete particle size distribution of suspended matter. The exchange between the various fractions is governed by the three flocculation agents mentioned above. They analysed the distribution of suspended particles in lakes using a sensitivity analysis; however, no comparison with observations was presented. Krishnappan (1990 and 1991) included the effects of Brownian motion and differential settling in a depth-averaged sediment transport model by solving the mass balance equations for various fractions; however, again no comparison with observations was presented. Later, Wiesner (1992) studied the initial flocculation effects by solving numerically three flocculation equations, accounting for the three agents mentioned above, for a discrete particle size distribution. He focused on the role of the aggregate structure (fractal dimensions) on the aggregation rate.

Not all collisions will result in aggregation. This effect can be captured with an aggregation efficiency e_c. Though little is known about this efficiency, it is probably low; O'Melia (1985), for instance, reported values of e_c of 10^{-3} to 10^{-1}. Such a low efficiency value agrees with the observations in Chapter 4.2 that the aggregation process

of fine-grained cohesive sediment falls within the class of Reaction Limited Cluster-Cluster Aggregation.

Stolzenbach and Elimelich (1994) studied the effect of differential settling in detail by analysing theoretical results presented in the literature (Wacholder and Sather, 1974) and by carrying out experiments in a settling column. They showed that the chance that a large, but less dense, rapidly falling particle will actually collide with a small, but denser, slowly falling particle is very small, because the trajectory of the smaller particle is deflected around that of the larger one. They concluded that the effect of differential settling on aggregation in marine environments is much smaller than predicted by the classical collision functions, and might even be entirely absent in many situations.

From these results we conclude that the effects of Brownian motion and differential settling are probably small in estuarine and coastal environments. Therefore, we focus on the effect of turbulence. A qualitative picture of this effect, shown in Fig. 4.1, was published by Dyer (1989), who conjectured that with increasing shear stress the floc diameter first increases and then decreases, and that the floc diameter also increases with sediment concentration. He attributed this to a dominance of aggregation effects at small shear stress and a dominance of floc breakup processes at larger shear stresses.

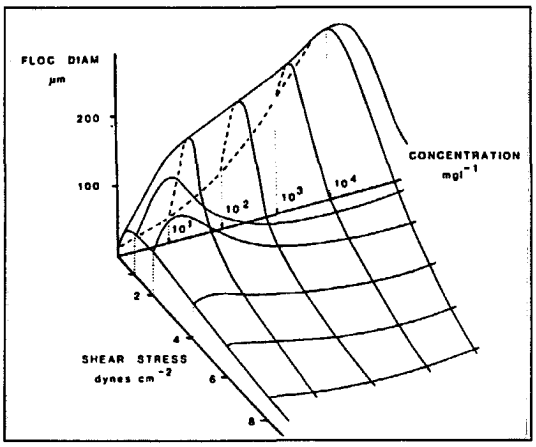

Fig. 4.1: Conceptual flocculation diagram of Dyer (1989).

A heuristic formula describing this effect was advocated by Van Leussen (1994), based on the work by Argaman and Kaufman (1970) described in the next paragraph:

$$w_s = w_{s,r}\frac{1+aG}{1+bG^2} \tag{4.1}$$

where w_s and $w_{s,r}$ are the actual and reference settling velocities, respectively[1)], a and b are empirical coefficients, and G is a dissipation parameter (often incorrectly referred to as the "velocity gradient"), defined as:

[1)] We will use capital letters for a constant settling velocity W_s, and small letters for w_s when the settling velocity varies because of flocculation and/or hindered settling effects.

$$G = \sqrt{\frac{\varepsilon}{\nu}} = \frac{\nu}{\lambda_0^2} \tag{4.2}$$

in which ε is the turbulent dissipation rate per unit mass, ν is the kinematic viscosity of the suspension, and λ_0 is the Kolmogorov micro-scale of turbulence: $\lambda_0 = (\nu/\varepsilon)^{1/4}$. Typical values of λ_0 in estuaries range from 100 to 1000 μm, depending on the water depth and flow velocity. For isotropic turbulence, the dissipation rate per unit mass ε is given by (e.g. Tennekes and Lumley, 1994; see also equ. (3.18)):

$$\varepsilon = 2\nu\overline{s_{ij}s_{ij}} \approx 15\nu\overline{\left(\partial u_1'/\partial x_1\right)^2} \tag{4.3}$$

in which s_{ij} is the turbulent rate of strain, u_1' is the turbulent velocity fluctuation in x_1-direction, and the coefficient 15 stems from all the components that contribute to the rate of strain. It follows that G is a measure of the turbulent shear of the flow.

It is illustrative to visualise the variation of $G(U,h,z)$ over the water depth h for various values of h and depth-averaged flow velocity U. For this purpose we apply the relation for ε given by Nezu and Nakagawa (1993):

$$\varepsilon \approx \frac{u_*^3}{\kappa h}\frac{1-\zeta}{\zeta} \tag{4.4}$$

in which u_* is the shear velocity, κ the Von Kármàn constant and $\zeta = z/h$ ($z = x_3 - Z_b$) the relative elevation above the bed. Substitution of (4.4) into (4.2) yields the mentioned variation in $G(U,h,z)$ for clear water ($\nu = 10^{-6}$ m^2/s), the results of which are plotted in Fig. 4.2, showing that G varies between 0.1 and 10 s^{-1} in general. Only for U of about 1 m/s and larger, G attains values beyond 10 s^{-1} near the bed.

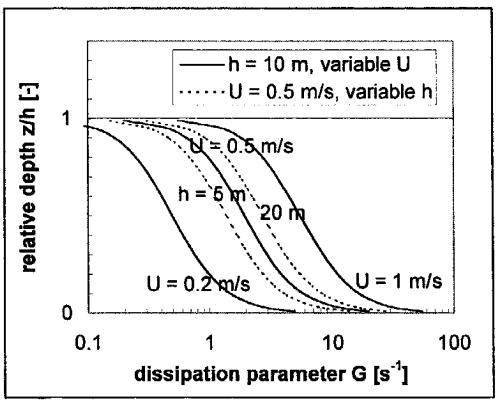

Fig. 4.2: Typical values for the dissipation parameter G in open channel flow (equ. (4.4)).

Formula (4.1) was applied by Malcherek (1995) in a numerical study with a three-dimensional model of the suspended sediment concentrations in the Weser estuary. That author reported that he was only able to simulate the observations properly when using this formulation.

The effects of turbulence on flocculation are widely addressed in the field of sanitary engineering. The two classical studies generally referred to are those by Argaman and

Kaufman (1970) and by Parker et al. (1972). These authors studied the simultaneous effects of aggregation and floc breakup; in the latter paper the processes of floc breakup were evaluated in greater detail. The various parameters in their models however are fairly unmeasurable and they ended up with a formulation similar to (4.1), describing the variation of the number of particles in a turbulent environment as a function of G and their residence time. Ayesa et al. (1991) developed an algorithm to calibrate the parameters of the model by Argaman and Kaufman against measured variations of the number of particles from experiments carried out in a mixing tank, obtaining an equilibrium concentration for large residence times. Lee et al. (1994) evaluated a slightly different model, and applied it to flocculation processes in a mixing tank for waste water treatment.

Boadway (1978) derived a model for the time evolution of floc size, including the effects of aggregation and floc breakup for massive, spherical (Euclidian) particles. Aggregation and breakup were assumed to be driven by velocity gradient. A simplified form of the Smoluchowski collision formula (see section 4.5.2) and a heuristic floc breakup description were used. The various parameters in the model were calibrated against experiments with alum flocs in a roto-viscometer-like instrument with a gap width of 6.75 mm. The velocity difference over the gap determines the mentioned velocity gradient. For equilibrium conditions, the floc diameter appeared to scale with the suspended sediment concentration.

Akers et al. (1987) tried to validate Parker's model for the maximal floc size D_{max} through experiments with a dilute suspension in a mixing tank. In agreement with theory, they found that $D_{\max} \propto \lambda_0$. On the basis of physical reasoning and experiments in a mixing tank with a paddle flocculator (impeller), Tambo and Hozimu (1979) found a similar result, i.e. $D_{\max} \propto \lambda_0^n$ with $\frac{1}{2} < n < \frac{3}{4}$.

In summary it can be concluded that many studies have been carried out on the effects of turbulence on the flocculation process. Some of these studies are rather descriptive, others highly fundamental, and some very empirical. They all describe the variation in the number of particles or estimate the maximal floc size that can be achieved. Only the model of Boadway (1978) explicitly describes the important variation in floc size and settling velocity with time.

In this chapter we derive an equation for the evolution of the floc size of cohesive sediment as a function of turbulence-induced aggregation and breakup processes. Our goal is threefold:

1. Derive a formulation for the relation between settling velocity and floc size,
2. Derive a formulation for the evolution of the floc size, hence through 1. a relation for the settling velocity as a function of space and time, and
3. Derive a formulation for the gelling point of the sediment.

We treat the mud flocs as fractal entities, which is a well-accepted approximation at present, e.g. Tambo and Watanabe (1979), Krone (1984), Huang (1994), Logan and Kilps (1995), Chen and Eisma (1995), and Kranenburg (1994). This approximation allows us to establish relations between size and settling velocity of the flocs.

4.2 Fractal structure of flocs of cohesive sediment

From the analysis in Chapter 1 we conclude that a relationship between the volumetric and mass concentrations ϕ and c of the flocs of cohesive sediment is required for a complete description of the dynamics of High-Concentrated Mud Suspensions. Such a relation is conveniently provided by fractal geometry, thus treating the sediment flocs as self-similar fractal entities. It is noted that the conceptual order-of-aggregate description of mud flocs by Krone (1984) is similar to this fractal picture. We distinguish between individual flocs in the water column, where each floc contains a large, but limited number of primary particles, and space-filling network structures in the fluid mud layer where all particles are more or less connected with each other.

Fractal theory implies that various physical processes obey power-law behaviour at all scales. However, in reality, structures are bounded within certain spatial ranges, and often are not self-similar at all scales. Yet, from many physical experiments it can be concluded that several processes governing fine-grained cohesive sediment obey such a power-law behaviour, amongst which viscosity, yield strength and permeability, see Kranenburg (1994), for instance. As a consequence, fractal theory is convenient for describing the dynamics of High-Concentrated Mud Suspensions.

The fractal dimension n_f is obtained from the description of a growing object with linear size La and volume $V(La)$, where a is the linear size of the seed (e.g. Viscek, 1992). Assuming that the linear size of the primary objects has unit dimension, $V(La) \propto N(La)$, where N is the number of primary objects (seeds), the fractal dimension n_f is defined as:

$$n_f = \lim_{L \uparrow \infty} \frac{\ln(N(L))}{\ln(L)} \tag{4.5}$$

From this approach it follows that the differential (or excess) density $\Delta\rho_f$ of mud flocs is given by (Kranenburg, 1994):

$$\Delta\rho_f = \rho_f - \rho_w = (\rho_s - \rho_w)\left[\frac{D_p}{D}\right]^{3-n_f} \tag{4.6}$$

where ρ_f, ρ_w and ρ_s are the densities of the mud flocs, the (interstitial) water and the sediment (primary particles), and D and D_p are the diameters of the flocs and of the primary particles. From (4.6) it follows that the relation between c and ϕ reads:

$$\phi = \left(\frac{\rho_s - \rho_w}{\rho_f - \rho_w}\right)\frac{c}{\rho_s} = \frac{c}{\rho_s}\left[\frac{D}{D_p}\right]^{3-n_f} \tag{4.7}$$

At the gelling point, the volumetric concentration of the flocs ϕ becomes unity by definition. Hence, the gelling concentration c_{gel} can be obtained from (4.7):

$$c_{gel} = \rho_s\left[\frac{D_p}{D}\right]^{3-n_f} \tag{4.8}$$

Note that, due to consolidation effects, the ratio c/c_{gel} can exceed unity within a fluid mud layer.

Measurements of the fractal dimension of flocs of cohesive sediment in the water column reveal values from about $n_f \approx 1.4$ for very fragile flocs, like marine snow to $n_f \approx 2.2$ for strong estuarine flocs. Typical values within estuaries and coastal waters range from $n_f \approx 1.7$ to 2.2, with an average value of $n_f \approx 2.0$. Within the bed much larger fractal dimensions are found, i.e. $2.6 < n_f < 2.8$ (e.g. Sections 5.2 and 5.3, and Kranenburg, 1994). We will not elaborate on the underlying processes of this transition, as this study is not dedicated to the kinetics of fractal growth of cohesive sediment flocs. However, we need a working hypothesis to accommodate for this transition in our physical description of the sediment dynamics. In this respect, we will follow Vicsek (1992) in the following paragraphs.

The aggregation process of particles moving in a fluid falls in either of two classes. In the class of Diffusion Limited Aggregation (DLA), the aggregation process starts from a single particle, the seed, while other, identical particles are released one by one to collide with the aggregate by diffusion processes to coagulate. It is clear that in sediment-water mixtures, particles are not released one by one, but that many particles are moving through the fluid simultaneously, approaching each other by diffusion processes. In this case the aggregation process falls within the so-called class of Cluster-Cluster Aggregation (CCA).

This CCA-class is commonly subdivided in two sub-classes (e.g. Weitz et al., 1985). When the sticking probability of two particles approaching each other is approximately unity, the diffusion process is the limiting agent in the particle growth. In this case the aggregation process falls within the sub-class of Diffusion Limited Cluster-Cluster Aggregation (DLCCA). Both from theoretical studies and from numerical and physical experiments the fractal dimension for DLCCA is established at about $1.7 < n_f < 1.8$ (e.g. Meakin, 1986).

If the sticking probability is much smaller than unity, for instance when the particles have to overcome a repulsive barrier, sticking becomes the limiting factor, and the aggregation process falls within the sub-class of Reaction Limited Cluster-Cluster Aggregation (RLCCA). From theoretical studies and numerical and physical experiments the fractal dimension for RLCCA is established at about $1.9 < n_f < 2.1$ (e.g. Brown and Ball, 1985).

When clay particles prevail in the suspension, RLCCA is likely, as the electrical charges on the clay particles generate short range repulsive forces. Indeed, the fractal dimensions of suspended cohesive sediment flocs with a major mineral component are of the order of $n_f \approx 2$, and the aggregation efficiency appears small in general (e.g. Section 4.1).

The presence of certain types of organic matter increases the sticking probability of approaching particles considerably through sticking filaments, polysaccharides etc. (e.g. Van Leussen, 1994). In that case DLCCA is more likely to occur, resulting in a decrease in fractal dimension (e.g. Weitz et al., 1985). It is postulated that it is the augmented sticking probability of organic compounds in a DLCCA process, that causes low excess density (see also Section 4.6.2), porous flocs of small strength in sediment suspensions rich of organic matter. Indeed Chen and Eisma (1995) found fractal dimensions of $1.7 < n_f < 1.8$ for mud aggregates with a fairly high organic content. However, we do not elaborate on this matter any further, as often, especially

in The Netherlansds, the organic content in marine and estuarine HCMS is small (e.g. Cornelisse et al., 1990, Kuijper et al., 1990 and Kuijper et al., 1991).

All theories and experiments, leading to the n_f-values given above, were derived for low-concentrated suspensions, i.e. $\phi << 1$. For HCMS near the bed this is no longer the case, particularly in the hindered settling regime around slack water. Kolb and Herrmann (1987) argue that a very abrupt transition from low-concentrated CCA to high-concentrated CCA (HCCCA) occurs when the average mutual distance between the clusters becomes of the order of the cluster dimensions themselves. When ϕ approaches unity, very compact clusters are formed with large fractal dimensions up to $n_f \approx 3$. This implies that on a micro-scale loose aggregates with $n_f \approx 2$ become densely packed at $n_f \approx 3$. On a macro-scale the overall fractal dimension attains a value somewhere in between, say $n_f \approx 2.6$ - 2.8. Similar conclusions are drawn by Haw et al. (1997) from a theoretical study on cluster-cluster aggregation near the gelling point.

4.3 A relation between settling velocity and floc size

The settling velocity of mud flocs is a function of their size D and differential density $\Delta\rho_f$, i.e. the excess density relative to water. For estuarine sediment this is discussed by Dyer (1989), Gibbs (1985), Hawley (1982) and Van Leussen (1994), amongst others. Due to aggregation effects, flocs form with relatively small $\Delta\rho_f$, typical values for $\Delta\rho_f$ are in the order of 50 to 300 kg/m^3.

The relation between the volumetric and mass concentrations, ϕ and c of the particle aggregates, and between ϕ and the number of particles per unit volume N for aggregates is given by:

$$\phi = \frac{\rho_s - \rho_w}{\rho_f - \rho_w}\frac{c}{\rho_s} = f_s N D^3 \tag{4.9}$$

where f_s is a shape factor; for instance for spherical particles $f_s = \pi/6$.

The settling velocity $w_{s,r}$ of individual mud flocs can be obtained from a balance between the gravitational and drag forces F_g and F_d for a single floc in a homogeneous fluid (e.g. Batchelor, 1983):

$$F_g = \alpha\frac{\pi}{6}D^3 g\Delta\rho_f \quad \text{and} \quad F_d = \beta c_D \frac{1}{2}\rho_w \frac{\pi}{4}D^2 w_{s,r}^2 \tag{4.10}$$

in which α and β are coefficients depending on the shape (sphericity) of the particles. According to Vanoni (1977), Raudkivi (1976) and Graf (1977) the formulation for the drag coefficient c_D that adequately matches most empirical data on non-cohesive sediment reads:

$$c_D = \frac{24}{Re}\left(1 + 0.15 Re_p^{0.687}\right) \tag{4.11}$$

in which $Re_p = w_{s,r} D/\nu$ is the particle Reynolds number. We assume that this relation is also valid for flocs of cohesive sediment, as no data on the drag coefficient for falling flocs are avilable.

Implicitly we assume that the fluid flows around, and not through the particles. This is, however, not a trivial assumption. Johnson et al. (1996) for instance studied the flow through flocs. They treated the flocs as self-similar fractal entities and reasoned that the size of the largest pores within the floc scale with the overall floc size. The absolute permeability of the flocs, hence the flow through the falling flocs, would therefore increase with increasing floc size. The effect of pore size was studied through a series of settling experiments with latex micro-spheres and numerical simulations. From these experiments, the settling velocity and floc density, the latter obtained through counting the number of primary particles within each floc, were established as a function of the floc diameter. It appeared that the measured settling velocities are consistently larger by an order of magnitude than the settling velocity computed with Stokes' law of impermeable flocs of the same size and mass. Next the settling velocity of flocs of similar size and mass were computed, allowing flow through these flocs; their permeability was assumed to be homogeneously distributed within each floc. The settling velocity of the permeable flocs appeared slightly larger than that of the impermeable flocs. From these studies Johnson et al. concluded that the settling velocity of porous flocs is affected by the flow through the pores of the flocs, and that the pore size distribution is an important parameter. It is not clear, however, why the settling velocity would increase if fluid can flow through the pores. One would expect the opposite, as the effective friction-affected floc surface would increase with permeability.

Gregory (1997) pointed out that fractal aggregates are hardly permeable at fractal dimensions beyond $n_f = 2$. However, the permeability rapidly increases with decreasing n_f, affecting largely the collision behaviour and frequency between the particles. This might have implications for the flocculation efficiency in the case of Diffusion Limited Cluster-Cluster Aggregation, which is hypothesised to be the governing aggregation process when the active organic content of the mud is high (see Section 4.2).

An interesting experiment was performed at the University of Florida, but unfortunately the results have not been published (Mehta, 1998). Settling experiments were carried out with clay flocs in a settling column under normal conditions, the results of which were compared with the settling velocity of frozen flocs of the same size and mass, and under the same conditions. No significant differences in settling velocity were found, from which the researchers concluded that, during settling, no fluid flows through the flocs.

Also from the experiments by Stolzenbach and Elimelich (1994), who studied the effects of differential settling, one can conclude indirectly that flow through flocs will be small. If not, larger and smaller particles would collide more often, and differential settling would not be negligible (e.g. Gregory, 1997).

From these arguments we conclude that we may treat flocs as porous, though impermeable entities as a fair approximation for the conditions studied, i.e. High-Concentrated Mud Suspensions in open-channel flow.

For mud flocs with a fractal structure, relations (4.6) and (4.11) can be substituted into formula (4.10), to yield an implicit formula for the settling velocity of single mud flocs in still water:

$$w_{s,r} = \frac{\alpha}{18\beta}\frac{(\rho_s - \rho_w)g}{\mu} D_p^{3-n_f} \frac{D^{n_f-1}}{1+0.15Re_p^{0.687}} \tag{4.12}$$

For spherical $(\alpha = \beta = 1)$, massive $(n_f = 3)$ particles in the Stokes' regime $(Re_p << 1)$, the well-known Stokes' formula for a stationary settling particle is obtained:

$$w_{s,r} = \frac{(\rho_s - \rho_w) g D^2}{18 \mu} \tag{4.13}$$

We recognise that the water temperature has a significant effect on the viscosity, hence on the settling velocity of the mud flocs. However, we will not elaborate on this, as this effect is well established in the literature.

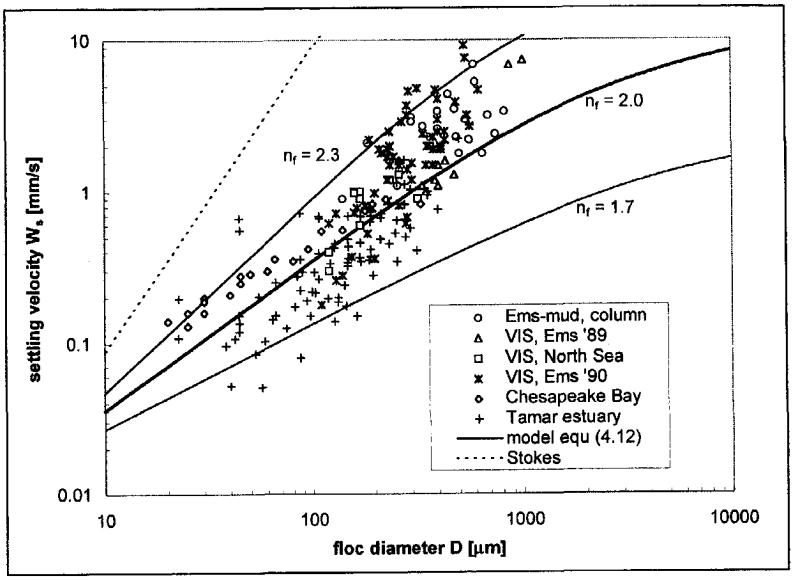

Fig. 4.3: Relation between settling velocity and floc size.

In Fig. 4.3 formula (4.12) with $\alpha = \beta = 1$, $D_p = 4$ µm (which is a typical value found by Van Leussen (1994) for Ems mud), $\rho_s = 2650$ kg/m^3, $\rho_w = 1020$ kg/m^3 and $\mu = 10^{-3}$ Pas, is plotted for three values of n_f, i.e. $n_f = 1.7$, 2 and 2.3, together with observations of settling velocity and floc size in the Delft Hydraulics settling column, in the Ems estuary and the North Sea (Van Leussen, 1994; VIS in Fig. 4.3 means optical size and settling velocity measurements with a Video In Situ camera system), in Chesapeake Bay (Gibbs, 1985), and in the Tamar estuary (Fennessy et al., 1994). It is observed that formula (4.12) matches the data adequately. This is also the case for data presented by Hawley (1982), who summarises the work of Japanese researchers in the ocean (not shown here). The overall trend of the data points seems slightly steeper than the fit with $n_f = 2$. However, when the individual data sets are studied, the slopes agree better with $n_f = 2$.

Figure 4.3 also shows that using formula (4.11) for the drag coefficient c_D does imply a relationship of the form $W_{s,r} \propto D^{n_f - 1}$ for diameters up to several mm. For particles

with a diameter up to a few 100 μm the data can be properly represented with the fit $W_{s,r} \propto D$, i.e. with an average fractal dimension $n_f = 2$.

At floc diameters beyond D = 1 mm equ. (4.12) predicts a rapid deviation from a simple power law behaviour because of the increasing role of the particle Reynolds number. We anticipate that the validity of (4.12) becomes limited at floc sizes beyond a few mm.

4.4 Hindered settling

We have inferred in Chapter 1 that hindered settling, which is the influence of neighbouring particles on the settling velocity of an individual particle within a suspension, is an important process governing the behaviour of HCMS. An extensive and detailed review was presented by Scott (1984), part of which was published in a paper by Mandersloot et al. (1986), summarising many theoretical and empirical studies on hindered settling in chronological order. That review is focused on the behaviour of massive, Euclidean particles (sand), however. As the flocs of cohesive sediment are not Euclidean, we cannot follow Scott in detail in our analysis of the hindered settling behaviour of mud flocs, as will be explained in this section. However, we use his analysis as a guide to ours.

From the literature and from physical reasoning, we can identify the following seven processes that affect the settling velocity of individual particles in a suspension:

1. **Return flow and wake formation**. A falling particle generates a return flow and a wake. When other particles in the vicinity of this falling particle are located within this return flow, their effective settling velocity (with respect to a fixed reference frame) will be affected, and the overall effective settling velocity of the suspension will decrease by a factor (1 - ϕ). We note that for Euclidean particles $\phi = \phi_p$, where ϕ_p is the volumetric concentration of the primary particles ($\phi_p = c/\rho_s$), whereas for cohesive sediment the volume fraction of the flocs is relevant. If, however, a second particle is caught in the wake of the falling particle, its settling velocity is increased, as is pointed out by Reed and Anderson (1980). The latter effect is often ignored but can be important (see point 7.).
2. **Dynamic or flow effect**. Several authors (e.g. Smith, 1998 and Darcovich et al., 1996) stress the role of neighbouring particles on the velocity gradients around a falling particle, as a result of which the pressure distribution around this particle, its hydrodynamic drag and added mass are affected. Some of the theoretical and numerical studies on hindered settling are focused on evaluating one or more of these processes (Reed and Anderson, 1980, Smith, 1998 and Darcovich et al., 1996). These effects are often lumped in an effective viscosity coefficient. It is noted that the influences of the return flow and wake formation discussed under 1. are of course also flow effects.
3. **Particle-particle collisions**. Collisions between particles cause additional stresses in the suspension. Since the pioneering work by Bagnold (1954), it is common to incorporate also this effect in an effective viscosity. As a consequence, the settling of individual particles is hindered, so that the effective settling velocity of the suspension decreases. This effect of course becomes more pronounced at higher

concentrations (e.g. Buscall, 1990). It is noted that this effect is expected to be unimportant for mud suspensions, as discussed in Chapter 1.

4. **Particle-particle interactions**. Batchelor (1982) discussed the role of mutual attraction and repulsion of particles by electrical charges or otherwise. Also Batchelor's analysis for small concentrations led to an augmented effective viscosity. In the case of fine-grained cohesive sediment attractive and repulsive forces will result in floc formation, or in a stable dispersion in the absence of a floc promoting solute.
5. **Viscosity**. Einstein was the first to realise that the effective viscosity of a suspension increases with particle concentration. Since then, many studies have been carried out and reported on this effect. A concise summary is given by Scott (1984). Most formulae are of the form $\mu_{eff} = \mu_0(1 - a\phi)^{-b}$, where a (≥ 1) and b (≥ 2.5) are coefficients; b is often assumed to depend on ϕ. Each individual particle within a suspension is then considered to be falling in the remainder of that suspension which has an increased viscosity. This would then decrease the effective settling velocity of all particles. The formulations in the literature for μ_{eff} differ widely, which is probably caused by implicitly accounting for the various effects discussed under 2, 3 and 4 through an (augmented) effective viscosity.
6. **Buoyancy or reduced gravity**. By the same argument, that is that an individual particle settles in the remainder of the suspension with an increased bulk density, the effective settling velocity of the suspension decreases by a factor $(1 - \phi)$.
7. **Cloud formation or settling convection**. Darcovich et al. (1996) and Tacker and Lavelle (1997) stress the role of cloud formation. Particles in the wake of another particle (see 1.) will be dragged by this particle. The wake around this group of particles increases, catching more particles, and a cloud of settling particles is formed. Such a cloud may behave as a settling entity by itself, as a result of which the effective settling velocity of or within the suspension may increase. This effect is probably important during dumping of dredge sludge, for instance, but less important in the more or less homogeneous suspensions encountered in estuarine and coastal environments.

Combining the effects mentioned under 1., 5. and 6. gives a formula for the effective settling velocity w_s of the form:

$$w_s = W_{s,r}(1 - k\phi)^n \tag{4.14}$$

which was the rationale of Scott (1984) to advocate the empirical hindered settling formula by Richardson and Zaki (1954), in which $k \approx 1$ and n is a function of the particle Reynolds number: $2.5 < n < 5.5$. Richardson and Zaki derived this formula from a dimensional analysis yielding the relevant parameters for hindered settling and an extensive series of sedimentation and fluidization experiments with particles of a large variety in shape and Reynolds numbers.

The larger particle Reynolds numbers in these experiments were obtained for fairly large particles with diameters up to about 0.5 to 1 cm. The mutual distance between the particles then becomes so large, that the suspension can no longer be regarded as a continuum, and the picture that each particle settles in a suspension with higher density and viscosity is no longer valid. Only the effects of return flow, uneven flow

distribution and particle-particle collisions are relevant. As a result the exponent attains a small value of about $n \approx 2.5$ for high Re_p.

The basic form of Richardson and Zaki's formula is confirmed by several experimental studies (e.g. Landman and White, 1992 and Davis and Birdsell, 1988) and by theoretical and numerical studies (e.g. Reed and Anderson, 1980 and Darcovich et al., 1996), amongst which studies with two-phase models are prominent (Tacker and Lavelle, 1980, Buscall, 1990, Ingber and Womble, 1994 and Smith, 1998). We note that hindered settling effects are automatically accounted for by means of a proper modelling of the sediment-fluid interactions in a two-phase system, as in the two-phase models by Teisson et al. (1992) and Le Hir (1997), for instance.

Recently, Cheng (1997) proposed an alternative approach for sand. He explicitly included the effects of return flow, augmented viscosity and density. The effective settling velocity of an individual particle in a suspension is obtained by assuming that this particle falls in the remainder of the suspension with larger viscosity and density. Cheng defined the grain parameters d_* and $d_{*,m}$:

$$d_* = \left(\frac{(\rho_s - \rho_w) g}{\rho \nu^2} \right)^{1/3} D, \quad \text{and} \quad d_{*,m} = \left(\frac{(\rho_s - \rho_m) g}{\rho_m \nu_m^2} \right)^{1/3} D \tag{4.15}$$

where ρ_w is the clear water density, ν is the clear water kinematic viscosity and subscript $_{,m}$ represents mixture characteristics. Cheng described the increase in viscosity by the sediment particles by:

$$\frac{\nu_m}{\nu} = \frac{2}{2 - 3\phi}, \quad \text{assuming } \phi_{\max} = \frac{2}{3} \tag{4.16}$$

Substitution into Stokes' expression led him to the following hindered settling formula:

$$w_s = W_{s,r} \frac{2 - 2\phi}{2 - 3\phi} \left(\frac{\sqrt{25 + 1.2 d_{*,m}^2} - 5}{\sqrt{25 + 1.2 d_*^2} - 5} \right)^{1.5} \tag{4.17}$$

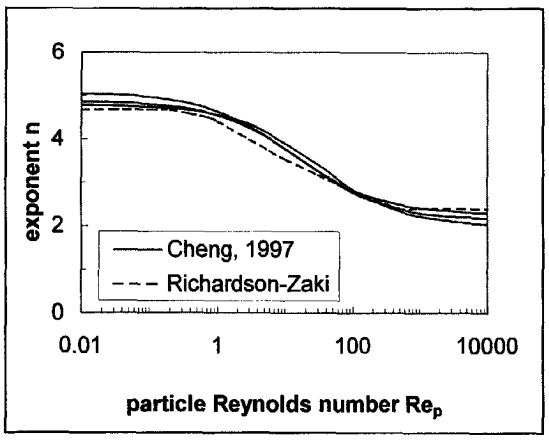

Fig. 4.4: Variation of n in (4.14) with Re_p according to Richardson and Zaki (1954) (ϕ_p = 0.05, 0.1 and 0.4) and Cheng (1997).

This formula can also be written in the "classical" Richardson and Zaki form. The resulting variation of the exponent n in (4.14) with particle Reynolds number Re_p for various concentrations (ϕ_p = 0.05, 0.1 and 0.4) is presented in Fig. 4.4, showing a good agreement between these approaches.

It is common to apply equ. (4.14) for cohesive sediment as well, using the overall volumetric concentration of the flocs for ϕ. This is probably not correct because:

- The viscosity of mud suspensions at concentrations below the gelling point does not scale with $(1 - a\phi)^{-b}$. Such a scaling law would lead to unrealistic large viscosity coefficients. From a large series of roto-viscometer measurements with natural mud from various sites in The Netherlands at c = 50 and 100 g/l (WL|delft hydraulics, 1992), it can be concluded that at the high shear rates occurring in turbulent flow, the viscosity of these muds does not increase by more than a factor of 2 to 3 with respect to the clear water viscosity. As we are not aware of any formulation for the viscosity of a suspension of cohesive sediment flocs in this range of concentrations, we therefore propose to apply the classical formula of Einstein:

$$\nu_m = \nu(1+2.5\phi) \tag{4.18}$$

- The buoyancy effect does not scale with $(1 - \phi)$, but with $(1 - \phi_p)$, where ϕ_p is the volumetric concentration of the primary particles ($\phi_p \equiv c/\rho_s$), i.e. with the bulk density of the sediment.

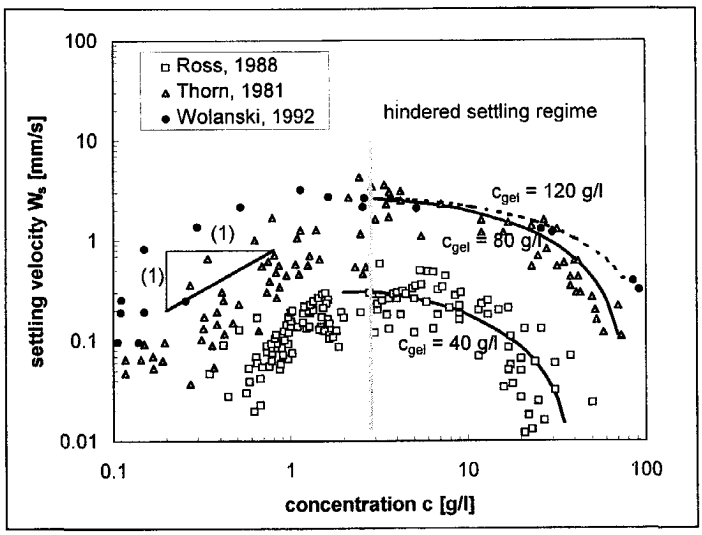

Fig. 4.5: Comparison of (4.19) with experimental data.

Following Cheng's procedure by substituting the effects of return flow, in equ. (4.12), we obtain the following hindered settling formula for cohesive sediment flocs:

$$w_s = w_{s,r}\frac{(1-\phi_*)^m(1-\phi_p)}{1+2.5\phi} \tag{4.19}$$

in which the factor (1 - ϕ_*) accounts for the return-flow effect, and the exponent m is an empirical parameter to account for possible non-linear effects (as mentioned under the items 2., 3. and 4. at the beginning of this section). The volumetric concentration is related to the sum of all fractions, i.e. $\phi = \sum c/c_{gel}$, and $\phi_* = \min\{1, \phi\}$, to account for the fact that c/c_{gel} can exceed unity in a consolidating fluid mud layer. In this study we will limit ourselves to the case where $m = 1$. Moreover, we have neglected the influence of the augmented viscosity and suspension density on the particle Reynolds number in (4.12), which is considered to be a secondary effect.

On the right-hand side of Fig. 4.5 ($c > 2$ to 3 g/l) the hindered settling formula (4.19) is compared with data of Thorn (1981), Ross (1988) and Wolanski et al. (1992). It is shown that the data can be described properly with (4.19), using reasonable values for the fitting parameter c_{gel}. This fit is certainly not less applicable than Mehta's using (4.14).

The left-hand side of Fig. 4.5 shows an increase in settling velocity with increasing sediment concentration. This is further discussed in Section 4.6.1.

4.5 Flocculation generated by turbulent shear

4.5.1 Balance equation for the number concentration

We restrict ourselves to the effect of turbulent shear on the flocculation process of cohesive sediment. All secondary effects, such as the influence of the particles on the turbulence structure itself, will be omitted. Only the influence of the suspension on the buoyancy effects in the fluid is accounted for. It is assumed that the particles are advected with the large scale turbulent movements of the fluid, which is correct even for fairly large sand particles with a diameter up to $D = 200$ μm, as discussed in Chapter 1.

Let us consider a control volume V at a fixed location in a Eulerian co-ordinate system which is enclosed by a closed surface A. At time t this volume contains fluid with N sediment particles per unit volume. The total amount of particles within this volume is given by $\iiint N \mathrm{d}V$. The total amount of particles entering or leaving this control volume reads $\iint N\vec{v}\cdot\vec{n}\mathrm{d}A$, where $\vec{n}$ is the unit vector normal to A, positive outward, and $\vec{v}$ the velocity of the particles.

Next, we introduce a flocculation function F_N describing the rate of change of the number of particles per unit volume as a result of turbulence-induced aggregation and floc breakup processes; F_N will be specified in the following sections. Then the rate of change of the number of particles in the control volume V is given by:

$$\frac{\mathrm{d}}{\mathrm{d}t}\iiint N\mathrm{d}V = -\iint N\vec{v}\cdot\vec{n}\mathrm{d}A + \iiint F_N\mathrm{d}V \tag{4.20}$$

Using Gauss theorem, the first integral on the right hand side of (4.20) can be transformed into a volumetric integral. As V is fixed in space we obtain:

$$\iiint\left(\frac{\partial N}{\partial t}+\nabla\cdot\vec{v}N-F_N\right)\mathrm{d}V=0 \tag{4.21}$$

This relation should be valid for all choices of the control volume V, which is only possible if the integrand is identically zero everywhere in the fluid (Batchelor, 1967). The convective velocity v consists of a fluid-induced part and the settling velocity of the particles induced by gravity, including the effects of hindered settling. It is convenient for our further analyses to rewrite the result in Einstein notation:

$$\frac{\partial N}{\partial t}+\frac{\partial}{\partial x_i}\left((u_i-\delta_{i3}w_s)N\right)=F_N \tag{4.22}$$

in which δ_{i3} is the Kronecker delta. This equation only differs from the dynamic equation for the number concentration of dust particles given by Friedlander (1977) in the settling and flocculation terms.

From (4.7) and (4.9) we find a relation between N and D:

$$N=\frac{1}{f_s}\frac{c}{\rho_s}D_p^{n_f-3}D^{-n_f} \tag{4.23}$$

where c is the suspended sediment concentration by mass. Substitution of (4.23) into (4.22) yields:

$$\frac{\partial}{\partial t}\left(cD^{-n_f}\right)+\frac{\partial}{\partial x_i}\left((u_i-\delta_{i3}w_s)cD^{-n_f}\right)=f_s\rho_sD_p^{3-n_f}F_N \tag{4.24}$$

In case we have no flocculation ($F_N = 0$, hence D = constant), (4.24) is identical to the mass balance for suspended sediment (3.13), prior to averaging. If we multiply (4.24) with D^{n_f+1}, and subtract the mass balance equation, we obtain an equation for the evolution of the floc size D:

$$\frac{\partial D}{\partial t}+(u_i-\delta_{i3}w_s)\frac{\partial D}{\partial x_i}=-f_s\frac{\rho_s}{c}D_p^{3-n_f}D^{n_f+1}F_N=-\frac{F_N}{N}D \tag{4.25}$$

in which N/F_N can be considered as a time scale for flocculation (see also equ. (4.22)). Again, considering the case without flocculation ($F_N = 0$), we observe that (4.25) then yields that the material derivative of D is identically zero (e.g. Kranenburg, 1996), i.e. the particle size remains constant along particle trajectories.

Next we apply the classical Reynolds averaging procedure to the turbulent quantities in (4.22). We define $N=\overline{N}+N'$, $c=\overline{c}+c'$, $D=\overline{D}+D'$, $u_i=\overline{u_i}+u_i'$, and $w_s=\overline{w_s}+w_s'$. The last decomposition is necessary, as w_s is a function of D, hence of N. The description of the flocculation function F_N is highly empirical and therefore we omit its turbulent contribution. Substitution and averaging over the turbulent time scale, applying Fick's law, and assuming isotropic turbulence, yields an equation for the number of mud flocs in a turbulent fluid:

$$\frac{\partial N}{\partial t}+\frac{\partial}{\partial x_i}\left((u_i-\delta_{i3}w_s)N\right)-\frac{\partial}{\partial x_i}\left((D_s+\Gamma_T)\frac{\partial N}{\partial x_i}\right)+\frac{\partial}{\partial x_i}\left(\delta_{i3}\overline{w_s'N'}\right)=F_N \tag{4.26}$$

in which Γ_T is the turbulent eddy diffusivity, defined earlier in Section 3.3. We have omitted the overbars for convenience. Note that in our derivation we have obtained the additional turbulent flux term $\overline{w_s' N'}$, which stems from the turbulent fluctuations in the settling velocity. A similar term is present in Chapter 3 in our mass balance, where we have reasoned that this term can be omitted as $w_s' << w'$.

As a result of the turbulent random motions, the particles will collide to form flocs. It was shown by Smoluchowski (1917) that these collisions can be described as a diffusion process. This conclusion is generally accepted, and all aggregation models presented in the literature are based on this concept. It is therefore only briefly summarised in Section 4.5.2.

Turbulence generates large deformations of the fluid; the resulting turbulent stresses can disrupt the flocs (Hinze, 1975). Several studies have been reported on floc breakup processes, e.g. Argamam and Kaufman (1970), Parker et al. (1972), Tambo and Huzumi (1979), Sontag and Russel (1987), and West et al. (1994). Most of the formulations given by these authors are not very practical and/or contain a number of unmeasurable coefficients; neither is there agreement on which of these formulations is most suitable. Therefore, a new, simple breakup function is proposed in section 4.5.3. In our derivation of the flocculation function we will follow small, homogeneous clouds of particles on their trajectory through the fluid.

4.5.2 Aggregation processes

Levich (1962) discussed the coagulation process in turbulent flow of particles smaller than the Kolmogorov scale λ_0. At this scale viscous effects are dominant. In his derivation, Levich assumed that small eddies with size λ $(\lambda \geq \lambda_0)$ bring these particles together. Integrating the Smoluchowski diffusion equation over a finite volume $>> \lambda_0$ yields the rate of coagulation between the particles in a turbulent fluid:

$$\frac{dN}{dt} = -\frac{3}{2}(1-\phi_*)e_c \pi e_d G D^3 N^2 \tag{4.27}$$

where t is time, e_c an efficiency parameter accounting for the fact that not all collisions will result in coagulation, and e_d is an (efficiency) parameter for diffusion. The efficiency parameter e_c is a function of the physico-chemical properties of the sediment and the water, of the organic compounds (coatings, polysaccharides, etc.) in the sediment, and of the form and structure of the flocs (Gregory, 1997). Hence e_c is basically an empirical parameter, see Van Leussen (1994), for example.

We have added the factor $(1-\phi_*)$ to guarantee that the aggregation processes will never result in volumetric concentrations beyond unity. From a conceptual point of view, the addition of this factor is consistent with the observations that at high concentrations the free path length of the particles is reduced, resulting in a decrease in effective diffusion at the scale of the floc forming eddies. This is discussed in Section 4.2.

Equ. (4.27), except for the $(1-\phi_*)$-factor, is used in most studies on flocculation mentioned in the literature. Moreover, Vicsek (1992) shows that (4.27) is valid for the Reaction Limited Cluster-Cluster Aggregation processes, described in Section 4.2, which are believed to govern the aggregation processes of cohesive sediment.

4.5.3 Floc breakup processes

The effects of floc breakup processes by inter-particle collisions are omitted as these effects will be small for flocs with a small excess density. Only the breakup by turbulence-induced stresses is analysed; this breakup process acts continuously, contrary to for instance breakup by collisions. Turbulence exerts fluctuating shear stresses on the flocs. It is therefore likely that the breakup rate of a floc will be a function of the ratio of the turbulence induced stresses τ_T and the strength of the floc τ_y. The flocs are considered as self-similar fractal entities, the smallest units being formed by the primary particles. The number of sub-flocs that can be generated by the breakup processes is therefore dependent on the size of the flocs D in relation to the size of the primary particles D_p. Finally, the breakup rate will be a function of the time scale T_ε of the disrupting turbulent eddies. On the basis of dimensional considerations, the breakup process should read:

$$\frac{1}{N}\frac{\mathrm{d}N}{\mathrm{d}t} \propto \frac{1}{T_\varepsilon} F\left(\frac{D}{D_p}, \frac{\tau_T}{\tau_y}\right) \tag{4.28}$$

For simplicity we assume that the function F can be written as a power function:

$$F = a\left(\frac{D - D_p}{D_p}\right)^p \left(\frac{\tau_T}{\tau_y}\right)^q \tag{4.29}$$

in which the coefficient a and the exponents p and q are to be determined later from experimental data.

We are considering flocs with the dimensions of the Kolmogorov scale or smaller. The disruptive stresses that have to be considered, are therefore in the viscous regime. As $Re_{\lambda_0} \approx 1$, eddies of scale $\lambda \approx \lambda_0$ have a velocity of about (e.g. Levich, 1962):

$$u_{\lambda_0} \approx \frac{\nu}{\lambda_0} \tag{4.30}$$

where ν is the kinematic viscosity of the fluid. The time scale for eddies of the Kolmogorov scale can be approximated by:

$$T_{\lambda_0} \approx \frac{\lambda_0}{u_{\lambda_0}} \approx \frac{\lambda_0^2}{\nu} \equiv \frac{1}{G} \tag{4.31}$$

According to Levich, turbulent eddy velocities scale with the eddy size λ:

$$u_\lambda \approx \frac{u_{\lambda_0}}{\lambda_0}\lambda \tag{4.32}$$

in which u_{λ_0} is the eddy velocity at scale $\lambda = \lambda_0$. This agrees with the normalised spectrum of the turbulent energy E at high wave numbers k around the Kolmogorov scale: E scales with k^{-3}, hence u with k^{-1}, thus with λ, as shown in Fig. 4.6 taken from Tennekes and Lumley (1994). As a consequence, the turbulent stresses in the viscous regime at scale $\lambda = D$ are given by:

$$\tau_T = \mu \frac{\partial u}{\partial z} \approx \mu \frac{u_{\lambda_0} D/\lambda_0}{D} \approx \mu G \tag{4.33}$$

in which μ is the dynamic viscosity of the fluid.

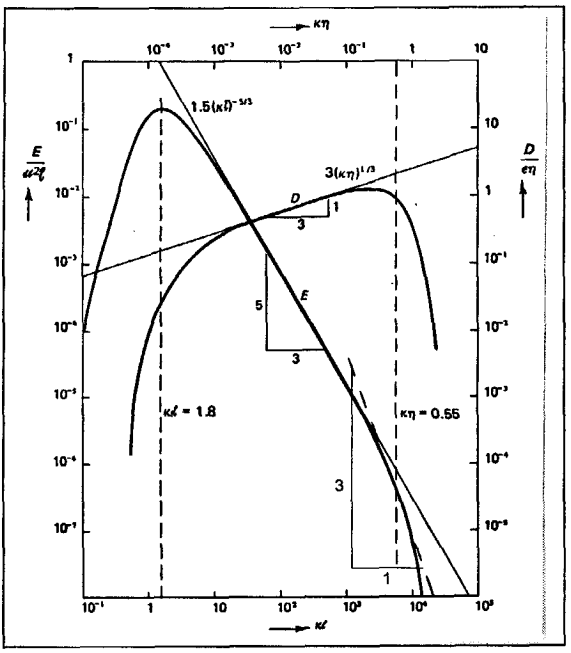

Fig. 4.6: Idealised 3D turbulent energy (E) and dissipation (D) spectra (from Tennekes and Lumley, 1994).

The yield strength of flocs F_y is determined by the number of bonds in a plane of failure, which, because of the fractal structure of the flocs, is independent of the size of the aggregate (e.g. Kranenburg, 1994). Hence F_y is constant, as a result of which τ_y scales with $1/D^2$. The actual value of F_y is determined by the physico-chemical properties of the sediment and the water, and can be related to the Zeta-potential of the water-sediment suspension; such relations are highly empirical though, and no explicit formulations are known at present.

Finally, the time scale for the eddies at $\lambda = D$, at which scale the relation $T_\varepsilon = T_D$ is valid, maintains the value of equ. (4.31), hence, $T_\varepsilon = 1/G$. By substitution, we obtain the growth rate of particle number concentration N by floc breakup:

$$\frac{dN}{dt} = a e_b G \left(\frac{D - D_p}{D_p} \right)^p \left(\frac{\mu G}{F_y / D^2} \right)^q N \tag{4.34}$$

in which e_b is an efficiency parameter for the breakup process.

4.5.4 A model for turbulence-induced flocculation

A complete flocculation model should include both aggregation and floc breakup processes. Because of the uncertainties in the formulations of these aggregation and floc breakup processes and the poorly known empirical parameters involved, a simple linear

combination of (4.26) and (4.34) is proposed, thus assuming a simultaneous acting of aggregation and floc breakup processes. The differential equation for the flocculation of cohesive sediment under the influence of turbulent shear then becomes:

$$\frac{\partial N}{\partial t}+\frac{\partial}{\partial x_i}\left(\left(u_i-\delta_{i3}\frac{(1-\phi_*)(1-\phi_p)}{(1+2.5\phi)}w_{s,r}\right)N\right)-\frac{\partial}{\partial x_i}\left((D_s+\Gamma_T)\frac{\partial N}{\partial x_i}\right)= \\ =-k_A'(1-\phi_*)GD^3N^2+k_BG^{q+1}(D-D_p)^pD^{2q}N \tag{4.35}$$

in which we have included the effects of hindered settling in the advection term and define the parameters k_A' and k_B as follows:

$$k_A'=\frac{3}{2}e_c\pi e_d\ ,\ \text{and}$$
$$k_B=ae_bD_p^{-p}\left(\frac{\mu}{F_y}\right)^q \tag{4.36}$$

When solving (4.35) we assume that no particles leave or enter the water column through the water surface. At the bed, flocs may enter or leave the computational domain through erosion or deposition processes. These processes are modelled in agreement with the description used for the mass balance, i.e. the Krone and Partheniades formulations (see Section 3.2). We assume that the flocs that leave the domain through deposition have the local floc size described by (4.35). We further assume that the particles that enter the domain will have a grain size equal to the local equilibrium conditions determined by the local bed shear stress (i.e. the local value of the dissipation parameter G at that time). This implies that the mass of sediment entering the water column through erosion is determined by the number of particles N, their volume V_f and density ρ_f, in which V_f and ρ_f are determined by equilibrium conditions[2)].

From (4.7) and (4.9) we find:

$$V_{f,e}=f_sD_e^3\ ,\ \text{and}$$
$$\rho_{f,e}=\rho_w+(\rho_s-\rho_w)\left[\frac{D_p}{D_e}\right]^{3-n_f} \tag{4.37}$$

The aggregation and floc breakup terms are set to zero at the water surface and at the horizontal water-bed interface. Hence the boundary conditions read:

$$\left\{(u_3-w_s)N-(D_s+\Gamma_T)\frac{\partial N}{\partial x_3}\right\}\Bigg|_{x_3=Z_s}=0$$
$$\left\{(u_3-w_s)N-(D_s+\Gamma_T)\frac{\partial N}{\partial x_3}\right\}\Bigg|_{x_3=Z_b}=E_{b,N} \tag{4.38}$$

The source-sink term $E_{b,N}$ represents the exchange with the bed and is modelled with the classical formulae of Partheniades and Krone, so that the water-bed exchange formulation is consistent with the one for the mass balance:

[2)] We use equilibrium parameters for the special case n_f=2 for convenience, see equ. (4.43).

$$E_{b,N} = -w_s N S(1-\theta_d) + \frac{M}{f_s D_e^3 \rho_{f,e}} S(\theta_e - 1) \tag{4.39}$$

in which the ramp function S, the threshold stress parameters θ_d and θ_e and the erosion parameter M have been defined in Section 3.2.

Our flocculation model consists of the coupled set of equations (3.13) for the mass balance, (4.35) and (4.36) for the number of particles, the geometrical relation (4.23), and the boundary conditions (4.38) and (4.39), together with the relations (4.37) and (4.43 - see below). A one-dimensional form of this flocculation model is obtained by neglecting the horizontal gradients in the various equations, which is implemented in the 1DV POINT MODEL - see Appendix B for details.

For the initial conditions in numerical simulations we propose to apply the conditions for equilibrium for $n_f = 2$. Given an initial flow field and sediment concentration (by mass), the equilibrium floc size can be established with (4.43) below. Formula (4.23) then gives the initial number of particles N_0.

4.6 Model characteristics and calibration

4.6.1 Behaviour of the simplified Lagrangean flocculation model

First, we study the behaviour of a simplified version of the flocculation model. We assume small volumetric concentration ($\phi << 1$) and apply (4.23). In the case where we have no net advective or turbulent transport (i.e homogeneous turbulence), as for instance in a settling column, the sediment concentration is constant, and (4.35) reduces to:

$$\frac{dD}{dt} = k_A c G D^{4-n_f} - k_B G^{q+1} \left(D - D_p\right)^p D^{2q+1} \tag{4.40}$$

in which the dimensional aggregation parameter k_A [m^2/kg] and floc breakup parameter k_B [s^{½}/m^2] are defined as:

$$k_A = k_A' \frac{D_p^{n_f-3}}{n_f f_s \rho_s} \tag{4.41a}$$

$$k_B = \frac{a e_b}{n_f} D_p^{-p} \left(\frac{\mu}{F_y}\right)^q = k_B' \frac{D_p^{-p}}{n_f} \left(\frac{\mu}{F_y}\right)^q \tag{4.41b}$$

where k_A' and k_B' are non-dimensional coefficients. This is the Lagrangean flocculation model elaborated in Winterwerp (1998). For equilibrium conditions, i.e. $dD/dt = 0$, an equilibrium floc size D_e can be defined. The exponents p and q can be obtained from empirical data available in literature. In many experimental studies it was found that D_e is proportional to λ_0 (e.g. Bratby (1980), Akers et al. (1987), Leentvaar and Rebhun (1983) and Van Leussen (1994)). This can be explained from the turbulent energy spectrum: at length scales beyond λ_0, the turbulent stresses increase rapidly, hence floc breakup becomes dominant.

Fig. 4.5 shows the variation of the settling velocity measured by Owen as published by Thorn (1981) and Mehta (1986), by Ross (1988) and by Wolanski et al. (1992). Here we concentrate on the left branch of the curve, representing data affected by flocculation effects. The scatter is large, and it is difficult to establish an accurate relation from these data. For the present analysis we assume that the data given represent variations around equilibrium values of $w_{s,e}$, and that $w_{s,e} \propto c$ (e.g. equ. (4.12)). We note that the measured w_s - c relation presented in Fig. 4.5 may be affected by spurious correlations: large values of c in general occur at large current velocity. At such large velocities larger sediment particles, with a larger settling velocity, may be mobilised. This effect will particularly take place in shallow and intertidal areas with a pronounced spring-neap tidal cycle.

By substituting these additional assumptions into (4.40) we find $q = 1/2$ and $p = 3 - n_f$, see Winterwerp (1998) for details. If we further set the fractal dimension at the average value for mud flocs in the water column at $n_f = 2$, we obtain a simple flocculation equation that can be used to study the behaviour of the model:

$$\frac{\mathrm{d}D}{\mathrm{d}t} = k_A c G D^2 - k_B G^{3/2} D^2 \left(D - D_p\right) \tag{4.42}$$

For small values of D, the first term on the right hand side of (4.42), e.g. the aggregation term dominates, whereas for large D the second term, e.g. the breakup term dominates. From this flocculation equation two conclusions can be drawn:

1. An equilibrium floc size D_e is obtained for $\mathrm{d}D/\mathrm{d}t = 0$. A mathematically trivial, but physically unsound and unstable solution is $D_e = 0$. In this case small particles always grow. The other equilibrium solution for the simplified model reads:

$$D_e = D_p + \frac{k_A c}{k_B \sqrt{G}} \tag{4.43}$$

   which is a stable equilibrium, as for $D < D_e$ the flocs grow and for $D > D_e$ the flocs break up.

2. Substituting from equ. (4.12) and neglecting the Re-term in the denominator gives a formula for the settling velocity under equilibrium conditions:

$$w_{s,e} = W_{s,p} + \alpha' \frac{k_A}{k_B} D_p \frac{\Delta g}{\nu} \frac{c}{\sqrt{G}} \tag{4.44}$$

   where $\alpha' = \alpha/18\beta$, $\Delta = (\rho_s - \rho_w)/\rho_w$, and $W_{s,p}$ is the settling velocity of the primary particles. Neglecting $W_{s,p}$, and using (4.2) and (4.4), the equilibrium settling velocity scales as $w_{s,e} \propto c/\sqrt{G} \propto c/\varepsilon^{1/4} \propto c\left(h/U^3\right)^{1/4}$.

This formula was already used to determine the coefficient q above, using $w_{s,e} \propto c$. It follows that $w_{s,e}$ is expected to be proportional to $1/\sqrt{G}$, consequently to λ_0, and it shows how $w_{s,e}$ varies with the primary flow parameters h and U.

From small scale experiments by Serra and Casamitjana (1998) with latex beads and by Lick and Lick (1988) with sediments from Lake Erie it was found that the equilibrium floc size D_e decreases with increasing sediment concentration. This is attributed to the effects of floc breakup by particle-particle collisions. This observation is not consistent with the many data presented in the literature that the settling velocity of

mud flocs increases with increasing sediment concentration. The scale of the experiments by Serra and Lick (wall effects) and/or strength of the flocs (dense flocs with a large fractal dimension) may explain this discrepancy. At present, we feel that the w_s - c data are more reliable and ignore the findings by Serra and Lick.

It should be noted that actually the flocculation process produces a distribution of particle sizes, with a large scatter, though. However, for flocculated sediment this distribution may be very steep (Migniot, 1968). Therefore size fractions are not accounted for in the present formulation. D_e should be considered as a characteristic floc size, something like the median particle size.

For the chosen fractal dimension $n_f = 2$, the differential equation (4.42) can easily be solved analytically, if the sediment concentration by mass c is constant. First a time scale parameter T' is defined:

$$T' = \left(k_B G^{3/2} D_e^2\right)^{-1} \tag{4.45}$$

The solution of equ. (4.42) then obtains the implicit form:

$$t = T'\left[\ln\left(\frac{D_e - D_0}{D_e - D}\frac{D}{D_0}\right) + \frac{D_e}{D_0} - \frac{D_e}{D}\right] \tag{4.46}$$

in which D_0 is the floc size at $t = 0$. This solution describes the aggregation/floc-breakup process for flocs initially either smaller or larger than the flocs at equilibrium size.

From (4.46) a time constant for flocculation T_f can be defined in the case that the initial floc size D_0 is much smaller or much larger than the equilibrium value, yielding the maximal time scales of the aggregation and floc breakup processes:

$$\begin{aligned}
&\text{for } D_e >> D_0 \quad T_f \approx T' D_e / D_0 \approx \frac{1}{k_A c G D_0} \\
&\text{for } D_e << D_0 \quad T_f \approx 2T' \approx \frac{2k_B}{k_A^2 c^2 \sqrt{G}} \\
&\text{hence:} \qquad T_f \propto \left(\frac{U^3}{h}\right)^{-n} c^{-m} \quad \text{with} \quad \frac{1}{4} \le n \le \frac{1}{2},\ 1 \le m \le 2
\end{aligned} \tag{4.47}$$

During the flocculation process, the flocs grow in size and their settling velocities increase. As a result, the residence time of the flocs in the water column is limited, hence the time available for flocculation. Two time scales are of importance: the residence time T_r itself and the time T_T during which the turbulent intensity remains more or less constant.

Let us consider a situation where the turbulence field is homogeneous over the water depth, as can be realised in a settling column, for example. Then $T_T \rightarrow \infty$, as the turbulent field is homogeneous. The mean residence time T_r for all particles in the water column with initial height Z_0 above the bottom of the water column can be obtained from:

$$\int_0^{T_r} w_s \mathrm{d}t = \alpha'' \int_0^{T_r} D \mathrm{d}t = Z_0 \tag{4.48}$$

in which $\alpha'' = \alpha' D_p g \Delta / \nu$ (≈ 3 s^{-1} for $D_p = 4$ μm). T_r can be solved directly from this equation using the simplified flocculation model (4.42) to yield:

$$T_r = \frac{Z_0}{\alpha'' D_e} + \frac{D - D_0}{k_A c G D D_0} = \frac{Z_0}{w_{s,e}} + T' \left[\frac{D_e}{D_0} - \frac{D_e}{D} \right] \tag{4.49}$$

in which $w_{s,e}$ is the equilibrium settling velocity.

The maximal settling velocity, as a function of a limited residence time, follows from (4.48) and (4.49) ($t = T_r$):

$$w_{s,max} = \frac{w_{s,0}}{\left(\frac{D_e - D_0}{D_e} \right) e^{-\frac{Z_0}{w_{s,e} T'}} + \frac{D_0}{D_e}} \tag{4.50}$$

This formula yields similar results as the heuristic formula (4.1), as will be shown in the next section.

4.6.2 Calibration of the simplified Lagrangean flocculation kinetics

The flocculation model contains a flocculation parameter k_A and a floc breakup parameter k_B, which have to be determined empirically. This has been done on the basis of flocculation experiments carried out in the settling column of WL|delft hydraulics (see Van Leussen, 1994). This column is a 4.25 m high perspex cylinder with an inner diameter of 0.29 m. Within the column a grid can be oscillated at various frequencies and amplitudes to generate a homogeneous turbulence field.

The dissipation parameter G can be varied by varying the frequency of the grid; the amplitude of the oscillations is always kept constant. Samples can be taken at various heights from the column. From the variations in measured suspended sediment concentration, the settling velocity distribution is assessed. During three experiments floc sizes at the bottom of the column were measured with a Malvern particle sizer.

To determine the model parameters k_A and k_B a series of experiments with mud from the Ems estuary were analysed. At the start of an experiment, the sediment is brought into the column and is mixed homogeneously by recirculating it through the column with a pump. Then at $t = 0$, the pump is stopped and the grid is set in oscillation. At regular time intervals samples are withdrawn at 10 positions over the height of the column. Two series of experiments are analysed. In the first series, the initial sediment concentration c_0 is kept more or less constant, and the frequency of the grid f (hence G) is varied. In the second series, G is kept constant, and suspensions with various initial concentrations are brought into the column. These tests are summarised in Table 4.1; the values of D and w_s given are the maximal values observed. For further details on the experimental set-up and these measurements - see Van Leussen (1994) and Cornelisse (1990).

It is assumed that at $t = 0$ the initial particle size equals the size of the primary particles, as measured with the Malvern, i.e. $D_0 = D_p = 4$ μm. Next k_A and k_B were determined from the results of test T73 only; it is assumed that the maximum floc size measured at the base of the settling column equals the equilibrium value, and that the

time at which this occurs is the time in which 95 % of the equilibrium value is obtained. In this way, the values given in Table 4.2 are found.

Test no	c_0 [kg/m^3]	f [Hz]	G [s^{-1}]	D_{50} [μm]	$w_{s,50}$ [mm/s]	w_s/c [(mm/s)/(g/l)]
T70	0.78	0.025	0.9	n.a.	1.6	2.05
T142	0.96	0.025	0.9	n.a.	1.8	1.87
T74	1.02	0.05	2.6	n.a.	1.50	1.51
T140	0.97	0.05	2.6	n.a.	1.8	1.86
T71	0.65	0.10	7.3	270	0.85	1.20
T137	0.98	0.1	7.3	n.a.	1.2	1.22
T69	1.17	0.25	28.9	241	0.17	0.15
T139	1.03	0.25	28.9	n.a.	0.2	0.19
T73	1.21	0.50	81.7	140	0.9	0.8
T141	1.01	0.5	81.7	n.a.	0.2	0.20
T113	0.79	0.025	0.9	n.a.	0.37	0.47
T114	0.15	0.025	0.9	n.a.	0.98	6.76
T142	0.97	0.025	0.9	n.a.	2.05	2.11

Table 4.1: Summary of settling column tests with Ems-Dollard mud (Cornelisse, '90)

From these values the non-dimensional coefficient k_A' can be determined, and k_B' can be estimated. For ρ_s = 2650 kg/m^3 and D_p = 4 μm, we find $k_A' \approx 0.31$ and e_c = O{0.01}, as $e_d \approx 0.5$ - 1 (e.g. Levich, 1962). This agrees fairly well with the values reported by O'Melia (1985), given in Section 4.1.

Test No	α' [-]	k_A [m^2/kg]	k_A' [-]	k_B [s^{½}/m^2]	ae_b [-]	$\sqrt{\mu/F_y}$ [s^{½}/m]
T73	1/18	14.6	0.31	14.0 10^3	2 10^{-5}	5.6 10^3

Table 4.2: Parameters of flocculation model established from test T73.

For the assessment of k_B', we have to know the floc strength F_y. Very little information about this strength is available, but from some literature (e.g. Van Leussen (1994) and Matsuo and Unno (1981)) F_y is estimated at $F_y \approx$ O{10^{-10}} N (though this can vary by several orders of magnitude), as a result of which k_B' is estimated at $k_B' =$ O{10^{-5}}. Apparently, the efficiencies of both the flocculation and floc breakup processes are very small, the latter being even much smaller than the

former. This was also concluded by Van Leussen (1994) on the basis of his estimates of the time scale for floc breakup.

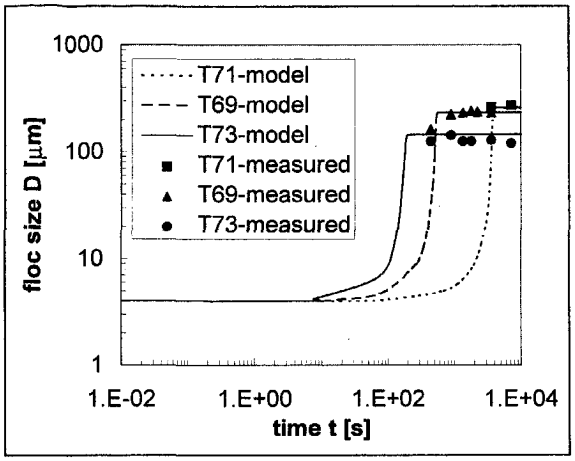

Fig. 4.7: Variation of floc size with time (parameters calibrated against test T73).

Using the parameters obtained from test T73, the solution (4.46) of the floc evolution model is plotted in Fig. 4.7, which shows the variation of the floc size with time for three tests. Initially the flocculation process is very slow, but after some time a rapid growth occurs. As D approaches its final equilibrium value, the growth rate decays rapidly. As a result a pronounced S-shaped curve is found. Qualitatively this is in agreement with observations reported by Boadway (1978), Tsai et al. (1987), Lick et al. (1993) and Lick and Huang (1994), for instance. Also from the theory of Reaction Limited Cluster-Cluster Aggregation such a behaviour is predicted (e.g. Vicsek (1992). In Fig. 4.7 the observed equilibrium values of D are also plotted. Predictions and observations are in good agreement for tests T69 and T71. Note that unfortunately we have only one data point on the growth-curve for test T69; all other data points represent more or less equilibrium values. Hence, more data are required to validate the model properly. At present, such data are not available though.

We also note that the flocculation time T_f for tets T73, obtained from (4.45) and (4.47), using the various parameters of Table 4.2, gives $T_f = 173$ s, which agrees well with the numerical solution, which predicts $T_f \approx 200$ s (see Fig. 4.7). This implies that the approximations of (4.47) are useful to estimate the flocculation time scale for cohesive sediment in a turbulent environment, provided the various model parameters are known.

Next, the maximal settling velocities measured in the settling column are compared with the model (4.50). As the simplified flocculation model assumes that the settling velocity is proportional to the concentration c, it is convenient to divide $w_{s,max}$ by c; in this way all tests presented in Table 4.1 can be compared with the model in one graph. The results are given in Figure 4.8. The solid line represents the model (4.50), showing an increasing $w_{s,max}/c$ with G at small G, and a decrease at large G. This behaviour is qualitatively similar to that of equ. (4.1); see Fig. 4.1. The dashed line represents the equilibrium curve (4.44). At small G the residence time of the flocs in the column becomes the limiting factor and the difference between the two curves is

considerable; at large G they coincide. It is not true that in the ascending branch flocculation effects dominate, and in the descending branch floc breakup processes, as is often suggested in the literature.

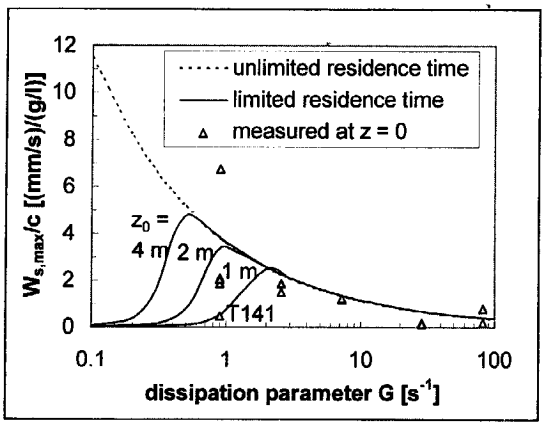

Fig. 4.8: Variation of settling velocity with dissipation parameter.

Figure 4.8 shows a reasonable agreement between observations and model, the largest differences occurring at small G; the measured settling velocity for test T141 is exceptionally low, which is attributed to a fairly high content of organic material in this particular sample (e.g. Van Leussen, 1994). These differences at small G may be attributed to the large sensitivity of the results to small variations in ambient conditions. This is predicted by the model. At small G, small variations in G itself, in the initial mixing process, which result in variations of effective column height and/or D_p, and variations in grain size distribution (presence of sand and organic material) may affect $w_{s,max}$ considerably. However, in the light of the large scatter in settling velocity data normally observed (e.g. Figs. 4.3 and 4.5), the agreement of model results and observations is satisfactory.

In the next two sections of this chapter we describe a series of sensitivity analyses of the simplified Lagrangean flocculation model, and a series of sensitivity analyses of the full Eulerian flocculation model in one (vertical) direction for open-channel flow.

4.7 Sensitivity analyses

4.7.1 The gelling point

When mud flocs settle on the bed, they may form a space-filling network structure, called a gel, and a measurable strength builds up (e.g. Section 2.4). The concentration at which this happens is called the gelling point. The volumetric concentration ϕ is then assumed to become unity, see equ. (4.8). If we assume that the flocculation model is also valid for these conditions, we can establish the gelling concentration c_{gel} for equilibrium conditions ($dD/dt = 0$) as a function of dissipation parameter G for various values of the fractal dimension n_f from the geometrical relation (4.8) and the simplified flocculation model (4.40) proposed in this chapter. We assume $D_e \propto \lambda_0$ and

$w_{s,e} \propto c$, as in Section 4.6, hence $q = 1/2$ and $p = n_f - 3$. We further assume that $D_p << D$ (e.g. equ. (4.43)) and that the sediment concentration is constant, yielding:

$$c_{gel} = \left(\frac{a e_b}{k_A'} \sqrt{\frac{\mu}{F_y}} \right)^{\frac{3-n_f}{4-n_f}} D_p^{\frac{3-n_f}{4-n_f}} \rho_s G^{\frac{3-n_f}{2(4-n_f)}} \tag{4.51}$$

Using the various model parameters assessed in Section 4.6, $c_{gel}(G,n_f)$ can be established for equilibrium conditions. The results are presented in Fig. 4.9, showing the high sensitivity of c_{gel} to n_f at larger values of n_f. For $n_f = 3$, we obtain the trivial result that $c_{gel} = \rho_s$. We observe that for $n_f = 2.6$ to 2.7, we find $c_{gel} \approx 100$ g/l, which is a characteristic concentration for fluid mud occurrences - see also Fig. 4.2 for typical values of G in open-channel flow.

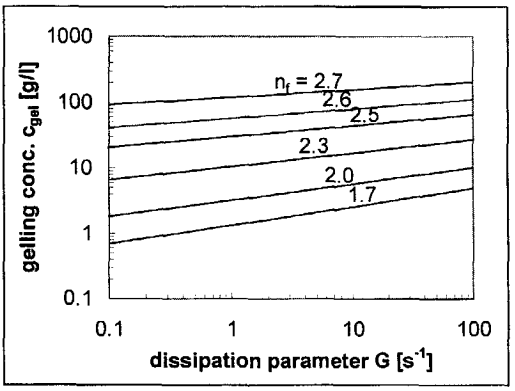

Fig. 4.9: Variation of gelling concentration c_{gel} with n_f and G for equilibrium conditions.

It is not possible to obtain c_{gel}-values of the order of 100 g/l by modifying the other parameters of the flocculation model within reasonable limits. Hence, by applying the flocculation model for equilibrium conditions, fluid-mud concentrations of about 100 g/l can only be obtained with fractal dimensions substantially larger than the average n_f-values encountered in the mud flocs in the water column. This is further elaborated in the Sections 4.8.2 and 7.3.

It is also noted that (4.51) yields unrealistic large values for c_{gel} at small G, because D_e becomes unrealistically large. Such large flocs would collapse, as their yield strength decreases with D^2, a process not accounted for in the present model.

4.7.2 Evolution of the settling velocity

Our flocculation model contains a number of parameters that have to be established indirectly from flocculation experiments. As only a limited set of experimental data is available, it is useful to study the sensitivity of the results of the flocculation model to variations in these parameters, prior to application of the model to practical situations.

First we observe from equ. (4.43) that the equilibrium floc size D_e varies linearly with k_A, c and $1/k_B$ for $D_e >> D_p$, and that the flocculation time T_f varies inversely proportional to k_A , c and D_0 (for $D_e >> D_0$). This implies that a doubling of k_A or c alone would result in a doubling of D_e and a halving of T_f . Doubling of k_B would

result in a halving of D_e, but does not have any effect on T_f, whereas a doubling of both k_A and k_B would halve T_f but not affect D_e. These conclusions are based on the simplified flocculation model, but numerical simulations with the complete flocculation model show the same trends. The results of these simulations are not presented here, though.

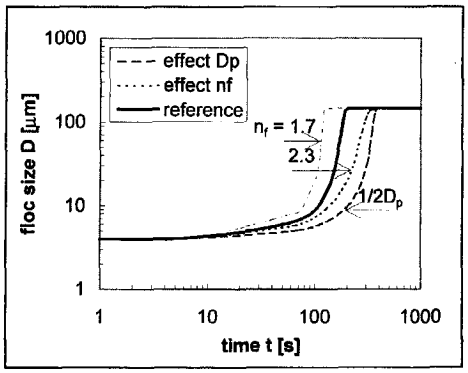

Fig. 4.10: Effect of some model parameters on flocculation time; reference conditions: n_f = 2, D_p = 4 µm.

The role of the size of the primary particles D_p and of the fractal dimension n_f are less obvious. Their effects have been assessed with numerical simulations with the complete flocculation model using the parameters established for calibration run T73 (e.g. Section 4.6.2). The results are presented in Fig. 4.10 showing that halving D_p (hence D_0 in the present case) leads to a doubling of T_f, but does not affect D_e. The same is true for the role of n_f: a variation in n_f does affect T_f, but not D_e. (This is only true for q = 0.5 in the flocculation model.)

From this simple analysis we can conclude that the equations (4.43), (4.45) and (4.47) are suitable to obtain a fair picture of the sensitivity of the model results to variations in the model coefficients, and as such of the behaviour of a flocculating suspension in open-channel flow.

In Section 4.6.1 it is shown that floc growth, hence settling velocity, can be limited by a limited residence time of the mud flocs in the water column. This analysis, however, is carried out for homogeneous turbulence conditions. So let us now study the flocculation process of a suspension in an open channel with steady uniform flow which initially consists of primary particles only. We are particularly interested in the variation in flocculation time over the water depth in comparison to the local settling time of the flocs. In Section 4.8 we study the behaviour of the entire flocculation model for open channel flow.

We apply the simplified flocculation model and the coefficients established in Section 4.6.2, including a sediment concentration c = 1.21 g/l (test T73). The variation of the flocculation time T_f with depth z then follows from the substitution of equ's (4.4), (4.43) and (4.45) into equ. (4.47). The settling time in still water T_s follows from $T_s = z/w_s$; the settling velocity is conveniently set at a constant value of w_s = 0.1 mm/s. The results are presented in Fig. 4.11 for a water depth h = 10 m and three flow velocities showing flocculation times of many hours over the major part of the water

column for flow velocities below 0.5 m/s. Only for $U = 1$ m/s T_f becomes of the order of a few minutes near the bed.

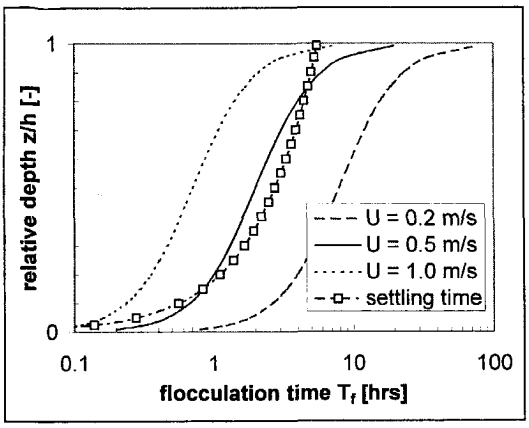

Fig. 4.11: Typical flocculation times for parameter setting given in the text.

We have to be careful when drawing quantitative conclusions from the results of Fig. 4.11. First we note that the model parameters have been based on a limited series of experiments only. Also the sediment concentration selected for this analysis is unrealistically high, by at least an order of magnitude, for the smaller flow velocities. For lower values of c, T_f would be proportionally larger. On the other hand, this would imply that the flocs and their settling velocity remain small, hence the residence time of the flocs at a specific height is large as the settling time T_s becomes large. Finally we note that Fig. 4.11 presents the maximal flocculation times, i.e. when the initial size of the particles equals the size of the primary particles.

The main observation from Fig. 4.11 is more qualitative: the flocculation time can be of the order of many hours and may vary by two orders of magnitude over the water column. In particular the following conclusions are relevant:

1. The initial floc size distribution is an important parameter. In a turbidity maximum in an estuary, sediment becomes trapped and the residence time of the mud flocs is large in general. Hence a dynamic equilibrium in floc size distribution may develop, depending on c and G. In coastal waters, HCMS's occur under short-duration episodic events, and the residence time of the flocs in the turbulent environment are expected to be small.
2. Near the water surface we expect small mud flocs in general: c near the water surface is small in general, hence T_f can become very large. On the other hand, also the residence time of these small mud flocs will become large, as their settling velocity will be small. The balance between these two processes determines the final floc size.
3. Because of the large vertical gradients in G (Fig. 4.2), hence D_e and T_f (Fig. 4.11), we expect large vertical gradients in floc size, hence settling velocity. This implies that the flocculation process by itself may be responsible for a considerable segregation effect.
4. Near the bed, where T_f becomes smaller, it is expected that the settling velocity will show a hysteresis effect over the tidal cycle: during decelerating tide the

settling velocity will be relatively large, hence promoting settling and during accelerating tide the settling velocity will be relatively small, hence promoting vertical mixing.

This qualitative picture will be further elaborated in Section 4.8 through a series of simulations with the 1DV POINT MODEL for open-channel flow under steady state and tidal conditions.

4.8 Floc evolution in open-channel flow - sensitivity analysis

No data are presently available on the evolution of the floc size and settling velocity in open-channel flow. As a consequence, the flocculation model can therefore not be calibrated against such data. Therefore we can only study the features of this model with a sensitivity analysis. This is done, using the 1DV POINT MODEL, in which the flocculation model is implemented. In none of the simulations have water-bed exchange processes been included. We have verified that the model reproduces the analytical solutions of the simplified model, presented in Section 4.6.1; however, these results are trivial, and are not presented herein.

4.8.1 Steady state flow conditions

First, a series of simulations for steady state flow conditions is carried out;

1. In the first series, $U = 0.5$ m/s and $W_s = 0.0$ mm/s,
2. In the second series the settling velocity is computed by the model ($U = 0.5$ m/s),
3. In the third series the effect of the flow velocity is studied ($U = 0.2$ and 1.0 m/s), whereas the settling velocity is computed by the model.

We start with a simulation with $U = 0.5$ m/s. In all simulations it is assumed that the sediment concentration is small and does not affect the density of the fluid, i.e. hindered settling nor feed back between suspended sediment concentration and turbulent processes is taken into account; these effects are treated in Chapter 6. The various parameters used in the model are listed in Table 4.3. The computed logarithmic velocity profile and related dissipation parameter G are presented in Fig. 4.12.

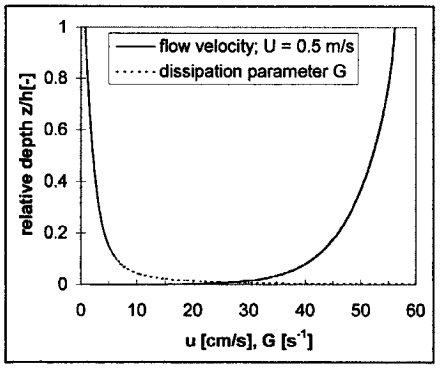

Fig. 4.12: Vertical profiles of flow velocity and dissipation parameter.

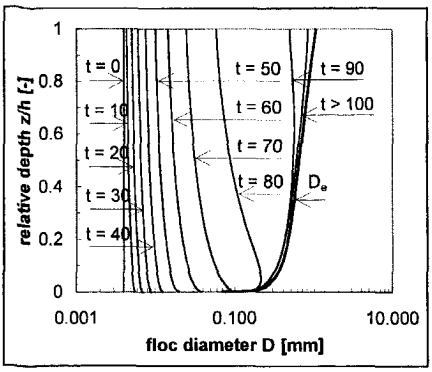

Fig. 4.13: Computed evolution of floc diameter with time [min] for $w_s = 0$.

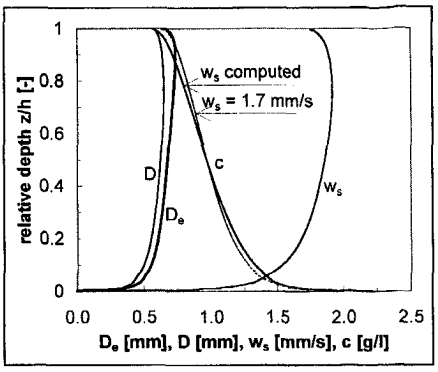

Fig. 4.14: Computed final sediment parameters for $w_s \neq 0$.

Fig. 4.13 presents the time evolution of the floc size from a simulation in which the settling velocity is set to zero, and starting with the primary size D_p at $t = 0$. It is shown that initially the flocs near the bed grow faster than higher in the water column. Only after 90 min. the flocs in the upper part of the water column become larger than near the bed. This behaviour is caused by the flocculation time: as G near the water surface is smaller than near the bed (see Fig. 4.12), T_f is larger, e.g. equ. (4.47). Hence it takes longer before the flocs reach their equilibrium value in the upper part of the water column, which is attained at $t = 100$ min. Note that the concentration profile remains uniform as $w_s = 0$.

parameter		value	remarks
water depth	h	8 m	constant; also for tidal flow
flow velocity	U	0.2, 0.5, 1.0 m/s	steady state
tidal flow amplitude	U_m	0.5 m/s	
bed roughness	z_0	1 mm	hydraulically rough
water density	ρ_w	1020 kg/m^3	
sediment density	ρ_s	2650 kg/m^3	
initial sediment concentration	C_0	1.0 & 0.5 kg/m^3	homogeneous profile
initial particle size	D_0	D_p & D_e	
settling velocity	W_s	0.5 mm/s	constant or computed
hindered settling		no & yes	
gelling concentration	c_{gel}	80 kg/m^3	constant or computed
fractal dimension	n_f	2.0	
flocculation parameters			see Table 4.2
water-bed exchange		no	
Prandtl-Schmidt-number	σ_T	0.7	
buoyancy coupling		no	
number of layers		105 layers	finer near the bed
time step	Δt	1 s	
relaxation time	T_{rel}	2 s	

Table 4.3: Parameter settings in numerical flocculation simulations.

It is also remarkable that the flocs do not attain their equilibrium value, represented by the D_e-curve in Fig. 4.13. Only very close to the bed, the floc size exceeds the equilibrium value. This has two reasons. First, D_e is the solution of the steady state simplified flocculation equation (4.42), whereas D_{final} is the solution of the steady state full flocculation equation (4.35); the latter also contains advection and diffusion terms. Second, the diffusion term in the flocculation model tends to oppose gradients in the number concentration N, thus limiting the growth of the flocs.

Next, the same simulation is carried out, but the settling velocity is computed by the 1DV POINT MODEL, using the relations of Section 4.3. The results for the final values (i.e. no variation with time any more) are presented in Fig. 4.14. The floc size and settling velocity show a moderate decrease near the water surface, and a large decrease near the bed, with an average value of about w_s = 1.7 mm/s. The first decrease is caused by a decrease in suspended sediment concentration, the second by the rapid increase in G near the bed. The vertical profile of the suspended sediment concentration has a realistic shape, though no measurements are available for comparison. However, comparison with the concentration profile computed for a constant settling velocity of 1.7 mm/s (i.e. no flocculation), also presented in Fig. 4.14, shows a slightly steeper profile: the variation of w_s with depth for the present conditions has apparently little effect on the vertical concentration profile.

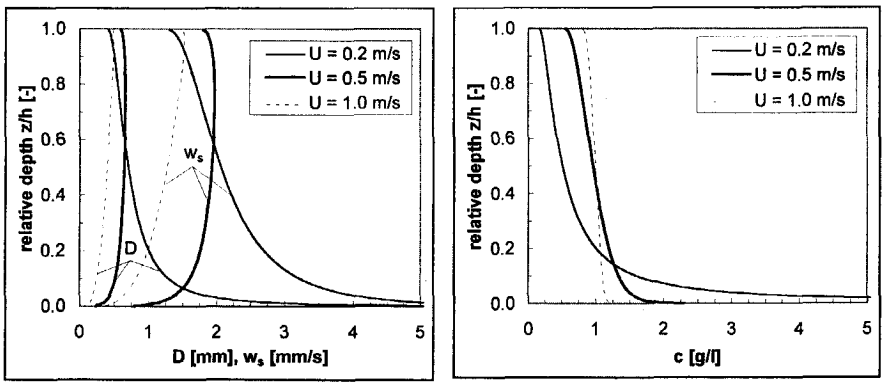

Fig. 4.15: Final distributions of floc size, settling velocity and suspended sediment concentration for U = 0.2, 0.5 and 1.0 m/s.

Fig. 4.15 presents the computed final floc size, settling velocity and suspended sediment concentration for various values of the mean flow velocity. The flocculation effects appear to become particularly important at smaller flow velocities, when large gradients in floc size and settling velocity are found in the lower part of the water column. As a result, the sediment concentration near the bed increases, which further augments the floc size, etc.

4.8.2 Tidal flow conditions

In this section the behaviour of the floc model for tidal flow conditions is studied. The depth is kept constant at h = 8 m, and the amplitude of the tidal velocity at U_m = 0.5 m/s, at a tidal period of T = 12.5 hrs. The following six simulations are carried out:

1. computed w_s, but no hindered settling effects, $U_m = 0.5$ m/s,
2. computed w_s, with hindered settling effects, but prescribed c_{gel},
3. computed w_s, with hindered settling effects, and c_{gel} computed with the flocculation model,
4. equilibrium settling velocity, i.e. $w_s = w_{s,e}$, with hindered settling effects, and c_{gel} computed with the flocculation model,
5. same as 3., but with $U_m = 0.2$, and
6. same as 4., but with $U_m = 0.2$.

The initial floc size D_0 is set at the equilibrium value for the initial flow profile. Other parameter settings are given in Table 4.3. Each simulation consists of 25 hrs, the results of the second period are presented at $t = 0.4\ T$, $0.5\ T$ (MEV = maximum ebb velocity), $0.6\ T$, $0.7\ T$, $0.75\ T$ (slack water), $0.8\ T$, $0.9\ T$ and $1.0\ T$ (MFV = maximum flood velocity). The results at $t = 0.5\ T$ and $t = 1.0\ T$ appear to be identical, indicating a spin-up period of about $1.5\ T$.

The computed vertical distributions of the flow velocity u and dissipation parameter G are presented in Fig. 4.16.

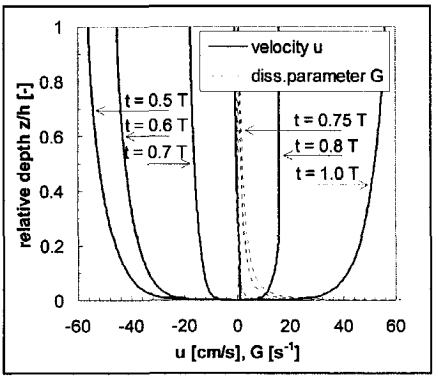

Fig. 4.16: Vertical profiles of flow velocity u and dissipation parameter G.

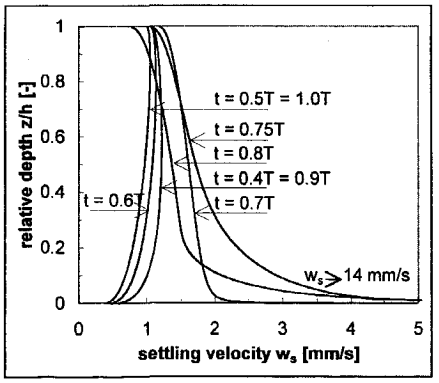

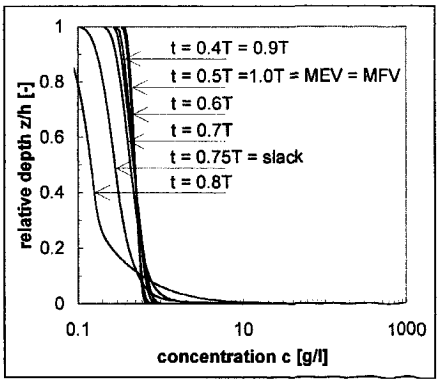

Fig. 4.17: Variation of settling velocity and vertical sediment concentration profiles with time; simulation without hindered settling.

Fig. 4.17 presents the results of a simulation without hindered settling, showing large settling velocities around slack water, especially near the bed, and subsequent extremely large sediment concentrations near the bed, with values up to 850 g/l at t = 0.8 T. This large concentration and the large settling velocity are directly related, as G is large near the bed, which by itself would result in small D, hence w_s. We must conclude that these results are fairly unrealistic.

Fig. 4.18 presents the results of a similar simulation, now including the effects of hindered settling. The gelling concentration has been prescribed and set at c_{gel} = 80 g/l. Qualitatively, Fig. 4.17 and 4.18 are comparable; the extreme values of the settling velocity and sediment concentration near the bed have been reduced considerably, though: the sediment concentration does not exceed its gelling value of 80 g/l in Fig. 4.18, and w_s at t = 0.8 T even slightly reduces near the bed due to the hindered settling effects.

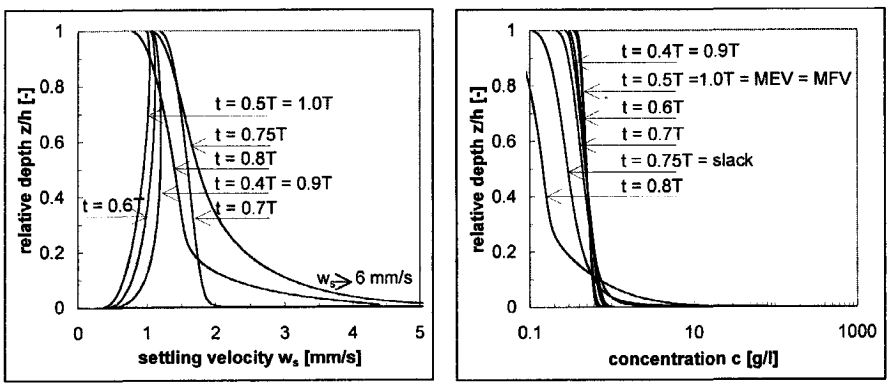

Fig. 4.18: Variation of settling velocity and vertical sediment concentration profiles with time; simulation with hindered settling: c_{gel} = 80 g/l.

The flocculation model can also be used to establish the gelling concentration from the floc size evolution itself by applying equ. (4.8), which is implemented in the 1DV POINT MODEL. The results of this simulation are presented in Fig. 4.19. The computed results now differ considerably, also in a qualitative sense, from the previous simulations: Fig. 4.19 does not show the large settling velocities and sediment concentrations found with the previous simulations. The vertical concentration profile in Fig. 4.19 looks quite realistic. Unfortunately, no experimental data are available for a quantitative comparison.

Fig. 4.19 also presents the results of the computed gelling concentration; the values vary with time and depth, as both G and c vary with time and depth. The values for c_{gel} range from about 10 g/l around slack water, when the flocs are large, till 50 to 100 g/l near the bed at larger flow velocities. Hence, the gelling concentration appears to be affected by history effects, and the fluid mud concentration may vary in time and space.

We note that the equilibrium conditions, discussed in Section 4.7.1, do not provide proper results: Fig. 4.9 suggests that gelling concentrations of 50 - 100 g/l can only be found at large fractal dimensions. In a dynamic simulation fluid-mud concentrations of 50 to 100 g/l are found for n_f = 2 because the flocs do not achieve their equilibrium

size. In Section 7.3 and 8.3 the gelling behaviour of HCMS and the formation of fluid mud is further elaborated.

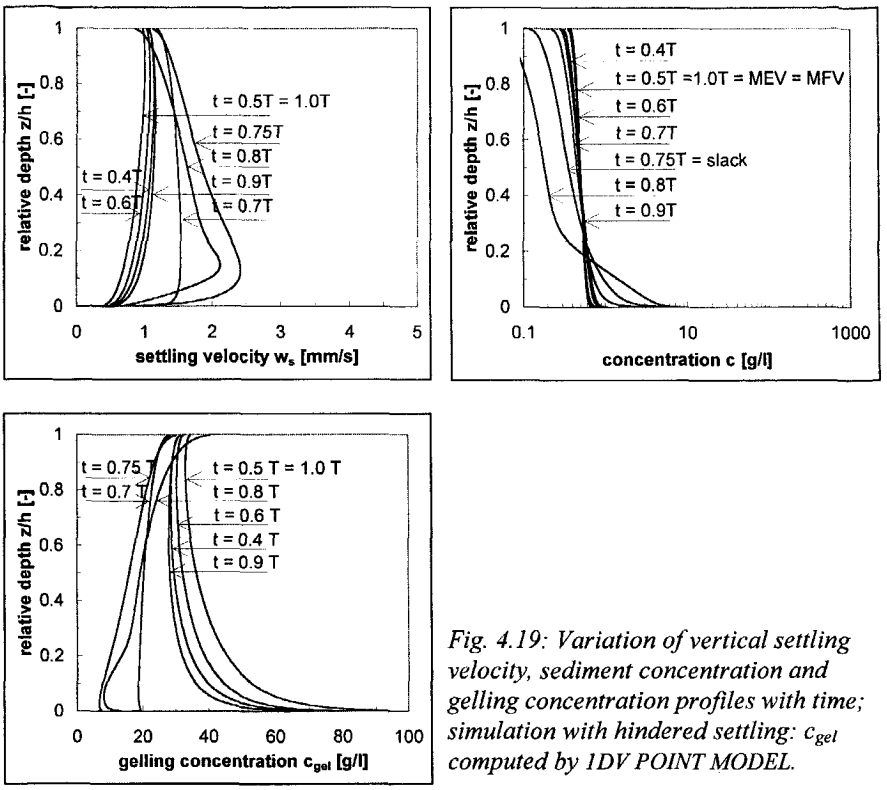

Fig. 4.19: Variation of vertical settling velocity, sediment concentration and gelling concentration profiles with time; simulation with hindered settling: c_{gel} computed by 1DV POINT MODEL.

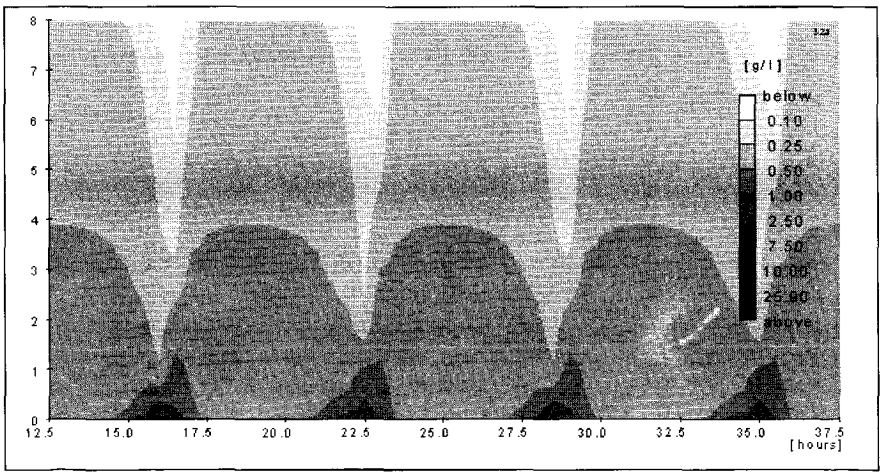

Fig. 4.20: Isolutals for the simulation with full flocculation model (same as Fig. 4.19).

The computed vertical concentration profile as a function of time is also plotted in Fig. 4.20 in the form lines of constant sediment concentration, which are called isolutals in this study, showing almost homogeneous conditions around t = 19, 25 and 32 hrs, i.e. around MFV and MEV, and large vertical gradients around t = 17, 22, 29 and 35 hrs, i.e. around slack water.

Simulations with the flocculation model are rather time consuming, as the vertical grid size and time step have to be small. It is therefore interesting to study whether it is possible to obtain reasonable results by applying equilibrium floc sizes only. In this case D_e is still a function of c and G; memory effects are omitted, however. The results, presented in Fig. 4.21, are fairly similar to those of Fig. 4.18, except for the irregular shape in the w_s-curve at t = 0.8 T; because of diffusion effects in the flocculation model, this irregular shape is less pronounced in Fig. 4.18.

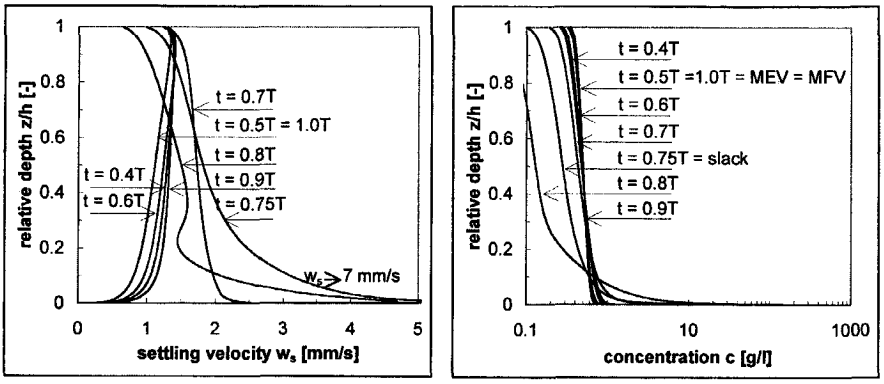

Fig. 4.21: Time variation of vertical profiles of settling velocity and sediment concentration; simulation with $w_s = w_{s,e}$ and hindered settling; c_{gel} computed.

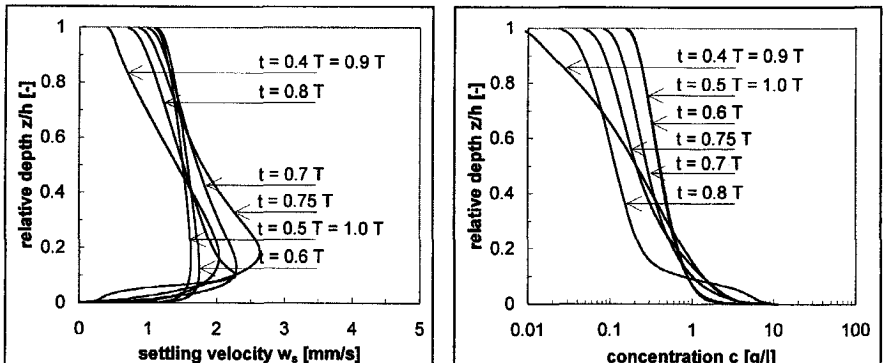

Fig. 4.22: Variation of vertical profiles of settling velocity and sediment concentration with time; simulation with U_m = 0.2 m/s and full flocculation model.

Comparison of Fig. 4.21 (and 4.18) with Fig. 4.19 shows that the vertical concentration profiles around maximal velocities are comparable to those of Fig. 4.19; large differences occur only around slack water. As long as the conditions around

slack water do not affect the water movement (e.g. Chapter 6 and 7), i.e. when the suspended sediment concentration is small, equilibrium values for the floc size and settling velocity may be used to assess horizontal transport rates.

Fig. 4.22 and 4.23 present the results of similar simulations, but for a tidal flow amplitude U_m = 0.2 m/s; Fig. 4.22 contains the results of the full flocculation model, whereas in Fig. 4.23 the results for a simulation with $w_s = w_{s,e}$ and computed c_{gel} are presented. We observe the same qualitative results as for U_m = 0.5 m/s (Fig. 4.19 and 4.21), i.e. little effect of the w_s-formulation around MEV and MFV, but large effects around slack water.

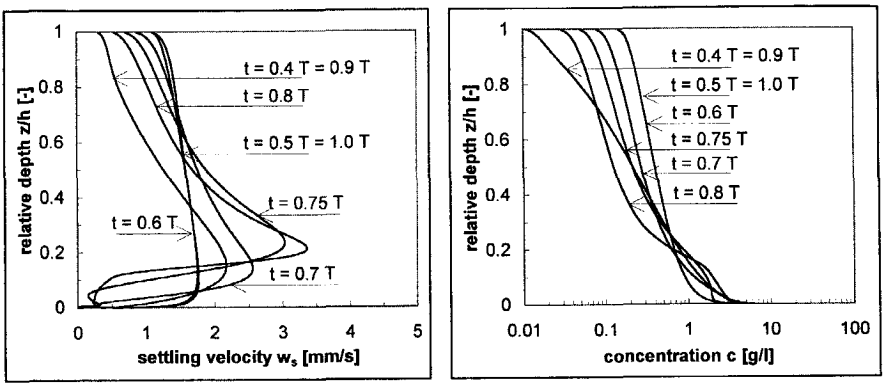

Fig. 4.23: Tome variation of profiles of settling velocity and sediment concentration; simulation with $\hat{u}$ = 0.2 m/s, $w_s = w_{s,e}$ and hindered settling; c_{gel} computed.

The various computational results presented in these sections seem reasonable, in the sense that realistic vertical concentration profiles are obtained, and that the computed settling velocity has reasonable values, though maybe a bit high (generally w_s-values of the order of 0.5 mm/s are encountered in estuarine and coastal areas; see also Section 7.3). We have to stress however that, before the flocculation model can be considered as operational, it should be calibrated against experimental data, which are not available at present.

5. Hindered settling and self-weight consolidation

5.1 Introduction

At the interface between the water column and a fluid mud layer, formed from the sedimentation of a High-Concentrated Mud Suspension, turbulence cannot be generated. Only when the fluid mud acquires sufficient strength, this interface becomes rigid and turbulence production is possible again. This process is elaborated in more detail in the Chapters 6 and 8. The present chapter proposes a model for self-weight consolidation and the related stress tensor of fluid mud layers. The main purpose of this model is to describe the development of a rigid interface between a fluid mud layer and the overlying water column, and the associated turbulence production at this interface.

We are interested in relatively short consolidation times only, i.e. periods around slack water during the tidal cycle. We do not study the consolidation processes of mud accumulations in navigation channels or harbour basins, for instance, nor do we assess the effects of strength build-up or strength break-down by external forces, such as turbulent stresses, wave loading, etc. However, when testing our model, we will apply it to simulate a long-term consolidation experiment.

In soil mechanics it is common to describe the rheological behaviour of fluid mud layers, subject to large deformations, with the Maxwell-approach, which involves a superposition of strain rates. However, with the limitations described above, we can simplify the mathematical-physical descriptions of the consolidation - strength evolution process considerably, and we can suffice with a superposition of the stresses (Van Kesteren, 1998). This approach matches our descriptions in Chapter 3 conveniently, as in the hydrodynamic equations stresses are also superposed. Moreover, by using this approach, the consolidation equation can be written as an advection-diffusion equation, as shown in the next sections. Hence, its mathematical treatment becomes identical to that of the mass balance equation presented in Section 3.2 (equ. (3.13)).

In our approach, the consolidation process and the subsequent strength evolution are established in two separate steps. Step 1 is dedicated to a description of self-weight consolidation, which follows Toorman's "unified theory" (1996), but in a Eulerian reference frame (e.g. Merckelbach, 1996). A similar approach was recently published by Bürger and Concha (1998) who derive a combined hindered settling and consolidation model in a Eulerian reference frame.

We use fractal power-law relations for the constitutive equations (Kranenburg, 1994, Merckelbach, 1998 and Merckelbach et al., 1998). This consolidation model provides the pressure and the sediment concentration (or void ratio) in the fluid mud layer as functions of time. In step 2, we establish the related stress tensor (e.g. Section 3.1) by modelling the fluid mud layer, when subject to shearing, as a Bingham visco-plastic fluid. The yield strength and viscosity are also determined as functions of the sediment concentration in the fluid mud layer, again using fractal power-law relations.

5.2 The consolidation equation

Toorman (1996) considers the settling and consolidation process of a suspension of cohesive sediment in a settling column, i.e. in still water, taking into account the effects of Brownian motion. In the present study we deal with turbulent open channel flow, and we augment the Brownian diffusion in the water column with the effects of turbulent diffusion. We follow Toorman's ideas to arrive at this Eulerian form; its derivation, though, is largely based on the work of Merckelbach (1996).

We start from the three-dimensional mass balance equation in Eulerian co-ordinates, but with the volumetric sediment concentration ϕ_p ($\equiv \Sigma c/\rho_s$) as the dependent variable (see also equ. (3.13)):

$$\frac{\partial \phi_p}{\partial t} + \frac{\partial}{\partial x_i}\left((u_i - \delta_{i3}\Xi_s)\phi_p\right) - \frac{\partial}{\partial x_i}\left(D_s \frac{\partial \phi_p}{\partial x_i}\right) = 0 \tag{5.1}$$

In (5.1) u_i and ϕ_p represent instantaneous quantities (fluctuating because of turbulence), and D_s is the molecular diffusion coefficient. The vertical velocity of the sediment particles with respect to the fixed reference frame is given by Ξ_s, where Ξ_s represents either the (hindered) settling velocity of the particles in the water column, denoted by w_s, or the particle velocity v_s within the fluid mud layer (i.e. during consolidation).

First we elaborate on the pressure gradients in the vertical direction (see also (3.9)):

$$\frac{\partial p}{\partial x_3} = -\rho g = -\phi_p g \rho_s - \left(1 - \phi_p\right) g \rho_w \tag{5.2}$$

where p is the pressure and ρ, ρ_s and ρ_w are the bulk density of the suspension, the density of the sediment and the density of the water, respectively. The relative velocity of the fluid v_f in vertical direction with respect to the sediment particles in our fixed reference frame is given by Darcy's law, and reads:

$$\left(v_f - v_s\right)\left(1 - \phi_p\right) = -\frac{k}{g\rho_w}\frac{\partial p_e}{\partial x_3} \tag{5.3}$$

where k is the permeability of the fluid mud layer and p_e is the excess pore water pressure defined as the difference between the actual pore water pressure p^f and the hydrostatic pore water pressure:

$$p_e = p^f - \int_{x_3}^{Z_s} g\rho_w \mathrm{d}x_3' \tag{5.4}$$

in which Z_s is the level of the water surface. Note that (5.3) implies that interstitial water can flow through all the pores of the mud, i.e. no distinction is made between likely variations in hydraulic resistance within the network-forming flocs and the space in between. This effect is empirically accounted for through the value of the gross permeability parameter k. Furthermore, because of continuity, the relation between v_f and v_s reads:

$$\phi_p v_s + \left(1 - \phi_p\right) v_f = 0 \tag{5.5}$$

Combining (5.3), (5.4) and (5.5) and introducing the effective stress concept, implying that the total stress at a specific level is the sum of the grain-induced effective stress p^s (commonly denoted by σ' in soil mechanics) and the pore pressure:

$$p = p^f + p^s \tag{5.6}$$

yields:

$$v_s = \frac{k}{g\rho_w}\frac{\partial\left(p^f + g\rho_w x_3\right)}{\partial x_3} = k + \frac{k}{g\rho_w}\frac{\partial p^f}{\partial x_3} = k + \frac{k}{g\rho_w}\left(\frac{\partial p}{\partial x_3} - \frac{\partial p^s}{\partial x_3}\right) \tag{5.7}$$

Substituting from (5.2) gives:

$$v_s = k - \frac{k}{g\rho_w}\left(\phi_p g\rho_s + \left(1-\phi_p\right)g\rho_w + \frac{\partial p^s}{\partial x_3}\right) = -k\frac{\rho_s - \rho_w}{\rho_w}\phi_p - \frac{k}{g\rho_w}\frac{\partial p^s}{\partial x_3} \tag{5.8}$$

Substituting v_s from (5.8) into Ξ_s in (5.1) gives an equation for self-weight consolidation processes in Eulerian co-ordinates for the volumetric concentration:

$$\frac{\partial \phi_p}{\partial t} + \frac{\partial}{\partial x_i}\left(\left(u_i - \delta_{i3}k\frac{\rho_s - \rho_w}{\rho_w}\phi_p\right)\phi_p\right) - \frac{\partial}{\partial x_i}\left(D_s\frac{\partial \phi_p}{\partial x_i} + \delta_{i3}\frac{k\phi_p}{g\rho_w}\frac{\partial p^s}{\partial x_3}\right) = 0 \tag{5.9}$$

Neglecting the advective velocity u_i and the diffusive term $D_s\partial\phi_p/\partial x_i$ yields the well-known Gibson equation, but in a Eulerian reference frame (e.g. Toorman, 1996 and Merckelbach, 1996). Equation (5.9) contains an advective and a diffusive-like part. Toorman's unified theory consists of a combination of (5.9) with the classical vertical advection-diffusion equation (3.13). This implies the decomposition of u_i and ϕ_p in ensemble averaged and fluctuating components, which is of course only relevant within the turbulent water column, and within the fluid mud layer. Note that, when consolidation is relevant, mud motions are not turbulent, and the terms containing the permeability contain no fluctuating components. The combined equation reads:

$$\frac{\partial \phi_p}{\partial t} + \frac{\partial}{\partial x_i}\left(\left(u_i - \delta_{i3}\Xi_s\right)\phi_p\right) - \frac{\partial}{\partial x_i}\left(\left(D_s + \Gamma_T\right)\frac{\partial \phi_p}{\partial x_i} + \delta_{i3}\frac{k\phi_p}{g\rho_w}\frac{\partial p^s}{\partial x_3}\right) = 0 \tag{5.10}$$

where u_i and ϕ_p now represent ensemble mean quantities. We propose, following Toorman, a simple superposition of the hindered settling effects (see Section 4.4) and the advective part of the consolidation process. This procedure was also followed by Bürger and Concha (1998). They stressed that the type of the combined equation changes from hyperbolic in the hindered settling regime to parabolic in the consolidation regime. In their numerical scheme this was overcome by the use of a continuous function for the increase in diffusivity from the hyperbolic regime to the parabolic regime. It is remarkable that they did not apply a similar continuous function for the advection term.

In (5.10) no problems arise with respect to this change in type, because of the diffusion coefficient D_s. The combination of hindered settling and consolidation is conveniently captured with:

$$\Xi_s(\phi) = f_{hs} + \frac{f_c}{1+\eta f_c}, \quad \text{with:}$$

$$f_{hs} = W_{s,r}\frac{(1-\phi_*)(1-\phi_p)}{1+2.5\phi}, \quad \text{and} \tag{5.11}$$

$$f_c = k\frac{\rho_s - \rho_w}{\rho_w}\phi_p$$

Note that ϕ ($\equiv \Sigma c/c_{gel}$) represents the volumetric concentration of the fluid mud forming mud flocs in the water column, but not of the flocs in the fluid mud layer itself. It can therefore exceed unity in the fluid mud, because of which the parameter $\phi_* = \min\{1,\phi\}$ is introduced - see also Chapter 4. In the range of interest, the product $\eta f_c << 1$,. where η is a user-defined parameter. This formulation yields a continuous transition between the effects of hindered settling and consolidation, as will be shown in the next paragraph.

We propose to apply fractal relations for the permeability and effective stress following Kranenburg (1994), see also Merckelbach et al. (1998):

$$k = K_k \phi_p^{\left(\frac{-2}{3-n_f}\right)} \tag{5.12}$$

and

$$p^s = K_p \phi_p^{\left(\frac{2}{3-n_f}\right)} \tag{5.13}$$

in which n_f is the fractal dimension and K_k and K_p are empirical coefficients. Typical values for soft mud deposits are (Merckelbach, 1998): $K_k \approx 2\cdot10^{-14}$ m/s and $K_p \approx 2\cdot10^{8}$ Pa at $n_f = 2.71$; these values were found from experiments with mud from the Caland-Beerkanaal in The Netherlands. In Section 4.2 we have argued that the fractal dimension n_f for consolidating bed conditions is considerably larger (i.e. $n_f \approx 2.6$ to 2.8) than for the aggregates suspended in the water column ($n_f \approx 2.0$). With these values, and assuming c_{gel} = 100 g/l and $\eta = 10^5$ s/m, we obtain the continuous relationship from (5.11) shown in Fig. 5.1.

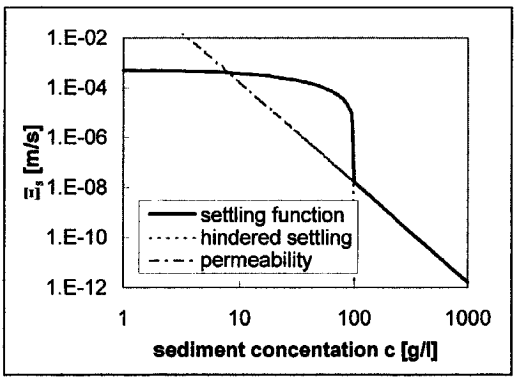

Fig. 5.1: Variation of settling function Ξ_s with concentration c for $n_f = 2.6$ and other parameter settings as given in the text.

We observe a jump of two decades in Ξ_s around the gelling point at the transition from the hindered settling regime (c < 100 g/l) to the consolidation regime (c > 100 g/l), i.e. at the water - fluid mud interface. This well-known phenomenon in consolidation theory (e.g. Sills, 1997, Toorman, 1992, Toorman and Huysentruyt, 1996) is not yet fully understood. However, it seems likely that the transition between hindered settling and consolidation takes place over a short distance (of the order of several floc sizes), as these two processes are different from a physical point of view. Moreover, this jump in Ξ_s corresponds to the rapid growth of the fractal dimension around the interface, as discussed in Section 4.2.

Our approach implies that we assume that the consolidating fluid mud layer is permanently at equilibrium, i.e. no thixotropic effects are taken into account. Substituting (5.12) and (5.13) into (5.10) yields a combined equation for the mass balance of cohesive sediment, both in the turbulent water column and in the consolidating fluid mud layer. It has the form of the classical advection-diffusion equation for suspended sediment:

$$\frac{\partial \phi_p}{\partial t} + \frac{\partial}{\partial x_i}\left((u_i - \delta_{i3}\Xi_s)\phi_p\right) - \frac{\partial}{\partial x_i}\left(\left(D_s + \Gamma_T + \delta_{i3}\phi_*^2\Gamma_c\right)\frac{\partial \phi_p}{\partial x_i}\right) = 0 \tag{5.14}$$

in which

$$\Gamma_c \equiv \frac{2K_k K_p}{(3-n_f)g\rho_w} \tag{5.15}$$

and Ξ_s is given by (5.11). Γ_c can be considered as a (constant) diffusion coefficient. A typical value of Γ_c would be $\Gamma_c = 3\cdot10^{-9}$ m^2/s, using Merckelbach's (1998) values for K_k and K_p. We have introduced the factor ϕ_*^2 in the diffusion term to ensure that the term containing Γ_c is very small for sub-gelling conditions. Note that Γ_c is comparable, but not identical to the coefficient of consolidation C_F, defined in classical consolidation literature (e.g. Gibson et al., 1967, Lee and Sills, 1980).

We solve (5.14) in a co-ordinate system relative to a horizontal base plane $x_3 = 0$ through which no sediment or pore water is transported, i.e. for single-drained conditions. Similarly, no sediment or water is transported through the water surface at $x_3 = Z_s$. Hence, the boundary conditions to (5.14) read:

$$\left\{(u_3 - \Xi_s)\phi_p - \left(D_s + \Gamma_T + \phi_*^2\Gamma_c\right)\frac{\partial \phi_p}{\partial x_3}\right\}\Bigg|_{x_3=Z_s} = 0 \tag{5.16}$$

$$\left\{(u_3 - \Xi_s)\phi_p - \left(D_s + \Gamma_T + \phi_*^2\Gamma_c\right)\frac{\partial \phi_p}{\partial x_3}\right\}\Bigg|_{x_3=Z_b} = 0 \tag{5.17}$$

If we omit the time derivative, the velocity component u_i, the hindered settling term, and the diffusion and eddy diffusivity in (5.14), an equation is obtained for the final equilibrium concentration distribution for consolidation only. This equilibrium concentration can be obtained by solving $\partial p^s / x_3 = -g(\rho_s - \rho_w)\phi_p$, which, upon substituting from (5.13), yields the expected result that the equilibrium concentration

distribution for consolidation is a function of the effective stress distribution of the sediment only, and not of its permeability. However, the time scale at which this equilibrium is attained is a function of the permeability.

From (5.14) we observe that two time scales T_c for consolidation can be defined, determined by the permeability term and by the diffusive consolidation term. The first time scale amounts to $T_{c,p} \approx \delta/\Delta k\phi_p$, where $\Delta = (\rho_s-\rho_w)/\rho_s$ and δ is the thickness of the fluid mud layer, and the second time scale to $T_{c,d} \approx \delta^2/\Gamma_c$. In general, the consolidation rate is governed by $T_{c,p}$, except possibly for very impermeable or very thin layers of fluid mud, when $T_{c,d}$ may become smaller than $T_{c,p}$. This is illustrated with a numerical example for a 0.1 m thick layer of fluid mud with an initial concentration of 100 g/l. If we take $K_k = 2{\cdot}10^{-14}$ m/s, $\Gamma_c = 3{\cdot}10^{-9}$ m^2/s and $n_f = 2.71$, we find $T_{c,p} \approx 3.4$ hrs and $T_{c,d} \approx 38$ days. This would mean that during slack tide already considerable consolidation can take place, possibly with some strength development, affecting the resuspension of the fluid mud layer and the turbulence production at the water - fluid mud interface.

The new combined mass balance equation (5.14) with the boundary conditions (5.16) and (5.17) has been implemented in our 1DV POINT MODEL, details of which are presented in Appendix B.

5.3 The stress tensor for consolidating fluid mud

Sections 5.2 and 5.3 deal with the development of the vertical normal stresses in the fluid mud layer under the influence of self-weight consolidation. In this section we propose a simple description for the shear stress in a sheared fluid mud layer. We assume local equilibrium, i.e. thixotropic effects are not accounted for. For this purpose we treat the fluid mud layer as a Bingham visco-plastic fluid (Malvern, 1969):

$$\begin{aligned} &\sqrt{\tau_{ij}^s \tau_{ij}^s} = \tau_B + 2\mu\sqrt{D_{ij}D_{ij}} \quad \text{for} \quad \tau_{ij}^s \geq \tau_B \\ &D_{ij} = 0 \qquad\qquad\qquad\quad \text{for} \quad \tau_{ij}^s < \tau_B \end{aligned} \tag{5.18}$$

in which τ_B is the Bingham or yield strength and μ is the viscosity of the fluid mud, and the rate of deformation tensor D_{ij} is defined as:

$$D_{ij} = \frac{1}{2}\left(\frac{\partial u_j}{\partial x_i} + \frac{\partial u_i}{\partial x_j}\right) \tag{5.19}$$

We assume that the fluid mud layers are thin compared to the horizontal dimensions and that shearing takes place in horizontal planes only. Because of this boundary layer approximation, the Bingham model reduces to:

$$\begin{aligned} &\tau_{ij}^s = \frac{D_{ij}}{|D_{ij}|}\tau_B + 2\mu D_{ij} \quad \text{for} \quad \tau_{ij}^s \geq \tau_B \\ &D_{ij} = 0 \qquad\qquad\qquad\quad \text{for} \quad \tau_{ij}^s < \tau_B \end{aligned} \tag{5.20}$$

The residual or remolded strength of the mud, measured after failure, can be regarded as the yield strength in (5.18) and (5.20). Kranenburg (1994) showed that in accordance with fractal theory this strength and the viscosity μ obey a power law behaviour. We omit the influence of the shear rate on the viscosity:

$$\tau_B = K_y \phi_p^{\frac{2}{3-n_f}} \tag{5.21}$$

and

$$\mu = K_\mu \phi_p^n \tag{5.22}$$

By applying (5.22) we neglect all effects of the structure of the flocs within the fluid mud. The exponent n can vary between about 2 and 6 for different muds and is dependent on the activity of the sediment (i.e. the fraction of fines). Equations (5.21) and (5.22) have to be established from rheological experiments. Note that (5.21) and (5.22) apply within the fluid mud layer only, i.e. for $c \geq c_{gel}$.

The value of K_y is closely related to K_p (e.g. Van Kessel, 1997). For a Poisson ratio of 0.5 for instance, $K_y = 0.5K_p$.

Substitution of (5.20) into (3.2), c.q. (3.6), provides us with a momentum equation for the fluid mud layer and its strength under the influence of self-weight consolidation, which makes the model particularly suitable to describe consolidation processes around periods of slack water, i.e. during the shorter times scale $T_{c,p}$. We have grossly neglected all time-dependent effects in the strength evolution of the mud and its response to deformations, as a result of which the effects of strength build-up or strength break-down by external forces, such as turbulent stresses, wave loading, etc. cannot accounted for.

Finally it is noted that a rheological model slightly different from (5.20) is implemented in the 1DV POINT MODEL; this formulation is given in Appendix B. The model of equ. (B.36) implies a general plastic model without any actual yield strength. This model is preferred above (5.20), as it yields only one value for the stress at zero strain rate, whereas the stress in (5.20) is undefined for zero strain rate.

5.4 Numerical experiments and comparison with literature

5.4.1 The numerical experiments by Townsend and McVay

Townsend and McVay (1990) presented a series of numerical consolidation experiments that have been used for an intercomparison of various numerical consolidation models in Florida's mining industries. It is regarded as a benchmark in the literature. All simulations have been carried out with numerical models based on the classical Gibson equation, which is generally accepted to yield a proper description of the consolidation process. The test case most suitable for validating our consolidation model is "Scenario A", a numerical single-drained, self-weight consolidation experiment with a slurry of initial height $\delta_0 = 9.55$ m and initial uniform void ratio $e_0 = 14.8$ ($e = (1-\phi_p)/\phi_p$), i.e. $\phi_{p,0} = 0.063$, which is beyond the gelling value.

This implies that hindered settling effects do not play a role. The material functions are given by:

$$k = 0.2532 \cdot 10^{-6} \mathrm{e}^{4.65}, \text{ and} \tag{5.23a}$$

$$e = 7.72 p^{s^{-0.22}}, \text{ yielding } p^s \approx 10.8 \cdot 10^3 e^{-4.55} \tag{5.23b}$$

where k has the dimension [m/day], p^s has the dimension [kPa] and where e is the void ratio. The minimal void ratio attained after a year of consolidation was computed to be about e_m = 6.4, hence the maximal concentration obtained was about $\phi_{p,m}$ = 0.14. In the range $0.06 < \phi_p < 0.2$, the functions (5.23) can be approximated with:

$$k = 4.12 \cdot 10^{-13} \phi_p^{-5.3} \text{ [m/s]}, \text{ and} \tag{5.24a}$$

$$p^s = 1.42 \cdot 10^8 \phi_p^{4.9} \text{ [Pa]} \tag{5.24b}$$

which values are close to Merckelbach's (1998). Comparison with (5.12) and (5.13) shows that (5.24a) corresponds to a fractal dimension n_f = 2.62 and (5.24b) to n_f = 2.59, which is in agreement with the values mentioned in Section 4.2.

Townsend and McVay's (1990) numerical consolidation experiment has been adopted as a bench mark for assessing the performance of consolidation models. The results of a series of simulations with various numerical consolidation models are intercompared in the paper by Townsend and McVay. We therefore also compare our model, as implemented in the 1DV POINT MODEL, with this benchmark experiment.

We discretise the column of 9.55 m height with an initial sediment concentration C_0 = 167.7 g/l in 200 equidistant layers and apply a time step of 12.0 hrs. The coefficients in the material functions (5.12) and (5.13) are set to $K_k = 4.12 \cdot 10^{-13}$ m/s and $K_p = 1.42 \cdot 10^8$ Pa, consistent with (5.20). After some trial and error, the best result is obtained for a fractal dimension n_f = 2.62. The diffusion coefficient D_s is set at 10^{-10} m^2/s and the reference settling velocity $W_{s,r}$ at 10^{-10} m/s. The computed lowering of the interface over a period of 10,000 days is presented in Fig. 5.2a and of the vertical distribution of the void ratio after 1 year of consolidation in Fig. 5.2b.

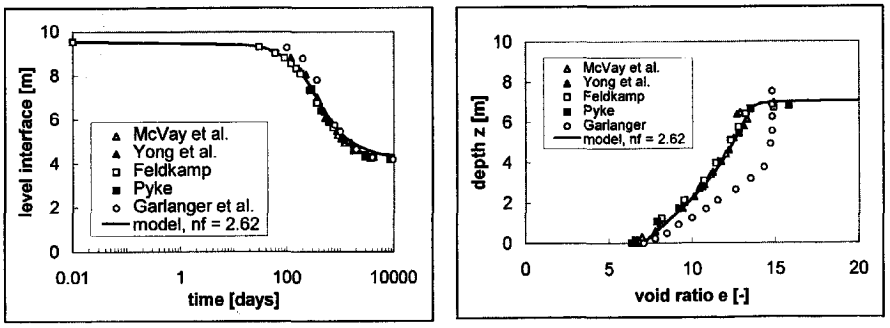

Fig. 5.2a and -b: Lowering of interface over 10,000 days and void ratio distribution after 1 year of consolidation.

The computed results are compared with the numerical results of various authors, presented in the paper by Townsend and McVay (1990). It is shown that our model

slightly underpredicts the final lowering of the interface at the end of the consolidation period, and slightly overpredicts the void ratio near the bed after one year of consolidation in comparison to most other models. These differences are attributed to the fact that it is not possible to match the material functions (5.23), as applied in the Gibson equation, exactly with the power-law form (5.12) and (5.13) as applied in our Eulerian description. However, the agreement is satisfactory and we conclude that our consolidation model is capable of correctly simulating the features of a consolidating mud column.

5.4.2 Consolidation experiments on Calandkanaal mud

At Delft University of Technology a series of experiments was carried out in an annular flume to establish the erosion of fluid mud layers (Winterwerp and Kranenburg, 1997). The experiments were carried out with mud from the silt traps in the Caland/Beerkanaal, one of the major navigation channels of the Port of Rotterdam, The Netherlands. The work included some simple consolidation experiments in the flume and in a settling column of 30 cm height with a suspension of initial concentration C_0 = 60 g/l. During these experiments, the location of the (upper) interface was monitored, and the vertical sediment concentration distribution at t = 3 hrs and t = 6 hrs was measured with a conductivity probe. From the initial settling rate, the settling velocity was estimated at $W_s = 4 \cdot 10^{-5}$ m/s at the initial sediment concentration. No other parameters, such as the pore pressure, were measured.

parameter		value	remarks
water depth	h	0.273 m	
flow velocity	U	none	
water density	ρ_w	1020 kg/m^3	
sediment density	ρ_s	2650 kg/m^3	
initial sediment concentration	C_0	60 kg/m^3	homogeneous profile
settling velocity	$W_{s,r}$	0.2 mm/s	constant
hindered settling		yes	
gelling concentration	c_{gel}	100 kg/m^3	
fractal dimension	n_f	2.71	
permeability coefficient	K_k	$1 \cdot 10^{-14}$ m/s	
effective stress coefficient	K_p	$1 \cdot 10^9$ Pa	
Bingham strength coefficient	K_y	$0.5 \cdot 10^9$ Pa	
number of layers		200	equidistant
time step	Δt	0.05 min	
relaxation time	T_{rel}	0.10 min	

Table 5.1: Parameter settings in numerical consolidation simulation.

In a separate experiment, with the same mud though, Van Kessel (1996), measured the yield strength of the consolidating mud at t = 1 hr with a miniature sounding technique. The results of these measurements can be used to establish whether the simple strength model proposed in Section 5.3 yields reasonable results. For this

purpose, the aforementioned consolidation experiment is simulated with the 1DV POINT MODEL. The relevant model parameters are established by trial and error, as they have not been measured; these parameters are summarised in Table 5.1.

From the kink in the measured level of the water-mud interface (Fig. 5.3), the gelling concentration c_{gel} is estimated at 100 g/l. The value of $W_{s,r}$ is chosen such to match the measured $W_s = 4 \cdot 10^{-5}$ m/s at $C_0 = 60$ g/l. This gelling concentration also implies that the initial phase of the experiment is in the hindered settling regime. The fractal dimension, and the coefficients for permeability and effective stress are first taken identical to those measured by Merckelbach (see Section 5.2) albeit for a different set-up. These parameters have been changed a bit, to obtain a better agreement between the model and the measurements.

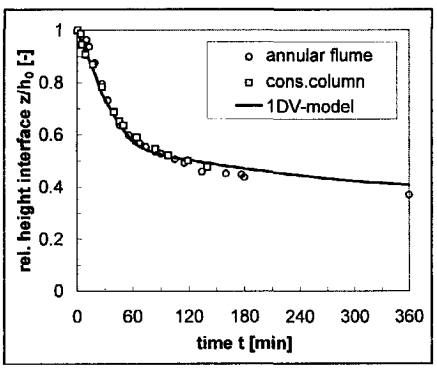

Fig. 5.3: Level of interface as a function of time.

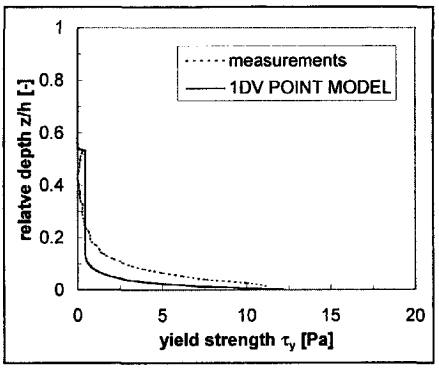

Fig. 5.4: Yield strength in consolidating bed at t = 1 hr.

The results of the numerical simulation are presented in Fig. 5.3 through 5.5. Fig. 5.3 shows that the settling rate is overpredicted in the hindered settling regime by the model, and underpredicted in the consolidation regime. The strength measured after 1 hr is underpredicted by a few Pa, see Fig. 5.4. The measurements suggest that in the upper part of the consolidating bed (i.e. beyond $z/h = 0.2$) hardly any strength has developed; this is also predicted by the model. Fig. 5.5 shows that the computed sediment concentration in the upper part of the consolidating bed is overpredicted, whereas lower in the bed higher concentrations are measured than computed. This difference seems to increase with time. This may be the result of segregation in the experiments, which is not accounted for in our model; the long tail in the concentration distribution near the bed is typical for segregation effects.

It is likely that a better match between measurements and model can be obtained by tuning the model parameters further (e.g. Merckelbach et al., 1998). This is however not an easy task, as no data on the material parameters are available and the number of degrees of freedom (model parameters) is large. Moreover, segregation effects probably have to be taken into account. As the major purpose of this exercise is to show that the present formulations allow the build up of a reasonable strength profile in a consolidating bed, we will not try to improve the numerical results further.

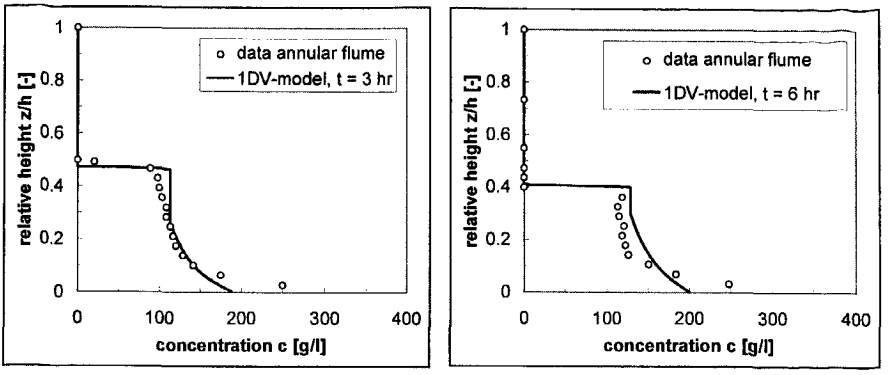

Fig. 5.5: Vertical concentration profiles at t = 3 hrs and t = 6 hrs.

6. The concept of saturation

In the next part of this study we concentrate on the processes in the vertical direction and neglect the advective contributions to the sediment transport in horizontal directions. It is therefore convenient to replace the notations for the horizontal co-ordinate and velocity x_1 by x and u_1 by u, respectively, and for the vertical co-ordinate x_3 and the vertical velocity u_3 by z and w, respectively. We maintain the orientation of the co-ordinate frame defined in Section 3.1 - see also Appendix B.

6.1 Saturation under steady state flow conditions

It is well known that the vertical concentration distribution of loose granular material attains an equilibrium profile under steady turbulent flow conditions. Such a distribution is generally known as a Rouse-profile. If the flow is over an alluvial bed, this equilibrium profile represents the equilibrium sediment transport by the flow, or its sediment carrying capacity. This fact is described and explained in all text books on sediment transport (e.g. Vanoni, 1977) and has been observed in numerous laboratory experiments and field measurements.

These equilibrium profiles are the result of a balance between the downward sediment flux by gravity (i.e. the settling of the sediment) and an upward flux by turbulent mixing. If the flow velocity would decrease, the vertical mixing, i.e. the upward flux, decreases, as a result of which less sediment can be kept in suspension. The surplus of sediment settles and a new equilibrium profile is formed, but at a lower concentration level. Vice versa, when the flow velocity would increase, an equilibrium profile is formed at a higher concentration level by entraining sediment from the bed. However, such equilibrium profiles are not formed instantaneously with changing flow velocity, as settling and mixing take time. These so-called relaxation effects have been elaborated by Galappatti and Vreugdenhill (1986), for instance. It is important to realise that in this concept it is implicitly assumed that the vertical mixing is not, or only slightly, affected by the presence of the sediment (i.e. buoyancy effects are small), and that the depositing particles form a rigid water-bed interface immediately, at which turbulence production is possible.

This is not the case for cohesive sediment. Because of flocculation, large flocs are formed and hindered settling becomes important, generating lutoclines and considerable buoyancy effects during deposition. Moreover, initially no rigid water-bed interface is formed by the depositing sediment. Turbulence production at the fluid mud - water interface is only possible after some time, when at this interface strength is built up by gelling and consolidation effects.

Let us analyse a sediment-laden flow over a rigid, horizontal bed with an amount of cohesive sediment equal to its sediment carrying capacity. When the flow velocity decreases slightly, sediment starts to settle, not to form a rigid bed, but a layer of fluid mud, thus creating a two-layer system. At the interface between the two layers vertical turbulence mixing is damped strongly, decreasing the sediment carrying capacity in the upper part of the flow further. This results in a snowball effect with a catastrophic

collapse of the vertical turbulence field and the vertical sediment concentration profile. In this study, the suspended sediment concentration for cohesive sediment just prior to this collapse is denoted by the term "saturation concentration" to distinguish it from the equilibrium concentration for sand.

The importance of this saturation concept for the behaviour of high-concentrated mud suspensions was discussed by Winterwerp (1996) and this terminology was introduced by Uittenbogaard et al. (1996). The first ideas, though, on the existence of such a saturation concentration for cohesive sediment were presented by Teisson et al. (1992); however, at that time no explicit physical meaning was attributed to this concentration. The concept of the saturation concentration for cohesive sediment is based on the empirical evidence (e.g. Turner, 1973) that a turbulent shear flow field collapses when the flux Richardson number Ri_f exceeds a critical value of about 0.15. Ri_f follows from the turbulent kinetic energy equation and is defined as the ratio of the buoyancy destruction and production terms (e.g. Section 3.3):

$$Ri_f = -\frac{g\overline{w'\rho'}}{\rho\overline{u'w'}\,\partial u/\partial z} = -\frac{\Delta g\overline{w'c'}}{\rho\overline{u'w'}\,\partial u/\partial z} \tag{6.1}$$

where a prime denotes the fluctuating part of the horizontal and vertical velocity components u and w, of the density of the water-sediment suspension ρ, and of the suspended sediment concentration c, g is the gravitational acceleration, z is the vertical co-ordinate (positive upward) and Δ ($\Delta = (\rho_s-\rho_w)/\rho_s$) is the relative excess sediment density. The overbar denotes averaging over the turbulent time scale. A more complete definition of Ri_f contains also the turbulent diffusion term in the denominator of (6.1) (e.g. Ivey and Imberger, 1991), but we have neglected this term in our analyses as it is small for shear flow: inclusion would only affect the level of saturation, not its concept.

Starting our evaluation of HCMS-dynamics at low, i.e. sub-saturated concentrations, a zero-order approximation is justified, in which the eddy diffusivity is not (yet) affected by buoyancy. By assuming a logarithmic velocity profile $\left(\partial u/\partial z = u_*/\kappa z\right)$, a parabolic viscosity profile $\left(\nu_T = \kappa u_* z(1-z/h)\right)$ and local equilibrium between settling and mixing $\left(\overline{w'c'} = -w_s c\right)$, we obtain an equation for the vertical concentration profile c_s at which saturation occurs:

$$c_s(z) = \frac{0.15\rho}{\Delta g\kappa}\frac{u_*^3}{hw_s}\left(\frac{h}{z}-1\right) \tag{6.2}$$

where u_* is the shear velocity, h the water depth, w_s the local settling velocity and κ the von Kármàn constant. At concentrations beyond c_s (super-saturated) the turbulence collapses and the flow is not able to carry the sediment in suspension. As c_s represents a vertical profile, a more convenient parameter is the depth-averaged saturation concentration C_s, which can also be regarded as a scaling parameter for saturated suspensions (e.g. Galland et al., 1997):

$$C_s \equiv \frac{1}{h}\int_0^h c_s \mathrm{d}z = K_s\frac{\rho}{\Delta g}\frac{u_*^3}{hW_s} \tag{6.3}$$

where K_s is a proportionality constant.

Let us next carry out a series of numerical experiments with the 1DV POINT MODEL to study this saturation concept further and to verify the scaling relation (6.3).

6.2 Numerical simulations for steady state flow conditions

The saturation concept is well illustrated through two simulations with the 1DV POINT MODEL for a hypothetical open-channel flow of 16 m depth, a constant depth-averaged flow velocity of $U = 0.2$ m/s and a constant settling velocity $W_s = 0.5$ mm/s. Initially, the sediment is distributed homogeneously over the water depth. The initial concentration C_0 was increased in small steps until saturation occurred. Other parameter settings are listed in Table 6.1 below; the grid size near the bed is set at $0.0002\times\Delta z$, which is increased by a factor 1.5 until a grid size of $0.01\times\Delta z$ is attained. Fig. 6.1 shows the time evolution of the sediment concentration for initial concentrations of $C_0 = 0.023$ g/l and Fig. 6.2 for 0.024 g/l.

It is clear that the 0.023 g/l case represents saturation conditions: a small increase in C_0 results in a catastrophic collapse of the concentration profile. The final concentration profile in the first case is more or less Rousean, whereas in the second case a fluid mud layer is formed. The coefficient K_s has a value of about $K_s \approx 0.7$.

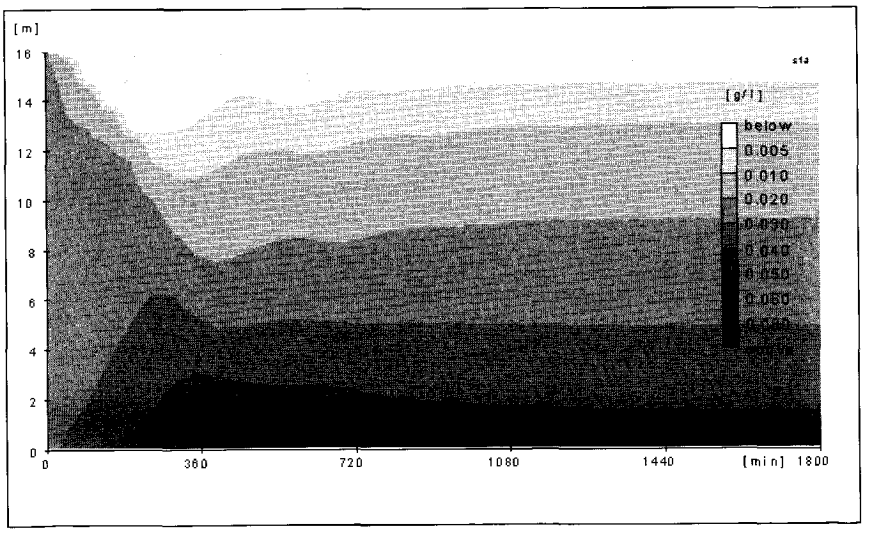

Fig. 6.1: Isolutals for saturated ($C_0 = 0.023$ g/l) suspensions in open-channel flow.

Fig. 6.3 shows the time development of the vertical distributions of suspended sediment concentration and eddy diffusivity for the 0.024 g/l case (note the logarithmic scales). From these profiles we observe that the eddy diffusivity in the upper part of the water column slowly collapses, which is caused by the buoyancy term in the turbulent energy equation. An equilibrium is obtained only after 3000 min., whereas the time scale for settling amounts to $h/W_s = 16$ m / $0.5\cdot10^{-3}$ m/s = 533

min. only. We also observe that after 1000 min., when the majority of the sediment is deposited in the fluid mud layer, the eddy diffusivity profile is restored a bit because some turbulence can be produced by the shear flow in the water column, but remains an order of magnitude smaller than in the non-buoyant case (t = 10 min.). This implies that this collapse is irreversible as long as the fluid mud layer remains soft, i.e. as long as no yield stress builds up, so that no turbulence can be generated at the water-mud interface. Hence, in addition to the scaling law (6.3), time scales for gelling and consolidation enter the physical description of HCMS-dynamics. Only when the flow velocity is increased sufficiently, can the fluid mud be remixed over the water column. This is further elaborated in the next section.

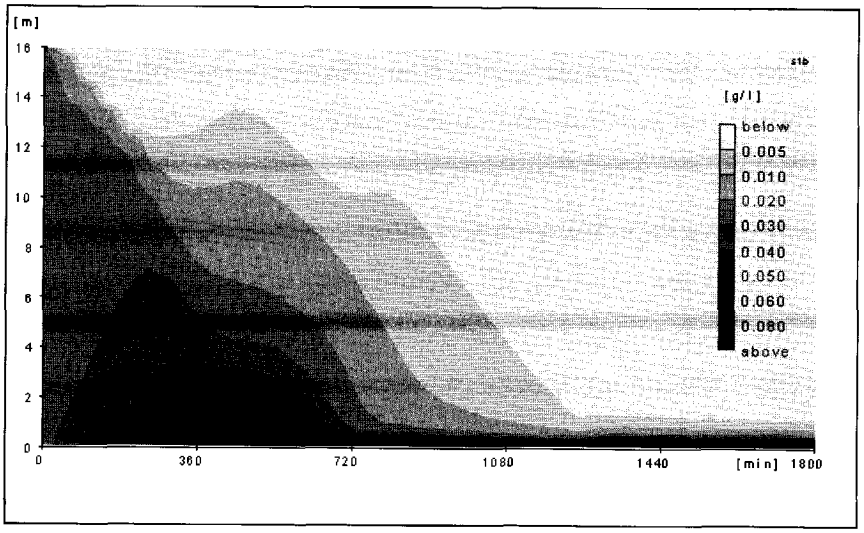

Fig. 6.2: Isolutals for super-saturated (C_0 = 0.024 g/l) suspensions in open-channel flow.

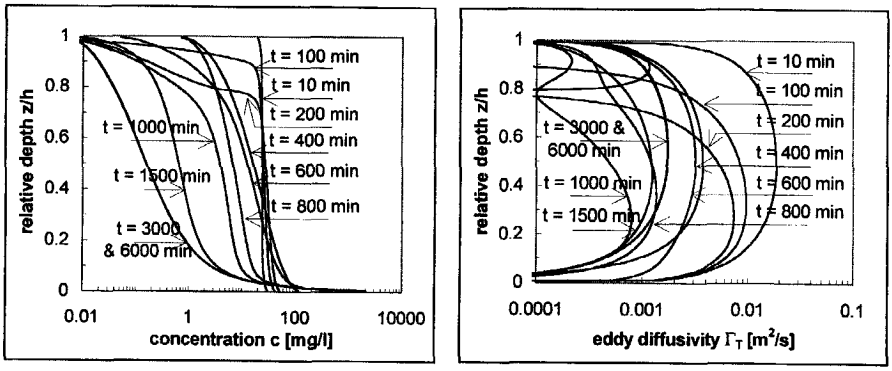

Fig. 6.3: Concentration and eddy diffusivity profiles for C_0 = 0.024 g/l.

Next, a series of numerical simulations is carried out to verify the scaling law (6.3), by increasing, for given hydrodynamic conditions, the initial sediment concentration in small steps until a collapse of the concentration profile is observed. The setting of the various parameters is given in Table 6.1 below. The results are presented in Fig. 6.4, where the computed vertical flux $W_s \times C_s$ is plotted versus the mean flow velocity U. We observe that the numerical results follow the functional relationship (6.3) properly. The influence of numerical parameters, e.g. the time step and the number of layers is also studied and can be seen to be negligible.

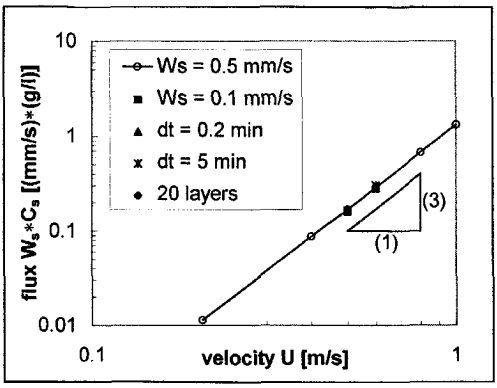

Fig. 6.4: Saturation flux $W_s \times C_s$ as a function of flow velocity (results from 1DV POINT MODEL).

We also carried out a series of simulations with a hindered settling formula, both for steady state and tidal flow conditions. In this case the absolute values of the saturation concentration increased slightly. However, the general trend, i.e. a catastrophic collapse of the concentration profile and turbulence remained the same.

parameter		value	remarks
water depth	h	8 & 16 m	constant; also for tidal flow
flow velocity	U	variable	steady state
tidal flow amplitude	U_m	variable	
bed roughness	z_0	1 mm	hydraulically rough
water density	ρ_w	1020 kg/m^3	
sediment density	ρ_s	2650 kg/m^3	
initial sediment concentration	C_0	variable	homogeneous profile
settling velocity	W_s	0.5 mm/s	constant
hindered settling		no	
water-bed exchange		no	
Prandtl-Schmidt-number	σ_T	0.7	
number of layers		109	logarithmic/equidistant
time step	Δt	1 min	
relaxation time	T_{rel}	2 min	

Table 6.1: Reference parameter settings in numerical simulations.

Also the effects of internal waves and of a change in the value of the coefficient $c_{3\varepsilon}$ (i.e. $c_{3\varepsilon} = 0$) in the k-ε turbulence model (3.20b) have been studied. Again a change in

the value of C_s has been found (considerable in the $c_{3\varepsilon}$-case), but the catastrophic behaviour is maintained. The results of these simulations are not presented herein.

6.3 Saturation under tidal flow conditions

In the preceding sections we have shown that for steady state flow conditions a saturation concentration C_s can be defined representing the maximal sediment load that can be carried by the flow. In Sections 6.3 and 6.4 we show that also for tidal conditions such a maximal sediment load exists. In this case we define the saturation concentration C_s as the amount of sediment, initially distributed homogeneously over the water depth, that can be carried by the turbulent flow in the form of a Rousean-like vertical profile during just one instant of the tidal cycle. From a formal dimensional analysis it can be shown that in this case the magnitude of C_s is also governed by other non-dimensional parameters, i.e. by the relative settling time $T_s' \equiv T_s/T = h/W_sT$ and the relative mixing time $T_m' \equiv T_m/T = h^2/\Gamma_T T \propto h/Tu_*$, where h is the water depth, W_s the settling velocity, Γ_T the vertical eddy diffusivity and T is one quarter of the tidal period, i.e. the acceleration or deceleration phase for a sinusoidal tide. Similarly, we define the sedimentation depth h_s as the distance a particle can travel during decelerating tide: $h_s \equiv W_sT$.

Let us sketch the variation of the sediment concentration profile with time during a tidal cycle in a water column of large depth, as shown in Fig. 6.5. We start with a homogeneous suspension of sediment of concentration C_0 at maximal flow velocity (MFV). If C_0 equals the saturation concentration C_s, the sediment will settle during decelerating tide. All sediment initially above the level $z > h_s$ will remain in the water column. The sediment below this level will form a layer of fluid mud on the bed at $z = 0$ (see Fig. 6.5). The maximal thickness of this layer δ_m around slack water (SW) amounts to $\delta_m = h_s c_{gel}/C_0 = h_s c_{gel}/C_s$. During accelerating tide this fluid mud will be remixed over the water column by entrainment processes.

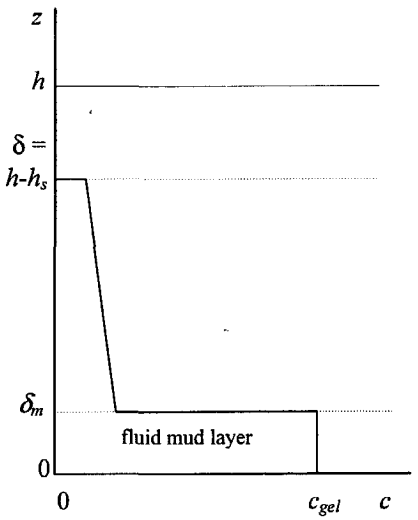

Fig. 6.5: Schematic concentration profile around slack water ($h_s < h$)

In the present analysis we do not account for consolidation or thixotropic effects in the fluid mud layer, hence the fluid mud layer is treated as a Newtonian fluid. When the fluid accelerates, it is therefore the fluid mud layer that becomes turbulent because of bed friction. This is illustrated in the series of graphs in Fig. 6.6 showing the evolution of the turbulent kinetic energy and eddy diffusivity profiles with time ($t = 0$,

60, 90, 120, 180, 300, 450, 600, 750 and 900 minutes) in a flow with constant acceleration, together with the related velocity and concentration profiles, as computed with the 1DV POINT MODEL. We start with zero velocity over the entire depth of 10 m and a fluid mud layer of 20 % of the total water depth at an initial concentration of 5 g/l; the settling velocity of the sediment is set at 0.1 mm/s.

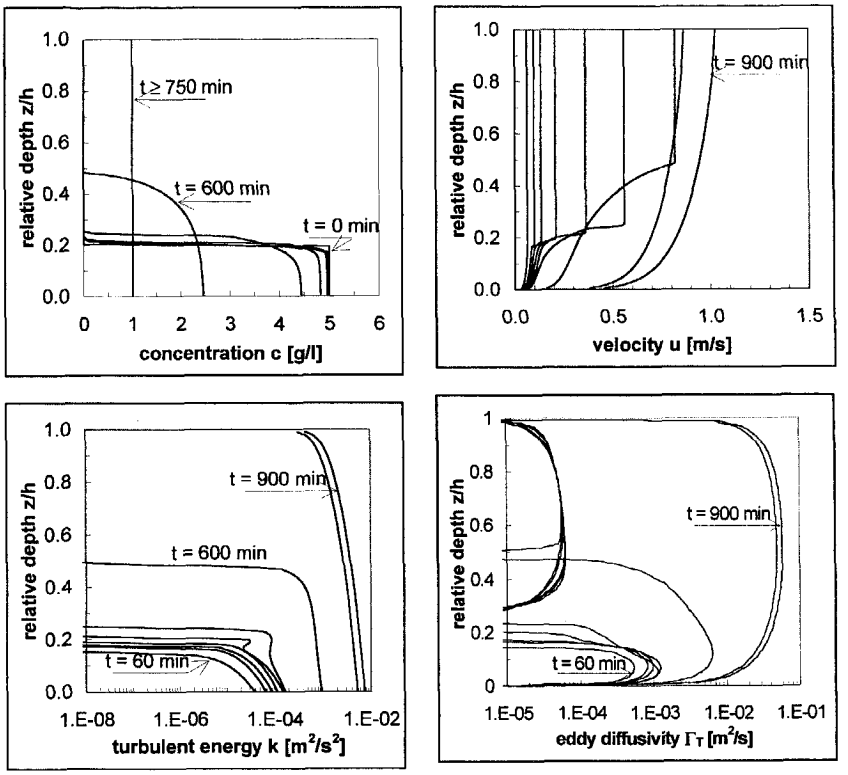

Fig. 6.6: Entrainment of fluid mud layer during accelerating flow; results of simulations with 1DV POINT MODEL.

These results clearly show that turbulence is generated at the bed, and that the water column is entrained by the fluid mud layer, which is thickened and diluted. The eddy diffusivity higher in the water column is not exactly zero, but one to two orders of magnitude smaller than within the fluid mud layer: the vertical sediment transport is effectively damped by the large density gradients near the water - fluid mud interface. Only at $t \geq 900$ min., when the sediment is fully mixed over the water column, is a parabolic eddy diffusivity profile obtained (note that the abscissa of Fig. 6.6d has a logarithmic scale).

Next, we investigate when the fluid mud may be treated as a turbulent viscous Newtonian fluid. The transition from laminar to turbulent flow occurs when the so-called effective Reynolds number exceeds a critical value $Re_{e,c}$, where Re_e is a

function of the common Reynolds number Re and a co-called "cohesive Reynolds number" Re_y. Re_e is defined as:

$$\frac{1}{Re_e} = \frac{1}{Re} + \frac{1}{Re_y} \quad \text{where} \quad Re = \frac{4U_m\delta_m}{\nu_m} \quad \text{and} \quad Re_y = \frac{8\rho_m U_m^2}{\tau_B} \tag{6.4}$$

where U_m is the mean velocity in the fluid mud layer, τ_B is the Bingham strength of the fluid mud (see also Section 5.3) and ν_m and ρ_m are the viscosity and density of the fluid mud. According to Liu and Mei (1989) the critical effective Reynolds number amounts to about $Re_{e,c}$ = 2,000 to 3,000. This criterion was recently validated by Van Kessel (1997) against experiments on laminar and turbulent mud flows over a sloping bed.

For a 1 m thick fluid mud layer with ρ_m = 1100 kg/m^3 and μ_m = 5 mPas, the fluid mud layer would become turbulent at a velocity of U_m = 0.2 to 0.6 m/s for τ_B = 0.1 to 1.0 Pa. From these figures we anticipate that the entrainment process described in this section will generally occur as long as the fluid mud layer has not gained too much strength. Indeed, this behaviour has been observed in the field, e.g. Wolanski et al. (1988, 1996), Kineke et al. (1995, 1996) and Le Hir (1997).

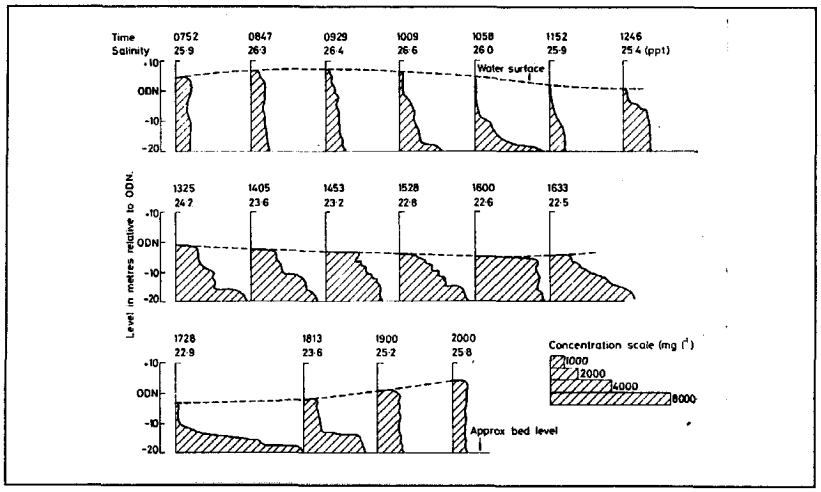

Fig. 6.7: Sediment concentration profiles measured in the Severn (Crickmore, '82).

Fig. 6.7 shows a diagram with a series of vertical sediment concentration profiles measured in the Severn (Crickmore, 1982). At the head of the Severn estuary, the tide behaves as a standing wave and mean water level more or less corresponds to maximal flow velocity, which occurs around t = 12:46 hr in Fig. 6.7. We observe that during accelerating tide, sediment is remixed over the water column. Of particular interest is the time period t = 13:25 hr through 15:28 hr when we observe that the fluid mud layer is diluted, whereas the concentration in the overlying water column remains virtually unchanged; around t = 16:00 hr, the sediment is well mixed over the water column at a concentration of almost 5 g/l. After that, the sediment starts to settle

again. It is noted that the profiles in Fig. 6.7 are probably also affected by horizontal advection. However, as deposition takes place throughout the estuary, the sediment must be remixed somewhere to attain the profiles shown.

When fluid mud gets time to consolidate, thus gaining strength, it can only be eroded by the floc erosion processes commonly described in the literature (e.g. Mehta et al., 1988). This is not further elaborated here.

The entrainment process described is elaborated by Kranenburg (1994, 1998), and his analysis is used to establish the scaling laws for C_s under tidal conditions. We start, following Kranenburg, with the balance equation for the turbulent kinetic energy k, neglecting horizontal advection (see also Section 3.3):

$$\frac{\partial k}{\partial t} = D + P - B - \varepsilon \tag{6.5}$$

where D is a diffusion term, P the turbulence production, B represents buoyancy destruction, i.e. the work required to keep the sediment in suspension, and ε the energy dissipation rate per unit mass. When this balance equation is integrated, using various approximations, over the turbulent layer, i.e. over the mud layer, we obtain an integral model describing the entrainment of water into the fluid mud layer. This is elaborated by Kranenburg (1994, 1998) to yield:

$$\begin{aligned} c_q \frac{\mathrm{d}}{\mathrm{d}t}\left(\delta u_*^2\right) &= c_q \delta \frac{\mathrm{d}u_*^2}{\mathrm{d}t} + c_q u_*^2 \frac{\mathrm{d}\delta}{\mathrm{d}t} = \\ &= c_s \left(U_w - U_m\right)^2 \frac{\mathrm{d}\delta}{\mathrm{d}t} + c_s' \left|U_w - U_m\right| u_*^2 + c_\sigma u_*^3 - 2\int_0^\delta B \mathrm{d}z \end{aligned} \tag{6.6}$$

where $\delta(t)$ is the thickness of the mixing layer with concentration c - see also Fig. 6.5. The various empirical coefficients have the following values: $c_q = 5.6$, $c_s = c_s' = 0.25$, and $c_\sigma = 0.42$. U_w is the mean velocity in the water column above the fluid mud layer and U_m is the mean velocity within the fluid mud layer. These two velocities have to be established from the momentum equations for the water and fluid mud layers, which should be solved simultaneously with (6.6). In the present analysis we assume $U_m = e_m U_w$, where e_m is a (time dependent) proportionality parameter, and $u_*^2 = \lambda U_m^2$. Hence $\left(U_w - U_m\right) = \left(1 - e_m\right)/e_m \sqrt{\lambda} u_* = \sqrt{\lambda'} u_*$. As $e_m \approx 0.2$ to 0.5 (see Fig. 6.6) and $\lambda \approx 0.0018$, and $\lambda' \approx 0.002$ to 0.03.

In the case where the upper (water) layer is turbulent, a similar integral model is obtained, which has been validated extensively against laboratory experiments (Winterwerp and Kranenburg, 1997).

In the following paragraphs we elaborate on the last term of (6.6). We have to distinguish between two regimes: REGIME 1: $h \le h_s$ and REGIME 2: $h > h_s$. In REGIME 1 all sediment in the water column can settle during decelerating tide to form a fluid mud layer and we do not have to deal with any sediment remaining above the fluid mud layer. In this case the thickness of the mixing layer δ in (6.6) equals the thickness of the fluid mud layer δ_m and the buoyancy term is described by:

$$\int_0^\delta B \mathrm{d}z = \int_0^{\delta_m} \left[\frac{\Delta g}{\rho_w} \overline{w'c'}\right] \mathrm{d}z \approx \frac{\Delta g}{\rho_w} \left[\delta_m W_s c_m + \frac{1}{2} \delta_m \Delta c_m \frac{\mathrm{d}\delta_m}{\mathrm{d}t}\right] \tag{6.7}$$

where $c_m(t)$ is the mean concentration in the fluid mud layer and $\Delta c_m(t) = c_m(t) - c_{z>\delta} = c_m(t)$; $c_{z>\delta}$ is the sediment concentration above the fluid mud layer. In deriving (6.7), we have used the mass balance equation - see Kranenburg (1994) or Kranenburg and Winterwerp (1997) for details. Substituting (6.7) into (6.6) and using conservation of mass ($c_m\delta_m = c_{m,0}\delta_{m,0} = hC_0$), where the subscript $_0$ refers to initial conditions (i.e. prior to entrainment, hence $c_{m,0} = c_{gel}$), a relation for the entrainment velocity $w_e = \mathrm{d}\delta_m/\mathrm{d}t$ is found:

$$\left[c_q u_*^2 + \Delta g \delta_m \frac{c_m}{\rho_w} - c_s\left(U_w - U_m\right)^2\right]\frac{\mathrm{d}\delta_m}{\mathrm{d}t} = \\ = c_s'\left|U_w - U_m\right|u_*^2 + c_\sigma u_*^3 - 2\Delta g \frac{c_m}{\rho_w} W_s \delta_m - c_q \delta \frac{\mathrm{d}u_*^2}{\mathrm{d}t} \tag{6.8}$$

From (6.8) Kranenburg (1998) concludes that entrainment can occur if:

$$c_s'\left(U_w - U_m\right)u_*^2 + c_\sigma u_*^3 > 2\Delta g \frac{c_{gel}}{\rho_w} W_s \delta_{m,0} + c_q \delta_{m,0} \frac{\mathrm{d}u_*^2}{\mathrm{d}t} \tag{6.9}$$

i.e. some time after slack water. This is also shown in Fig. 6.6. The entrainment rate w_e would become very large if:

$$c_s\left(U_w - U_m\right)^2 \uparrow c_q u_*^2 + \Delta g \delta_m c_m/\rho_w \tag{6.10}$$

However, for non-stratified conditions, w_e cannot become larger than $0.28u_*$ (e.g. Tennekes and Lumley, 1994). An order of magnitude estimate shows that in stratified flow, the first and last terms of (6.8) are small in comparison to the other terms.

Our definition of C_s implies that during accelerating tide, all fluid mud has to be remixed over the whole water depth. This means that the entrainment velocity w_e has to be sufficiently large to mix the entire fluid mud layer during accelerating tide over the water depth. Thus:

$$\int_0^T w_e \mathrm{d}t = h, \quad \text{hence } w_e \approx h/T \tag{6.11}$$

For saturated conditions in REGIME 1 we have to substitute $C_s = C_0$, and upon substitution of (6.11) into (6.8) we find:

$$\frac{C_s}{\rho_w} \approx \frac{\frac{c_s}{\lambda'}\frac{h}{u_* T} + \frac{c_s'}{\sqrt{\lambda'}} + c_\sigma}{\frac{\Delta g h}{u_*^2}\frac{h}{u_* T} + \frac{2\Delta g h}{u_*^2}\frac{W_s}{u_*}} = \frac{\frac{c_s}{\lambda'}T_m' + \frac{c_s'}{\sqrt{\lambda'}} + c_\sigma}{\left(T_m' + 2\beta\right)Ri_*} \tag{6.12}$$

where we have defined the Rouse number $\beta \equiv W_s/u_*$ and a bulk Richardson number $Ri_* \equiv \Delta g h/u_*^2$.

Under REGIME 2 not all sediment settles during decelerating tide. This implies that the fluid mud layer obtains a thickness $\delta_{m,0} = h_s c_{gel}/C_0$, and that, in addition to the work given by (6.7), work has to be done to remix the sediment beyond $z = h_s$ over the rest of the water column. We distinguish between two phases. In Phase 1, the fluid mud layer becomes turbulent and is remixed over the sedimentation depth; the related

entrainment velocity is referred to as w_{e1}. We ignore the fact that during this process the sediment beyond $z = \delta_m$ may continue to settle because of the small eddy diffusivity above the water - fluid mud interface. In Phase 2, all the sediment is remixed over the entire water column; the related entrainment velocity is referred to as w_{e2}. Our definition of C_s implies that during accelerating tide, both the fluid mud and the suspension above have to be remixed over the whole water depth. This means that:

$$T \approx \frac{h_s}{w_{e1}} + \frac{h - h_s}{w_{e2}} \tag{6.13}$$

In Phase 1, the concentration difference over the water - fluid mud interface for a saturated suspension follows form $\Delta c_m \delta_m \approx (c_m - C_0)\delta_m = C_s W_s T - C_0 \delta_m \approx C_s W_s T$, which is correct for the major part of the accelerating tide. We may again neglect the storage term in (6.6). Hence, upon integration of the buoyancy term of (6.6) over the thickness of the fluid mud layer δ_m, as in (6.7), the entrainment rate w_{e1} becomes:

$$\frac{w_{e1}}{u_*} \approx \frac{\dfrac{c_s'}{\sqrt{\lambda'}} + c_\sigma - \dfrac{2\Delta g h C_s}{\rho_w u_*^2}\dfrac{W_s}{u_*}\dfrac{W_s T}{h}}{\dfrac{\Delta g h C_s}{\rho_w u_*^2}\dfrac{W_s T}{h} - \dfrac{c_s}{\lambda'}} = \frac{\left(\dfrac{c_s'}{\sqrt{\lambda'}} + c_\sigma\right)T_s' - 2Ri_*\beta\dfrac{C_s}{\rho_w}}{Ri_*\dfrac{C_s}{\rho_w} - \dfrac{c_s}{\lambda'}T_s'} \tag{6.14}$$

In Phase 2 of the entrainment process, the concentration difference over the water - fluid mud interface for a saturated suspension follows from $\Delta c\delta \approx c\delta = C_0 h = C_s h$. In Phase 2, the Richardson number is not too large in general, as a consequence of which the storage term in (6.6) may not be neglected a priori. Hence, the entrainment velocity w_{e2} becomes:

$$\frac{w_{e2}}{u_*} \approx \frac{\dfrac{c_s'}{\sqrt{\lambda'}} + c_\sigma - \dfrac{2\Delta g h C_s}{\rho_w u_*^2}\dfrac{W_s}{u_*} - \dfrac{2c_q}{u_*}\dfrac{\delta}{u_*}\dfrac{\mathrm{d}u_*}{\mathrm{d}t}}{c_q + \dfrac{\Delta g h C_s}{\rho_w u_*^2} - \dfrac{c_s}{\lambda'}} = \frac{\dfrac{c_s'}{\sqrt{\lambda'}} + c_\sigma - Ri_*\beta\dfrac{C_s}{\rho_w} - \dfrac{2c_q}{u_*}\dfrac{\delta}{u_*}\dfrac{\mathrm{d}u_*}{\mathrm{d}t}}{c_q + Ri_*\dfrac{C_s}{\rho_w} - \dfrac{c_s}{\lambda'}} \tag{6.15}$$

Substitution of (6.15) and (6.14) into (6.13) yields a scaling equation for the saturation concentration under REGIME 2. It is obvious that the result is not very practical; even the explicit form of (6.12) for REGIME 1 is too complicated to get a clear picture of the functional relation between C_s and the various physical parameters like U, u_*, h and W_s. However, we can establish some workable relations for extreme conditions. For this purpose, we distinguish for REGIME 2 between $h_s/w_{e1} >> (h-h_s)/w_{e2}$, which implies $h \approx h_s$, but $h > h_s$, and $h_s/w_{e1} << (h-h_s)/w_{e2}$, which implies $h >> h_s$. We will not elaborate on the case $\beta >> 1$, as this represents the suspension of (coarse) sand, which, of course, does not form fluid mud layers upon deposition. This gives the scaling relations summarised in Table 6.2:

	$\beta << 1$		
	$T_m' << 1$ $T_m' << \beta$	$T_m' << 1$ $T_m' >> \beta$	$T_m' >> 1$ $T_m' >> \beta$
REGIME 1: $h \le h_s$	$C_s \propto \frac{1}{\beta Ri_*}$ $\propto \frac{\rho_w u_*^3}{\Delta g h W_s}$	$C_s \propto \frac{1}{T_m' Ri_*}$ $\propto \frac{\rho_w T u_*^3}{\Delta g h^2}$	$C_s \propto \frac{1}{Ri_*}$ $\propto \frac{\rho_w u_*^2}{\Delta g h}$
REGIME 2; phase 1: $h > h_s$	$C_s \propto \frac{T_s'}{\beta Ri_*} \propto \frac{\rho_w u_*^3}{\Delta g T W_s^2}$		
REGIME 2; phase 2: $h >> h_s$	$C_s \propto \frac{1}{\beta Ri_*}$ $\propto \frac{\rho_w u_*^3}{\Delta g h W_s}$	$C_s \propto \frac{1}{T_m' Ri_*}$ $\propto \frac{\rho_w T u_*^3}{\Delta g h^2}$	$C_s \propto \frac{1}{Ri_*}$ $\propto \frac{\rho_w u_*^2}{\Delta g h}$

Table 6.2: Scaling relations for C_s under tidal conditions.

Table 6.2 shows that the saturation conditions are governed by four sets of non-dimensional parameters, i.e. a bulk Richardson number Ri_*, the relative sedimentation time T_s' (or relative sedimentation depth h_s/h), the Rouse number β and the relative mixing time T_m'. In the next section we investigate whether these scaling relations are supported by simulations with the 1DV POINT MODEL.

6.4 Numerical simulations for tidal flow conditions

Similar to the simulations described in Section 6.2, we study the evolution of the sediment concentration profile as a function of time for various initially homogeneous concentration profiles, increasing C_0 in small steps until the flow is no longer able to remix the sediment for just one instant over the entire water column. The value of C_0 just prior to this total collapse is defined as the saturation concentration for tidal flow conditions.

These simulations are carried out for a constant water depth of 8 m, a 12.5 hrs period semi-diurnal, sinusoidal tide with a velocity amplitude of 0.5 m/s, and a settling velocity of 0.5 mm/s including hindered settling with c_{gel} = 80 g/l; the other parameters are identical to those listed in Table 6.1. Fig. 6.8 presents this evolution for initial concentrations of C_0 = 0.28 and 0.29 g/l, showing a dynamic equilibrium for the 0.28 g/l case with alternating periods of fluid mud formation and periods of complete mixing over the water column, and a complete collapse for the 0.29 g/l case. The 0.28 g/l case obviously represents the saturation conditions defined in Section 6.3.

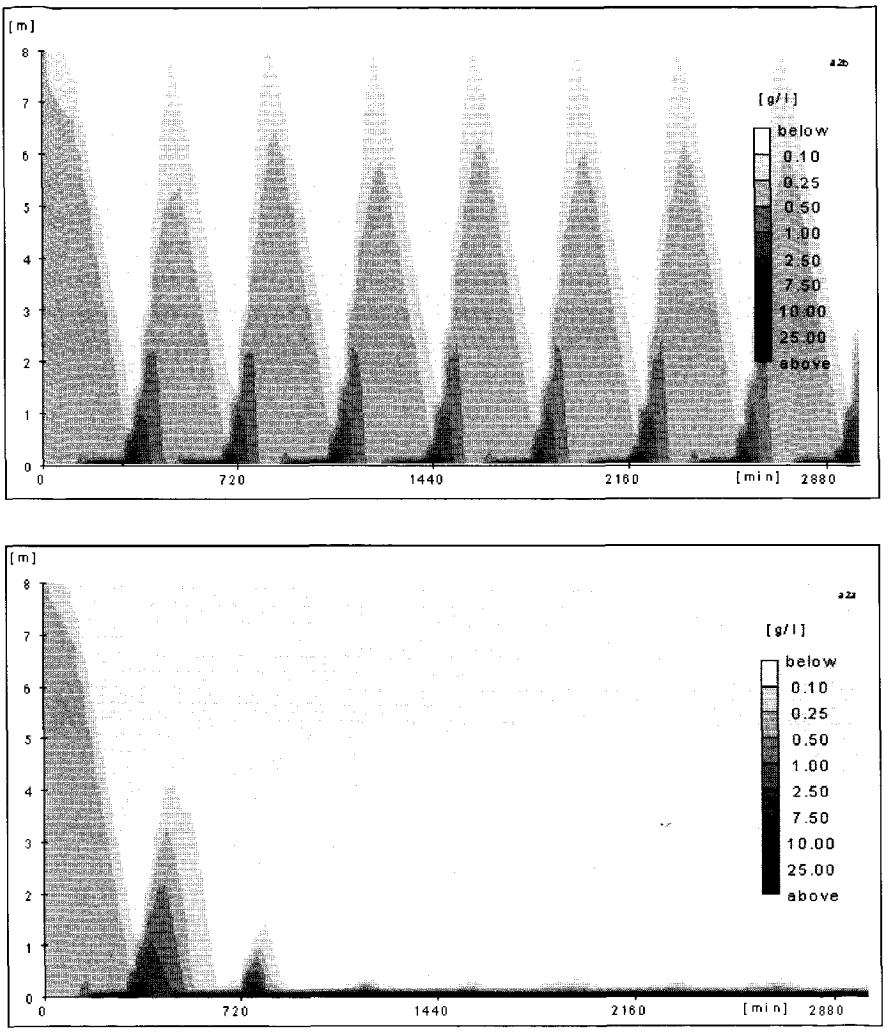

Fig. 6.8: Time evolution of the concentration profile for saturated conditions (above: C_0 = 0.28 g/l) and for super-saturated conditions (below, C_0 = 0.29 g/l).

We conclude that, similar to the case of steady state flow situations, also for tidal flow conditions a saturation concentration C_s can be defined which represents the maximal sediment load that can be carried in suspension by a turbulent flow. At a sediment load beyond this saturation condition, the flow is not able to mix the entire fluid mud layer over the whole water depth. As a result, the vertical concentration (density) gradient grows with time, eventually resulting in a complete collapse of the turbulence. This process is irreversible, as long as the fluid mud has not gained sufficient strength to re-enable turbulence production at the water - fluid mud interface.

Before we study the scaling relations derived in Section 6.3, we first have to elaborate on some numerical aspects that do not play a role under steady flow conditions. We note that fluid mud is temporarily formed at (near) saturation conditions in tidal flow, which process cleanses the water column for the larger part. As a result, the density gradient, hence the Richardson number at the lower grid points in the 1DV POINT MODEL, are functions of the local grid size if the grid size is too large: if the lowest grid size would be very large, for instance, the maximal concentration that could occur is determined by the total amount of sediment in the water column (up to the sedimentation depth), whereas for much smaller grid sizes the maximal possible concentration equals the gelling concentration. Hence we expect that the saturation concentration is a function of the grid size, or in other words, convergence of the numerical solution of the 1DV-equations requires a small grid size. This is illustrated in Fig. 6.9 showing computed C_s-values as a function of the first grid size from the bed for the conditions of Fig. 6.8. The abscissa shows the relative grid size of the first grid point from the bed; the size of the next grid cell is increased by a factor 1.5, etc., until a relative grid size of 1 % is obtained. The time step is varied consistently (see Appendix B).

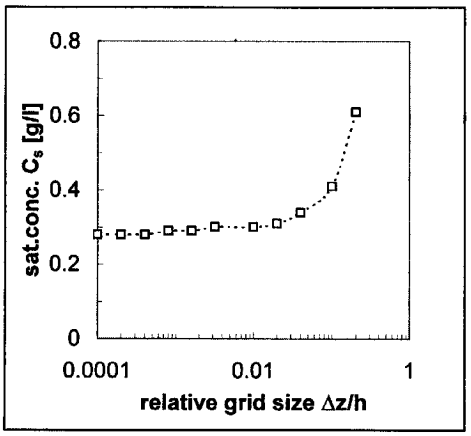

Fig. 6.9: Variation of saturation concentration C_s as a function of the first relative grid size $\Delta z/h$ at the bed.

We observe that for these particular conditions, a relative near-bed grid size beyond 1 % yields very inaccurate results, whereas grid-size-independent results are obtained for a relative near-bed grid size of 0.04 % or smaller.

Next, the results of a series of simulations is presented to show the variation of C_s as a function of flow parameters. The first grid size near the bed is set at $\Delta z/h$ = 0.02 %. The results are presented in Fig. 6.10 and 6.11 - the parameter settings are summarised in Table 6.1.

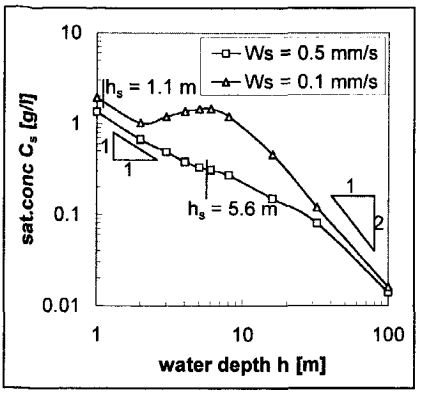

Fig. 6.10: Variation of C_s with h for different settling velocities

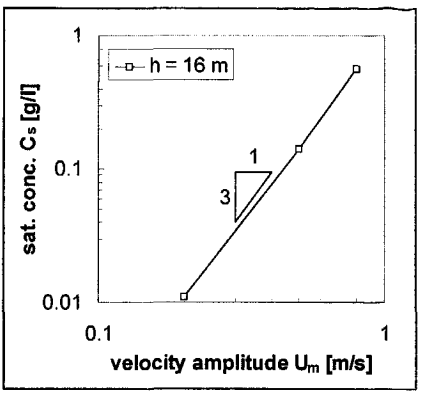

Fig. 6.11: Variation of C_s with U_m for W_s = 0.5 mm/s

The variation of C_s with h for a semi-diurnal tide with a velocity amplitude of U_m = 0.5 m/s shows a fairly irregular trend - see Fig. 6.10 - especially for W_s = 0.1 mm/s. However, this trend is consistent with the classification of Table 6.2. By increasing the water depth, as in Fig. 6.10, we follow the path represented by the dotted arrow in Table 6.2. We observe that at small depth, C_s scales with $1/h$. In REGIME 2, phase 1, the h-dependency disappears, but C_s becomes proportional to W_s^{-2}: indeed Fig. 6.10 shows that the influence of differences in settling velocity becomes more important. Finally, at large h, C_s scales with $1/h^2$, and becomes independent of W_s, which is also shown in Fig. 6.10.

Fig. 6.11 represents conditions for which $T_m' \approx T_s' \approx 1$. The variation of C_s with U_m can therefore not be read from Table 6.2. Instead, we have to use the full formulation given by equ. (6.12), from which it follows that C_s scales with U_m^n, where $2 < n < 3$ (but n is almost 3).

We conclude that also for tidal flow conditions a saturation concentration C_s can be defined, and that the numerical analyses with the 1DV POINT MODEL support the analyses of Section 6.3. For extreme conditions simple scaling relations for C_s can be derived, but in general this is not the case and C_s has to be established separately for each site, and probably for varying flow conditions at that site as well.

6.5 Other effects on saturation

In the two next sections we elaborate a bit further on the effects of waves and flocculation on the saturation behaviour of the flow, with the help of a series of numerical experiments with the 1DV POINT MODEL

We have no experimental data available to sustain our numerical experiments. However, we use reasonable parameter settings, and the results appear to match our experience, in a qualitative sense anyway

6.5.1 The effects of waves on saturation

The erosive capacity of waves largely exceeds their mixing capacity. Hence one may expect that under storm conditions coastal sites may become super-saturated when abundant amounts of mud are available in the sea bed.

The mud in the sea bed may be mobilised by liquefaction of the bed by the stresses induced by the waves (e.g. De Wit, 1995, Van Kessel, 1997 and Van Kesteren et al., 1997). If this does not occur, the bed still may be eroded by the wave-induced shear stresses at the bed, which generally exceed the flow-induced shear stresses by an order of magnitude. At present, only the latter process is accounted for in the 1DV POINT MODEL.

parameter	symbol	value	parameter	symbol	value
water depth	h [m]	16	velocity amplitude	U_m [m/s]	0.5
bed roughness	z_0 [m]	0.001	Pr-Sch. number	σ_T [-]	0.7
water density	ρ_w [kg/m^3]	1020	sediment density	ρ_s [kg/m^3]	2650
initial concentration	C_0 [g/l]	0	gelling point	c_{gel} [g/l]	80
hindered settling		yes	flocculation		no
buoyancy		yes			
settling velocity	W_s [mm/s]	0.5	crit. stress deposit.	τ_d [Pa]	0.5
erosion parameter	M [kg/m^{2}s]	10^{-4}	crit. stress erosion	τ_e [Pa]	0.1
wave height	$H_{1/3}$ [m]	1.8	wave period	T_{rms} [s]	4.8
mean wave height	H_{rms} [m]	1.3	time step	Δt [min]	1.0
relaxation time	t_{rel} [min]	2.0	grid size	$\Delta z/h$ [-]	0.01

Table 6.3: Parameter settings 1DV-simulation of wave effect on saturation.

Fig. 6.12 presents the results of a simulation for a hypothetical case, showing the effect of 1.8 m waves on the suspended sediment concentration in steady state open-channel flow, initially containing no sediment. The various numerical parameters are summarised in Table 6.3.

Fig. 6.12 shows that initially the suspended sediment concentration increases with time. However, after about 500 min. the vertical concentration profile starts to collapse and a fluid mud layer is formed. We have some doubt that the erosion mechanism under wave action is described fully by the classical Partheniades formulation, presently used in the 1DV POINT MODEL. For instance, the simulation of Fig. 6.12 predicts that the flow and waves continue to erode the sea bed, as a result of which the amount of sediment in the fluid mud layer continues to grow. In reality, one would expect that the waves are damped by the fluid mud layer and that the underling bed becomes protected from further erosion.

However, from a conceptual point of view the picture sketched in Fig. 6.12 seems realistic in the sense that the flow becomes super-saturated due to the wave action. Such a result can only be obtained if sediment-induced buoyancy effects are included in the simulations. We conjecture that this mechanism is responsible for the occurrence of the mud banks encountered in many coastal zones (e.g. Kerala coast, India; west coast of Korea; coast of Surinam, etc.).

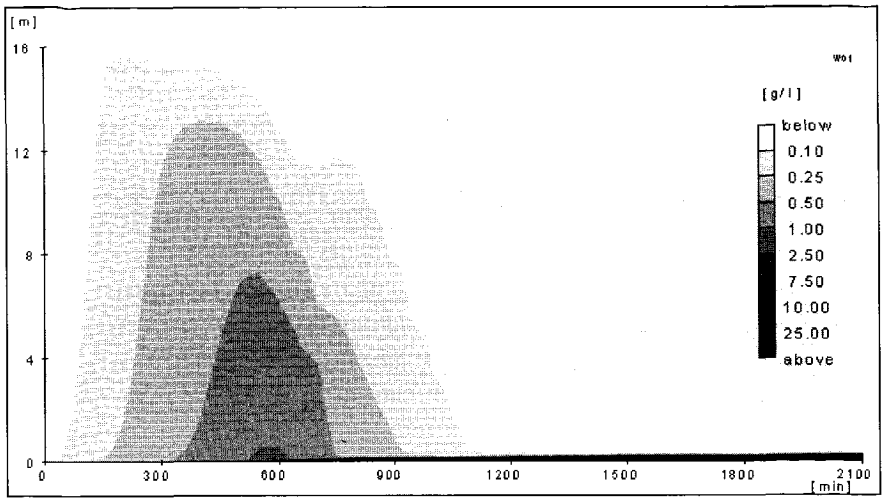

Fig. 6.12: Auto-saturation by wave action - results of 1DV-simulation.

We conclude from our analyses that waves have two opposing effects on the saturation behaviour in coastal areas. First, waves augment the vertical mixing by increasing the effective bed roughness, as a result of which the saturation concentration C_s increases. Second, waves can erode the sea bed, augmenting the available amount of cohesive sediment. When the sea bed contains abundant amounts of mud, the latter mechanism is dominant, and mud banks are generated because of a process, that can be called auto-saturation.

6.5.2 The effects of flocculation on saturation

In the Sections 6.1 through 6.4 we have studied the saturation behaviour of HCMS under stationary and tidal flow conditions. However, we carried out the simulations with a constant settling velocity, omitting the flocculation processes, characteristic of cohesive sediment. From our analysis presented in Section 4.8.1 we have deduced that the flocculation largely affects the value of the settling velocity. Especially around slack water, when the mixing capacity of the flow is small, flocs will grow, further destabilising the concentration profile. Thus, we may expect that flocculation also affects the saturation behaviour of HCMS.

Flocculation effects on the saturation behaviour are studied through a series of simulations similar to those described in Section 6.4, i.e. simulations are carried out, starting with a homogeneous initial suspended sediment concentration C_0. This concentration is increased in small steps until the flow becomes super-saturated. The relevant parameter settings are summarised in Table 6.4. The parameters of the flocculation model are set at the reference values of Section 4.6.2, except for the aggregation efficiency parameter e_c, which is halved to obtain a larger flocculation time, so that the lutocline formation happens less fast.

parameter	symbol	value	parameter	symbol	value
sinusoidal tide			tidal period	T [hrs]	12.5
water depth	h [m]	16	velocity amplitude	U_m [m/s]	Fig. 6.13
bed roughness	z_0 [m]	0.001	Pr-Sch. number	σ_T [-]	0.7
water density	ρ_w [kg/m^3]	1020	sediment density	ρ_s [kg/m^3]	2650
initial concentration	C_0 [g/l]	varies	buoyancy		yes
hindered settling		yes	flocculation		yes
settling velocity	w_s [mm/s]	comp.	gelling point	c_{gel} [g/l]	comp.
efficiency parameter	e_c [-]	0.066	efficiency parameter	e_c [-]	0.066
efficiency parameter	e_c [-]	0.066	shape factor	f_s [-]	1.0
form factor	α [-]	1.0	form factor	β [-]	1.0
exponent	p [-]	1.0	exponent	q [-]	0.5
time step	Δt [s]	10.0	relaxation time	t_{rel} [s]	20.0
grid size	$\Delta z/h$ [-]	0.001-0.01: log. distribution near wall			

Table 6.4: Parameter settings 1DV-simulation of flocculation effect on saturation.

The results for two simulations with U_m = 0.7 m/s and C_0 = 0.41 and 0.42 g/l are presented in Fig. 6.13 and 6.14, showing that the sudden collapse, found in Chapter 6, is also found with the flocculation model. Note that the collapse of the concentration profile in Fig. 6.14 is not complete, as in Fig. 6.8. The saturation concentration for these conditions apparently amounts to C_s = 0.41 g/l. The results at other velocity amplitudes are summarised in Fig. 6.15, which is to be compared with Fig. 6.11, obtained for a constant settling velocity of W_s = 0.5 mm/s.

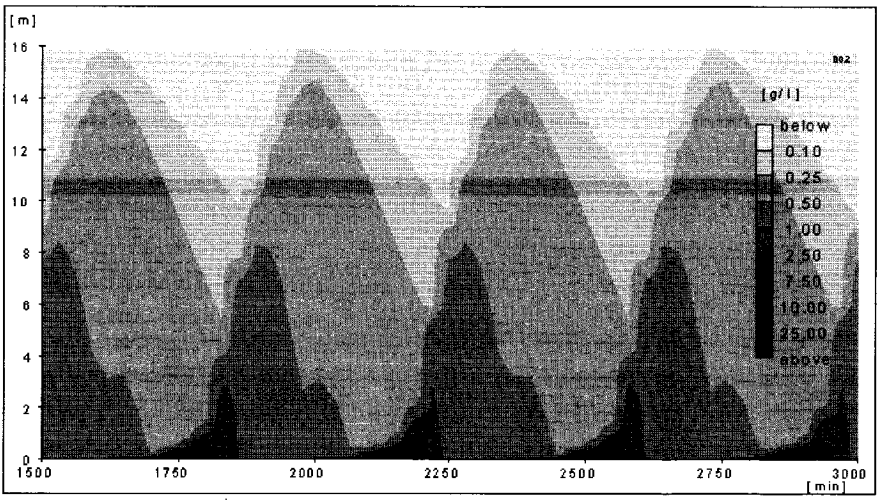

Fig. 6.13: Time evolution of the concentration profile for saturated conditions: flocculation model and C_0 = 0.41 g/l.

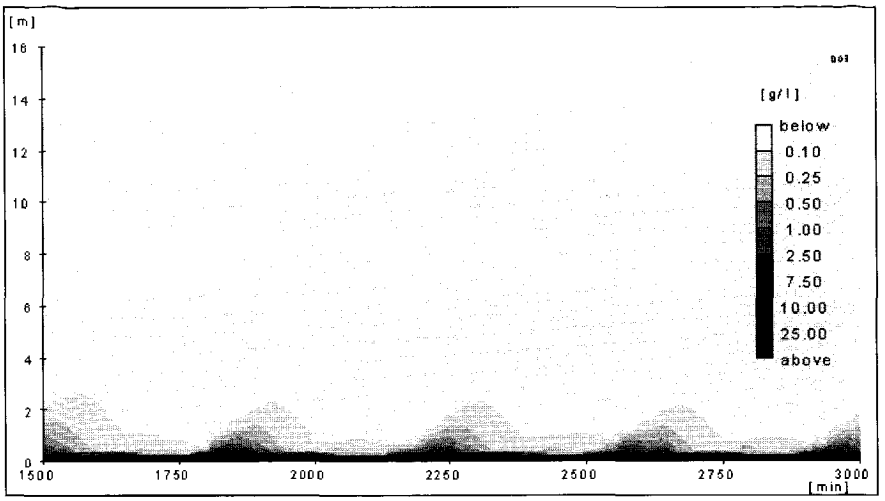

Fig. 6.14: Time evolution of the concentration profile for super-saturated conditions: flocculation model and C_0 = 0.42 g/l.

Fig. 6.15 shows that for the smaller tidal flow velocities, C_s, as computed with the flocculation model, is larger than in the case of a constant settling velocity. A direct comparison is not possible however, as the computed w_s cannot directly be compared with a constant value W_s = 0.5 mm/s, as used for Fig. 6.11. It is interesting though to observe that for increasing U_m the two saturation concentrations become comparable. For even larger values of U_m, the flocculation model is likely to predict lower values of C_s than in case of a constant settling velocity: the sediment concentration itself progressively augments the settling velocity as computed with the flocculation model (e.g. equ. (4.44)), and, as a result, affects the value of C_s.

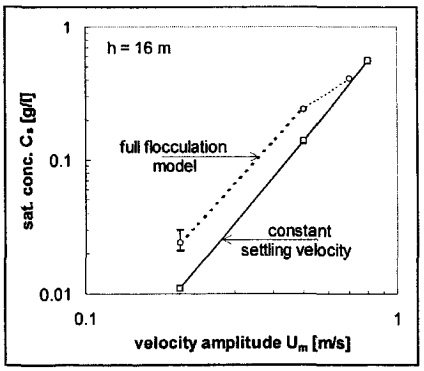

Fig. 6.15: Variation of saturation concentration C_s with velocity amplitude U_m - effect of flocculation (see also Section 6.4 and Fig. 6.11).

Fig. 6.16 presents computed vertical profiles for the saturated case (C_0 = 0.41 g/l) of the flow velocity u, the eddy diffusivity Γ_T, the dissipation parameter G, the gelling concentration c_{gel}, the settling velocity w_s and the suspended sediment concentration c at various instants.

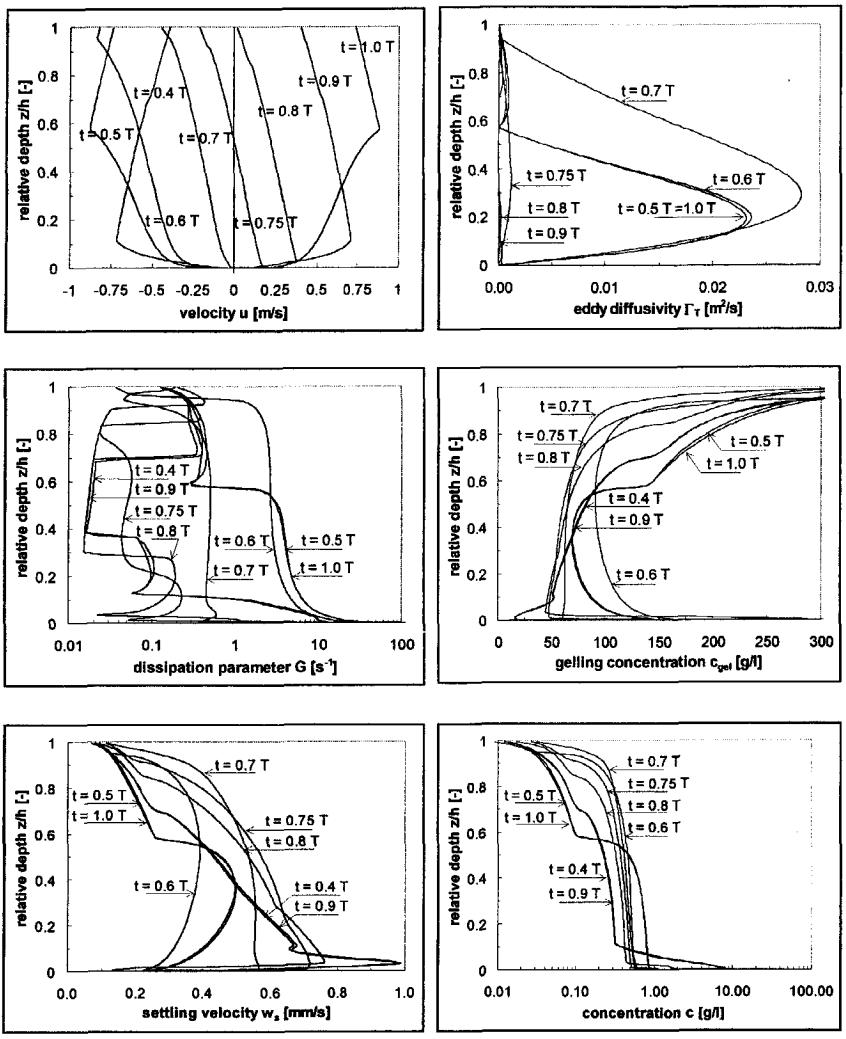

Fig. 6.16: Vertical profiles computed with flocculation model of u, Γ_T, G, c_{gel}, w_s and c at various times for $C_0 = 0.41$ g/l

From Fig. 6.13 and 6.16 it can be concluded that a dynamic equilibrium has been established, as the various curves at $t = 0.5\ T$ and $t = 1.0\ T$ are virtually identical. We also observe that in the period $0.5\ T \leq t \leq 0.7\ T$, i.e. after maximal flood (or ebb) velocity, the sediment is fairly well mixed over the water depth with a substantial eddy diffusivity. Towards slack and during the accelerating phase of the tide, up to $t = 0.9\ T$, vertical mixing is almost completely damped and large concentrations are found near the bed. The irregular G-profiles are related to irregular ε-profiles (not shown), which are affected by the large gradients in the vertical concentration profiles.

Large values of c_{gel} are predicted in the upper part of the water column, which is caused by small floc sizes (and settling velocities) resulting from the low suspended sediment concentrations. Closer to the bed c_{gel} ranges from about 20 to 300 g/l, the latter value is found directly after slack water (t = 0.8 T). It is noted that the entire behaviour is very dynamic and varies considerably with the hydrodynamic and sedimentological conditions. For super-saturated conditions, obtained for C_0 = 0.42 g/l (Fig. 6.14), c_{gel} near the bed amounts 20 to 30 g/l, which is therefore the fluid mud concentration for these conditions.

From these numerical experiments we conclude that saturation is also predicted with the flocculation model. The collapse of the concentration profile is a little less dramatic as found with a constant settling velocity, as can be seen by comparing Fig. 6.14 and 6.8.

7. Applications and comparison with measurements

7.1 The effects of sediment-induced buoyancy

The experiments and analyses, carried out by Coleman to study the influence of suspended sediment particles on the velocity profile in open-channel flow, were published in two papers. Coleman (1981) contains the primary data and analyses, whereas Coleman (1986) provides additional tables with the raw data and some additional analyses. Some further details were given in Coleman's reply to Gust's (1984) discussion of the results in the 1981-paper - see also Section 2.2.

The experiments were carried out in a tilting, recirculating flume with a plexiglass channel of 15 m length and 0.356 m width, operated at a water depth of about 0.17 m. The flow rate was measured with a venturi meter, the flow velocity with a traversible Pitot-tube, the bed shear stress with a Preston-tube, the surface slope with two point gauges 6 m apart, and the water temperature with a thermometer. Vertical profiles of the suspended sand concentration were also measured with the Pitot-tube, deployed to withdraw isokinetic samples. The Pitot-tube and Preston-tube measurements were carried out in the centreline of the flume, 12 m downstream from the inlet. No data on experimental accuracy were given by Coleman. Note that the length scale for settling amounts to $L_s \approx h \times U/W_s$ = 0.17 m × 0.95 m/s / 0.0107 m/s ≈ 15 m (see table 7.1), hence equilibrium of the concentration profile may not have been established fully at this measuring location.

The sediment used was composed predominantly of quartz and feldspar; the finest sample had a diameter between 88 and 125 μm, with a median diameter of 105 μm, and its settling velocity is established from Stokes' law. The experiments with this finest sample are analysed in this section.

The bed and wall of the flume were smooth; no roughness elements were installed, and during the experiments, no sand was allowed to settle on the bed. All experiments were carried out at uniform flow conditions.

The depth-mean velocity in the centreline of the flume can be established from the flow rate and water depth given by Coleman ($U_{m,Q}$), and from an integration of the presented measured velocity profile (U_m); the latter contains an uncertainty related to the extrapolation of the velocity data to the bed, c.q. the water surface. Both mean velocities are given in Table 7.1, showing a considerable difference. It is remarkable that $U_{m,Q}$ is larger than U_m, whereas in general one would expect the opposite, as wall friction effects are smaller in the centreline of the flume. This is a strong indication for important secondary current effects in the flume, with possibly some meandering. These secondary currents are also the cause of the decreasing flow velocity measured in the upper 30 % of the water column, as shown in Fig. 7.1a, indicating that almost the entire upper half of the water column is affected by such secondary currents[1)].

[1)] If the upper half of the velocity profile is indeed affected by secondary currents, it is impossible to use these data to establish an effect of suspended sediment in the upper part of the velocity profile, either in log-law form, or in defect-law form. We are therefore of the opinion that these data do not prove Coleman's claim that the effective Von Kármàn constant κ_s is not affected by sediment.

In our analyses we apply the velocity obtained from integration, i.e. U_m = 0.96 m/s, as also the sediment concentration profiles are measured in the centreline of the flume. The depth-mean suspended sediment concentration is also obtained from integration of the measured data. All other data, relevant for the analysis with the 1DV POINT MODEL, are also summarised in Table 7.1.

parameter	symbol	test 1	test 10	remarks
flume experiments				
flume length	l [m]	15	15	
flume width	b [m]	0.356	0.356	
water depth	h [m]	0.172	0.171	measured
flow rate	Q [m^3/s]	0.064	0.064	measured
water temperature	T [^{0}C]	21.1	23.9	measured
viscosity	ν [m^2/s]		0.93 10^{-6}	
cross-sect.-mean velocity	$U_{m,Q}$ [m/s]	1.05	1.05	from flow rate
depth-mean velocity	U_m [m/s]	0.96 ± 0.02	0.96 ± 0.02	by integration
shear velocity	u_* [m/s]	0.041	0.041	measured
volume sand	[kg]	0	8.18	
mean concentration	C_m [g/l]	0	6 ± 0.2	by integration
maximum diameter	D_{max} [μm]	-	125	
minimum diameter	D_{min} [μm]	-	88	
median diameter	D_{50} [μm]	-	105	
settling velocity	$W_{s,50}$ [mm/s]	-	10.7	from Stokes
bed friction coefficient	f [-]	0.0149	0.0149	
wall friction coefficient	f_w [-]	0.0142	0.0145	Vanoni-Brooks
1DV-simulations				
relative grid size	$\Delta z/h$ [-]	0.01	0.01	
time step	Δt [s]	1	1	
simulation period	T_{sim} [s]	1000	1000	
roughness		hydraulically smooth		
buoyancy		-	yes/no	
shear velocity	u_* [m/s]	0.042	0.039/0.042	computed
side wall friction in momentum equ.		yes/no	yes/no	
side wall friction in energy equ.		yes/no	no	
shear velocity	u_* [m/s]	0.049/0.042	0.039	computed
Prandtl-Schmidt number	σ_T [-]	0.7	0.7	
hindered settling		-	yes	

Table 7.1: Conditions of Coleman ('81/'86) experiments.

Despite these fairly strong secondary current effects, the data are suitable for analysis with our 1DV POINT MODEL, as can be concluded from the successful simulations by Galland with a Reynolds-stress model (1996), see Section 2.7. Moreover, we are not aware of any other data in the literature on sediment-laden flow with sufficient detail to carry out such analyses. For instance, Vanoni (1946) presents

data in the lower part of the water column only, whereas the experiments by Einstein and Chien (1955) are carried out for hyper-concentrated conditions.

Vanoni and Brooks (1957) showed that for experiments in straight flumes with width to depth ratios less than five, side wall friction can have a considerable effect on the experimental results, and should therefore be corrected for. They present a method to establish the effective wall shear stress coefficient for hydraulically smooth conditions, given the bed shear stress and Reynolds number. This correction method consists of a scalar summation of the bed- and wall-induced shear stresses. Vanoni-Brooks promote the following friction coefficient f_w for smooth walls:

$$f_w = 0.0026\left(\log\left(\frac{Re}{f}\right)\right)^2 - 0.0428\log\left(\frac{Re}{f}\right) + 0.1884 \tag{7.1}$$

in which f is the bed shear stress coefficient, defined as $f = 8(u_*/U)^2$, and the Reynolds number is defined as $Re = 4UR/\nu$, where R is the hydraulic radius. Substituting the various parameters given in Table 7.1 yields $f_w = 0.0142$, which is only slightly smaller than the bed shear stress coefficient, amounting to $f = 0.0149$.

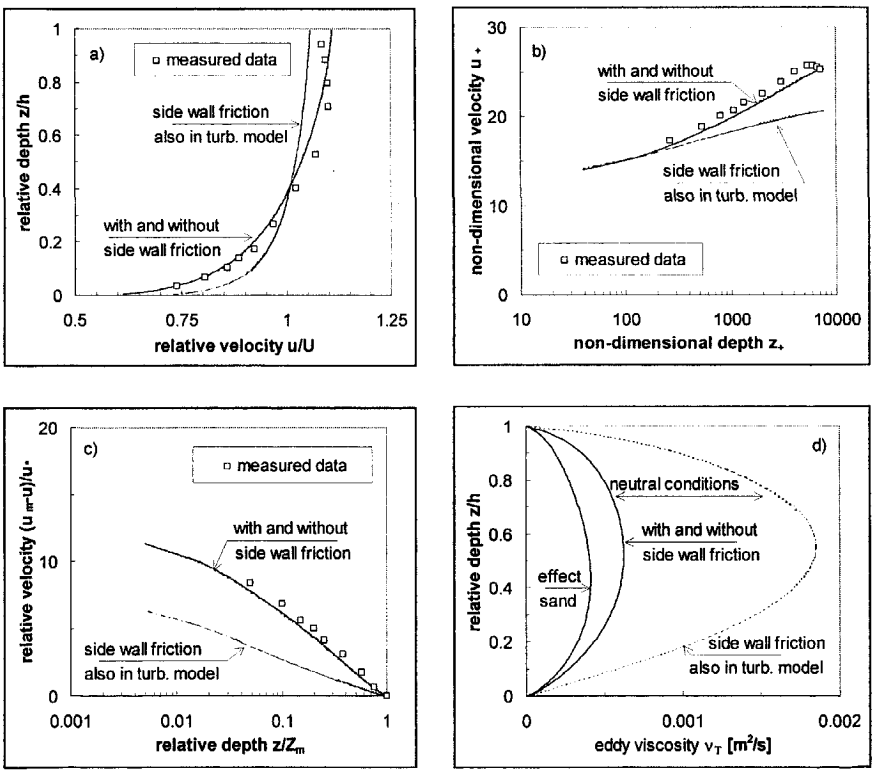

Fig. 7.1: Simulation of Coleman's (1981) clear water experiments, showing vertical velocity profiles: a) non-dimensional form, b) log-law form, c) defect-law form d) vertical eddy viscosity profile.

In the following paragraphs the experiments by Coleman are used to analyse the effects of sediment-induced buoyancy on the vertical velocity and concentration profile. This is done with a series of numerical experiments with the 1DV POINT MODEL:

1. In the first series, Coleman's clear water experiments are simulated, and the effect of side wall friction is studied,
2. In the second series, Coleman's sediment-laden experiments are simulated with the complete 1DV-model, and
3. In the third series the effect of sediment-induced buoyancy on the vertical velocity and concentration profile is explicitly studied.

First, Coleman's test 1 (clear water) experiment is first simulated with the 1DV POINT MODEL. The relevant numerical parameters are summarised in Table 7.1. Three simulations are carried out: 1) without side wall friction effects, 2) with side wall friction effects included in the momentum equation only, and 3) with side wall friction effects both in the momentum equation and in the turbulent energy and dissipation equations - see Appendix B for the relevant mathematical formulations in the 1DV POINT MODEL. The results are presented in normal linear, but non-dimensional form in Fig. 7.1a, in log-law form in Fig. 7.1b and in defect-law form in Fig. 7.1c. In these figures the following nomenclature is used: u = local flow velocity, U = depth-mean flow velocity, z = vertical co-ordinate, h = water depth, $u_+ = u_*/U$, u_* = shear velocity, $z_+ = zu_*/\nu$, ν = kinematic viscosity, and u_m = maximal flow velocity measured at height Z_m (which is about half water depth).

All these graphs clearly show that in the simulations the role of side wall friction in the momentum equation is negligible (compare the solid line and the almost coinciding dashed line in the graphs). This is consistent with the estimates by Coleman (1986). He computed the shear velocity u_* from the energy gradient:

$$u_*^2 = gh(S_e - S_w) \tag{7.2}$$

where S_e is the overall energy gradient and S_w is that part of the energy gradient associated with the side walls of the flume. Coleman found $S_w \approx 0.03 \times S_e$, hence side wall effects are expected to be small. If there is an effect, it is a slight steepening of the velocity profile in the upper part of the water column, as expected, accompanied by a decrease in slope near the bed, because continuity has to be fulfilled.

The influence of side wall friction in the turbulence model on the other hand is dramatic: the velocity profile steepens beyond reasonable values, which is caused by the large increase in eddy viscosity as shown in Fig. 7.1d. The reason for this overestimation is that the side-wall-induced turbulence production in the vicinity of the side wall is largely balanced by dissipation effects. As a result, the net contribution to the vertical mixing is much smaller than the (local) increase in turbulent kinetic energy. In our further analyses we will therefore only take into account the (small) effects of side wall friction in the momentum equation, and omit its influence in the turbulent kinetic energy equation. The legend "with and without side wall friction" in the various figures in this section therefore relates to friction effects in the momentum equation only.

Fig. 7.1b and 1c show that near the bed and near the water surface the computed velocity profile is not entirely logarithmic. This is due to the Dirichlet boundary

conditions of the k-ε equations, chosen to guarantee a robust numerical scheme - this was mentioned earlier in Section 3.3. Note that the logarithmic scale in the figures exaggerates this non-logarithmic behaviour near the wall; actually only the lower four to five computational points deviate from a logarithmic profile.

Fig. 7.1a shows that the computed velocity profile is in reasonable agreement with Coleman's data, except in the upper half of the water column, which is affected by secondary currents not accounted for in the 1DV POINT MODEL. Note that the computed and measured shear velocity (see Table 7.1) agree within experimental accuracy, which also supports our choice to use U_m in stead of $U_{m,Q}$.

Fig. 7.1b shows that the lower half of Coleman's data up to $z_+ \approx 4{,}000$ follow the logarithmic trend fairly well. The deviation between computed and measured velocity profile is a bit larger than in Fig. 7.1a, because of the small difference in shear velocity used to scale the axes of Fig. 7.1b and 1c.

We also observe that, by presenting experimental data in defect-law form, the three data points near the water surface have to be omitted, as these would yield negative defect velocities. Another consequence of this presentation is that all velocity curves converge, as they have to go through (1,0) (see also equ. (2.2)).

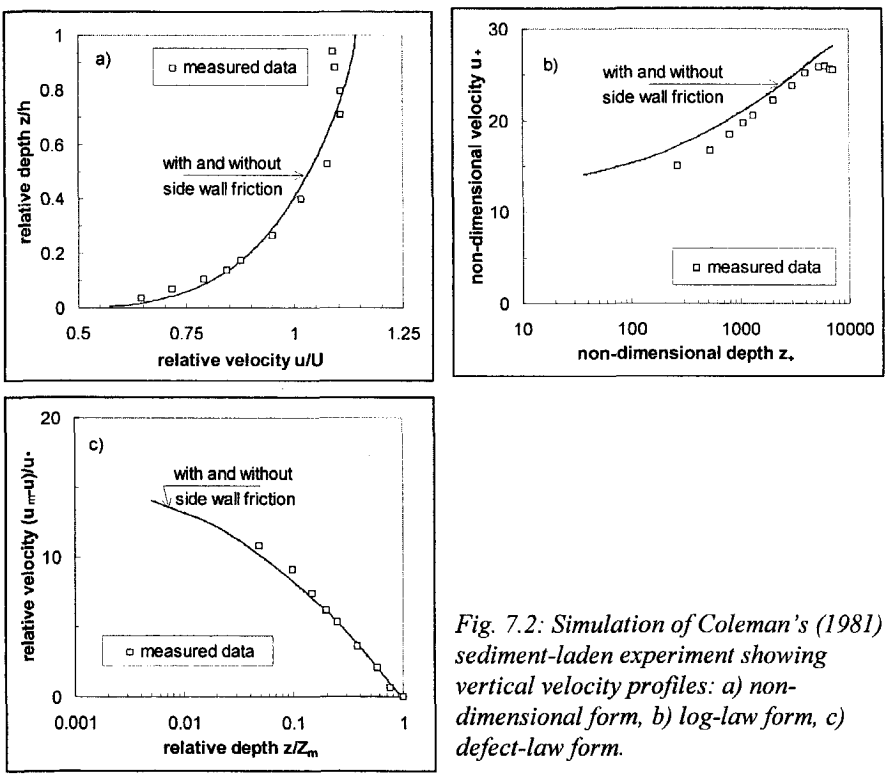

Fig. 7.2: Simulation of Coleman's (1981) sediment-laden experiment showing vertical velocity profiles: a) non-dimensional form, b) log-law form, c) defect-law form.

The computed and measured velocity profiles for the sediment-laden test 10 are presented on linear scale in Fig. 7.2a, in log-law form in Fig. 7. 2b and in defect-law form in Fig. 7.2c. We observe that the agreement between computed and measured

data near the wall in Fig. 7.2a is slightly less than in Fig. 7.1a. We will elaborate on this below.

It is remarkable that the computed velocity profile lies above the measured data in Fig. 7.2b, whereas it lies below the data in Fig. 7.1b. This difference is entirely due to the difference in computed and measured shear velocity. By the same cause, the agreement between computed and measured data in defect-law form seems to have improved in comparison to Fig. 7.1c.

The agreement between computed and measured vertical suspended sediment concentration is fair - see Fig. 7.3a (linear scales) and 7.3b (logarithmic scales). An even better agreement can be obtained by tuning the settling velocity, but this was not done.

In summary we conclude that the agreement between the computed and measured velocity and concentration profiles is fair and of the same quality as the results presented by Galand (1996), presented in Fig. 2.4.

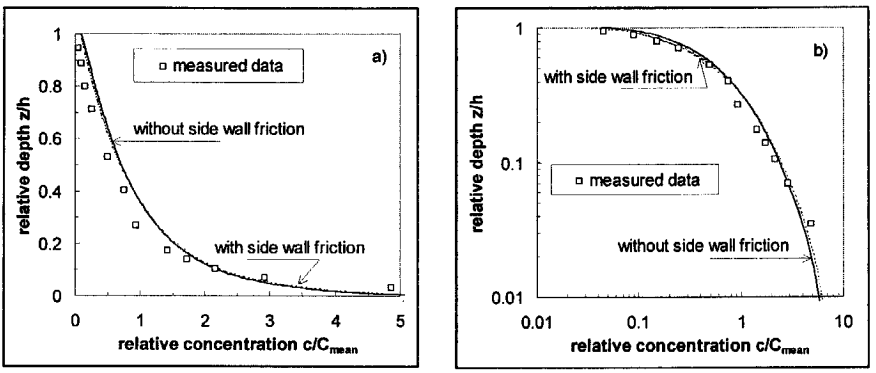

Fig. 7.3: Simulation of Coleman's (1981) sediment-laden experiment: sediment concentration profiles.

Next a series of simulations of test-10-conditions is carried out, but without sediment-induced buoyancy effects. The results are presented in Fig. 7.4a in linear form, in Fig. 7.4b in log-law form and in Fig. 7.4c in defect-law form; the effects on the vertical concentration profiles are presented in Fig. 7.5. The computed velocity profile with sand, but without buoyancy effects is of course identical to the computed clear water profile (e.g. Fig. 7.1). Fig. 7.4a clearly shows that the sediment-induced buoyancy effects reduce the vertical mixing, as expected. This is also shown in Fig. 7.1d where the eddy viscosity profile with and without buoyancy effects are compared.

These buoyancy effects may also be the cause of the underprediction of the measured flow velocity near the bed. The sediment used in the experiments is (slightly) graded and it may be expected that as a result, the coarser material will generate larger buoyancy effects closer to the bed. To test this hypothesis an additional simulation is carried out, assuming a Gaussian grain size distribution, as no data on this distribution were given by Coleman. The results of this simulation indeed show the expected trend, i.e. the buoyancy effects on the velocity profile are augmented, but the effect is so small that the results are not presented here.

The comparison in log-law form is again hindered by different values of the shear velocity. Fig. 7.4c on the contrary, showing the results in defect-law-form, is very illuminating. It is this form of presentation that inspired Coleman to his analysis of the effect of suspended sediment on the wake function of the velocity profile. This figure clearly shows that the effect of suspended sand on the measured velocity profile is properly predicted by the simulations through adding a sediment-induced buoyancy term in the turbulent energy equation of the numerical model. Comparison of the computed sediment concentration profile with and without buoyancy effects (e.g. Fig. 7.5) clearly shows a considerable overestimation of the measured data for the simulation without buoyancy effects. This could, but only partly, be compensated for by an increase in settling velocity.

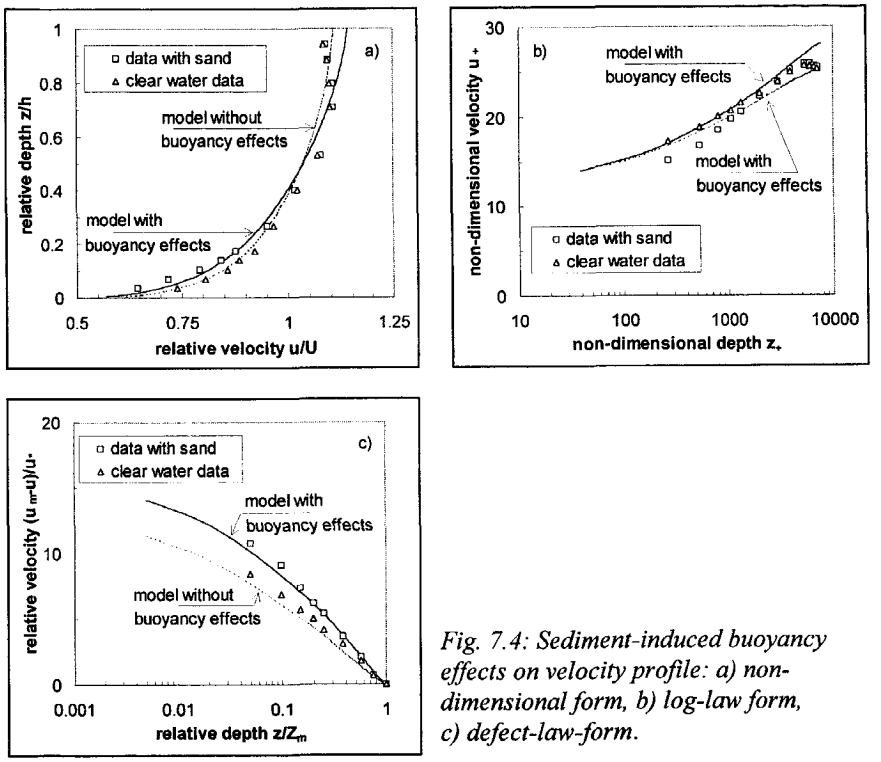

Fig. 7.4: Sediment-induced buoyancy effects on velocity profile: a) non-dimensional form, b) log-law form, c) defect-law-form.

From these analyses we conclude that the 1DV POINT MODEL is able to reproduce the major features of sediment-laden flow, and that the effects of the suspended sediment on the velocity profile is explained largely through sediment-induced buoyancy effects, as hypothesised by Vanoni in 1946.

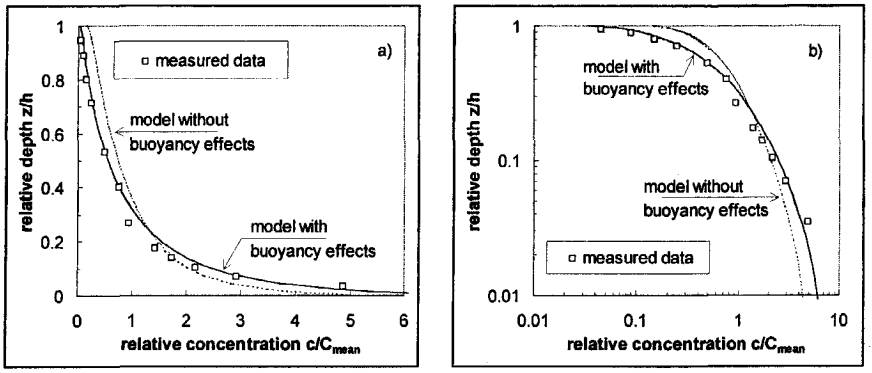

Fig. 7.5: Sediment-induced buoyancy effects on vertical concentration profile.

7.2 Entrainment and the effects of consolidation

At Delft University of Technology three series of entrainment experiments have been carried out in an annular flume with an outer diameter of 4.0 m, an inner diameter of 3.4 m and a maximal height of 0.4 m. The fluid within the flume is driven by a screen on the fluid surface; the flume itself can rotate in the opposite direction to minimise secondary currents near the bed. For fresh water, the three-dimensional flow and shear stress distributions in the flume have been measured in detail with a Laser-Doppler Anemometer (LDA) system (Winterwerp and Kranenburg, 1997).

During the entrainment experiments the height of the screen was set at 27.3 cm above the bottom and the ratio of the rotational speeds of lid and flume was set at -1.8, which is the optimal value for this water depth to minimise the near-bed secondary currents.

In the first series, entrainment experiments with saline and fresh water have been carried out, and in the second series, entrainment experiments were carried out with a kaolinite - saline water suspension. These experiments were reported by Winterwerp and Kranenburg (1994). The major conclusion of those studies is that initially the fluid mud behaves as a dense fluid and the initial entrainment rates of a saline layer and of a fluid mud layer by a turbulent fresh water layer can be described by the same entrainment relations, and that the entrainment rate decreases when the bed strength increases.

In the third series, entrainment experiments were carried out with mud from the Caland/Beerkanaal, the entrance to the Port of Rotterdam in The Netherlands. The experimental procedure was as follows. Sea water at a salinity of about 30 ppt was let into the flume. Then a dense suspension of the mud was added to obtain a concentration of about 60 g/l. This suspension was rotated and mixed in the flume for a week, after which it was allowed to settle and consolidate for a preselected period. Prior to and after the entrainment experiments, samples were taken to carry out additional consolidation experiments in separate columns (see also Section 5.4.2). After the selected settling/consolidation period, an entrainment experiment was started by accelerating both flume and screen gradually in the same direction and at the same rate till the rotational speed selected for the flume was reached. In this way it was achieved that the lower fluid mud layer remained stagnant with respect to the flume, so that no turbulence was generated in this layer. Then the screen was accelerated in the opposite direction, up to the selected speed, which was kept constant during the entrainment experiment. The latter procedure took about 20 s in general.

During such an experiment, the following parameters were measured:

- the rotational speeds of flume and lid,
- the suspended sediment concentrations in the centre line of the flume at two heights (15 and 20 cm above the bottom of the flume) with turbidity sensors (OSLIM, WL|delft hydraulics); two sensors were used in series at each depth, one to measure at low sediment concentration, the second to measure at high concentrations; the accuracy of these measurements is estimated at ±2.5 g/l,
- prior to and after each test samples were taken to calibrate the turbidity sensors, and
- the height of the interface was measured visually and from video-recordings at the inner and outer walls of the flume.

In a separate consolidation experiment in the annular flume, the vertical distribution of the dry bed concentration in the fluid mud layer was measured in still water for various consolidation periods with an electrical conductivity probe (ECP).

The experimental programme is set up such that both the hydrodynamic parameters (Richardson number Ri_*) and the mud properties (consolidation time T_c) are varied. The bulk Richardson number is defined as $Ri_* = \Delta\rho g\delta/\rho u_*^2$, where $\Delta\rho$ is the density difference between upper and lower layers, δ is the thickness of the mixed (upper) layer, ρ is the density of the upper layer, and u_* is the friction velocity at the location where the turbulence is mainly produced, that is at the screen for the present study.

parameter	symbol	clear water exp.	test C5	remarks
flume experiments				
outer diameter flume	$2R$ [m]	4.0		
flume width	b [m]	0.3		
water depth	h [m]	0.273		
screen velocity	U_s [m/s]	0.78	0.58	
flume velocity	U_f [m/s]	-0.58	-0.33	
initial mean concentration	C_0 [g/l]	-	60	before cons.
initial vertical density profile	ρ_0 [g/l]	-		see Fig. 5.5
initial thickness mud layer	δ_0 [m]	-	0.101	
settling velocity	W_s [mm/s]	-	0 & 0.2	
1DV-simulations				
relative grid size	$\Delta z/h$ [-]	0.005		
time step	Δt [s]	0.05		
simulation period	T_{sim} [s]	1500		
screen roughness length	z_s [m]	$1.0\cdot10^{-5}$		variable
bed roughness length	z_0 [m]	$1.0\cdot10^{-5}$		variable
wall friction coefficient	f_w [-]	0.0018		Blasius' law
buoyancy		-	yes	
Prandtl-Schmidt number	σ_T [-]	-	0.7	
hindered settling		-	yes	
viscosity coefficient	K_μ [Pas]		140.0	~ 10 × water
viscosity exponent	n [-]		3.0	
yield strength coefficient	K_y [Pa]		variable	Fig. 7.11 & 12
fractal dimension	n_f [-]		2.7	

Table 7.2: Conditions of annular flume experiments and simulations.

In this section we describe the simulations of these experiments with the 1DV POINT MODEL. In particular test C5 is suitable, which is characterised by a consolidation time of six hours, and an initial Richardson number $Ri_* = 204$, implying a fairly slow entrainment process. The experimental conditions correspond to the consolidation experiment discussed in Section 5.4.2. In our analysis, we carry out the following numerical experiments:

1. In the first series establish the effects of the roughness height of the screen of the flume on the vertical velocity profile and initial entrainment rate,
2. In the second series establish the effects of the settling velocity on the entrainment rate,
3. In the third series establish the effects of consolidation, i.e. the initial bed density profile, on the entrainment rate, and
4. In the fourth series study the effects of bed strength on the entrainment rate.

First we investigate whether the vertical velocity profile in clear water can be simulated properly. This profile was measured with an LDA-system in the centre plane of the annular flume during an experiment at which the screen is rotated at 0.87 m/s, and the flume is rotated at -0.58 m/s (e.g. Booij et al., 1993). Fig. 7.6 presents the results of four simulations, studying the effect of the roughness of the screen and bottom and of the side wall:

1. $z_s = z_0 = 1.0 \cdot 10^{-5}$ m, no side wall roughness,
2. $z_s = z_0 = 1.0 \cdot 10^{-4}$ m, with side wall roughness; $\lambda_s = 0.0018$,
3. $z_s = z_0 = 1.0 \cdot 10^{-5}$ m, with side wall roughness; $\lambda_s = 0.0018$,
4. $z_s = z_0 = 1.0 \cdot 10^{-6}$ m, with side wall roughness; $\lambda_s = 0.0018$,

It is shown that a reasonable simulation of the measured velocity profile is only possible when side wall friction is taken into account, and that the computed vertical velocity profile is greatly affected by the roughness length of screen and bottom. The smaller z_s, the steeper the velocity profile, and a value of $z_s = 1.0 \cdot 10^{-6}$ m seems appropriate at first sight. This value is close to the roughness length for hydraulically smooth conditions, amounting to $z_s = 0.11\nu/u_* = 3 \cdot 10^{-6}$ m. However, the roughness length $z_s = 1.0 \cdot 10^{-5}$ m corresponds better to the roughness coefficient $\lambda = 0.0017$, which was used by Winterwerp and Kranenburg (1997). Furthermore, the shear velocity at the screen at this z_s is computed at $u_{*,s} = 0.041$ m/s, which agrees more or less with measured values, amounting to $u_{*,s} = 0.035$ to 0.038 m/s (Winterwerp and Kranenburg, 1997).

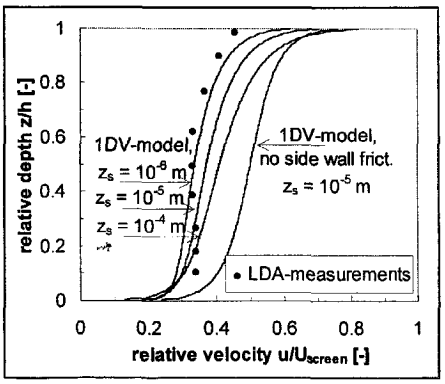

Fig. 7.6: Measured and computed vertical velocity profiles in annular flume.

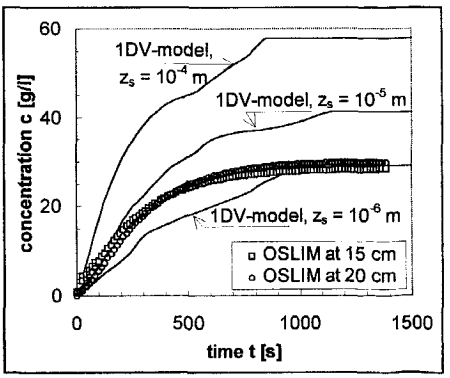

Fig. 7.7: Time histories of concentration for various z_s and $W_s = 0$.

Next, we study the effect of z_s on the (initial) entrainment rate of the fluid mud layer. The results are given in the form of time histories of the suspended sediment concentration in the fluid above the mud bed, as in Fig. 7.7, which represents the results of a simulation starting with the measured bed density profile (Fig. 5.5) and zero settling velocity. It is shown that the best simulation is obtained for $z_s = 1.0 \cdot 10^{-5}$ m. We must conclude that it is not possible to obtain a better agreement between the measured and computed velocity distribution, as the effects of the secondary currents in the annular flume cannot be accounted for in a 1DV-model. These secondary currents generate a fairly rigid kernel in a major part of the cross section of the flume, with more or less constant velocity, and large velocity gradients in the boundary layers at the flume wall (Booij et al., 1993). Apparently however, the velocity gradient near the fluid mud layer, i.e. in the lower part of the annular flume, is simulated with sufficient accurately to compute a fair initial entrainment rate for the first 200 s of the experiment. It is noted that the wavy character of the computed suspended sediment concentration variation with time is caused by the scatter in the initial density data (see Fig. 5.5).

In all our following simulations we use $z_s = 1.0 \cdot 10^{-5}$ m, though the vertical velocity profile seems a bit better when using $z_s = 1.0 \cdot 10^{-6}$ m.

Next, we study the effect of the settling velocity on the entrainment process. The settling velocity is set at $W_{s,r} = 0.2$ mm/s, as described in Section 5.4.2. The results of this simulation are presented in Fig. 7.8, showing that a fair agreement between experimental and numerical data is obtained for the first 500 s. The entrainment rate in this simulation is smaller than in the zero-settling-velocity simulation, because part of the available turbulent kinetic energy is now required to keep the sediment in suspension.

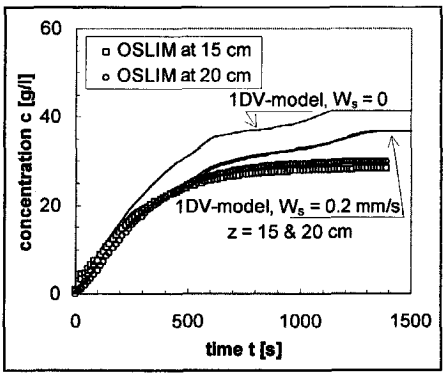

Fig. 7.8: Effect of settling velocity on concentration.

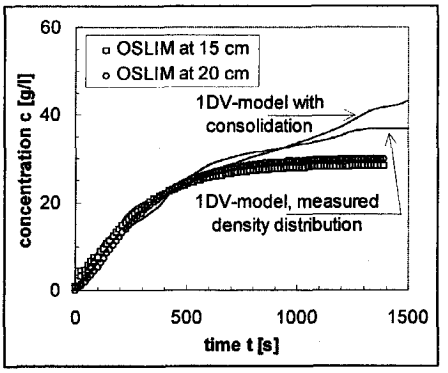

Fig. 7.9: Effect computed consolidation (see also Fig. 5.5) on concentration.

These entrainment experiments also allow us to study the hindered settling - consolidation - re-entrainment cycle. For this purpose, the 1DV POINT MODEL is run for this entire cycle, starting with an initially homogeneous sediment concentration of $C_0 = 60$ g/l at $t = -6$ hrs. The computational results for the settling-consolidation phase of this cycle are presented in Section 5.4.2. The entrainment phase of this cycle is presented in Fig. 7.9, showing a fair agreement with the data up to 700 s. Thereafter,

the computational results start to deviate; in fact, eventually, the entire mud layer will be eroded, which is not the case using the measured initial density profile.

Part of this difference is attributed to buoyancy effects, as shown in Fig. 7.10, presenting the computed vertical profiles of velocity, turbulent kinetic energy, eddy viscosity and suspended sediment concentration for the measured bed density profile. It is shown that the concentration gradient near the bottom of the flume becomes so large, that the lower part of the sediment cannot be resuspended anymore. In the case of the computed bed density profile, the near-bed sediment concentration is lower (e.g. Fig. 5.5), hence these buoyancy effects are smaller.

Fig. 7.10 shows that below the upper interface, at $z \approx 3$ cm, some turbulence appears to be produced by the local velocity gradients. As a result, the gentle gradients, present in the initial density distribution, steepen around the lower interface at $z \approx 2$ cm. This is shown by the stepwise concentration distribution around $z \approx 2.5$ cm.

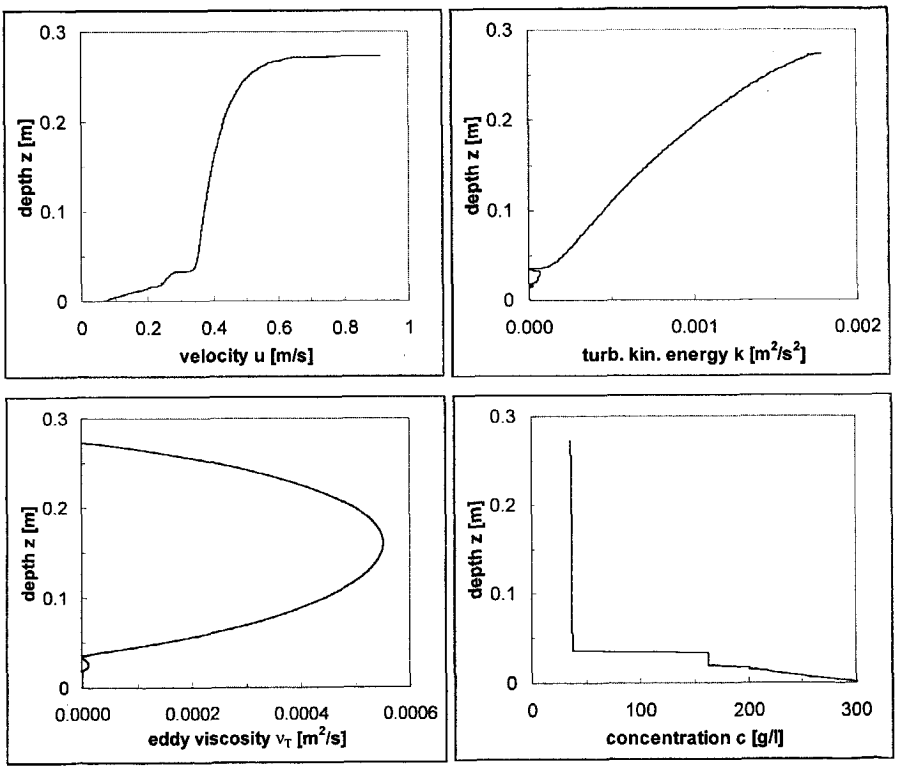

Fig. 7.10: Computed vertical profiles of u, k, ν_T and c for the measured bed density profile at t = 1500 s, i.e. when the entrainment has stopped.

The entrainment process not only stops because of these buoyancy effects, but also because the mud layer has attained sufficient strength to withstand the turbulent mixing processes. This effect is modelled by including the strength formulation given in Section 5.3. The relevant parameters are presented in Tables 7.2 and 7.3:

yield strength parameter K_y [Pa]		comments
measured bed density	$1.0 \cdot 10^8$	after Merckelbach with c.o.l.s. = 0.5
measured bed density	$1.0 \cdot 10^8$	after calibration
computed bed density	$5.0 \cdot 10^8$	from consolidation with c.o.l.s. = 0.5
computed bed density	$5.0 \cdot 10^6$	after calibration

Table 7.3: Setting of yield strength parameter in 1DV-simulations (c.o.l.s. is coefficient of lateral stress).

Fig. 7.11 presents the results for a simulation starting with the measured bed density profile, with a bed strength coefficient K_y related to Merckelbach's (1998) effective stress data, which amounts to $K_p = 2.0 \cdot 10^8$ Pa and a coefficient of lateral stress of 0.5. This ratio is chosen on the basis of results presented by Van Kessel (1997). The agreement between the measurements and simulations is satisfactory, though the computed concentration shows a small kink around t = 700 s. This is caused by the rheological model chosen, which does contain two linear parts, divided by the Bingham strength.

Fig. 7.12 presents the results for the entrainment phase of the hindered settling - consolidation - erosion cycle, where K_y is set at $5.0 \cdot 10^8$ Pa, which corresponds to the effective stress coefficient K_p used in the consolidation phase of the cycle (see Section 5.4.2) and a coefficient of lateral stress of 0.5. This graph shows that in this case the entire mud layer is so strong that no sediment can be entrained. Only if we decrease K_y down to $5.0 \cdot 10^6$ Pa, a fair agreement with the measured entrainment curve is obtained.

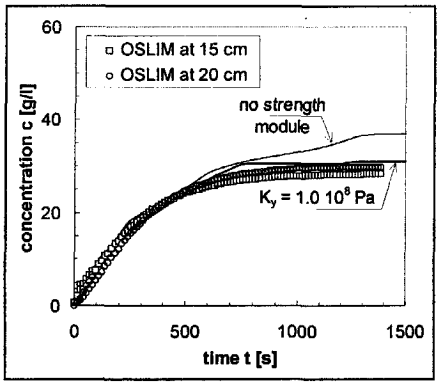

Fig. 7.11: Effect of strength module on entrainment rate; measured initial density.

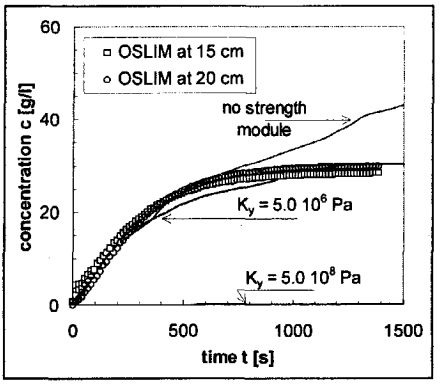

Fig. 7.12: Effect of strength module on entrainment rate; consolidation model.

Fig. 7.13 presents the computed vertical distributions of the flow velocity and of the total stress (i.e. the contribution of molecular viscosity, turbulent shear stress and yield strength), of the turbulent shear stress alone and of the yield strength for the simulation presented in Fig. 7.11 for t = 150 s and 900 s. Above the water-mud interface the total and turbulent shear stresses are virtually equal. Around the interface, the turbulent stresses vanish, apart from a small increase in the upper part of the mud layer. The total shear stress first decreases and then increases again towards

the bed. The latter is a result of the rapid increase in concentration near the flume bottom, as the yield strength is explicitly related to the sediment concentration (equ. (5.21)). The flow velocity in the lower part of the mud layer is zero.

The picture at t = 900 s (Fig. 7.13c and 13d) is very similar, except that the lower layer is now slightly dragged with the main flow. The mud layer does not remain stagnant, as the mud is not modelled as an ideal plastic fluid with Bingham behaviour, but as a general plastic fluid with zero stress only at zero deformation (e.g. Appendix B). Note that this mud flow has not been observed in (at the side wall of) the flume. However, no further entrainment occurs, as the turbulent shear stresses remain well below the yield strength of the mud.

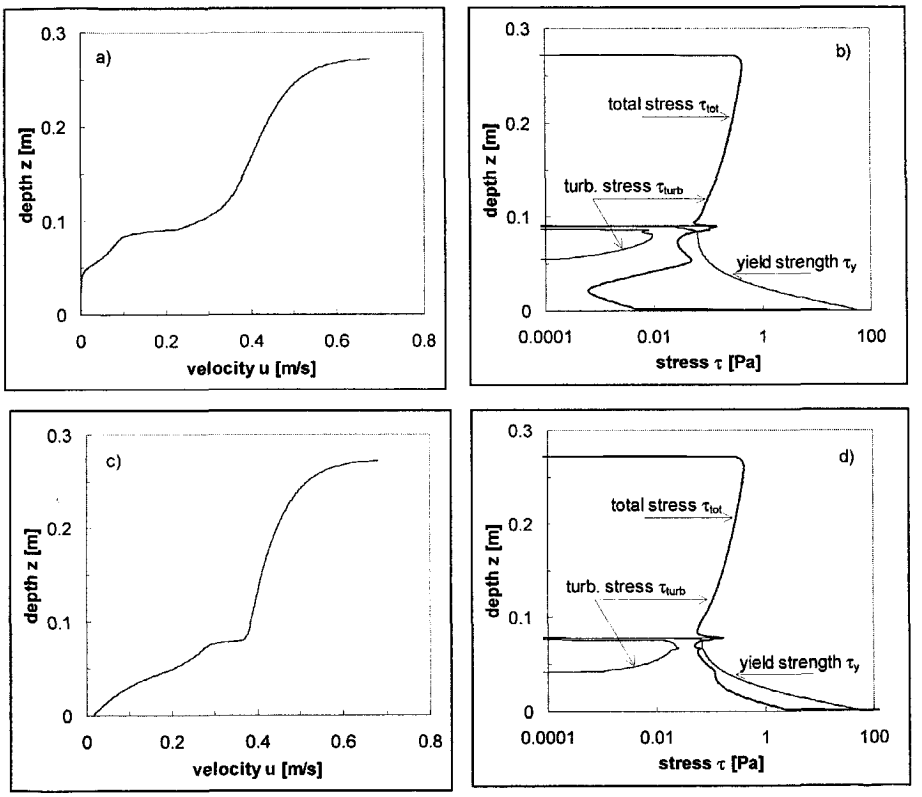

Fig. 7.13: Velocity and stress profiles for simulation with measured bed density profile and $K_y = 1.0 \cdot 10^8$ Pa at t = 150 min (a & b), and at t = 900 min (c & d).

From the numerical simulations in this section we conclude that it is possible to simulate the entire hindered settling - consolidation - re-entrainment process, as occurs around slack water in tidal environments, with the model formulations proposed herein. However, a proper simulation of the experimental data requires severe tuning of the rheological model coefficients, especially of the yield strength, to values that do not match the effective stress formulation required to simulate the

consolidation process properly. A big handicap in these simulations is the lack of proper rheological data of the mud with which the entrainment experiments have been carried out. As a result the rheological and consolidation parameters had to be found by trial and error. Moreover, it is not known whether the effective stress in a consolidating mud layer is directly related to the yield strength in a general plastic rheological model. However, the major shortcoming seems to be generated in the consolidation model, as the application of the measured initial bed density profile shows a fair agreement between the measurements and simulations, using realistic parameter settings. A possible cause for this shortcoming is segregation, which is suggested by the pronounced tail in the measured density distribution (e.g. Section 5.4.2 and Fig. 5.5). Generalisation of this conclusion requires more research, though.

Also the effects of low Reynolds numbers and the effects of the sediment itself on the turbulence field are not taken into account. It is expected that such effects further decrease the computed entrainment rates, but should not be studied in detail before the strength evolution itself has been described properly. However, this task is beyond the scope of the present study.

We also recognise that the present model formulations do not include weakening of consolidating mud layers, necessary to describe the erosion process implicitly in a computational domain covering water column and consolidating bed. Hence, the present model cannot cope with the effect of spring-neap cycles for instance, which is so important for the behaviour of HCMS in many high-energetic estuaries, such as the Severn estuary.

7.3 HCMS in the Ems estuary

Van Leussen (1994) presented the results of a series of hydro-sedimentological measurements in the Ems estuary in Germany and The Netherlands. These measurements were carried out in June 1990 along five stretches of the river. At each stretch, two anchor stations at a mutual distance of approximately 1 km were deployed to measure the flow velocity with an impeller flow meter (Ott mill), the salinity from conductivity and temperature measurements and the suspended sediment concentration with a Partech turbidity meter or by taking water samples when suspended sediment concentrations were high. During 13 hours, these parameters were measured every half hour at 0.3 m, 0.5 m, 1 m, 2 m, etc. above the bed, till 1.5 m below the water level. Along these stretches, measurements were also taken from a floating vessel, determining the flow velocity, salinity and suspended sediment concentration with identical instruments, and the floc size and settling velocity with an in-situ video-system (VIS). A summary of the measuring locations is presented in Fig. 7.14, which is copied from Van Leussen (1994).

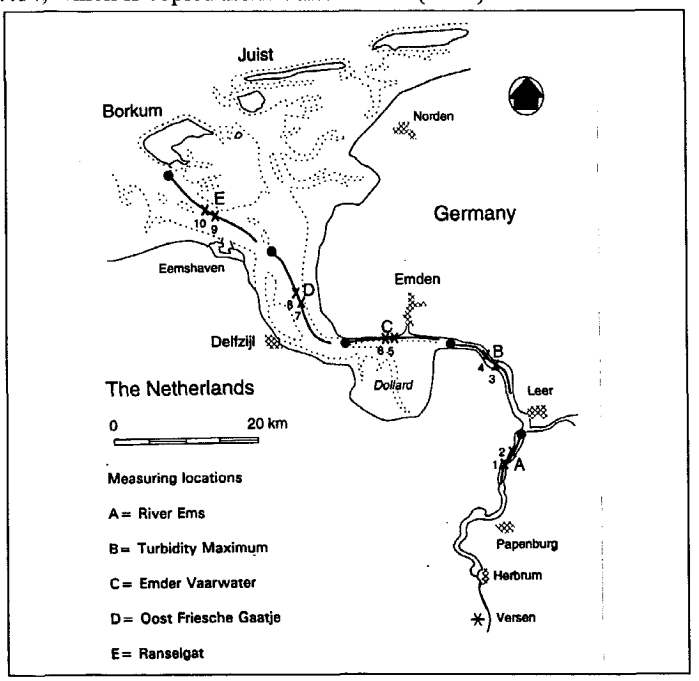

Fig. 7.14: Locations of field measurements in the Ems estuary (from Van Leussen, 1994).

The river flow during the measurements was about 10 to 25 m^3/s, which is very low. As a result the turbidity maximum was located around stretch B, about 15 km upstream of its usual location in the Emder Fahrwasser (stretch C). Because of this low river flow, vertical salinity gradients were virtually absent during the entire measuring campaign.

The variations in water level and depth-averaged values of flow velocity, salinity and suspended sediment concentration at Station 3 and 4, located in the turbidity maximum, are presented in Fig. 7.15a through 15d. To establish these depth-averaged values, the measured data have been extrapolated linearly to the water surface and

river bed, respectively. Vertical distributions of velocity and suspended sediment concentration at two specific times at Station 3 and 4 are presented in Fig. 7.16. The concentration distribution during the entire measuring period at Station 3 is given in the form of isolutals in Fig. 7.17.

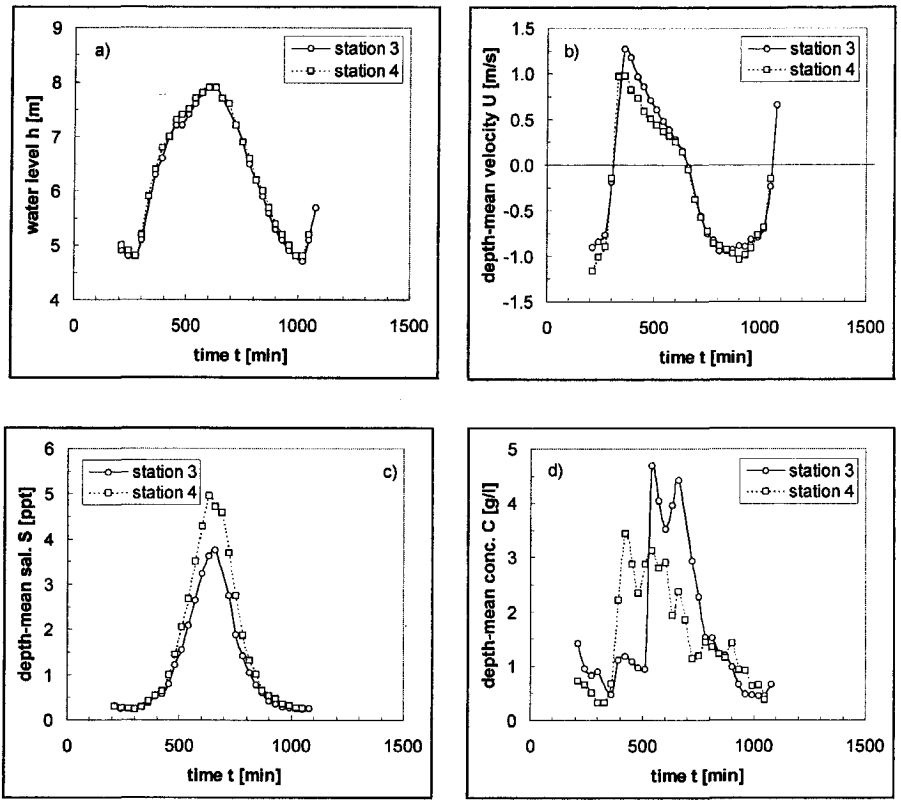

Fig. 7.15: Data at turbidity maximum (June 20, 1990): a) water level h, and depth-averaged values of b) flow velocity U, c) salinity S and d) sediment concentration C.

From these graphs, the following conclusions can be drawn:

- The variation with time of h and U at Station 3 and 4 are almost in phase. The flood velocity at Station 3 is about 30 % larger than at Station 4.
- The tidal velocity shows a strong asymmetry with a peaked flood velocity and a more gradually varying ebb velocity. Moreover, the flood period is shorter than the ebb period. Such asymmetry is typical for many estuaries and generates a net upstream sediment flux.
- High water slack (HWS) and low water slack (LWS) are observed about 0.5 hrs after high water (HW), respectively low water (LW), hence the tide behaves almost as a standing wave.
- The vertical salinity distribution is virtually homogeneous. As peak in the depth-averaged salinity is observed exactly at HWS, we can conclude that the saline water is transported by advection only (i.e. no gravition circulation).

- The depth-averaged suspended sediment concentration C at Station 4 starts to rise by almost a factor ten directly after LWS and to decrease after HWS. These large concentrations are indicative for the occurrence of fluid mud, as is shown below. The large fluctuations in C are likely to be due to inaccuracies in the assessment of the depth of the measuring instruments - an error of a few dm may easily occur, causing large errors in C in the vicinity of lutoclines.

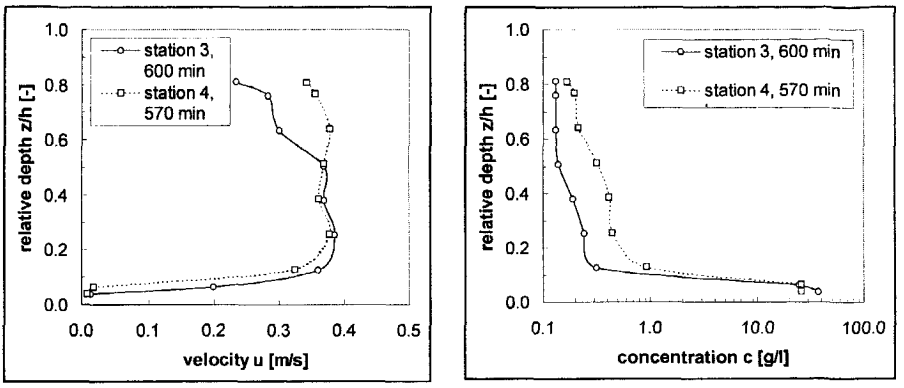

Fig. 7.16: Vertical profiles of velocity and sediment concentration in fluid mud layer.

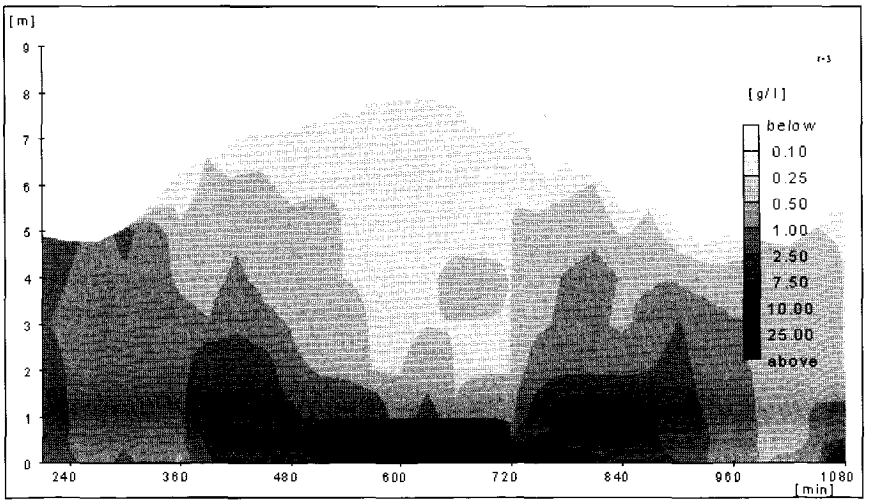

Fig. 7.17: Isolutals from measurements at Station 3.

- It is remarkable that the increase in C at Station 3 starts almost 2.5 hrs later than at Station 4. This is a strong indication of advective effects. This is further substantiated by Fig. 7.16, presenting the vertical profiles of flow velocity u and suspended sediment concentration c during the period of high C: the mean velocity in the fluid mud layer amounts to about 0.1 to 0.2 m/s, yielding a travel time from Station 4 to Station 3 of about 1.5 to 3 hrs.

From these observations we have to conclude that the sediment dynamics in the turbidity maximum are highly affected by advection. It is therefore senseless to try and simulate the observed concentration distribution in detail with the 1DV POINT MODEL, which of course does not take such advective effects into account. However, we can use the model and the data to establish some properties of the HCMS in the turbidity maximum.

Van Leussen (1994) presented data on the size of the so-called macro-flocs in the turbidity maximum throughout the tide. His results are presented in Fig. 7.18, showing floc sizes between 250 and 400 μm. From these floc sizes the gelling concentration c_{gel} can be established, using equ. (4.8). For various parameter settings c_{gel} is given in Table 7.4.

parameter combination	D [μm]	D_p [μm]	n_f	c_{gel} [g/l]
1	200	4.0	2.0	53
2	400	4.0	2.0	26.5
3	200	4.0	2.7	820
4	400	4.0	2.7	660
5	200	$1.7 \cdot 10^{-4}$	2.7	40
6	400	$3.4 \cdot 10^{-4}$	2.7	40

Table 7.4: Gelling concentration as a function of mud parameters.

Note that values of $n_f \approx 2.7$ are expected in a consolidating bed, and that $D_p = 4$ μm is found from measurements by Van Leussen. From Table 7.4 we conclude that only the parameter combination 1 and 2 with $n_f = 2$ yield reasonable results, i.e. values for c_{gel} consistent with the near-bed concentrations presented in Fig. 7.16 and 7.17.

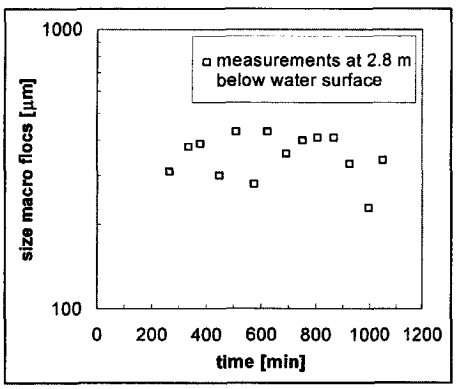

Fig. 7.18: Measured variation in floc size 2.8 m below water surface at Station 3, turbidity maximum.

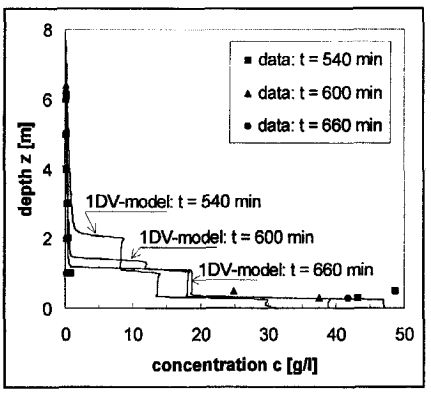

Fig. 7.19: Comparison of computed and measured concentration distributions and formation of fluid mud at Station 3, turbidity maximum.

Though we cannot hope to simulate the observed HCMS-dynamics in the turbidity maximum properly with a 1DV-model, we can try to establish whether the 1DV POINT

MODEL can predict some characteristics of the fluid mud formation properly. For this purpose we have run the model with the standard settings of the flocculation model parameters, as presented in Chapter 4, with an initial concentration C_0 = 5 g/l, which is characteristic for the depth-mean sediment concentration around the period of fluid mud occurrences (e.g. Fig. 7.15). We have used the measured tidal variations in water depth h and in depth-averaged flow velocity U as forcing parameters. Computed and measured data for three times when fluid mud occurs are presented in Fig. 7.19. The simulations shows the existence of two lutoclines, indicating deposition in the hindered settling regime. These two lutoclines are not observed in the present field data; however, they have been measured once (Van Leussen, 1999a). We conclude that the agreement between measurements and simulations is reasonable in the sense that the measured concentrations in the fluid mud layer are more or less predicted by the model.

From these analyses we conclude that the fractal dimension n_f in the fluid mud layer in the Ems estuary is about $n_f \approx 2$, yielding gelling concentrations in the fluid mud layer of 30 to 40 g/l. The very large fractal dimensions of $n_f \approx 2.6$ - 2.7, sometimes observed in consolidating mud layers, apparently do not occur in mud layers formed in the Ems estuary.

Table 7.5 presents a summary of fluid mud concentrations in some estuaries as reported in the literature, showing that fluid mud concentrations of the order of several tens of g/l are quite common, though larger values are reported, especially in the Amazon estuary. The Amazon values, however, have been measured further offshore, where wave action may play a role. This is further discussed in Section 7.4.

estuary	reference	fluid mud conc. [g/l]	remarks
Severn	Crickmore ('82) Kirby & Parker ('83)	appr. 10	
Parret	Odd et al. ('93)	40 - 80	above cons. bed
Ems Estuary	Van Leussen ('94)	appr. 40	0.35 from bed
Amazon	Kineke et al. ('95) Kineke et al. ('96)	40 - 250	0 - 2 m from bed
Loire	Le Hir ('97)	appr. 40	1 m thick layers
Jiaojiang River	Guan et al. ('98)	appr. 40	0.35 from bed

Table 7.5: Typical fluid mud concentrations in estuaries.

The suspended sediment concentrations further upstream, measured at the Stations 1 and 2, are presented in the form of time series in Fig. 7.20 and in the form of isolutals for Station 2 in Fig. 7.21. These concentrations are still large, but less extreme than in the turbidity maximum. Fig. 7.20 also presents the variations in water level h_r with respect to the mean water level, and the depth-averaged values of the flow velocity U, the salinity S and suspended sediment concentration C for both stations. Qualitatively, the picture for the water level and flow velocity is similar to that of Fig. 7.15, i.e. h and U at Station 1 and 2 are almost in phase; the salinity, however, remains almost constant at $S \approx 0.2$ ppt, indicating more or less fresh water conditions.

It is also remarkable that the suspended sediment concentration at both stations is almost identical, though during maximal flow velocity, the measured values at Station 1 are a bit larger than at Station 2. This indicates that, though advection certainly will

play a role, horizontal gradients in sediment concentration are small, which is a good basis for 1DV-simulations. Maximal values of C vary from about 0.7 to 1.0 g/l during maximal flood and maximal ebb velocities down to about 0.3 g/l during slack water. This variation can be attributed both to settling and remixing processes over the water depth and/or to horizontal advection effects, as the travel time between the two stations is estimated at 20 to 30 min.

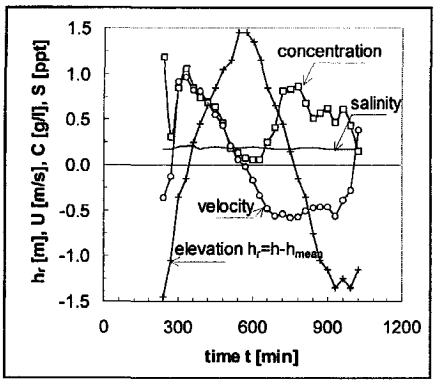

Fig. 7.20a: Measured variation in h_r, U, S and C at Station 1.

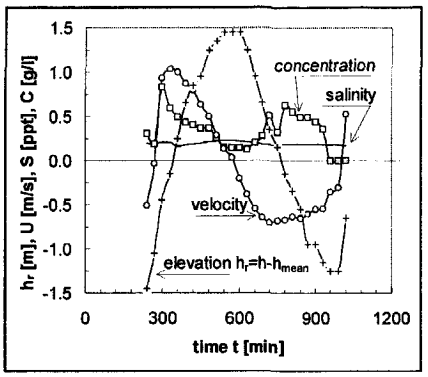

Fig. 7.20b: Measured variation in h_r, U, S and C at Station 2.

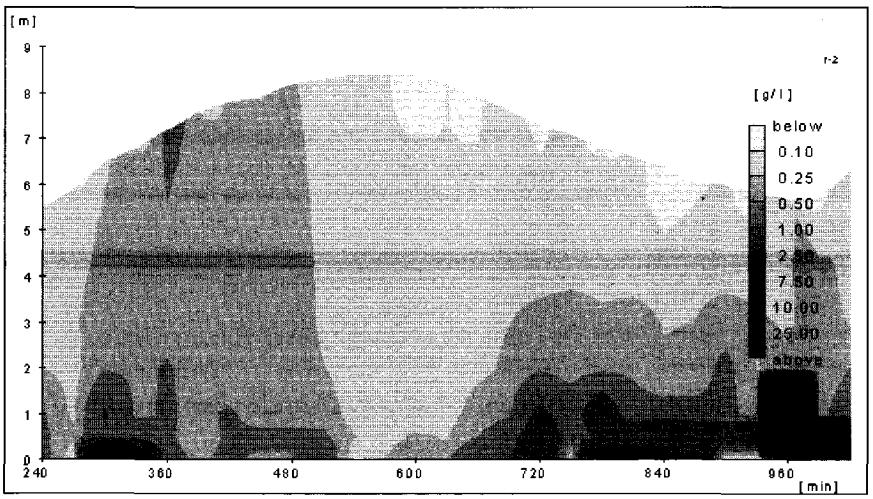

Fig. 7.21: Isolutals from measurements at Station 2.

Fig. 7.21 shows that during flood, the sediment is almost homogeneously mixed over the water depth, whereas during ebb, a more stratified condition occurs. This picture is qualitatively consistent with the larger peak flood velocity, e.g. Fig. 7.20. The very large concentrations around t = 1000 min. are attributed to instabilities of the mud on the steep river banks, supplying large amounts of mud to the river (Van

Leussen, 1999b), and will be ignored in our further analysis. Note that no data have been measured below $z = 0.3$ m.

In the next paragraphs we present the results of the numerical experiments with the 1DV POINT MODEL. We have carried out the following series of simulations:

1. In the first series the concentration distribution at Station 2 is simulated with a constant settling velocity, its value was determined by trial and error,
2. In the second series the concentration distribution at Station 2 is simulated with the full flocculation model, using the calibrated model parameters (e.g. Section 4.6),
3. In the third series also the full flocculation model was applied, but, contrary to the series 1 and 2, sediment-induced buoyancy effects are not taken into account, and
4. In the fourth series the settling velocity is computed from the equilibrium floc size, i.e. time effects are omitted. Sediment-induced buoyancy effects are included though.

The first series of simulations is carried out with a constant settling velocity and a gelling concentration c_{gel} = 40 g/l, as found from our earlier analyses. The constant settling velocity of w_s = 0.6 mm/s, which yields the best approximation of the field data, was found by trial and error. Other parameter settings are given in Table 7.6.

parameter	symbol	constant w_s	flocc. model	remarks
relative grid size	$\Delta z/h$ [-]	0.001 - 0.01		
time step	Δt [min]	0.5		
simulation period	T_{sim} [min]	4040		
bed roughness length	z_0 [m]	0.001		
buoyancy		yes		
water-bed exchange		no		
initial concentration	C_0 [g/l]	0.61		
Prandtl-Schmidt number	σ_T [-]	0.7		also smaller
hindered settling		yes		
settling velocity	$w_{s,r}$ [mm/s]	0.6	computed	
gelling concentration	c_{gel} [g/l]	40	computed	
parameters flocculation model				
efficiency parameter	e_c [-]		0.1	75 % ref.
efficiency parameter	e_d [-]		0.5	
efficiency parameter	ae_b [-]		$2.0 \cdot 10^{-5}$	
floc strength	F_y [N]		$0.32 \cdot 10^{-10}$	
form factor	α [-]		1.0	
form factor	β [-]		1.0	
shape factor	f_s [-]		1.0	
exponent	p [-]		1.0	
exponent	q [-]		0.5	

Table 7.6: Conditions for simulations Ems estuary, Station 2.

The results of the best simulation are presented in the form of isolutals in Fig. 7.22, which is to be compared with Fig. 7.21. It is noted that 1000 min. should be subtracted

from the values on the time-axis in Fig. 7.22, which is the spin-up time for all simulations. Though both pictures are qualitatively comparable, many of the features, characteristic for the measured pattern in Fig. 7.21 are missing, amongst which the rapid settling around high water (high water slack), and the vertical structure during the ebb period for $1700 < t < 1900$ min. (i.e. $700 < t < 900$ min.). We did not succeed in obtaining these features by changing the parameter settings. In fact a slightly larger initial concentration C_0 (or W_s) resulted in a total collapse of the concentration profile during the mentioned ebbing period, indicating that the conditions are close to saturation.

We also carried out some simulations with smaller Prandtl-Schmidt numbers (e.g. $\sigma_T = 0.3$, 0.5 and 0.6) with the idea of accounting for some additional mixing induced by ambient turbulence, but did not obtain an improvement of the results.

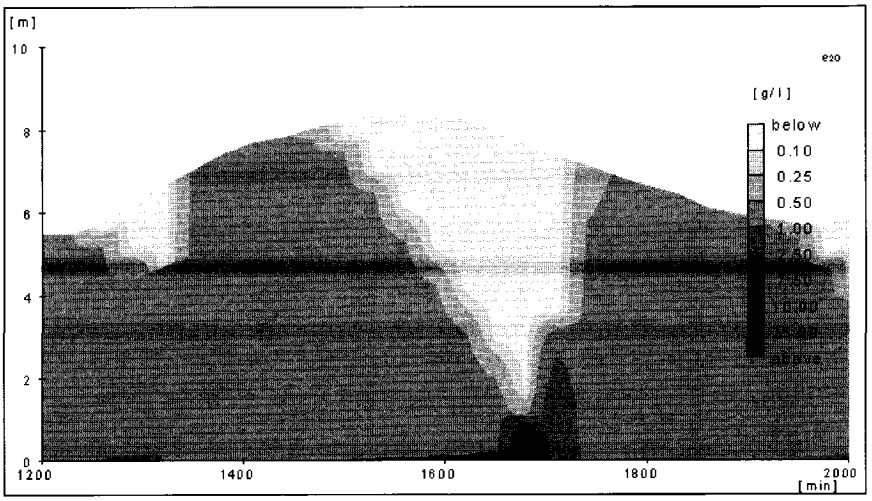

Fig. 7.22: Isolutals from 1DV POINT MODEL for optimal simulation with constant settling velocity.

The second series of simulations is carried out with the full flocculation model, using the calibrated parameter settings described in Section 4.6.2, apart from a small, 25 % decrease in the efficiency parameter e_c. In this case the settling velocity is variable, contrary to the first series of simulations. The results are presented in the form of isolutals in Fig. 7.23 and vertical concentration profiles at regular time intervals in Fig. 7.24.

The rapid decrease in suspended sediment concentration around High Water Slack is now reproduced, and also some of the vertical structure during the ebb period is found. Also the vertical profiles, as presented in Fig. 7.24, are reasonably reproduced, though the agreement becomes less towards the end of the ebb period.

When the initial concentration is lowered to $C_0 = 0.6$ g/l, the concentration profile during ebb becomes almost homogeneous. On the other hand, the picture of Fig. 7.23 remains virtually unchanged for values of C_0 ranging from 0.61 through 0.7 g/l. At still larger C_0, the concentration profile first collapses during ebb, and a further

increase in C_0 results in a complete collapse during the entire simulation period. The results of these simulations are not presented here, however.

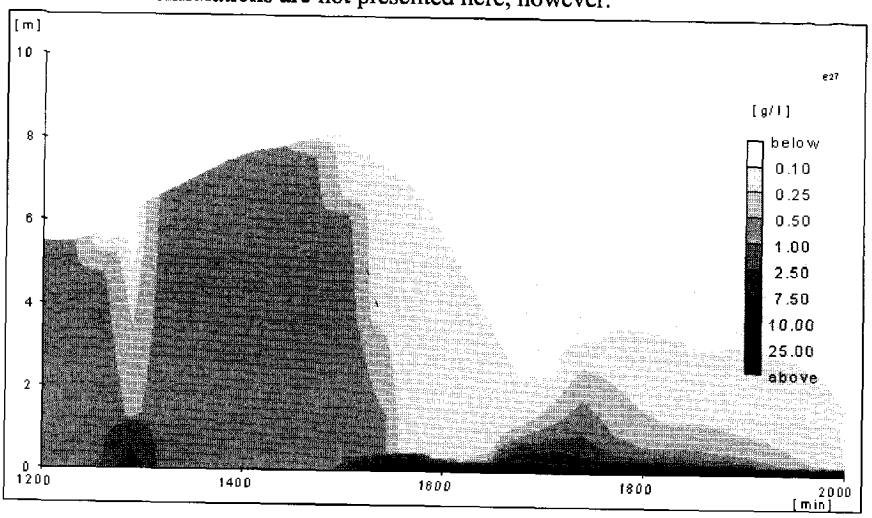

Fig. 7.23: Isolutals from 1DV POINT MODEL with flocculation model.

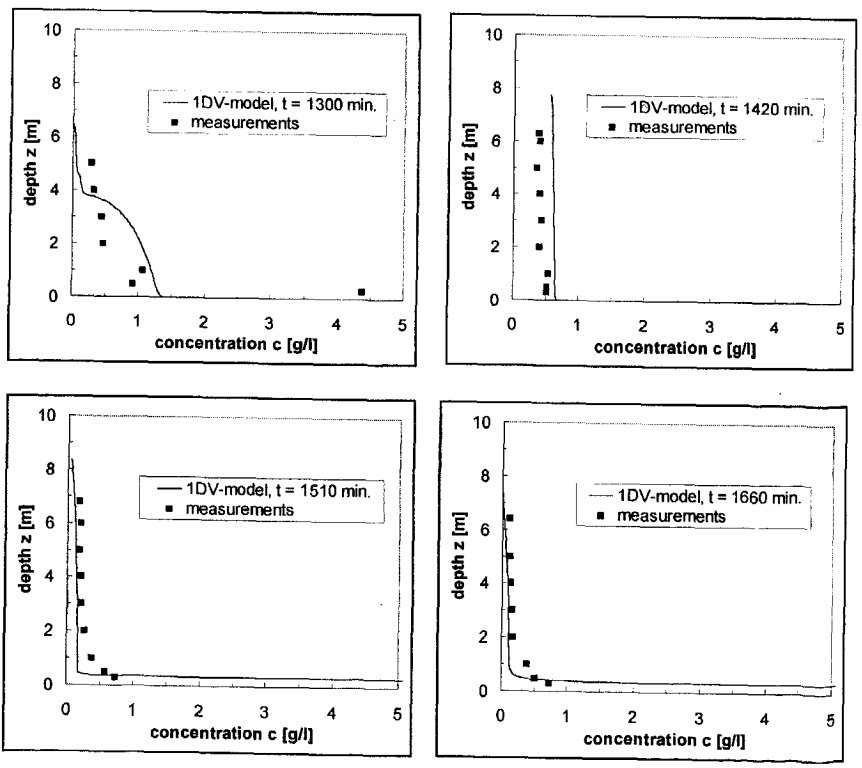

Fig. 7.24: Computed and measured vertical concentration profiles.

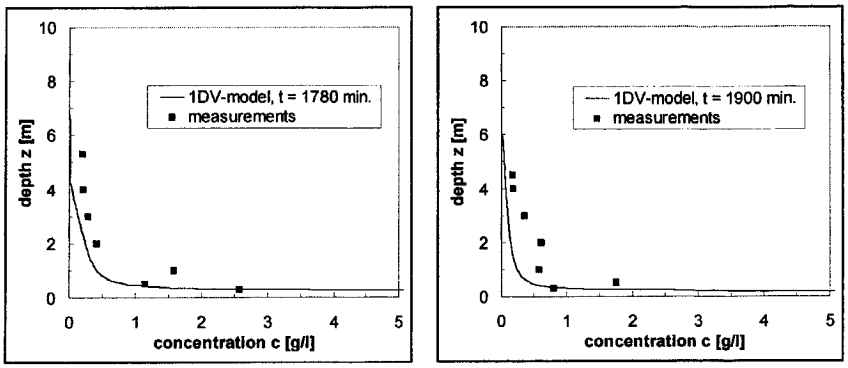

Fig. 7.24-continued: Computed and measured vertical concentration profiles.

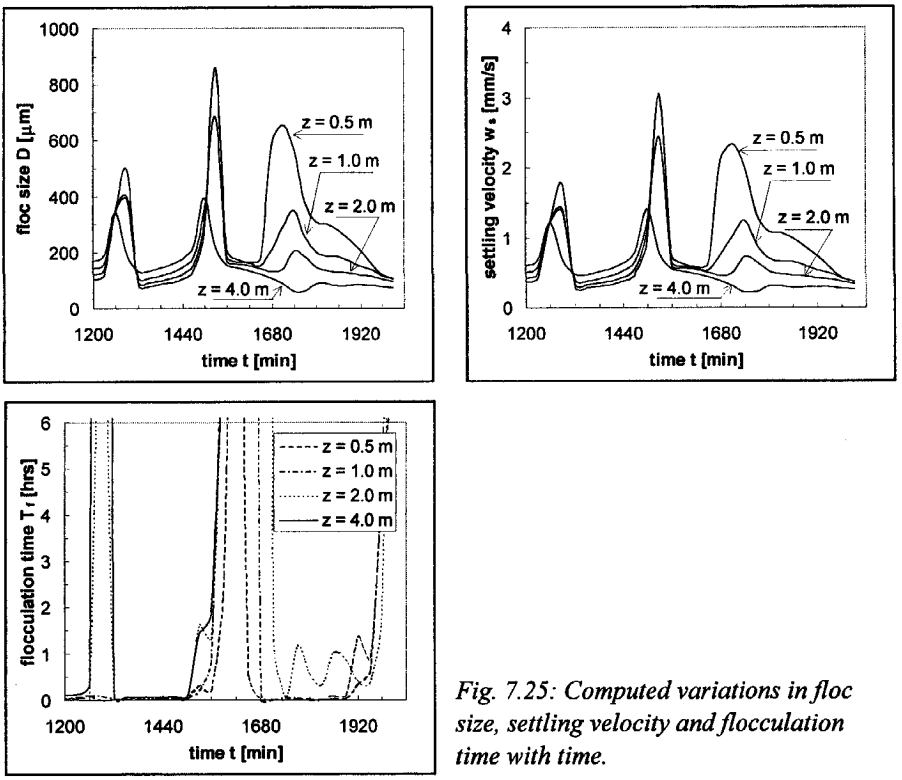

Fig. 7.25: Computed variations in floc size, settling velocity and flocculation time with time.

In Fig. 7.25 the computed variation with time of the floc size D, settling velocity $w_{s,r}$ (without hindered settling effects) and flocculation time T_f with time at four depths are presented. T_f is defined as the time still required for the flocs to achieve 95 % of their equilibrium size, assuming that the hydrodynamic and sedimentological conditions remain unchanged long enough. It is shown that during the flood period ($1300 < t < 1500$ min.), when the sediment is well mixed over the water depth, the settling velocity higher in the water column is larger than near the bed. This is the result of the

smaller values of the dissipation parameter G higher in the water column (e.g. Fig. 4.2). During the ebb period ($t > 1600$ min.) the larger settling velocities are found near the bed; now the effect of the larger sediment concentration becomes important and dominates the G-effect.

Fig. 7.25 also shows that D and $w_{s,r}$ vary significantly with time, with a pronounced peak during HWS. This peak explains the rapid settling observed around this period. The floc size varies between 100 and 900 μm, with typical values of about 100 to 200 μm, which agrees reasonably with Van Leussen's (1994) data, presented in Fig. 7.18, though the latter were obtained above the fluid mud in the turbidity maximum.

From an analysis of the measured vertical concentration profiles at Station 1 and 2, Van Leussen estimated the so-called effective settling velocity $w_{s,eff}$ at 0.3 to 1.5 mm/s, where $w_{s,eff}$ implicitly includes the effects of vertical mixing. Upon a correction for these mixing effects, values for the actual settling velocity w_s are obtained, which are a factor 2 to 4 larger than $w_{s,eff}$. Direct measurements of w_s with the VIS-system yielded values of $0.3 < w_s < 3$ mm/s. The computed values agree well with all these measured data.

The flocculation time T_f appears to vary considerably. Around slack water T_f amounts to many hours, whereas around maximal flood velocity ($1300 < t < 1500$ min.) and at the lower two levels during maximal ebb velocity ($1700 < t < 1900$ min.) $T_f \leq 5$ min. This would imply that around slack water the flocs will not get the time to achieve their equilibrium value, hence characteristic settling velocities for the entire tidal period are merely determined by the conditions prevailing during maximal ebb and maximal flood velocity.

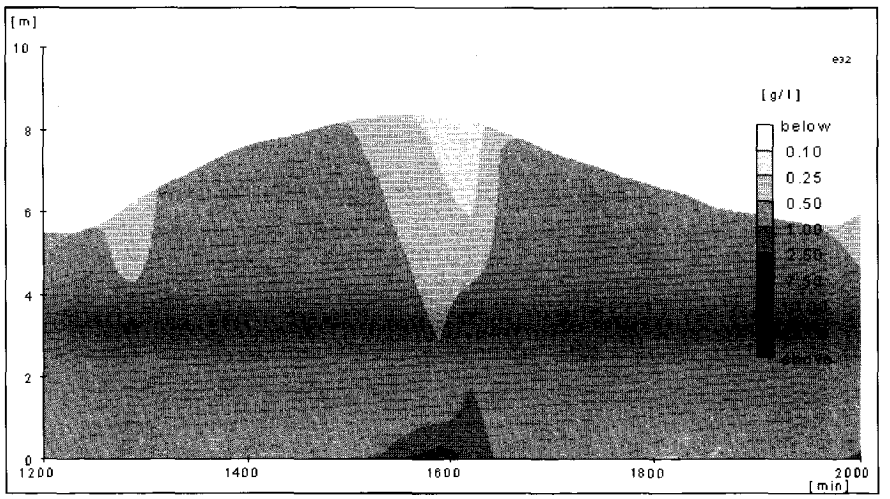

Fig. 7.26: Same as Fig. 7.23, but without sediment-induced buoyancy effects.

We have also studied the sediment-induced buoyancy effects and the role of the flocculation time through two simulations with the 1DV POINT MODEL in which these buoyancy effects are switched off, and in which the settling velocity is computed from the equilibrium floc size, respectively. The results are presented in Fig. 7.26 and

7.27 in the form of isolutals. These figures are to be compared with Fig. 7.21 and 7.23.

Fig. 7.26 shows that the vertical structure in the concentration profiles almost vanishes when sediment-induced buoyancy effects are not taken into account. If also a constant settling velocity is used (W_s = 0.6 mm/s), than even less vertical structure is maintained (not shown here).

The results presented in Fig. 7.27 are qualitatively comparable to those of Fig. 7.23, especially during the flood phase of the tide. Around HWS, though, a more pronounced vertical profile is found, which of course is directly related to the long flocculation times that limit the floc growth, hence settling velocity, in the flocculation model. The vertical concentration structure of Fig. 7.27 in the ebb period resembles the observations in Fig. 7.21 a little better even than that of Fig. 7.23, which might indicate that the flocculation time in the flocculation model is a bit large.

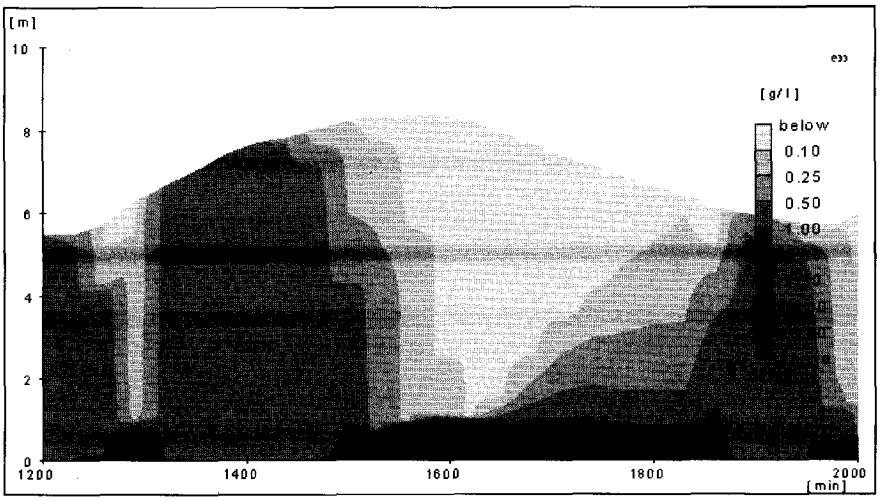

Fig. 7.27: Same as Fig. 7.23, but with equilibrium floc size.

From the analyses and simulations described in this section we can draw the following conclusions:

1. The gelling concentration in many estuaries amounts to about $c_{gel} \approx 40$ g/l, which is the sediment concentration for unconsolidated (mobile) fluid mud layers. This value is also predicted by the flocculation model, provided that the fractal dimension $n_f = 2$.
2. The observed variations over the tidal cycle in the vertical concentration profiles can only be simulated properly if the effects of sediment-induced buoyancy and flocculation are both taken into account in the 1DV POINT MODEL.
3. The flocculation model predicts that floc size, hence settling velocity, varies by an order of magnitude over the tidal cycle. Flocculation times around slack water appear to be very large, indicating that the flocs will never attain their equilibrium size around slack water. During maximal flood velocity and during maximal ebb

velocity in the lower part of the water column, flocculation times amount to a few minutes only.

These conclusions are consistent with observations (e.g. Van der Lee and Van der Ham, 1999) that the constant settling velocity, required to reproduce measured vertical concentration profiles with a 1DV-model, may be much lower than the settling velocities measured directly in the field.

7.4 HCMS in the Maasmond area (Dutch coastal zone)

The Directorate-General "Rijkswaterstaat", The Netherlands Ministry of Transport, Public Works and Water Management, installed four semi-permanent anchor stations on the sea bed at either side of the Maasgeul, the access channel to the Port of Rotterdam, within the framework of the SILTMAN-project, see Fig. 7.28. At these anchor stations, suspended sediment concentration at 0.15, 0.55, 2 and 7 m and flow velocity and direction at 0.35 m above the sea bed were monitored with an optical turbidity sensor and an EMS-flowmeter, respectively. The instruments were operated continuously during the winter periods 1995/'96 and 1996/'97. Also data on wave height, wind speed and direction and tidal elevation at stations nearby are available.

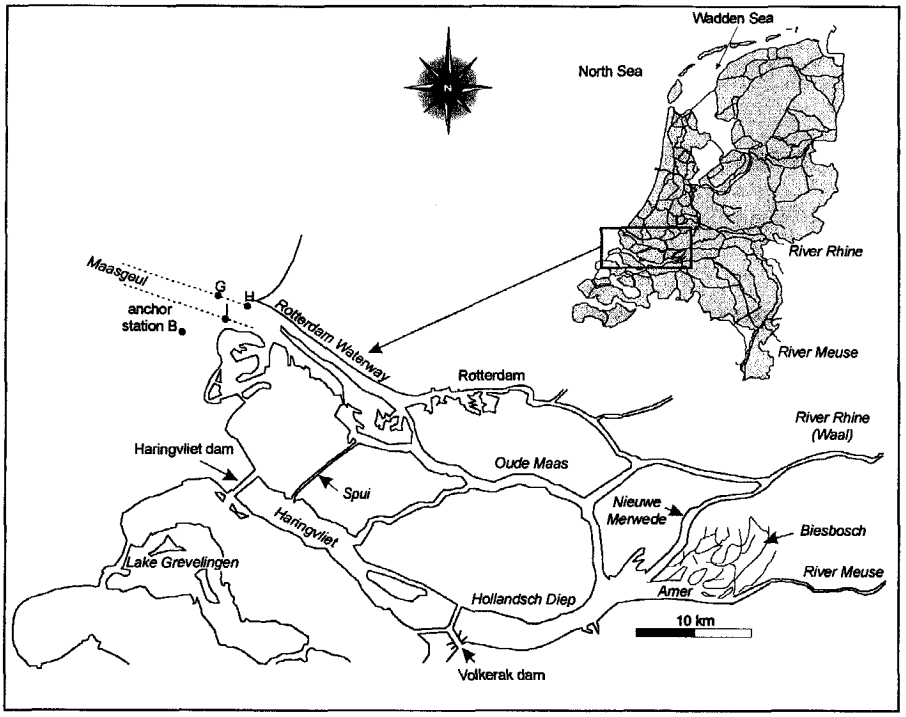

Fig. 7.28: Location of measuring stations around Maasgeul.

The season 1995/'96 is characterised by exceptionally calm weather conditions with no long and/or frequent stormy periods. During the entire season the measured sediment concentration remained small, rarely exceeding the mean summer values of several tens of mg/l. Occasionally, concentrations up to a few hundreds of mg/l were measured. This season is also renowned for an exceptionally low siltation rate and consequently small dredging needs in the navigation channels and harbour basins.

The winter season 1996/'97 is more typical of the meteorological conditions in this part of the North Sea, and dredging operations had to be carried out as usual. During this period, high suspended sediment concentrations were measured frequently, larger

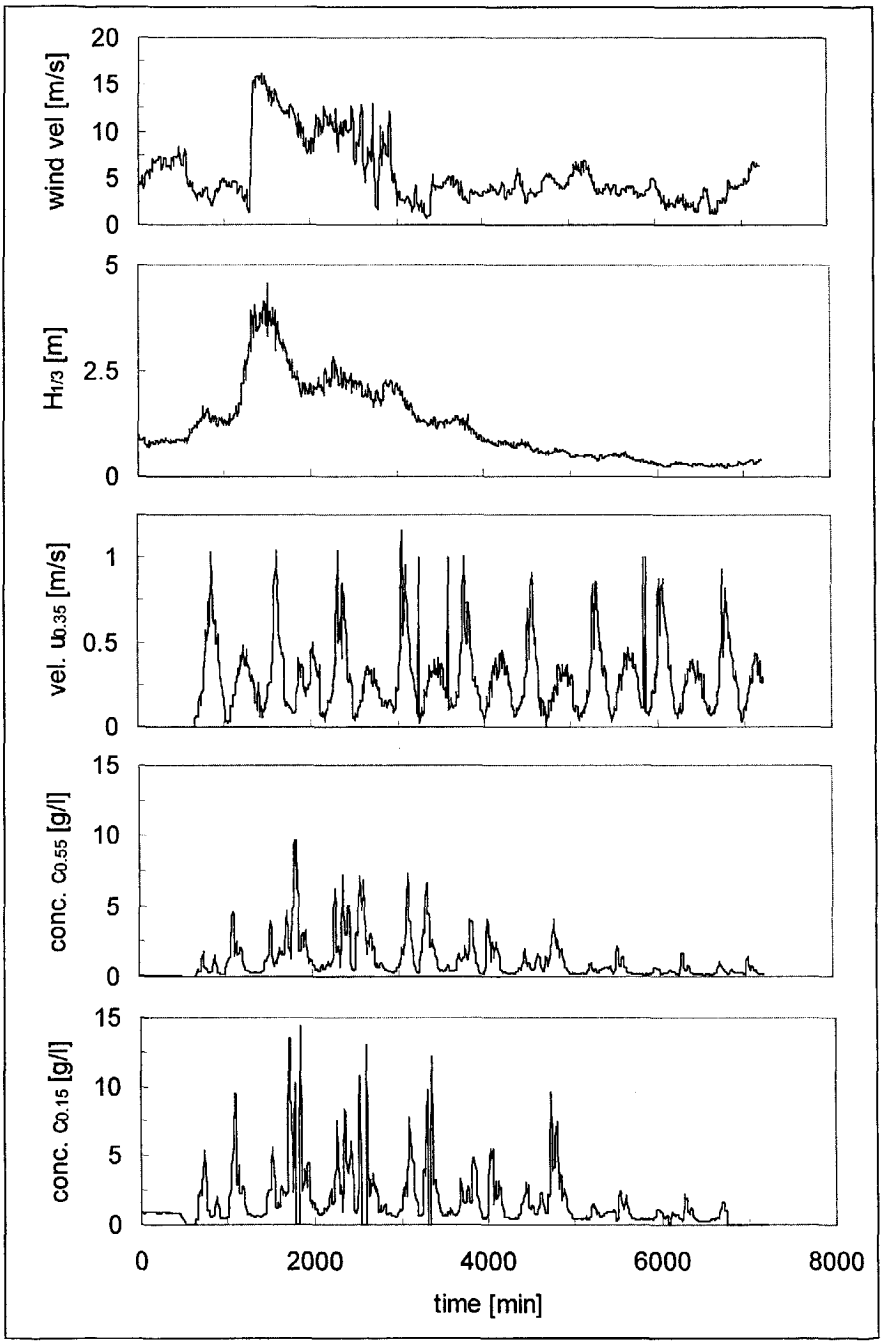

Fig. 7.29: Measurements of wind speed, wave height, flow velocity $u_{0.35}$ and sediment concentrations $c_{0.15}$ and $c_{0.35}$ at Station B, November 13 & 14, 1996.

than 10 g/l at the lower measuring stations. Fig. 7.29 shows the data at anchor station B for November 13 and 14, 1996, as an example. Wind speed and wave height were considerable, but not extreme. It is probably a sequence of rough weather conditions that results in the availability of the sediment; being available for transport, local hydro-meteo conditions govern its dynamics.

Measurements were also carried out simultaneously inland from the breakwaters. Vertical profiles of salinity, velocity and suspended sediment concentration revealed a sharp lutocline low in the water column. The sediment concentration below this lutocline amounted to more than several tens of g/l, whereas above this lutocline, virtually no suspended sediment was found, e.g. concentrations of a few tens of mg/l at most (Van Woudenberg, 1998).

The following paragraphs discuss the analysis of these measurements. We have selected the data from anchor station B, as the flow at this location is only slightly distorted by the converging flow effects near the head of the breakwaters.

We have run the 1DV POINT MODEL to simulate the measurements of November 13/14, 1996. The depth-averaged flow velocity is estimated using the measured data at 0.35 m above the bed assuming a logarithmic velocity profile - see Fig. 7.30. The time-varying significant wave height is schematised into a few time functions (blocks with wave height either constant or linearly varying with time). Rms-values for the wave height are obtained from a procedure outlined in Van der Velden (1989) and the relevant wave period is deduced from Roskam's (1995) data base on the wave climate in the Dutch coastal zone.

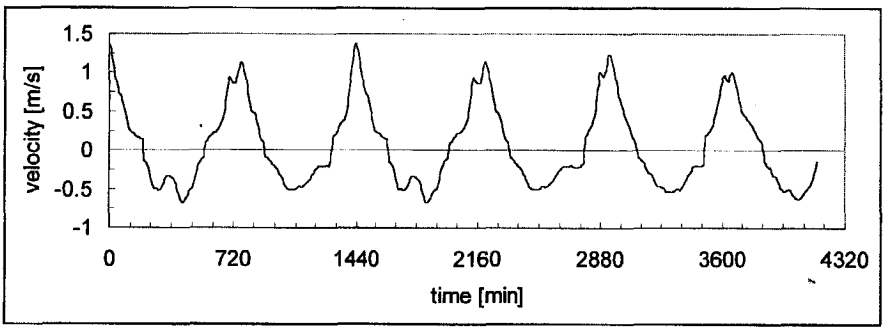

Fig. 7.30: Time series of depth-averaged velocity used in 1DV POINT MODEL.

The Dutch coastal zone in this area exhibits a strong vertical fresh-saline water induced stratification, caused by the outflow of the River Rhine. As no salinity profiles are available during the measuring period, we apply the vertical salinity profile measured at April 8, 1997, which is believed to be typical for conditions throughout the year, and is characterised by a constant salinity of about $S \approx 30$ ppt in the lower 8 to 9 m of the water column, with a gradually decreasing salinity on top down to $S \approx 10$ to 15 ppt at the water surface. With respect to the vertical salinity distribution, the 1DV POINT MODEL is run in a so-called diagnostic mode, which implies that the initial salinity profile remains constant during the simulations and only affects the vertical density profile, hence the vertical mixing processes.

parameter	value	parameter	value
h	16 m	c_{gel}	80 & ∞ kg/m^3
H_{rms}	from data	W_s	0.6 mm/s
U	from data	C_0	0.5 kg/m^3
z_0	0.001 m	n	109 grid points$^{\dagger)}$
ρ_w	1020 kg/m^3	Δt	1 min
ρ_s	2650 kg/m^3	T_{rel}	2 min
buoyancy effects		yes	no; see Fig. 7.34
surface waves		yes	no; see Fig. 7.35
salinity profile		yes	no; see Fig. 7.37
water-bed exchange		no	
wind stress		no	
flocculation model		no/yes	yes; see Table 7.6

Table 7.7: Parameters in 1DV POINT MODEL ($^{\dagger)}$ n = number of grid points; near the bed a logarithmic grid size distribution is used).

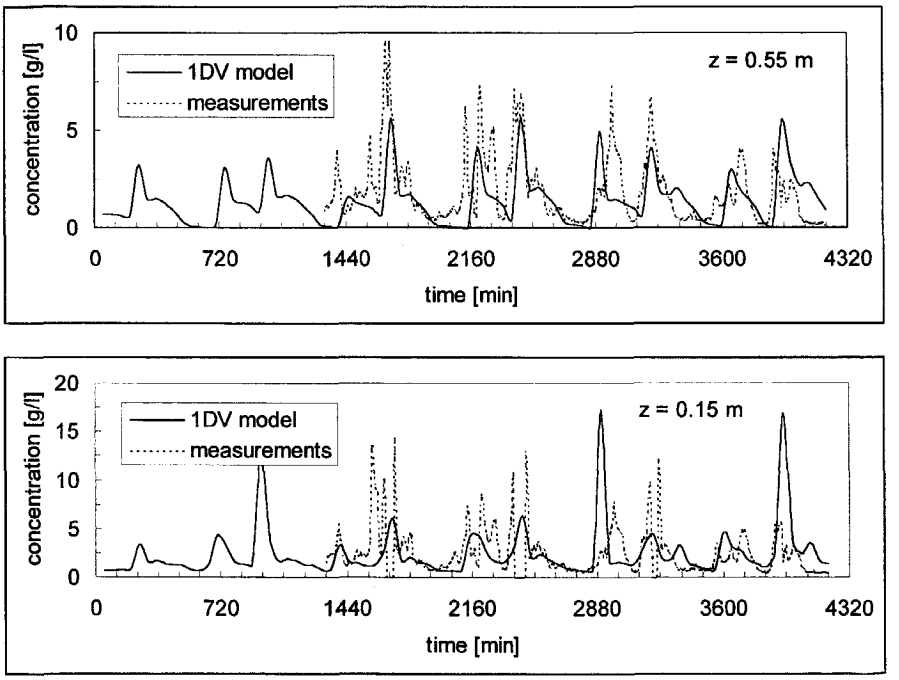

Fig. 7.31: Computed and measured concentrations at Station B, Nov. 13 & 14, 1996.

All simulations are carried out for one sediment fraction only and they start with an initially homogeneous concentration profile C_0 and a spin-up time of 24 hours. After some trial and error, a fair agreement with the measurements is obtained for the parameters summarised in Table 7.7. We recognise that the total amount of sediment available, defined by C_0 in the simulations, may not be constant in reality - no data are available however.

Fig. 7.31 compares the computed and measured suspended sediment concentration at 0.55 m and 0.15 m above the bed; unfortunately, data at 2 and 7 m above the bed are not available. We observe that the numerical results follow the measured trend and variations properly, though some of the detailed patterns are missed, amongst which a series of individual peaks in the concentration measurements. The latter may be related to episodic events (bursts?), which are not accounted for in the model. These deviations can also be attributed, though, to short time variations in wave activity or fresh/saline water stratification (note that our simulations are not run with the actual salinity profile), and to horizontal advection and/or patchiness of the suspension. We conclude however that the agreement between simulations and measurements is sufficiently accurate to assess the dominant physical processes governing the sediment dynamics around the Maasgeul.

Fig. 7.32 shows the variation in concentration at four levels for the same simulation. At $z = 2$ m, c varies around 1 g/l. At this height, no data are available for Station B, but the measurements at Station H give concentrations within the same range. Close to the bed, a temporal, about 1 dm thick layer of fluid mud appears to be formed around slack tide (with $c_{max} = c_{gel}$). This layer is remixed rapidly over the water column with increasing flow velocity, causing some of the peaks in $c_{0.15}$ and $c_{0.55}$ in Fig. 7.31. The numerical results are also plotted in Fig. 7.33, showing that no sediment can penetrate into the upper part of the water column due to the low vertical mixing caused by the salinity-induced stratification effects.

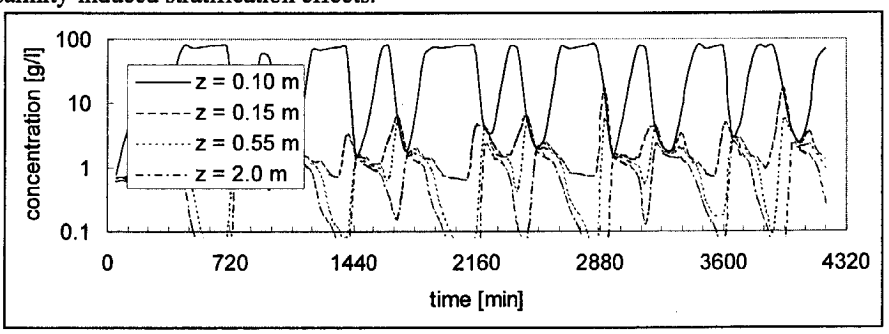

Fig. 7.32: Computed concentration at 4 heights at Station B, Nov. 13 & 14, 1996.

We have also carried out simulations with the Partheniades-Krone bed-boundary conditions, the results of which are not presented here. However, in this case we are not able to reproduce the measurements in any reasonable way for any realistic or unrealistic parameter setting. The erosion formula causes the water column to load up with sediment until it becomes super-saturated causing a collapse of the concentration profile like in Section 6.5.1; the deposition formula causes the water column to unload, as a result of which buoyancy effects vanish. We note that this assessment is consistent with the sediment composition of the sea-bed, which contains only about 3 % of cohesive sediment.

We stress however, that we do not conclude that erosion-deposition processes are not important with respect to the dynamics of HCMS in general, as ultimately they are of course responsible for the amount of sediment available.

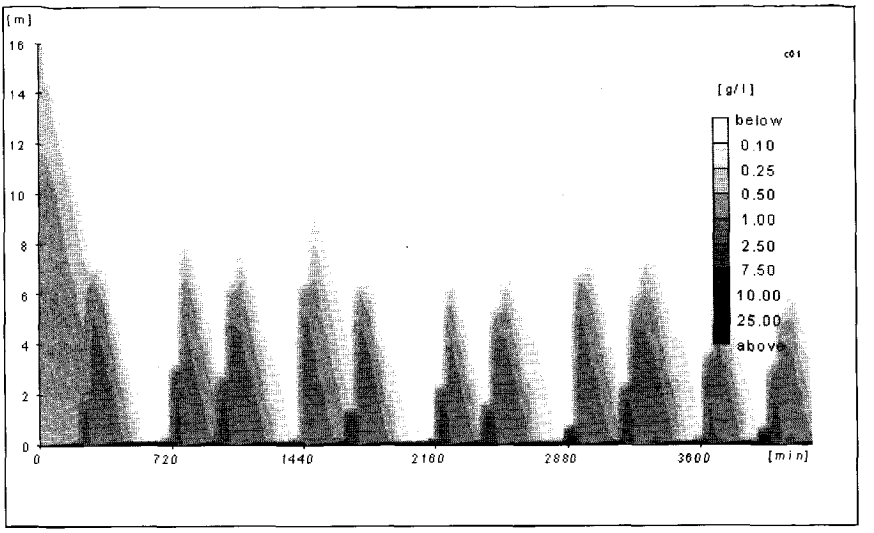

Fig. 7.33: Computed isolutals at Station B, Nov. 13 & 14, 1996; reference conditions: with buoyancy, waves, salinity and hindered settling.

The results, as presented in Fig. 7.33, are the basis for a series of sensitivity analyses in which we switch off the various processes in the 1DV POINT MODEL one by one. The following series of simulations is carried out:

1. In the first series the effects of sediment-induced buoyancy is studied.
2. In the second series the effects of waves is studied,
3. In the third series the effects of a vertical salinity profile is studied,
4. In the fourth series the effect of hindered settling is studied,
5. In the fifth series a simulation with the full flocculation model is carried out,
6. In the sixth and seventh series so-called prognostic simulations are carried out; in the sixth series the effect of a navigation channel is studied, using the reference conditions, and
7. The seventh series is identical to the sixth, but the effect of sediment-induced buoyancy is excluded.

Fig. 7.34 shows the results of a simulation without buoyancy effects. Quantitatively this picture is considerably different from Fig. 7.33, and it is not possible to obtain results that resemble the measurements. However, from a qualitative point of view Fig. 7.34 and 7.33 are comparable. This qualitative comparison is lost if we exclude the effect of waves (Fig. 7.35 and 7.36), or the vertical salinity profile (Fig. 7.37), or switch off the effects of hindered settling ($c_{gel} \rightarrow \infty$), see Fig. 7.38. Close inspection of Fig. 7.35 shows much less agreement between computational and experimental results in comparison to the reference situation - Fig. 7.31. Fig. 7.38 even shows a complete collapse of the concentration profile, which is caused by the very large vertical gradients in suspended sediment concentration, as the near-bed concentration can grow without limits when gelling is not accounted for. We estimate that the contribution of waves to the vertical mixing is about 20 %, implying that the suspension is close to its saturation value. Our analysis shows further that hindered

settling locally tends to maximise the vertical density gradients, which results in considerable buoyancy effects, and also appears to be crucial for a proper reproduction of the vertical sediment concentration profile. Simulations with slightly different values for c_{gel}, i.e. $60 < c_{gel} < 110$ g/l yield comparable results; however, when c_{gel} is lowered to about $c_{gel} = 40$ g/l, the computational results start to deviate considerably from the observed time series of $c_{0.15}$ and $c_{0.55}$.

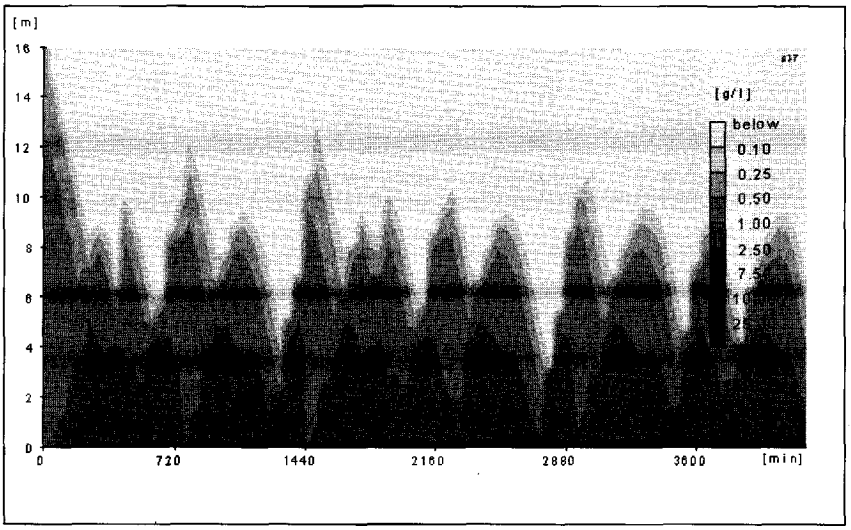

Fig. 7.34: Computed isolutals at Station B, Nov. 13 & 14, 1996; sensitivity analysis: with waves, salinity and hindered settling, no buoyancy.

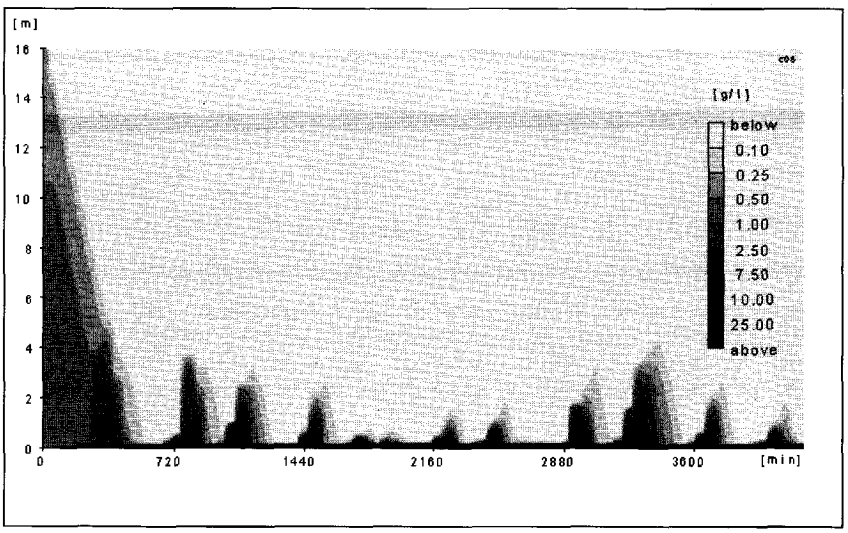

Fig. 7.35: Computed isolutals at Station B, Nov. 13 & 14, 1996; sensitivity analysis: with buoyancy, salinity and hindered settling, no waves.

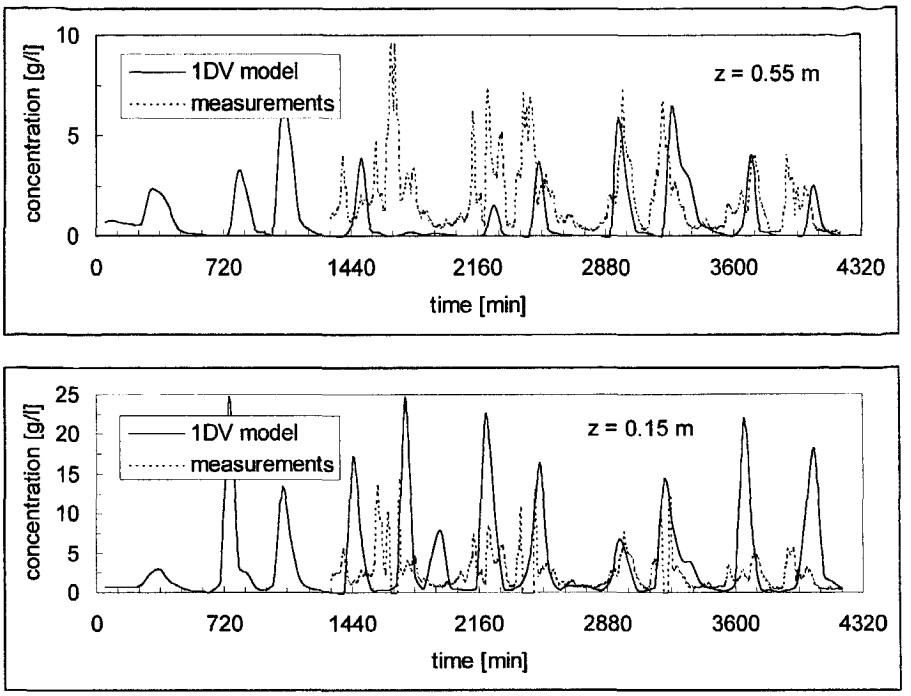

Fig. 7.36: Computed evolution of concentration profile at Station B, Nov. 13 & 14, 1996; sensitivity analysis: with buoyancy, salinity and hindered settling, no waves.

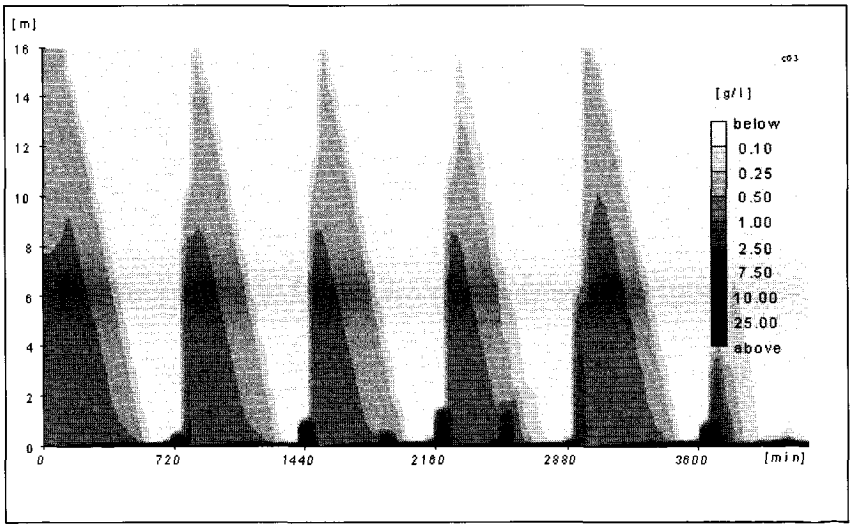

Fig. 7.37: Computed isolutals at Station B, Nov. 13 & 14, 1996; sensitivity analysis: with buoyancy, waves and hindered settling, no salinity.

We conclude that the vertical salinity profile prevents the sediment being mixed over the entire water column. This effect appears to be important in the Maasmond area and it agrees with remote-sensing observations, c.q. aerial photographs which have never revealed highly turbid waters in this area, as such observations are limited to the near-surface water layers. We note however, that no data are available on the suspended sediment concentration in the upper part of the water column to quantify this conclusion.

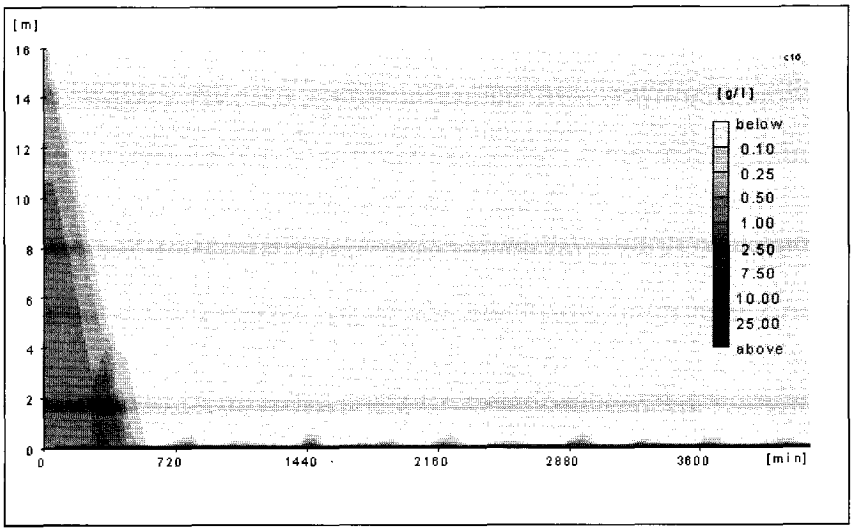

Fig. 7.38: Computed isolutals at Station B, Nov. 13 & 14, 1996; sensitivity analysis: with buoyancy, waves and salinity, no hindered settling.

From our analyses we conclude that the sediment concentration, measured at anchor station B, is close to its saturation value, and we infer that this is the case for a large area in the Dutch coastal zone. During slack water a thin, temporal layer of fluid mud is formed, which is mixed rapidly during accelerating tide. These dynamics are governed strongly by the effects of the tide, surface waves and vertical fresh-saline water induced stratification. As the sea bed locally contains only small amounts of cohesive sediment, water-bed exchange processes are not important. A proper reproduction of the measurements is only possible if salinity- and sediment-induced buoyancy effects, and the effects of surface waves, tidal velocity variations and hindered settling are all taken into account.

We have also carried out two simulations with the full flocculation model and with an equilibrium settling velocity. The results of the first simulation are presented in the form of isolutals in Fig. 7.39 and of time series of $c_{0.15}$ and $c_{0.55}$ in Fig. 7.40. The picture in Fig. 7.39 qualitatively resembles that of Fig. 7.33. On close inspection we observe major differences near the bed however, which become very clear from the

$c_{0.15}$-time series (with log-scale) in Fig. 7.40[2]. The reason for this large discrepancy is the small gelling concentration, hence fluid mud concentration, predicted by the flocculation model. Whereas the reference conditions of Fig. 7.33 required $c_{gel} \approx 80$ g/l to obtain a fair agreement between measured and computed time series of $c_{0.15}$ and $c_{0.55}$, the flocculation model predicts $c_{gel} = 20$ to 40 g/l.

It is noted that simulations with different initial sediment concentrations did not improve the results either. These results are not presented however.

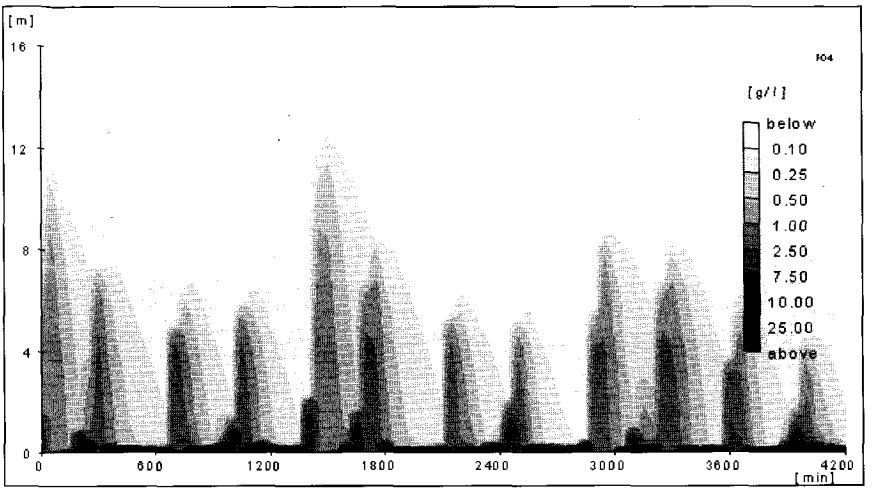

Fig. 7.39: Computed isolutals at Station B, Nov. 13 & 14, 1996; full flocculation model.

Two possible reasons can be identified to explain this underestimation of the gelling concentration:

1. The fractal dimension in the flocculation model is set at $n_f = 2$. Larger values of c_{gel} can be obtained with $n_f = 2.5$ - 2.7 (see Fig. 4.9). Applying such values would also require retuning of the other parameters of the flocculation model. As no data on the settling velocity and its time evolution are available, and no physical reason is known why n_f in the water column should be so high, we have made no attempt to improve the agreement between measurements and computations with the full flocculation model. Moreover, a better agreement would not necessarily imply realistic values of the model parameters.
2. Within the wave boundary layer large instantaneous stresses occur. The thickness of this boundary layer is estimated at 2 to 6 cm, applying equ. (3.25) of Section 3.4. The peak instantaneous shear stresses are about twice the mean stress, averaged over the wave period (e.g. Van Rijn, 1993), implying that $G_{peak} \approx 2^{3/4} \times G_{mean}$, where G is the dissipation parameter. Moreover, the local sand bed is not smooth, but contains ripples and other irregularities. It is imaginable that the mud flocs in a fluid mud layer, that is moved back and forth by the orbital motion over such an

[2] We have also compared the measurements with the computed time series 0.3 m higher in the water column to account for the increased thickness of the fluid mud layer when using the full flocculation model. However, this did not improve the agreement.

irregular bed, will be fractured, as a result of which the gelling concentration increases.

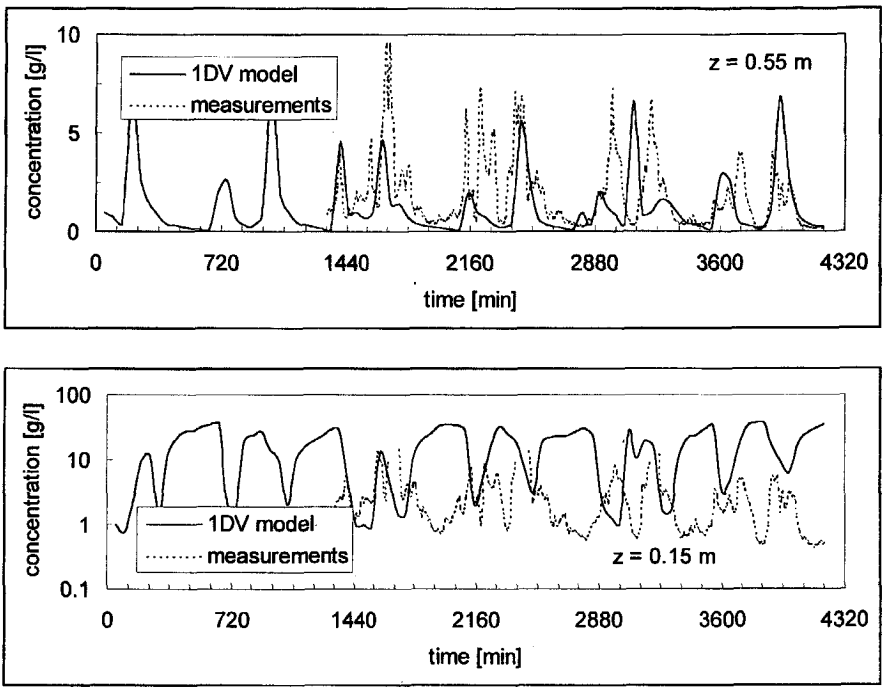

Fig. 7.40: Computed evolution of concentration profile at Station B, Nov. 13 & 14, 1996; full flocculation model.

At present we are tempted to believe that waves have a significant effect on c_{gel}, hence on the properties of the fluid mud. An effort to substantiate this hypothesis further by another simulation was not successful however. In this simulation an equilibrium settling velocity $w_{s,e}$, using the calibrated parameters of Chapter 4, is applied, together with a prescribed gelling concentration of c_{gel} = 80 g/l. It was found that near the bed settling velocities of 0.7 to 1.5 mm/s are computed, which results in a total collapse of the concentration profile, forming a fluid mud layer with c = 80 g/l. By trial and error a parameter set for $w_{s,e}$ can probably be found that results in a reasonable agreement between measurements and simulations. This however has not been done, as it would not help to understand the effect of waves on the flocculation process. Nevertheless, the results of Fig. 7.39 and 7.40 show however that this may be an important aspect in modelling the behaviour of HCMS in coastal areas. The research required to quantify this effect is beyond the scope of the present study, though.

Next, the 1DV POINT MODEL is used in a Lagrangean sense, i.e. a package of water with sediment at Station B is followed on its course into the Maasgeul. Along this route, the water depth increases from 16 m at Station B to 24 m within the access channel. We assume that the flow crosses the channel perpendicularly, as a result of which the flow velocity will decrease by 1/3. In reality, a considerable along-channel

component will be generated, caused by the in- and outflow through the Rotterdam Waterway and the various harbour basins. However, for the present analysis our assumption is sufficient, as the suspension is almost saturated, and a small decrease in flow velocity will already be sufficient to cause a complete collapse of the vertical profile. Moreover, the contribution of the waves to the vertical mixing processes will become small or even disappear entirely, because the channel's width is too small to allow (re-)generation of long waves that would affect the bed.

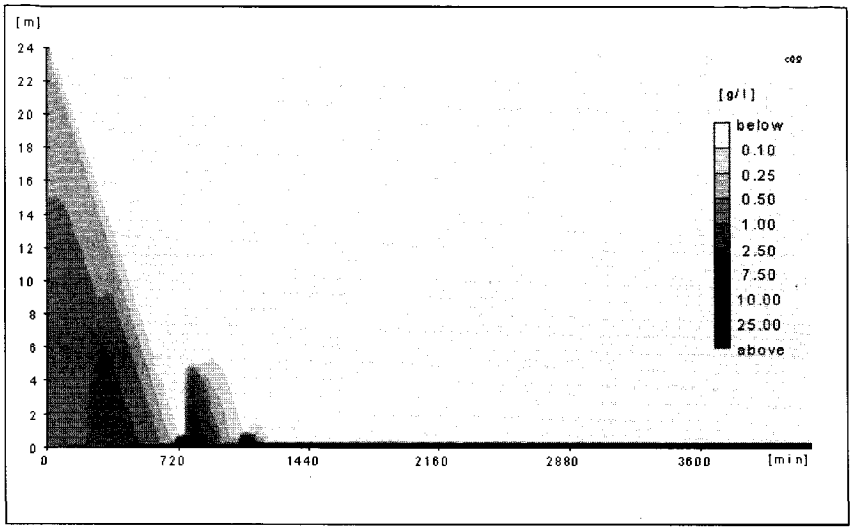

Fig. 7.41: Prognostic simulation of concentration profile in the Maasgeul, Nov. 13 & 14, 1996; reference conditions: with buoyancy, waves, salinity and hindered settling.

Apart from an increase in water depth and decrease in flow velocity, all other parameters are kept at the settings of Fig. 7.33. The results of this prognostic simulation are presented in Fig. 7.41, showing a catastrophic collapse of the vertical sediment profile. The flow within the access channel to Rotterdam Port, the Maasgeul, is no longer able to carry the available sediment in suspension, and the conditions become super-saturated. The computed Richardson numbers show very high values near the sediment-water interface, with a corresponding collapse of the turbulent kinetic energy and eddy diffusivity, very similar to the picture presented in Fig. 6.2.

Finally, this simulation is repeated, but without buoyancy effects. The results are presented in Fig. 7.42, showing a picture not widely different from that of Fig. 7.34, and predicting fairly large concentrations within the Maasgeul.

We conclude that the sediment dynamics around the Maasgeul can only be represented properly by a numerical model that does include sediment-induced buoyancy effects, the effects of the local salt-stratification and the contribution of surface waves to the vertical mixing. It seems that the sediment suspension in the vicinity of the Maasgeul is almost saturated for the hydro-meteo conditions under consideration. During slack water, a temporal thin layer of fluid mud is formed on the sea bed that is mixed

rapidly during accelerating tide causing pronounced peaks beyond 10 g/l in the suspended sediment concentration at 0.15 and 0.55 m above the bed.

When the water body moves over the Maasgeul, the suspension becomes super-saturated and the vertical turbulence and concentration profile collapse, forming a fluid mud layer. However, this collapse however will take place at the time scale of settling T_s, which amounts to about $T_s = h/W_s = 12$ m / $0.6 \cdot 10^{-3}$ m/s ≈ 6 hrs ($h_{eff} \approx h/2$ because of the salt-fresh water stratification). Hence, this collapse cannot explain the observed absence of suspended sediment in the water column between the breakwaters, as the travel time of this package of water-sediment mixture between the two locations of observation is only one to two hours. However, from soundings and dredging needs we know that sediment enters the channels and basins within the breakwaters frequently.

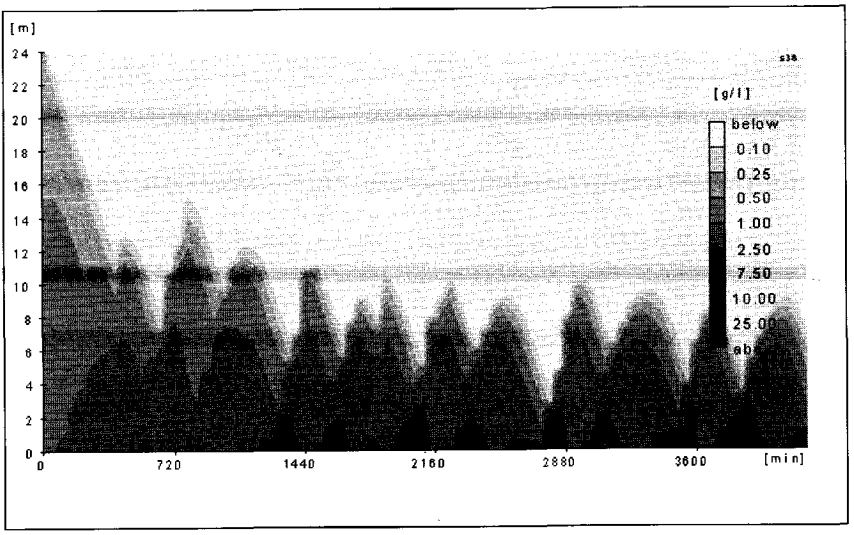

Fig. 7.42: Prognostic simulation of concentration profile in Maasgeul, Nov. 13 & 14, 1996; sensitivity analysis: with waves, salinity and hindered settling, no buoyancy.

We infer therefore that the collapse of the concentration profile is a necessary, but not a sufficient condition to form such a high-concentrated near-bed suspension in the inner channels and harbour basins. It is hypothesised that this collapsing suspension triggers the generation of a sediment-driven density current, which cleanses the water column rapidly, causing the rapid siltation through the transport and accumulation of fluid mud into the channels and harbour basins. This hypothesis is subject of ongoing research.

8. Transport and fate of HCMS

8.1 Scaling parameters for HCMS

In Chapter 3 through 5 we have studied the various individual processes that govern the behaviour of High-Concentrated Mud Suspensions in an isolated way, and in Chapter 6 we have studied the interaction between the suspended sediment and the turbulent flow. In Chapter 7 we have validated our model concept against a limited set of laboratory and field data. In the present chapter we discuss how the various processes interact to obtain an integrated picture. For this purpose we sketch the transport and fate of a near-saturated mud suspension in an estuary or coastal zone. The time scale of the primary driving force is the tidal period T, or more accurately, the period of the decelerating and accelerating phase of the tide. We have argued in Section 3.3 that the adaptation time of the turbulence parameters, like the eddy viscosity and eddy diffusivity, to changes in hydrodynamic conditions is small compared to other time scales, so that the turbulence time scale T_T can be neglected in our analyses.

The mud flocs in a near-saturated HCMS start to settle during decelerating tide to form a layer of fluid mud, which is mixed over the water column entirely during the accelerating phase of a tide cycle. This cyclical process is governed by one or a combination of four scaling parameters, i.e. the relative settling time T_s', the relative mixing time T_m', the Richardson number Ri_*, and the Rouse number β, depending on the hydrodynamic and sedimentological conditions prevailing, as shown in Chapter 6.

The settling process itself is controlled by flocculation processes. In the upper part of the water column the dissipation parameter G, which is a measure for the floc forming diffusion processes and floc disrupting turbulent stresses, is relatively small, and we expect large (equilibrium) values of the floc size D and settling velocity w_s, whereas in the lower part of the water column G is large, hence we expect small values of D, c.q. w_s. Of course the sediment concentration c is smaller in the upper part of the water column than near the bed, reversing the trend in D and w_s. In general the effect of G, which varies also with tidal phase, dominates, except when c becomes very large. Around slack water G decreases, and large values of D and w_s may be expected, further enhancing the settling process in this phase of the tide. Whether such variations in D and w_s with time and over the water depth are relevant depends on the time scale for flocculation T_f, as discussed in Chapter 4 and Section 7.3. Note that, especially in shallow areas, D and w_s may be determined primarily by the composition of eroded bed material rather than by the flocculation processes in the water column. This may lead to spurious correlations in w_s-c graphs, as both the amount of sediment and the size of the eroded particles may increase with increasing flow velocity.

Flocculation processes also cause considerable hindered settling effects and determine the gelling conditions at which fluid mud formation takes place. The resulting large gradients in sediment concentration, known as lutoclines, damp the vertical exchange of turbulence through buoyancy effects, as a result of which T_m' is affected. Because of this decrease in vertical mixing, less sediment can be kept in suspension, enhancing the lutocline formation further through a positive feed-back.

The vertical mixing processes are generated by the flow. Waves may augment vertical mixing considerably through their effect on the apparent bed roughness, hence waves form an important parameter in the dynamics of HCMS in coastal zones. The influence of waves on the flocculation process itself and on the gelling concentration of the mud is not clear at present, however.

Following the hindered settling phase, the fluid mud formed during decelerating tide may gain strength through consolidating processes. Whether this is the case depends on the time scale for consolidation T_c in relation to the relevant time scale of the driving force. The latter may be attributed to waves and is therefore not necessarily the tidal period. The re-entrainment process of this fluid mud layer is governed by two additional scaling parameters, i.e. the effective Reynolds number Re_e, determining whether the fluid mud layer can be mixed through turbulent processes, and by a relative bed shear stress parameter θ_e. If $\theta_e > 1$, re-entrainment by floc-erosion will take place, whereas for $\theta_e < 1$, no re-entrainment of the fluid mud layer is to be expected. We anticipate that θ_e is related to the yield strength of the fluid mud layer through the consolidation process (e.g. Van Kesteren et al., 1997).

In our analysis of the saturation concept, we assumed that the mud flocs form a fluid mud layer upon deposition, damping the turbulence production at the mud-water interface. However, if the bed is irregular, for instance due to ripples, small dunes, cavities, etc., the first amounts of depositing mud will collect in the depressions of these irregularities. If this amount is limited, turbulence production is still possible at the protruding tops of the ripples, for instance. A commonly used measure for such irregularities is the Nikuradse roughness height k_s, and we deduce that an additional scaling parameter is given by the ratio δ_m/k_s, where δ_m is the thickness of the fluid mud layer. Only if $\delta_m/k_s >> 1$, saturation can occur.

These various scaling parameters are summarised in Table 8.1; all time scales are made non-dimensional with respect to the tidal period T, or its decelerating or accelerating phase:

scaling parameter		comments / effects on:
tidal period	T	major driving agent
turbulence generation	T_T/T	negligible for tidal flow
effective Reynolds number	Re_e	turbulence level fluid mud layer
Rouse number	β	concentration profile; saturation parameter
particle Richardson number	Ri_*	overall buoyancy effects; saturation parameter
relative sedimentation time	T_s/T	relaxation time; saturation parameter
relative sedimentation depth	h_s/h	sediment available for fluid mud formation
relative mixing time	T_m/T	relaxation time; saturation parameter
relative flocculation time	T_f/T	relevance of variations in settling velocity; fluid mud concentration
relative consolidation time	T_c/T	strength in fluid mud & turbulence production
relative erosion strength	θ_e	floc erosion of consolidating bed
relative bed irregularities	δ_m/k_s	saturation; damping of turbulence production

Table 8.1: Scaling parameters for HCMS-dynamics.

If the hydrodynamic conditions are cyclical and the amount of sediment is constant, the behaviour of the near-saturated HCMS is cyclical as well, in the sense that a period of settling and fluid mud formation during decelerating tide is followed by a period of re-entrainment of the fluid mud and the subsequent mixing over the water column during accelerating tide. If, however, by some mechanism, either the tidal flow velocity or the wave effects decrease, or the amount or properties of the sediment change, the HCMS may become super-saturated, resulting in a total collapse of the turbulence field and the vertical concentration profile. Such effects may occur in the following cases, for instance:

1) an increase in water depth in the direction of the flow, for instance in a navigation channel,
2) a decrease in flow velocity, for instance in a harbour basin, or towards neap tide,
3) a decrease in wave height, for instance after a storm, resulting in a decrease in vertical mixing capacity,
4) an increase in wave height, for instance during a storm, eroding consolidated mud deposits,
5) dredging works, increasing the volume of sediment in the environment,
6) algae bloom, increasing the concentration of poly-saccharides, hence the floc size,
7) a decrease in bed friction, for instance above mud deposits, decreasing the vertical mixing capacity, etc.

This collapse will result in fluid mud formation; the turbulent mixing capacity of the flow above the fluid mud will be very small until the fluid mud has gained sufficient strength to re-enable turbulence production at the water-mud interface. The time scale at which this fluid mud is formed is the sedimentation time. Prior to fluid mud formation, the HCMS may behave as a density current, entering for instance harbour basins. It is conjectured that this process is the basic mechanism behind the rapid siltation processes described in the Introduction.

8.2 Discussion

In the Introduction we identified the various processes that govern the dynamics of High-Concentrated Mud Suspensions in estuarine and coastal environments. We studied the various processes separately and developed new mathematical-physical formulations where necessary. These new formulations could be validated against data from the literature; direct validation of the flocculation model, however, is meagre because of a limited amount of available data. Moreover, the effects of waves on the flocculation process is not clear at present. Further calibration and validation is a necessity before this flocculation model can be deployed with confidence for practical situations. However, the results from numerical experiments with this model are promising. The characteristic features of the sediment dynamics in the Ems River, for instance, could only be simulated realistically if flocculation processes were taken into account.

Next we established the relevant time scales and other scaling parameters. Upon implementation of these processes in the 1DV POINT MODEL, we carried out numerical experiments to study their combined influence on HCMS-dynamics and

obtained plausible results. Application of the 1DV POINT MODEL to laboratory experiments and field data yielded fair simulations of the measurements.

We are therefore tempted to conclude that the relevant physical processes have been captured properly in our model, enabling us to predict the transport and fate of High-Concentrated Mud Suspensions in estuaries and coastal areas. However, we have to stress that the occurrence of a saturation condition, which is identified as one of the most important and characteristic features of HCMS-dynamics, is derived from an extrapolation beyond generally accepted regimes, and no direct concrete data are available to validate these results. We have several indications, though, that this extrapolation is allowed and that the results are physically sound:

1. Abundant data from laboratory experiments and field measurements show the existence of an equilibrium concentration for non-cohesive sediment, e.g. sand, which can be regarded as the equivalent to the saturation concentration for mud. However, in the sand case, the turbulence does not collapse, because upon deposition, the settling sand grains directly form a particle matrix, a rigid bed at which turbulence production is possible.
2. Laboratory experiments, field measurements and theoretical analyses on the behaviour of two-layered fluid systems show a more or less complete collapse of the vertical turbulent transport, when this system becomes too stratified, i.e. when the Richardson number exceeds a critical value. In HCMS-dynamics, such a two-layer system is generated when the mud flocs settle to form a layer of fluid mud.
3. Field measurements in Namyang Bay, Korea, in the Tamar and Conway estuaries in the UK, and in the Dollard Estuary, The Netherlands revealed the existence of stratified sediment-laden flows with a considerable damping of the vertical turbulent exchange processes.
4. Numerical simulations of the water movement in the Yangtze River and in the Amazon River and on the Amazon shelf require exceptionally small hydraulic roughness coefficients to simulate the tidal propagation properly, indicating strong damping of the vertical turbulent exchange by near-bed sediment suspensions.
5. In the Botlek harbour in The Netherlands, for instance, fluid mud layers are encountered frequently, contrary to the situation in the Rotterdam Waterway, where the mud suspensions show a more homogeneous profile (Blokland, 1999). This suggests sub-saturated conditions in the river and super-saturated conditions in the harbour basin.
6. Dual-frequency echo soundings in the channels of Cochin Port, India (WL|delft hydraulics, 1990) revealed frequent fluid mud occurrences during the monsoon season in the offshore approach channel and the inshore navigation channel, but never in the Gut, the narrow tidal inlet to the Port and the lagoon in the hinterland. This observation suggests the existence of super-saturated conditions in the two channels and sub-saturated conditions in the Gut, where large flow velocities ($U >$ 2 m/s) prevail.
7. The results of a series of field measurements in the Maasmond area, The Netherlands, can be reasonably simulated with the 1DV POINT MODEL only if sediment- and salinity-induced buoyancy effects, hindered settling, fluid mud formation and wave-augmented vertical mixing are all taken into account. Prognostic simulations for this area reveal a complete collapse of the turbulence

field and the suspended sediment concentration profile, yielding the formation of a thin layer of fluid mud in the navigational channel.

Summarising, we have circumstantial evidence supporting our ideas on the saturation behaviour of HCMS resulting from the interaction between the vertical suspended sediment concentration profile and the turbulent flow field, but we have no definite experimental evidence. Such evidence could be obtained from laboratory experiments and/or field measurements. Laboratory experiments would require a set-up yielding:

- No, or little turbulence production at the water surface (as with a rotating screen of an annular flume) or at the side wall of a flume,
- No, or little secondary currents that might destabilise stratification effects,
- A layer of fluid mud formed upon deposition, sufficiently thick to prevent bottom effects; this implies fairly large amounts of sediment in the water column, hence large initial sediment concentrations at small water depth, and
- Sufficient length of the experimental set-up to allow full deposition of the slowly settling mud flocs (to match the sedimentation time).

Field measurements would have to be carried out when saturation conditions can be expected, i.e. during, or shortly after stormy periods in coastal areas or near the turbidity maximum in estuaries. Moreover, horizontal gradients should be small to minimise the effects of longitudinal advection. Such measurements should include:

- Continuous recording of the response of dual-frequency echo soundings, to detect the occurrence of fluid mud layers,
- Measurements of the vertical distribution of the mean flow velocity (and direction), the mean salinity (and the temperature), and of the suspended sediment concentration,
- Measurements of tidal elevation and wave height and period or length, when relevant,
- Measurements of the turbulence intensities and the turbulent shear stress and vertical sediment transport, above and below the lutocline, and
- Preferably, also the settling velocity of the mud flocs should be measured.

Such laboratory experiments and/or field measurements are not easy to perform, and therefore costly. This will therefore remain a challenge for the future. However, whether or not the predicted catastrophic transition from sub- to super-saturated conditions exists, the existence of sediment-induced buoyancy effects on the turbulence field is beyond doubt. These effects give rise to sediment-induced density currents of estuarine and coastal systems. This implies that rapid siltation processes in harbour basins and navigational channels from High-Concentrated Mud Suspensions can only be simulated properly with a full three-dimensional numerical model, in which the sediment dynamics and the turbulent flow field are fully coupled. The implementation of these effects should have the highest priority in the further development of three-dimensional cohesive sediment transport models.

It is interesting to note that multiplication of c_s from (6.2) with u and integration over the water depth h yields a transport formula for HCMS $F_s = \int_h c_s u dz \propto \tau_b u_* U / \Delta g W_s$, which is almost identical to the transport formula by Bagnold (1966) for suspended sand transport:

$$F_{Bag} = \frac{e_s(1-e_b)\tau_b U^2}{(\rho_s - \rho_w)gW_s} \tag{8.1}$$

The latter equation was obtained from energy considerations for uniform, steady flow in open channels with an unlimited amount of sediment on the bed. In analogy to Bagnold's transport formula, the sediment transport capacity of the flow F_s can be regarded as a transport formula for HCMS. Gradients in F_s would indicate whether the flow can adsorb more sediment, or whether super-saturated conditions may occur. Hence, F_s (or likewise, C_s) may be a parameter for rapid assessment by engineers to establish whether channels, trenches, etc. might be subject to rapid siltation by fluid mud.

Equation (6.3) can also be interpreted as the depth h over which a certain amount of sediment, represented by the depth-averaged concentration C_s, can entirely be mixed against its buoyancy over the water column. Similar formulations have been derived for many stratified flow problems, including entrainment of two-layer systems, thermocline formation, etc. (e.g. Turner, 1973).

The simulations with the flocculation model of the measurements in the Ems River are very illustrative. These measurements can only be reproduced properly if sediment-induced buoyancy effects as well as the effects of flocculation are taken into account. Large variations in floc size, hence settling velocity are predicted, especially around slack water. It is therefore worth while to develop the flocculation model further and to collect data for its validation. Deployment of a flocculation model also requires an efficient methodology to establish the various model parameters.

From these observations we generalise that the sediment transport in and around the turbidity maximum of many estuaries is governed by an interaction between the often high-energetic tidal flow, the turbulence field, flocculation effects, salt-fresh water induced gravitation circulation, and sediment-induced buoyancy effects and density currents. All these effects should be implemented in full three-dimensional numerical models, which, amongst other things, requires a proper parameterisation of the flocculation effects, as the model proposed in this study is too laborious for a full three-dimensional simulation.

Another remark concerns the settling velocity in estuarine HCMS, which may vary by an order of magnitude over the water depth and with the tidal phase, if we may generalise our findings for the Ems Estuary. This means that the use of a flocculation model can facilitate the analysis and interpretation of experimental data of in situ measurements of the settling velocity of mud flocs in estuarine HCMS considerably. A conceptual flocculation model will be necessary anyway to relate the measured settling velocities to floc forming hydrodynamic parameters. The development of an explicit relation between the settling velocity and the physico-chemical properties of the cohesive sediment and pore water is beyond the state-of-the-art, however.

From our literature survey we concluded that HCMS can also occur in coastal areas under a wide variety of conditions; abundant availability of mud seems to be a sufficient condition. When this mud is locally available in the sea bed in the form of mud banks, for instance, fluid mud layers may be generated by auto-saturation. Such fluidised mud banks will strongly damp the surface waves. These phenomena are

observed at several locations, amongst which the coasts of Korea, south India and Surinam.

The sea bed of the Dutch coastal zone does not possess large amounts of cohesive sediment. Yet, HCMS can occur, the mud being mobilised elsewhere during (a sequence of) storms and transported by the tidal currents. No agreement exists at present on the sources of these sediments. These High-Concentrated Mud Suspensions can enter navigation channels and harbour basins by tidal filling and in the form of sediment-driven density currents.

These suspensions can also settle in other sheltered areas, the mouth of the Haringvliet in the Netherlands is a likely candidate. Such areas may serve as a temporary storage area: abundant mud is stored during, or directly after stormy periods, from which it is released gradually during calm whether periods, when these temporary deposits are eroded slowly by tidal currents and/or local wind waves.

Our understanding of the dynamic behaviour of HCMS also allows us a qualitative analysis of the aerial photograph on the front cover of this thesis, showing the turbid waters around the Port of Zeebrugge. This photograph clearly reveals a marked difference in the colour of the water within and outside the harbour basin, indicating sub-saturated conditions outside the basin, where sediment can be mixed up to the water surface, and super-saturated conditions within the basin, where the concentration profile collapses. At the northern breakwater (left hand side of the picture) we observe a plume of turbid water entering the basin, which may be responsible for the turbid cloud in the central part of the basin.

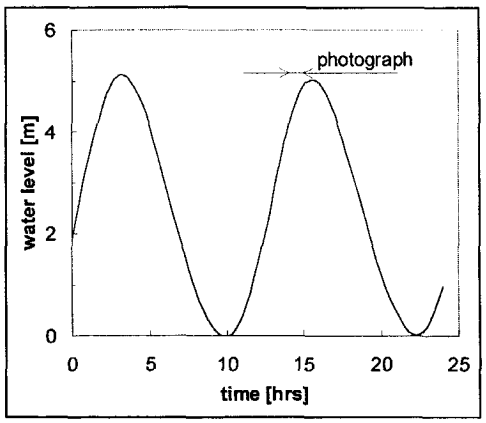

Fig. 8.1: Variation in water level at Zeebrugge on October 18, 1993, obtained from tidal prediction.

This aerial photograph was taken around spring tide on October 18, 1993, between 14:00 and 15:00 hrs, which is 1 to 2 hours before high water. The flow in this phase of the tide is north, with an estimated velocity of about 1 m/s (Royal Navy, 1986).

From this information, the following picture can be deduced. The tide is still rising, hence there is a net inflow of water through the harbour entrance. As the surface area of the basin is about 7 km^2, and the cross section of the entrance measures about 650×15 m^2, the mean velocity of the inflow in the entrance is about 0.1 m/s. However, at the water surface we observe a distinct outflow. This is only possible if an exchange

flow exists in the harbour mouth. This exchange flow is generated by density currents, induced by the horizontal gradients in suspended sediment concentration across the harbour entrance (note that virtually no fresh or warm water is released in the basin). The outflow at the water surface should have a velocity larger than 0.1 m/s to counterbalance the tidal inflow. For simplicity we assume double critical flow conditions in the entrance and zero sediment concentration in the upper part of the water column in the harbour. The suspended sediment concentration at sea in front of the harbour mouth can then be estimated from $u = 0.5\sqrt{0.6cgh/\rho}$ to amount at least 0.4 g/l, which is in the range of the observed values of several hundreds of mg/l (Bastin et al., 1984). Therefore, it is concluded that, at the time the photograph was taken, a two-layered system existed in the harbour entrance with some outflow in the upper layer and a significant ($U > 0.2$ m/s) inflow of sediment-laden water in the lower layer.

The northerly current separates near the southern breakwater in front of the outflowing clear water and forms a mixing layer in the harbour mouth. Probably due to three-dimensional effects, some inflow from this mixing layer occurs near the northern breakwater. The inflowing sediment is caught in an eddy in the mouth of the basin with a clockwise rotation. Possibly, the cloud in the central part of the basin emerges from leakage from this primary eddy, and is captured in a secondary eddy, with opposite rotation.

However, it is the sediment-laden inflow in the lower layer through the entrance of the basin, together with the import by tidal filling effects, that is deemed to be responsible for the rapid siltation with soft sediments (fluid mud), not only in the harbour basin of the Port of Zeebrugge, but probably also in many other basins all over the world. It is this rapid siltation which forces the managing authorities to carry out regular maintenance dredging works to safeguard navigation.

9. Conclusions and recommendations

9.1 Conclusions

In this thesis we have studied the behaviour of High-Concentrated Mud Suspensions (HCMS) in estuaries and coastal zones. From an extensive literature survey it was established that HCMS is encountered frequently all over the world under a large variety of hydrodynamic and meteorological conditions. Their occurrence may vary largely with time and in space, however. Abundant availability of mobilisable mud seems to be a sufficient condition for such occurrences. Moreover, it was found that sediment-induced buoyancy effects are notable already at moderate sediment concentrations, for both cohesive and non-cohesive sediments. Deviation of the velocity profile, measured in sediment-laden flow, from the universal logarithmic profile can be explained by these buoyancy effects in many cases.

The effect of low-concentrated clay additives on the effective hydraulic resistance is probably not important in estuaries and coastal zones, where hydraulically rough flow conditions prevail.

We reasoned that a complete description of the behaviour of HCMS requires a proper formulation of the relevant advection and diffusion effects across the water column. This implies, amongst other things, a relation between the mass and volumetric concentration of the sediment. Such a relation is conveniently provided by fractal theory, yielding power law behaviour of varoious mud properties, both in the water column and within the bed.

The conclusions that have been drawn from our study on the behaviour of High-Concentrated Mud Suspensions (HCMS) in estuaries and coastal zones can be grouped in five categories:

1. Settling velocity

a) Because of their fractal structure, the settling velocity w_s of mud flocs does not scale with D^2, where D is the floc diameter, as predicted by Stokes' theory, but as $w_s \propto D^{n_f-1}$, where n_f is the fractal dimension of the mud flocs. Agreement of this new relation with data from literature is satisfactory.

b) The Richardson-Zaki formulation, derived for hindered settling of non-cohesive, granular material, in principle seems not appropriate for cohesive sediment. A new hindered settling relation, which accounts for the typical properties of cohesive sediment, is proposed herein. This formulation matches data from the literature properly.

2. Turbulence-induced flocculation

a) Flocculation processes in estuarine and coastal waters are mainly governed by turbulence-induced aggregation and breakup processes. The effects of Brownian motion and differential settling on the flocculation process are negligible in estuarine and coastal waters. The three-dimensional Eulerian flocculation model, developed in this thesis, predicts that, starting from small flocs or primary particles

after a slow initial phase, the flocculation process can proceed rapidly. This behaviour is characteristic for fractal growth processes.

b) The fractal dimension of mud flocs formed in the turbulent water column amounts to about $n_f \approx 2$, which is a typical value for growth processes in the regime of so-called Reaction Limited Cluster-Cluster Aggregation. The fractal dimension of mud flocs in fluid mud layers in estuaries seems to have a similar magnitude, corresponding to fluid mud concentrations of about 10 to 80 g/l. These are typical values found in nature.

c) When the residence time of the settling flocs in a turbulent water column is too small, the flocs cannot attain their equilibrium size. This is particularly relevant at low turbulent levels (small flow velocity), at small sediment concentrations, and/or in very shallow water. Experimental data showing an increase in "equilibrium" floc size at small values of the dissipation parameter G with increasing turbulent level (i.e. G), followed by a decrease in size at large G, are biased by a limited residence time in the experimental set-up. It is not true that the flocculation process at small G is governed by aggregation processes and by breakup processes at large G, as is often assumed in the literature.

d) The rapid deposition observed in the Ems River around slack water can only be simulated properly with the 1DV POINT MODEL if the effects of flocculation as well as sediment-induced buoyancy are taken into account. These simulations also show that the size of the mud flocs varies considerably over the tidal cycle. The computed floc sizes and settling velocities agree reasonably with measured data.

e) This computed variation in floc size may explain the discrepancies in the values of settling velocity, which have been measured directly, and those which are required to describe observed vertical concentration profiles with numerical simulations using a constant settling velocity.

f) The flocculation time in the turbidity zone in the River Ems seems to vary significantly over the tidal cycle. During maximal flood velocity the flocculation time amounts to several minutes, which is also the case in the lower part of the water column during maximal ebb velocities. During slack water, however, the flocculation time amounts to many hours, indicating that equilibrium conditions will not be met during this phase of the tide. It is conjectured that this behaviour will occur in most highly dynamic environments, such as meso- and macro-tidal estuaries and in coastal zones.

3. Consolidation and re-entrainment

a) The introduction of the fractal concept in consolidation theory leads to a simple advection-diffusion formulation of the Gibson equation in a Eulerian reference frame with a constant diffusion coefficient. This formulation can easily be combined with the classical mass balance equation for suspended sediment in turbulent flow, including the effects of hindered settling. From the literature it was found that the fractal dimension of the mud in a consolidating bed ranges from about 2.6 to 2.75, which is considerably larger than that of the mud flocs in the water column.

b) This new consolidation model compares well with numerical benchmark experiments on consolidating mud layers, presented in the literature.

c) At present, a proper simulation of the entire cycle of hindered settling - consolidation - re-entrainment and horizontal transport is limited by a limited predictive capability of the consolidation and strength-evolution formulations derived herein.

4. Saturation and fluid mud formation

a) The maximal amount of sediment that can be carried by a turbulent flow is limited by sediment-induced buoyancy effects in combination with the large consolidation times typical of soft mud deposits. These large consolidation times allow the formation of fluid mud layers, at the interface of which little turbulence production is possible initially. This sediment carrying capacity is characterised by the so-called saturation concentration C_s, which scales as $C_s \propto \rho u_*^3 / \Delta g h W_s$ for steady flow conditions. C_s can be compared with, but is not identical to, the equilibrium concentration for non-cohesive sediment.

When fluid mud layers are left alone for sufficient time, they become rigid because of consolidation processes. Then turbulence production at the interface is possible again, and the mixing capacity of the flow is restored. If the height of bed irregularities (ripples, dunes, etc.) exceeds the thickness of fluid mud deposits formed in the depressions of the bed, turbulence production is still possible at the top of the protruding irregularities, as a result of which the fluid mud can be easily mixed over the water depth during accelerating tide.

b) Also under tidal flow conditions a saturation concentration can be identified, which characterises the capacity of tidal flows to transport cohesive sediment in suspension. In this case, scaling relations can be derived from more classical entrainment theory, which, however, does lead to complicated relations that cannot be used easily in practice.

c) Super-saturated conditions can occur when the flow velocity decreases, the water depth increases, and/or the amount of sediment increases. In that case the turbulence profile collapses, the available sediment can no longer be kept in suspension and a fluid mud layer is formed.

d) Such fluid mud layers can be remixed over the water column when the flow velocity increases again sufficiently, provided that the mud has not gained too much strength because of consolidation. In general this mixing takes place because the fluid mud layer becomes turbulent, entraining water from the fluid above, unless the mud deposits are too confined in space.

e) Waves may significantly increase the apparent hydraulic roughness, hence contribute to the vertical mixing. As a result the value of C_s may increase substantially under wave action.

f) When the amount of transportable sediment in a sub-saturated system is augmented by wave activity, super-saturated conditions may emerge, as the contribution of waves to vertical mixing is much smaller than to the erosion of the bed. It is conjectured that this results in a state of auto-saturation, which may be observed in fluidised mud banks in coastal areas.

g) HCMS in the North Sea is transported in a very dynamic form: during slack water a more or less stagnant high-concentrated near-bed suspension (fluid mud layer) is formed and upon acceleration of the flow this suspension is remixed over the water

column and subsequently transported in horizontal directions by the tidal flow. The behaviour in the vertical can be properly simulated with the 1DV POINT MODEL only if the effects of hindered settling, sediment-induced buoyancy, stratification by vertical salinity gradients and augmented mixing by surface waves are all included in the model.

h) It is conjectured that when the sediment-laden flow crosses the Maasgeul, the navigational channel to the Port of Rotterdam, The Netherlands, the suspension becomes super-saturated and a sediment-induced density current is generated, which eventually forms the fluid mud layers commonly observed in the silt traps of the Caland/Beerkanaal.

i) Stratification by salt and fresh water decreases the effective water depth with respect to the vertical mixing of the sediment. In general, sediment suspended in the lower, saline part of the water column cannot penetrate into the fresher upper layer. This occurs in the Maasmond area, i.e. the entrance to the Port of Rotterdam, which explains why aerial photographs of this area never reveal the turbidity that is commonly observed around the Port of Zeebrugge, Belgium, for instance, which has no fresh water inflow.

5. Scaling parameters

The behaviour of HCMS in estuarine and coastal environments is governed by the dimensionless groups summarised in the table below. The Rouse number β, the bulk Richardson number Ri_*, the settling time T_s and the mixing time T_m determine whether the flow can carry the available amount of cohesive sediment in suspension, or whether fluid mud layers are formed.

dimensionless groups		comments
turbulence generation	T_T/T	negligible in estuaries and coastal zones
effective Reynolds number	Re_e	turbulent fluid mud layer
Rouse number	β	concentration profile; saturation parameter
particle Richardson number	Ri_*	overall buoyancy effects; saturation parameter
relative sedimentation time	T_s/T	relaxation time; saturation parameter
relative sedimentation depth	h_s/h	sediment available for fluid mud formation
relative mixing time	T_m/T	relaxation time; saturation parameter
relative flocculation time	T_f/T	relevance of variations in settling velocity, fluid mud concentrations
relative consolidation time	T_c/T	strength in fluid mud & turbulence production
relative erosion strength	θ_e	floc erosion of consolidating bed
relative bed irregularities	δ_m/k_s	saturation; damping of turbulence production

The relative thickness of fluid mud layers with respect to the size of bed irregularities δ_m/k_s determines whether local turbulence production at these irregularities is possible. The effective Reynolds number Re_e and the consolidation time T_c determine whether a fluid mud layer can become turbulent, when accelerated by the tide and whether turbulence can be produced at the mud-water interface. The flocculation time T_f determines the variation in settling velocity over the tidal cycle and the fluid mud concentration. The erosion parameter θ_e

determines whether HCMS dynamics are affected by water-bed exchange processes. The tidal period T is the time scale for the major driving agent.

9.2 Recommendations

On the basis of this study, many recommendations for future work can be given. The most urgent issues to be addressed are:

1. The flocculation model presented herein is a promising tool to study mud dynamics in the sense that various features of mud flocs in turbulent environments are predicted realistically. However, the model needs further validation before it can be applied with confidence under a wide variety of conditions. Especially the variability of the various model coefficients should be established. As such, the present model should be regarded as a research tool.
2. An efficient methodology should be developed to establish the various parameters of the flocculation model.
3. Waves seem to have a considerable effect on the concentration in fluid mud layers. However, no data are available to study this effect. An experimental laboratory study under well-defined conditions is a first step towards its understanding.
4. An extension of the flocculation model to incorporate more sediment fractions may shed light on the ongoing dispute on the discrepancy between the value of the settling velocity measured directly from settling mud flocs with optical systems in the field, and the (constant) settling velocity applied in mathematical models to describe the observed vertical distributions of suspended sediment concentration. It is noted that such population models require extensive data sets for calibration.
5. The numerical solution of the present flocculation model requires considerable computational efforts, which forbids its deployment in three-dimensional models of estuarine and coastal systems on a routine basis. If possible, this model concept and/or the model results should therefore be parameterised.
6. The saturation concept and its relation to the formation of fluid mud layers presented herein is new. Though our model concept compares favourably with experimental data, no direct evidence exists at present whether fluid mud formation actually coincides with a collapse of the turbulence field. It is recommended that turbulence measurements are carried out in areas renowned for fluid mud formation and/or that laboratory experiments are carried out to study the saturation concept under well-controlled conditions.
7. This saturation concept leads to the conjecture that sediment-induced density currents may play an important role in the processes of rapid siltation in navigation channels and harbour basins. It is therefore recommended to study this hypothesis with high priority, and upon verification, incorporate these sediment-induced buoyancy effects in three-dimensional numerical models used for engineering studies on siltation.
8. Upon deposition, the structure of the mud flocs seems to change dramatically, which is characterised by a sudden increase in the fractal dimension. Little is

known about the underlying physical processes. Basic research is required to enhance our understanding of the relevant phenomena.

9. The weak links in simulating the full (hindered) settling - consolidation and re-entrainment cycle is formed by proper formulations of the material functions of the consolidating mud and the related strength evolution, i.e. the rheological model. Further basic research is required to improve these formulations.
10. Field measurements on the behaviour of suspended sediment should contain sufficient data to allow a proper discrimination between local effects, i.e. the processes in the water column, and advective effects.

References

Adams, C.E. and Weatherly, G.L, 1981a, "Suspended-sediment transport and benthic boundary-layer dynamics", Marine Geology, Vol 42, pp 1-18.

Adams, C.E. and Weatherly, G.L, 1981b, "Some effects of suspended sediment stratification on an oceanic bottom boundary layer", Journal of Geophysical Research, Vol 86, No C5, pp 4161-4172.

Adams, C.E., Wells, J.T. and Park, Y.-A., 1990, "Internal hydraulics of a sediment-stratified channel flow", Marine Geology, Vol 95, pp 131-145.

Akers, R.J, Rushton, A.G. and Stenhouse, J.I.T., 1987, "Floc breakage: the dynamic response of particle size distribution in a flocculated suspension to a step change in turbulent energy dissipation", Chemical Engineering Sciences, Vol 42, pp 787-798.

Allen, G.P., Salomon, J.C., Du Penhoat, Y. and Grandpré, C. de, 1980, "Effects of tides on mixing and suspended sediment transport in macro tidal estuaries", Sedimentary Geology, Vol 26, pp 69-90.

Arai, M. and Takahashi, T., 1986, "The Kármàn constant of the flow laden with high sediment", 3rd International Symposium on River Sedimentation, University of Mississippi, pp 824-833.

Argamam, Y. and Kaufman, W.J., 1970, "Turbulence and flocculation", Journal of the Sanitary Engineering, ASCE, Vol 96, No SA2, April 1970, pp 223-241.

Arundale, A.M.W., Darbyshire, E.J., Hunt, S.J., Schmitz, K.G. and West, J.R., 1997, "Turbidity maxima formation in four estuaries", in Proceedings of the 4th Nearshore and Estuarine Cohesive Sediment Transport Conference, INTERCOH'94, Wallingford, UK, July 1994, ed. by N. Burt, R. Parker and J. Watts, John Wiley and Sons, pp 135-146.

Ayesa, E., Margeli, M.T., Flórez, J. and García-Heras, J.L., 1991, "Estimation of breakup and aggregation coefficients in flocculation by a new adjustment algorithm", Chemical Engineering Science, Vol 46, No 1, pp 39-48.

Bagnold, R.A., 1954, "Experiments on a gravity-free dispersion of large solid spheres in a Newtonian fluid under shear", Proceedings of the Royal Society, London, Vol A225, pp 49-63.

Bagnold, R.A., 1966, "An approach to the sediment transport problem from general physics", Geological Survey Professional Paper 422-I, Physiographic and hydraulic studies of rivers.

Barenblatt, G.F., 1953, "On the motion of suspended particles in a turbulent stream", Prikladnaja Matematika i Mekhanika, Vol 17, pp 261-274 (English translation).

Bastin, A., Caillot, A. and Malherbe, B, 1982, "Sediment transport measurements on and off the Belgium coast by means of tracers", Proceedings of the 8th International Harbour Congress, KVIV, Antwerp, 1982.

Batchelor, G.K, 1982, "Sedimentation in a dilute poly-disperse system of interacting spheres. Part I - general theory", Journal of Fluid Mechanics, Vol 119, pp 379-408.

Batchelor, G.K., 1983, "An introduction to fluid dynamics", Cambridge University Press.

Baumert, H. and Radach, G., 1992, "Hysteresis of turbulent kinetic energy in non-rotational tidal flows: a model study", Journal of Geophysical research, Vol 97, No C3, pp 3669-3677.

Beardsley, R.C., Candela, J., Limeburner, R., Geyer, W.R., Lentz, S.J., Castro, B.M., Cacchione, D. and Carneiro, N., 1995, "The M_2 tide on the Amazon shelf", Journal of Geophysical Research, Vol 100, pp 2283-2319.

Been, K. and Sills, G.C., 1981, "Self-weight consolidation of soft clays: an experimental and theoretical study", Geotechnique, Vol 31, No 4, pp 519-535.

Blokland, T, 1999, personal communication.

Boadway, J.D., 1978, "Dynamics of growth and breakage of alum flocs in presence of fluid shear", ASCE, Journal of the Environmental Engineering Division, Vol 104, No EE5, pp 901-915.

Booij, R., Visser, P.J. and Melis, H., 1993, "Laser-Doppler measurements in a rotating annular flume", Proceedings of the 5th International Conference on Laser Anemometry Advances and Applications, Veldhoven, The Netherlands, pp 409-416.

Borgas, M.S., Flesh, T.K. and Sawford, B.L., 1997, "Turbulent dispersion with broken reflectional symmetry", Journal of Fluid Mechanics, Vol 332, pp 141-156.

Bratby, J., 1980, "Coagulation and flocculation, with an emphasis on water and waste water treatment", Uplands Press Ltd, Croydon, England.

Brown, W.D. and Ball, R.C., 1985, "Computer simulation of chemically limited aggregation", Journal of Physics, Section A: Mathematics and General, Vol 18, pp L517-L521.

Bürger, R. and Concha, F., 1998, "Mathematical model and numerical simulation of the settling of flocculated suspensions", International Journal of Multiphase flow, Vol 24, pp 1005-1023.

Buscall, R., Mills, P.D.A., Goodwin, J.W. and Lawson, D.W., 1988, "Scaling behaviour of the rheology of aggregate networks formed from colloidal particles", Journal of the Chemical Society, Faraday Transactions I, Vol 84, No 12, pp 4249-4260.

Buscall, R., 1990, "The sedimentation of concentrated colloidal suspensions", Colloids and Surfaces, Vol 43, pp 33-53.

Casamitjana, X. and Schladow, G., 1991, "A dynamic model for particle distribution in a stratified lake", Proceedings of the XXIV Congress of the International Association for Hydraulic Research, Madrid, Vol C, pp 509-516.

Casamitjana, X. and Schladow, G., 1993, "Vertical distribution of particles in stratified lake" , ASCE, Journal of Environmental Engineering, Vol 119, No 3, pp 443-462.

Chen, S. and Eisma, D., 1995, "Fractal geometry of in situ flocs in the estuarine and coastal environments", Netherlands Journal of Sea Research, Vol 32, No 2, pp 173-182.

Cheng, N.-S., 1997, "Effect of concentration on settling velocity of sediment particles", ASCE, Journal of Hydraulic Engineering, Vol 123, No 8, pp 728-731.

Coleman, N.L., 1981, "Velocity profiles with suspended sediment", Journal of Hydraulic Research, Vol 19, No 3, pp 211-229.

Coleman, N.L., 1986, "Effects of suspended sediment on the open-channel velocity distribution", Water Resources Research, Vol 22, No 10, pp 1377-1384.

Coles, D., 1956, "The law of the wake in the turbulent boundary layer", Journal of Fluid Mechanics, Vol 1, pp 191-226.

Cornelisse, J.M., 1990, "Flocculation and settling velocity - Data report of experiments carried out in the settling column in 1987 through 1989", Delft Hydraulics (in Dutch).

Cornelisse, J.M., Kuijper, C. and Winterwerp, J.C., 1990, "Erosion and deposition characteristics of natural muds; sediments from the Ems-Dollard (Eems harbour)", Rijkswaterstaat & Delft Hydraulics, Cohesive Sediments, Report 26.

Crickmore, M.J., 1982, "Data collection - tides, tidal currents and suspended sediment", The Dock & Harbour Authority, Vol LXIII, No 742, pp 183-186.

Dalrymple, R.A. and Liu, P.L., 1978, "Waves over soft muds: a two layer fluid model", Journal of Physical Oceanography, Vol 8, pp 1121-1131.

Darcovich, K., Gierer, C. and Capes, C.E., 1996, "The application of dynamic clustering data to the sedimentation rate of concentrated suspensions", Advances in Powder Technology, Vol 7, No 1, pp 1-19.

Davis, R.H. and Birdsell, K.H., 1988, "Hindered settling of semi-dilute mono-disperse and poly-disperse suspensions", American Institute of Chemical Engineers, AICHE Journal, Vol 34, No 1, pp 123-129.

Dong, L., Wolanski, E. and Li, Y., 1997, "Field and modelling studies of fine sediment dynamics in the extremely turbid Jiaojianng River estuary, China", Journal of Coastal Research, Vol 13, No 4, pp 995-1003.

Dyer, K.R., 1989, "Sediment processes in estuaries: future research requirements", Journal of Geophysical Research, Vol 94, No C10, October 1989, pp 14,327 - 14,339.

Einstein, H.A. and Chien, 1955, "Effects of heavy sediment concentration near the bed on velocity and sediment distribution", MRD Sediment Series No 8, University of California, Berkeley.

Elata, E. and Ippen, A.T., 1961, "The dynamics of open channel flow with suspensions of neutrally buoyant particles", M.I.T., Hydrodynamics Laboratory, Technical Report 45, Cambridge.

Faas, R. and Wartel, S., 1985, "Resuspension potential of fluid mud and its significance to sediment transport in the Western Scheldt estuary, Belgium", Estuaries, Vol 8, No 2b.

Felderhof, B.U. and Ooms, G., 1990, "Effect of inertia, friction and hydrodynamic interactions on turbulent diffusion", European Journal of Mechanics, Part B/Fluids, Vol 9, No 4, pp 350-368.

Fennessy, M.J., Dyer, K.R. and Huntley, D.A., 1994, "INSSEV: An instrument to measure the size and settling velocity of flocs in situ", Marine Geology, Vol 117, pp 107-117.

Fowler, L., 1953, "Notes on the turbulence function k", Missouri River Division, U.S.Army, Corps of Engineers.

Friedlander, S.K., 1977, "Smoke, dust and haze - fundamentals of aerosol behavior", John Wiley and Sons, New York.

Galland, J.-C., 1996, "Transport de sédiments en suspension et turbulence", Electricité de France, Direction des Etudes et Recherches, Rapp. HE-42/96/007/A.

Galland, J.-C., Laurence, D. and Teisson, C., 1997, "Simulating turbulent vertical exchange of mud with a Reynolds stress model", Proceedings of the 4th Nearshore and Estuarine Cohesive Sediment Transport Conference INTERCOH'94, July 1994, Wallingford, UK, ed. T. N. Burt, W.R. Parker and J. Watts, John Wiley & Sons, pp 439-448.

Gallappatti, G. and Vreugdenhill, C.B., 1987, "A depth-integrated model for suspended sediment transport", Journal of Hydraulic Research, Vol 23, N0 4, pp 359-377.

Gibbs, R.J., 1985, "Estuarine flocs: their size, settling velocity and density", Journal of Geophysical Research, Vol 90, No C2, March 1985, pp 3249-3251.

Graf, W.H., 1977, "Hydraulics of Sediment Transport", McGraw-Hill Book Company, New York.

Grant, W.D. and Madsen, O.S., 1979, "Combined wave and current interaction with a rough bottom", Journal of Geophysical Research, Vol 84, No C4, pp 1797-1808.

Gregory, J., 1997, "The density of particle aggregates", Water Science Technology, Vol 36, No 4, pp 1-13.

Gust, G., 1976, "Observations on turbulent-drag reduction in a dilute suspension of clay in sea water", Journal of Fluid Mechanics, Vol 75, Part 1, pp 29-47.

Guan, W.B., Wolanski, E. and Dong, L.X., 1998, "Cohesive sediment transport in the Jiaojiang River Estuary, China", Estuarine, Coastal and Shelf Science, Vol 46, pp 861-871.

Gust, G., 1984, discussion of N.L. Coleman's "Velocity profiles with suspended sediment", and reply by the author, IAHR, Journal of Hydraulic Reserach, Vol 22, No 4, pp 263-289.

Ham, R. van der, 1999, "Turbulent exchange of fine sediments in tidal flow", PhD-thesis, Delft University of Technology, Faculty of Civil Engineering and Geotechnical Sciences.

Ham, R. van der, Kranenburg, C. and Winterwerp, J.C., 1998, "Turbulent vertical exchange of fine sediments in stratified tidal flows", proceedings of the Conference on Physical Processes in Estuaries and Coastal Seas (PECS), ed. by J. Dronkers and M.B.A.M. Scheffers, The Hague, September 1997, pp 201-208.

Haw, M.D., Poon, W.C.K. and Pusey, P.N., 1997, "Structure and arrangement of clusters in cluster aggregation", The American Physical Society, Physical Review E, Vol 56, No 2, pp 1918-1933.

Hawley, N., 1982, "Settling velocity distribution of natural aggregates", Journal of Geophysical Research, Vol 87, No C12, pp 9489-9498.

Hino, M., 1963, "Turbulent flow with suspended particles", ASCE, Journal of the Hydraulics Division, Vol 89, No HY4, pp 161-185.

Hinze, J.O., 1975, "Turbulence", McGraw-Hill Book Company.

Hir, P. le, 1997, "Fluid and sediment "integrated" modelling application to fluid mud flows in estuaries", in: Proceedings of the 4th Nearshore and Estuarine Cohesive Sediment Transport Conference, INTERCOH'94, Wallingford, UK, July 1994, ed. by N. Burt, R. Parker and J. Watts, John Wiley & Sons, pp 417-428.

Hir, P. le, Bassoulet, P, Jestin, H. and Sottolichio, A., 1998, "Application of the continuous modelling concept to the simulation of highly concentrated suspended sediment: comparison with measurements in a macro-tidal estuary", Presentation at the 5th International Conference on Cohesive Sediment Transport, INTERCOH'98, May 1998, Seoul, Korea, paper no 49.

Huang, H., 1994, "Fractal properties of flocs formed by fluid shear and differential settling", Physics of Fluids, Vol 6, No 10, pp 3229-3234.

Hydraulics Research Station, 1980, "The Severn Estuary; Measurements of the vertical and lateral distribution of mud suspensions", Report No EX 965.

Ingber, M.S. and Womble, D.E., 1994, "Hindered settling computations using a parallel boundary element method", American Society of Mechanical Engineers, Fluid Engineering Division, Parallel Computing in Multi-phase Flow Systems Simulations, Vol 199, pp 53-59.

Inglis, C.C. and Allen, H.H., 1957, "The regimen of the Thames Estuary as affected by currents, salinities and river flow", Proceedings of the Institution of Civil Engineers, Maritime and Waterways Engineering Division Meeting, Vol 7, pp 827-879.

Ivey, G. and Imberger, J., 1991, "On the nature of turbulence in stratified flows; Part I: the energetics of mixing", Journal of Physical Oceanography, Vol 21, No 5, pp 650-658.

IOS Taunton, 1977, "Investigation of turbidity structures in the Severn Estuary and Inner Bristol Channel", Institute of Oceanographic Sciences, Taunton, Cruise Report No 92.

Itakura, T. and Kishi, T., 1980, "Open channel flow with suspended sediments", ASCE, Journal of the Hydraulics Division, Vol 106, No HY8, pp 1325-1343.

James, A.E., Williams, D.J.A. and Williams, P.R., 1988, "Small strain, low shear rate rheometry of cohesive sediments", in: Physical Processes in Estuaries, ed. J. Dronkers and W. van Leussen, Springer-Verlag, pp 488-502.

Johnson, C.P, Li, X.Y. and Logan, B.E., 1996, "Settling velocities of fractal aggregates", Environmental Science & Technology, Vol 30, No 6, pp 1911-1918.

Karelse, M. and Kester, J.A.Th.M. van, 1995, "Validation of DELFT3D with tidal flume measurements", Delft Hydraulics, Report Z810 (in Dutch).

Kessel, T. van, 1996, "Accurate sounding tests for soft cohesive soils", Delft University of Technology, Department of Civil Engineering, Report 7-96

Kessel, T. van, 1997, "Generation and transport of subaqueous fluid mud layers", PhD-thesis, Delft University of Technology, Department of Civil Engineering

Kester, J.A.Th.M. van, 1994, "Validation of DELFT3D against mixing layer experiment; Phase 1: improved implementation of k-ε model", Delft Hydraulics, Report Z810 (in Dutch).

Kester, J.A.Th.M. van, Uittenbogaard, R.E. and Stelling, G.S., 1994, "Sensitivity analysis of 3D-Noordwijkerraai-model", Delft Hydraulics, Report Z691 (in Dutch).

Kesteren, W.G.M., Cornelisse, J.M. and Kuijper, C., 1997, "DYNASTAR BED MODEL: bed strength, liquefaction and erosion", Rijkswaterstaat and WL|delft hydraulics, Cohesive Sediments, Report No 55.

Kesteren, W.G.M. van, 1998, personal communication.

Kihara, T., Sasajima, H., Yoshinaga, K., Koizuka, T., Sasayama, H., Yoshinaga, H. and Fujimoto, T., 1994, "Field surveys on siltation-prevention effects in waterways and anchorage by submerged walls", Hydro-Port'94, International Conference on Hydro-Technical Engineering for Port and Harbour Construction, October, Yokosuka, Japan, pp 1225-1242.

Kineke, G.C., 1993, "Fluid muds on the Amazon continental shelf", PhD-thesis, University of Washington.

Kineke, G.C. and Sternberg, R.W, 1995, "Distribution of fluid muds on the Amazon continental shelf", Marine Geology, Vol 125, pp 193-233.

Kineke, G.C., Sternberg, R.W., Trowbridge, J.H. and Geyer, W.R., 1996, "Fluid mud processes on the Amazon continental shelf", Continental Shelf Research, Vol 16, No 5/6, pp 667-696.

Kirby, R. and Parker, W.R., 1980, "Settled mud suspensions in Bridgewater Bay, Bristol Channel", Institute of Oceanographic Sciences, Taunton, IOS Report, No 107.

Kirby, R. and Parker, W.R., 1983, "Distribution and behaviour of fine sediment in the Severn estuary and inner Bristol Channel, UK", Canadian Journal of Fisheries and Aquatic Science, Vol 40 (suppl.1), pp 83-95.

Kolb, M. and Herrmann, H.J., 1987, "Surface fractals in irreversible aggregation", Physical Review Letters, Vol 59, No 4, pp 454-457.

Kranenburg, C., 1992, "Hindered settling and consolidation of mud - analytical results", Delft University of Technology, Department of Civil Engineering, Report 11-92.

Kranenburg, C., 1994, "An entrainment model for fluid mud", Delft University of Technology, Faculty of Civil Engineering, Communications on Hydraulic and Geotechnical Engineering, Report 93-10.

Kranenburg, C., 1994, "On the fractal structure of cohesive sediment aggregates", Estuarine, Coastal and Shelf Science, Vol 39, pp 451-460.

Kranenburg, C., 1996, personal communication.

Kranenburg, C. and Winterwerp, J.C., 1997, "Erosion of fluid mud layers - I: Entrainment model", ASCE, Journal of Hydraulic Engineering, Vol 123, No 6, pp 504-511.

Kranenburg, C., 1998, "Effects of floc strength on viscosity and deposition of cohesive sediment suspensions", to appear in Continental Shelf Research, Focused Issues on Nearshore and Coastal Oceanography.

Kranenburg, C., 1998, personal communication.

Krishnappan, B.G., 1990, "Modelling of settling velocity and flocculation of fine sediments in still water", Canadian Journal of Civil Engineering, Vol 17, pp 763-770.

Krishnappan, B.G., 1991, "Modelling of cohesive sediment transport", Proceedings of the International Symposium on The Transport of Suspended Sediments and its Mathematical Modelling, Florence, September 2-5, pp 433-448.

Krone, R.B., 1984, "The significance of aggregate properties to transport processes", Proceedings of a Workshop on Cohesive Sediment Dynamics with Special Reference to Physical Processes in Estuaries, Tampa, Florida, Springer Verlag, Lecture Notes on Coastal and Estuarine Studies, Vol 14, Estuarine and Cohesive Sediment Dynamics, pp 66-84.

Kuijper, C., Cornelisse, J.M. and Winterwerp, J.C., 1990, "Erosion and deposition characteristics of natural muds; sediments from Loswal Noord", Rijkswaterstaat & Delft Hydraulics, Cohesive Sediments, Report 37.

Kuijper, C., Cornelisse, J.M. and Winterwerp, J.C., 1991, "Erosion and deposition characteristics of natural muds; sediments from the Ems-Dollard (Delfzijl)", Rijkswaterstaat & Delft Hydraulics, Cohesive Sediments, Report 35.

Kynch, G.J., 1952, "A theory of sedimentation", Transactions of the Faraday Society, Vol 48, pp 166-176.

Landman, K.A. and White, L.R., 1990, "Determination of the hindered settling factor for flocculated suspensions", American Institute of Chemical Engineers, AICHE Journal, Vol 38, No 2, pp 184-192.

Lau, Y.L, 1982, "Suspended sediment effect on flow resistance", ASCE, Journal of Hydraulic Engineering, Vol 109, No 5, pp 757-763.

Lau, Y.L and Chu, V.H., 1987, "Suspended sediment effect on turbulent diffusion", Proc. 22nd IAHR Congress, Lausanne, pp 221-226.

Launder, B.E. and Spalding, D.B., 1974, "The numerical computation of turbulent flows", in: Computer Methods in Applied Mechanics and Engineering, Vol 3, pp 269-289, North-Holland Publishing Company.

Lee, D.I., 1969, "The viscosity of concentrated suspensions", Transactions of the Society of Rheology, Vol 13, No 2, pp 273-288.

Lee, K. and Sills, G.S., 1980, "The consolidation of a soil stratum, including self-weight effects and large strains", International Journal for Numerical and Analytical Methods in Geomechanics, Vol 5, pp 405-428.

Lee, W.T.B. van der and Ham, R. van der, 1999, "Settling velocities in the tidal channel Groote Gat (Ems-Dollard estuary, The Netherlands)", International Conference on Intertidal Mudflats: properties and processes, ed. K.R. Dyer, April, 1999, Plymouth, UK.

Lee, S.-I., Seo, I.-S. and Koopman, B., 1994, "Effect of mean velocity gradient and mixing time on particle removal in sea water induced flocculation", Water, Air and Soil Pollution,Vol 78, pp 179-188.

Leentvaar, J. and Rebhun, M., 1983, "Strength of ferric hydroxide flocs" Water Research, Vol 17, pp 895-902.

Leussen, W. van and Velzen, E. van, 1989, "High concentration suspensions: their origin and importance in Dutch estuaries and coastal waters", Journal of Coastal Research, Special Issue No 5, pp 1-22.

Leussen, W. van, 1994, "Estuarine macroflocs and their role in fine-grained sediment transport", PhD-thesis, University of Utrecht, February 1994.

Leussen, W. van, 1999a, "Fluid mud layers in the Ems Estuary", to be submitted.

Leussen, W. van, 1999b, personal communication.

Levich, V.G., 1962, "Physico-chemical Hydrodynamics", Prentice Hall, Inc.

Lick, W. and Lick, J., 1988, "Aggregation and disaggregation of fine-grained lake sediments", Journal of Great Lakes Research, Vol 14, no 4, pp 514-523.

Lick, W. and Huang, H., 1993, "Flocculation and the physical properties of flocs", in Proceedings of the 3rd Conference on Nearshore and Estuarine Cohesive Sediment Transport, ed. A.J. Mehta, American Geophysical Union, Coastal and Estuarine Studies, Vol. 42, pp 21-39.

Lick, W., Huang, H. and Jepsen, R., 1993, "Flocculation of fine-grained sediments due to differential settling", Journal of Geophysical Research, Vol 98, No C6, June 1993, pp 10,279-10,288.

Lienhard, J.H. and Van Atta, C.W., 1990, "The decay of turbulence in thermally stratified flow", Journal of Fluid Mechanics, Vol 210, pp 57-112.

Liu, K. and Mei, C.C., 1989, "Effects of wave-induced friction on a muddy seabed as a Bingham plastic fluid", Journal of Coastal Research, Vol 5, No 4, pp 777-789.

Logan, B.E. and Kilps, J.R., 1995, "Fractal dimensions of aggregates formed in different fluid mechanical environments", Water Resources, Vol 29, No 2, pp 443-453.

Lueck, R.G. and Lu, Y.Y., 1997, "The logarithmic layer in a tidal channel", Continental Shelf Research, Vol 17, No 14, pp 1785-1801.

Lumley, J.L., 1969, "Drag reduction by additives", in: Annual Review of Fluid Mechanics, Vol 1, ed. W.R. Sears and M. van Dyke, pp 367-383.

Lyn, D.A., 1986, "Turbulence and turbulent transport in sediment-laden open-channel flows", W.M. Keck Laboratory of Hydraulics and Water Resources, Division of Engineering and Applied Science, California Institute of Technology, Report No KH-R-49.

Lyn, D.A., 1988, "A similarity approach to turbulent sediment-laden flows in open channels", Journal of Fluid Mechanics, Vol 193, pp 1-26.

Malcherek, A., 1995, "Mathematische Modellierung von Strömungen und Stofftransportprozessen in Ästuaren", Dissertation, Institut für Strömungsmechanik und Elektronisch Rechnen im Bauwesen der Universität Hannover, Bericht Nr. 44/1995 (in German).

Malvern, L.E., 1969, "Introduction to the Mechanics of a Continuous Medium", Prentice-Hall, Series in Engineering of the Physical Sciences, New Jersey.

Mandersloot, W.G.B., Scott, K.J. and Geyer, C.P., 1986, "Sedimentation in the hindered settling regime", in Advances in Solid-Liquid Separation, ed. H.S. Muralidhare, Battle Press, Columbia, USA, Ch 3, pp 63-77.

Matsuo, T. and Unno, H., 1981, "Forces acting on floc and strength of floc", ASCE, Journal of the Environmental Engineering Division, Vol 107, No EE3, pp 527-545.

McCave, I.N., 1984, "Size spectra and aggregation of suspended particles in the deep ocean", Deep Sea Research, Vol 31, No 4, pp 329-352.

Meakin, P., 1986, "Computer simulations of growth and aggregation processes", in On Growth and Form, Fractal and Non-fractal Patterns in Physics, ed. H.E. Stanley and N. Ostrowsky, Martinus Nijhoff Publishers, pp 111-135.

Mehta, A.J., 1986, "Characterisation of cohesive sediment properties and transport processes in estuaries", in Lecture Notes on Coastal and Estuarine Studies, Vol 14, Estuarine Cohesive Sediment Dynamics, Proceedings of a Workshop on Cohesive Sediment Dynamics with Special Reference to Physical Processes in Estuaries, ed. A.J. Mehta, Tampa, Florida, USA, 1984.

Mehta, A.J., Hayter, E.J., Parker, W.R., Krone, R.B. and Teeter, A.M., 1989, "Cohesive Sediment Transport - I: Process Description", ASCE, Journal of Hydraulic Engineering, Vol 115, No 8, pp 1076-1093.

Mehta, A.J., 1998, Personal communication.

Merckelbach, L., 1996, "Sedimentation in the Maasmond; a correlation analysis", Netherlands Ministry of Transport and Public Works, Rjkswaterstaat, North Sea Directorate, Report NZ-96.02.

Merckelbach, L.M., 1996, "Consolidation theory and rheology of mud - a literature survey", Delft University of Technology, Department of Civil Engineering, Report 9-96.

Merckelbach, L.M., 1998, "Laboratory experiments on consolidation and strength evolution of mud layers", Delft University of Technology, Department of Civil Engineering, Report 9-96.

Merckelbach, L.M., Sills, G.C. and Kranenburg, C.,1998, "Laboratory experiments on consolidation and strength evolution of mud layers", submitted to the Proceedings of the 5th Nearshore and Estuarine Cohesive Sediment Transport Conference INTERCOH'98, Seoul, Korea.

Migniot, C., 1968, "A study of the physical properties of various forms of very fine sediments and their behaviour under hydrodynamic action", Communications présenté au Comité Technique de la Société Hydrotechnique de France, La Houille Blanche, Vol 23, No 7, pp 591-620.

Migniot, C., 1968, "A study on the physical properties of various forms of very fine sediments and their behaviour under hydrodynamic action", La Houille Blanche, Vol 7, pp 591-620.

Muste, M. and Patel, V.C., 1997, "Velocity profiles for particles and liquid in open-channel flow with suspended sediment", ASCE, Journal of Hydraulic Engineering, Vol 123, No 9, pp 742-751.

NEDECO, 1968, "Surinam transportation study", Netherlands Engineering Consultants, The Hague.

Nezu, I. and Rodi, W., 1986, "Open-channel flow measurements with a laser Doppler anemometer", ASCE, Journal of Hydraulic Engineering, Vol 112, No 5, pp 335-355.

Nezu, I and Nakagawa, H., 1993, "Turbulence in open-channel flows", International Association for Hydraulic Research, Monograph Series, Balkema, Rotterdam.

Odd, N.V.M., 1988, "Mathematical modelling of mud transport in estuaries", in Physical Processes in Estuaries, ed. by J. Dronkers and W. van Leussen, Springer Verlag, pp 503-531.

Odd, N.V.M and Cooper, A.J., 1989, "A two-dimensional model of the movement of fluid mud in a high energy turbid estuary", Journal of Coastal Research, Special Issue No 5, pp 175-184.

Odd, N.V.M, Bentley, M.A., Waters, C.B., 1993, "Observations and analysis of the movement of fluid mud in an estuary", in Proceedings of the 3rd International Conference on Nearshore and Estuarine Cohesive Sediment Transport, ed. A.J. Mehta, Coastal and Estuarine Studies, Vol. 42, American Geophysical Union, pp 430-446.

Olphen, H. van, 1977, "An introduction to Clay Colloid Chemistry", 2nd edition, John Wiley & Sons, New York, London.

O'Melia, C.R., 1980, "Aquasols: the behaviour of small particles in aquatic systems", Environmental Science and Technology, Vol 14, No 9, pp 1052-1060.

O'Melia, C.R., 1985, "The influence of coagulation and sedimentation on the fate of particles, associated pollutants, and nutrients in lakes", Chemical Processes in Lakes, ed. Werner Stum, John Wiley and Sons, New York, pp 207-224.

Ooms, G. and Schinkel, W.M.M, 1998, "Effect of particle properties on turbulence intensity of a suspension", Presented at the European Turbulence Conference, Cap Ferrat, France, pp 1-4.

Parker, D.S., Kaufman, W.J. and Jenkins, D., 1972, "Floc breakup in turbulent flocculation processes", ASCE, Journal of the Sanitary Engineering Division, Vol 98, No SA1, pp 79 - 97.

Partker, W.R. and Hooper, P.M., 1994, "Criteria and methods to determine navigable depth in hyperconcentrated sediment layers", in: Proceedings of Hydro-Port'94, International Conference on Hydro-Technical Engineering for Port and Harbour Construction, October, Yokosuka, Japan, pp 1211-1224.

PDC, 1995, "Regulation of the Yangtze Estuary, Volume B: Hydro-morphological assessment and mathematical models", Port and Delta Consortium and Ministry of Water Resources of the People's Republic of China, Shanghai Investigation Research and Design Institute (confidential).

Penhout, Y. du and Salomon, J.C., 1979, "Numerical simulation of estuarine mud layers - application to the Gironde", Oceanologica Acta, Vol 2, No 3, pp 253-260 (in French).

Pope, S.B., 1983, "A Lagrangean two-time probability density function equation for inhomogeneous turbulent flows", Physics of Fluids, Vol 26, No 12, pp 3448-3450.

Raudkivi, A.J., 1976, "Loose boundary hydraulics", Pergamon Press, New York.

Reed, C.C. and Anderson, J.L., 1980, "Hindered settling of a suspension at low Reynolds number", Journal of the American Institute of Chemical Engineering, Vol 26, No 5, pp 816-827.

Reynolds, A.M., 1997, "A Lagrangean stochastic model for particle trajectories in non-Gaussian turbulent flows", Fluid Dynamics Research, Vol 19, pp 277-288.

Richardson J.F. and Zaki, W.N., 1954, "Sedimentation and fluidization, Part I", Transactions of the Institution of Chemical Engineers, Vol 32, pp 35-53.

Rijn, van L.C., 1993, "Principles of sediment transport in rivers, estuaries and coastal seas", AQUA Publications, The Netherlands.

Rodi, W., 1984, "Turbulence models and their applications in hydraulics - a state-of-the-art review", IAHR monograph, Delft, The Netherlands.

Roskam, B., 1995, "Wave climate at EUR- and LEG- observation platform for Maasvlakte-studies", EIA-working document, RWS-RIKZ, Report RIKZ/OS-95.111x (in Dutch).

Ross, M.A., 1988, "Vertical structure of estuarine fine sediment suspensions", PhD-thesis, Coastal & Oceanographic Engineering Department, University of Florida, Gainesville, Florida, USA.

Royal Navy, 1986, "Current Atlas of the Western Scheldt", Dienst der Hydrografie van de Koninklijke Marine, Nederland (in Dutch).

Scott, K.J., 1984, "Hindered settling of a suspension of spheres; critical evaluation of equations relating settling rate to mean particle diameter and suspension concentration", CSIR, Chemical Engineering Research Group, South Africa, Report CENG 497.

Serra, T. and Casamitjana, X., 1998, "Effect of the shear and volume fraction on the aggregation and breakup of particles", Journal of the American Institute of Chemical Engineers, Vol 44, No 8, pp 1724-1730.

Shen, H., Li, J., Zhu, H., Han, M. and Zhou, F., 1993, "Transport of suspended sediment in the Changjiang Estuary", International Journal of Sediment Research, Vol 7, No 3, pp 45-63.

Sills, G.S., 1997, "Consolidation of cohesive sediments in settling columns", in Cohesive Sediments, Proc. 4th Nearshore and Estuarine Cohesive Sediment Transport Conference INTERCOH'94, July 1994, ed. N. Burt, R. Parker and J. Watts, John Willey & Sons, Chichester, pp 107-120.

Simonin, O., Uittenbogaard, R.E., Baron, F. and Viollet, P.L., 1989, "Possibilities and limitations of the k-ε model to simulate turbulent fluxes of mass and momentum, measured in a steady, stratified mixing layer", Proceedings of the XXIII bi-annual Congress, Ottawa, p A55-A62.

Smith, T.N., 1998, "A model of settling velocity", Chemical Engineering Science, Vol 53, No 2, pp 315-323.

Smoluchowski, M., 1917, "Versuch einer Mathematischen Theorie der Koagulations-kinetik Kolloid Lösungen", Zeitschrift für Physikalische Chemie, Leipzig, Vol 92, pp 129-168 (in German).

Sonntag, R.C. and Russel, W.B., 1987, "Structure and breakup of flocs subjected to fluid stresses", Journal of Colloid and Interfacial Science, Vol 115, No 2, pp 378-389.

Soulsby, R.L. and Wainwright, B.L.S.A., 1987, "A criterion for the effect of suspended sediment on near-bottom velocity profiles", Journal of Hydraulic Research, Vol 25, N0 3, pp 341-356.

Soulsby, R.L., Hamm, L., Klopman, G., Myrhaug, D., Simons, R.R. and Thomas, G.P., 1993, "Wave-current interaction within and outside the bottom boundary layer", Coastal Engineering, Vol 21, pp 41-69.

Stolzenbach, K.D. and Elimelich, M., 1994, "The effect of density on collisions between sinking particles: implications for particle aggregation in the ocean", Journal of Deep Sea Research I, Vol 41, No 3, pp 469-483.

Sukhodolov, A., Thiele, M. and Bungartz, H., 1998, "Turbulence structure in a river reach with sand bed", Water Resources Research, Vol 34, No 5, pp 1317-1334.

Tambo, N. and Watanabe, Y., 1979, "Physical characteristics of flocs - I. The floc density function and aluminium floc", Water Research, Vol 13, pp 409-419.

Tambo, N. and Hozumi, H., 1979, "Physical characteristics of flocs - II. Strength of floc", Water Research, Vol 13, pp 421-427.

Taylor, P.A. and Dyer, K.R., 1977, "Theoretical models of flow near the bed and their implications for sediment transport", The Sea, Vol 6, pp 579-601.

Teisson, C. and Fritsch, D., 1988, "Numerical modelling of suspended sediment transport in the Loire estuary", in Proceedings of the 21st International Conference on Coastal Engineering, ICCE, Malaga, Spain, pp 2707-2722.

Teisson, C., Simonin, O., Galland, J.-C. and Laurence, 1992, "Turbulence modelling and mud sedimentation: a Reynolds stress model and a two-phase flow model", Proceedings of the 23rd International Conference on Coastal Engineering, ICCE, Venice 1992, Vol 3, pp 2853-2866.

Tennekes, H. and Lumley, J.L., 1994, "A first course in turbulence", The MIT press, Cambridge, Massachusetts.

Thacker, W.C. and Lavelle, J.W., 1977, "Two-phase flow of hindered settling", The Physics of Fluids, Vol 20, N0 9, pp 1577-1579.

Thorn, M.F.C., 1981, "Physical processes of siltation in tidal channels", Proceedings of Hydraulic Modelling applied to Maritime Engineering Problems, ICE, London, pp 47-55.

Toorman, E.A., 1992, "Modelling of fluid mud flow and consolidation", PhD-thesis, Katholieke Universiteit Leuven, Faculteit Toegepaste Wetenschappen.

Toorman, E.A. and Huysentruyt, H., "Towards a new constitutive equation for effective stress in self-weight consolidation", in Cohesive Sediments, Proc. 4th Nearshore and Estuarine Cohesive Sediment Transport Conference INTERCOH'94, July 1994, ed. N. Burt, R. Parker and J. Watts, John Willey & Sons, Chichester, pp 121-132.

Toorman, E.A., 1996, "Sedimentation and self-weight consolidation: general unifying theory", Géotechnique, Vol 46, No 1, pp 103-113.

Toorman, E.A., 1997, "Modelling the thixotropic behaviour of dense cohesive sediment", Rheology Acta, Vol 36, pp 56-65.

Townsend, F.C. and McVay, M.C., 1990, "SOA: Large strain consolidation predictions", ASCE, Journal of Geotechnical Engineering, Vol 116, No 2, pp 222-243.

Tsai, C-H., Iacobellis, S. and Lick, W., 1987, "Flocculation of fine-grained lake sediments due to a uniform shear stress", Journal of Great Lakes Research, Vol 13, No 2, pp 135-146.

Turner, J.S., 1973, "Buoyancy effects in fluids", Cambridge University Press.

Uittenbogaard, R.E., Kester, J.A.Th. M. van and Stelling, G.S., 1992, "Implementation of three turbulence models in TRISULA for rectangular horizontal grids, including 2DV test cases", Delft Hydraulics, report Z162.

Uittenbogaard, R.E., Kester, J.A.Th.M. van, and Stelling, G.S., 1992, "Implementation of an algebraic eddy-viscosity, a k-L and the k-ε turbulence model in TRISULA for rectangular horizontal grids - including 2DV-test cases", Delft Hydraulics, Report Z78.

Uittenbogaard, R.E., 1994, "Physics of turbulence; MAST-VERIPARSE technical report on subtask 5.2", Delft Hydraulics, Report Z649.

Uittenbogaard, R.E., 1994, "Physics of turbulence: technical report on sub-task 5.2", MAST VERIPARSE project, delft hydraulics, Report Z649.

Uittenbogaard, R.E., 1995, "Modelling seasonal temperature stratification with TRIWAQ", Delft Hydraulics, Report Z978.

Uittenbogaard, R.E., 1995, "The importance of Internal Waves for Mixing in a Stratified Estuarine Tidal Flow", PhD-thesis, Delft University of Technology, September 1995.

Uittenbogaard, R.E., Winterwerp, J.C., Kester, J.A.Th.M. van and Leepel, H.H., 1996, "3D Cohesive Sediment Transport - A preparatory study about implementation in DELFT3D", delft hydraulics, Report Z1022, March 1996.

Valiani, A., 1988, "An open question regarding shear flow with suspended sediments", Meccanica, No 23, pp 36-43.

Vanoni, V.A., 1946, "Transportation of suspended sediment by water, ASCE Transactions", Vol 111, Paper no 2267, pp 67-133.

Vanoni, V.A. and Brooks, N.H., 1957, "Laboratory studies of the roughness and suspended load of alluvial streams", California Institute of Technology, Sedimentation Laboratory, Pasadena, USA, Report E-68.

Vanoni, V.A., 1977, "Sedimentation engineering", ASCE Manuals and Reports on Engineering Practice, No 54.

Velden, E.T.J.M. van der, 1990, "Coastal Engineering, Volume II", Delft University of Technology, Department of Civil Engineering, lecture series f7.1.

Verlaan, P.A.J. and Spanhoff, R., 1994, "Sedimentation in the Maasmond; inventory and re-analyses", OCN, Oceanographic Company of The Netherlands (in Dutch).

Vicsek, T., 1992, "Fractal growth phenomena", World Scientific, Singapore.

Villaret, C. and Trowbridge, J.H., 1991, "Effects of stratification by suspended sediments on turbulent shear flows", Journal of Geophysical Research, Vol 96, No C6, pp 10659-10680.

Villaret, C., Teisson, C. and Boeuf, C., 1996, "Two-phase modelling of cohesive sediment transport", Electicité de France, Laboratoire National d'Hydraulique, Report HE-42/97/012.

Visser, P.J., Booij, R. and Melis, H., 1994, "Flow field observations in a rotating annular flume", Proceedings of the Conference on the Remediation of Sediments", Rutgers University, New Brunswick, New Jersey, USA.

Vreugdenhil, C.B., 1994, "Numerical methods for shallow water flow", Water Science and Technology Library, Vol 13, Kluwer Acadamic Publishers, Dordrecht, The Netherlands.

Wacholder, E. and Sather, N.F., 1974, "The hydrodynamic interaction of two unequal spheres moving under gravity through quiescent viscous fluid", Journal of Fluid Mechanics, Vol 5, pp 417-437.

Wang, Z.Y., Larsen, P., Nestmann, F. and Dittrich, A., 1998, "Resistance and drag reduction of flows of clay suspensions", ASCE, Journal of Hydraulic Engineering, Vol 124, No 1, pp 41-49.

Weitz, D.A., Huang, J.S., Lin, M.Y. and Sung, J., 1985, "Limits of the fractal dimension for irreversible kinetic aggregation of gold colloids", Physical Review Letters, Vol 54, No 13, pp 1416-1419.

Wells, J.T., 1983, "Dynamics of coastal fluid muds in low-, moderate- and high-tide-range environments", Canadian Journal of Fisheries and Aquatic Science, Vol 40 (suppl 1), pp 130-142.

West, A.H.L., Melrose, J.R. and Ball, R.C., 1994, "Computer simulations of the breakup of colloid aggregates", Physical Review E, Vol 49, No 6, pp 4237-4249.

West, J.R. and Oduyemi, K.O.K., 1989, "Turbulence measurements of suspended solids concentration in estuaries", ASCE, Journal of Hydraulic Engineering, Vol 115, No 4, pp 457-474.

Wiesner, M.R., 1992, "Kinetics of aggregate formation in rapid mix", Water Research, Vol 26, No 3, pp 379-387.

Williams, P.R. and Williams D.J.A., 1989, "Rheometry for concentrated cohesive suspensions", Journal of Coastal Research, Special Issue No 5, pp 151-164.

Winterwerp, J.C., Groot, M.B. de, Mastbergen D.R. and Verwoert, H., 1990, "Hyperconcentrated sand-water mixture flows over a flat bed", ASCE, Journal of Hydraulic Engineering, Vol 116, No 1, pp 36-54.

Winterwerp, J.C. and Kranenburg, C., 1994, "Erosion of fluid mud by entrainment", in: Proceedings of the 4th Nearshore and Estuarine Cohesive Sediment Transport Conference, INTERCOH'94, Wallingford, UK, July 1994, ed. by N. Burt, R. Parker and J. Watts, John Wiley & Sons, pp 263-278.

Winterwerp, J.C., 1996, "HCBS - High Concentrated Benthic Suspensions - SILTMAN desk study", delft hydraulics, Report Z1013. January 1996 (in Dutch).

Winterwerp, J.C. and Kranenburg, C., 1997, "Erosion of fluid mud layers - II: Experiments and model validation", ASCE, Journal of Hydraulic Engineering, Vol 123, No 6, pp 512-519.

Winterwerp, J.C. and Uittenbogaard, R.E., 1997, "Sediment transport and fluid mud flow - physical mud properties and parameterization of vertical transport processes, SILTMAN; set-up of a POINT-MUD MODEL", WL|delft hydraulics, Report Z2005.

Winterwerp, J.C., 1998, "A simple model for turbulence induced flocculation of cohesive sediment", IAHR, Journal of Hydraulic Engineering, Vol 36, No 3, pp 309-326.

Wit, P.J. de, 1995, "Liquefaction of cohesive sediments caused by waves", PhD-thesis, Delft University of Technology, Faculty of Civil Engineering, also: Communications on Hydraulic and Geotechnical Engineering, Report 95-2.

WL|Delft Hydraulics, 1990, "Vallarpadam Container Transshipment Terminal, Cochin Port, India; morphological aspects - feasibility study", Report Z338 (confidential).

WL|Delft Hydraulics, 1992, "Erosion of natural sediments from The Netherlands - analysis of laboratory experiments", Cohesive Sediments, Report 38.

Wolanski, E., Chapell, J., Ridd, P. and Vertessy, R., 1988, "Fluidization of mud in estuaries", Journal of Geophysical Research, Vol 93, No C3, pp 2351-2361.

Wolanski, E., Gibbs, R.J., Mazda, Y., Mehta, A.J. and King, B., 1992. "The role of turbulence in settling of mudflocs", Journal of Coastal Research, Vol 8, No 1, pp 35-46.

Wolanski, E., Huan, N.N., Dao, L.T., Nhan, N.H. and Thuy, N.N., 1996, "Fine-sediment dynamics in the Mekong River estuary, Vietnam", Estuarine, Coastal and Shelf Science, Vol 43, pp 565-582.

Woudenberg, C. van, 1998, "First results of preliminary measurements of suspended sediment in the Caland/Beerkanaal", Rijkswaterstaat, Directorate North Sea, report N98.02 (in Dutch).

Wright, L.D., Wiseman, W.J., Yang, Z.-S., Bornhold, B.D., Keller, G.H., Prior, D.B. and Suhayda, J.N., 1990, "Processes of marine dispersal and deposition of suspended silts off the modern mouth of the Huanghe (Yellow River)", Continental Shelf Research, Vol 10, No 1, pp 1-40.

Zhou, D. and Ni, J.R., 1995, "Effects of dynamic interaction on sediment-laden turbulent flows", Journal of Geophysical Research, Vol 100, No C1, pp 981-996.

Appendix A - nomenclature

a_{eb}	floc breakup efficiency parameter in flocculation model
B	buoyancy destruction in turbulence model
C_0	initial suspended sediment concentration, homogeneous over water depth
C_s	depth-averaged saturation concentration
c	suspended sediment concentration by mass
c_D	drag coefficient
c_{gel}	gelling concentration
c_m	concentration in fluid mud layer
c_q	coefficient in integral entrainment model
c_s	local saturation concentration
c_s	coefficient in integral entrainment model
c_s'	coefficient in integral entrainment model
$c_{1\varepsilon}$	coefficient in k-ε turbulence model
$c_{2\varepsilon}$	coefficient in k-ε turbulence model
$c_{3\varepsilon}$	coefficient in k-ε turbulence model
c_μ	coefficient in k-ε turbulence model
c_σ	coefficient in integral entrainment model
D	floc size
D	self-diffusion term in turbulence model
D_e	equilibrium floc size
D_{ij}	deformation tensor
D_{max}	maximal attainable floc size
D_p	diameter primary mud particles
D_s	molecular diffusion coefficient of mud flocs
D_0	initial floc size
D_{50}	median floc size
E_b	rate of sediment exchange between bed and water column
e	void ratio
e_c	efficiency coefficient for coagulation in flocculation model
e_d	efficiency coefficient for diffusion in flocculation model
F_N	flocculation and floc breakup function in flocculation model
F_y	yield strength of flocs
f_w	wave-induced bed friction coefficient
f_s	shape factor in flocculation model
G	dissipation parameter in flocculation model
g	acceleration of gravity
H	wave height
H_{rms}	root mean square wave height
h	water depth
h_s	sedimentation depth
K_B	coefficient in power law description of Bingham strength
K_k	coefficient in power law description of permeability
K_p	coefficient in power law description of effective stress

K_μ	coefficient in power law description of viscosity in Bingham model
k	turbulent kinetic energy
k	permeability
k	Boltzman constant
k_A	aggregation coefficient in flocculation model
k'_A	non-dimensional aggregation coefficient in flocculation model
k_B	floc breakup coefficient in flocculation model
k'_B	non-dimensional floc breakup coefficient in flocculation model
k_s	Nikuradse's roughness height
l	turbulent length scale (mixing length)
M	erosion parameter in erosion law of Partheniades
m	exponent in hindered settling formula accounting for non-linear effects
N	number concentration of mud flocs
N_0	initial number concentration of mud flocs
n	exponent in hindered settling formula by Richardson and Zaki
n_f	fractal dimension of mud flocs
P	production term in turbulence model
p	exponent in flocculation model
p	isotropic stress (pressure)
p_e	excess pore water pressure
p^s	effective stress
q	exponent in flocculation model
Re	overall Reynolds number
Re_e	effective Reynolds number
Re_p	particle Reynolds number
Re_T	turbulent Reynolds number
Re_y	yield stress Reynolds number
Ri	gradient Richardson number
Ri_f	flux Richardson number
Ri_*	bulk Richardson number
S	salinity
T	tidal period or accelerating or decelerating phase of tide
T	absolute temperature
T'	time parameter in flocculation model
T_c	consolidation time
T'_c	relative consolidation time
T_f	flocculation or floc breakup time scale
T_m	vertical mixing time
T'_m	relative vertical mixing time
T_r	residence time
T_{rel}	relaxation time
T_s	sedimentation time
T'_s	relative sedimentation time
T_T	turbulent time scale
t	time
U	depth-averaged horizontal flow velocity

U_m	amplitude tidal flow velocity
u	horizontal flow velocity
u_i	flow velocity in i-direction
$\hat{u}_{orb}$	amplitude orbital flow velocity near the bed
u_*	shear velocity
u_{*f}	flow-induced shear velocity
u_{*w}	wave-induced shear velocity
V_f	volume of mud flocs
v_f	vertical fluid velocity in bed relative to fixed reference frame
v_s	vertical velocity of sediment particles relative to fixed reference frame
W_s	constant or characteristic settling velocity
w	vertical velocity
w_e	entrainment velocity
w_s	effective settling velocity, varying with depth and/or time
$w_{s,r}$	settling velocity of individual mud floc in still water
$w_{s,max}$	maximal settling velocity, bounded by limited residence time
x_i	co-ordinate in i-direction
Z_b	bed level
Z_s	level of water surface
z	vertical co-ordinate
z_{wc}	roughness height for waves and current
z_0	roughness height for current alone
α	shape factor sediment
α'	shape parameter in settling velocity formula: $\alpha' \equiv \alpha/18\beta$
β	Rouse parameter
β	shape factor sediment
Γ_c	diffusion coefficient in consolidation formula
Γ_T	eddy diffusivity
Δ	relative sediment density: $\Delta \equiv (\rho_s - \rho_w)/\rho_w$
Δt	time step in 1DV POINT MODEL
Δz	grid size in 1DV POINT MODEL
Δz_b	size near bed grid in 1DV POINT MODEL
$\Delta\rho_f$	excess floc density: $\Delta\rho_f \equiv \rho_f - \rho_w$
δ_m	thickness fluid mud layer
δ_w	thickness wave boundary layer
ε	turbulent energy dissipation
ζ	relative height above bed: $\zeta = z/h$
η	parameter in settling function
θ_d	non-dimensional threshold shear stress for deposition: $\theta_d = \tau_b/\tau_d$
θ_e	non-dimensional threshold shear stress for erosion: $\theta_e = \tau_b/\tau_e$
κ	Von Kármàn constant
λ	friction coefficient
λ	size floc forming eddies
λ_0	Kolmogorov micro-scale of turbulence
μ	dynamic viscosity

ν	kinematic viscosity
ν_m	kinematic viscosity of fluid mud
ν_T	eddy viscosity
Ξ_s	settling function
ρ	bulk density of water-sediment suspension
ρ_f	density of mud flocs
ρ_s	density of primary sediment particles
ρ_w	density of water
σ_{ij}	stress tensor
σ_k	Prandtl-Schmidt number for the diffusion of k in k-ε turbulence model
σ_T	Prandtl-Schmidt number relating eddy diffusivity and eddy viscosiy
σ_ε	Prandtl-Schmidt number for the diffusion of ε in k-ε turbulence model
σ_{ij}^f	fluid-induced part of stress tensor
σ_{ij}^s	sediment-induced part of stress tensor
τ_B	Bingham strength
τ_b	bed shear stress (flow- and wave-induced contributions)
τ_c	flow-induced bed shear stress
τ_d	critical shear stress for deposition
τ_e	critical shear stress for erosion
τ_{ij}	dviatoric stress tensor
τ_s	surface shear stress
τ_y	yield stress
ϕ	volumetric concentration of mud flocs
ϕ_*	min $\{1, \phi\}$
ϕ_p	volumetric concentration of primary particles
ω	wave frequency

subscripts

ξ_0	initial conditions
ξ_e	equilibrium conditions
ξ_m	conditions in fluid mud layer
ξ_r	reference conditions
ξ_T	turbulent conditions

superscripts and other symbols

ξ^f	fluid-related parameter
$\xi^{(i)}$	sediment fraction (i)
ξ^s	sediment related parameter
ξ'	turbulent fluctuating part of ξ
$\overline{\xi}$	mean value of ξ averaged over turbulent time scale

Appendix B - The 1DV POINT MODEL

The 1DV POINT MODEL was developed on the basis of DELFT3D-FLOW, the software system of WL|delft hydraulics to simulate the water movement and transport of matter in three-dimensions, by stripping all horizontal gradients, except the horizontal pressure gradient. This model was originally developed to study the implementation of the k-ε turbulence model in DELFT3D-FLOW by Uittenbogaard et al. (1992) and Van Kester (1994). Later, the model was extended (Uittenbogaard, 1995) by incorporating the effects of temperature-induced stratification. The version that is used as a basis to implement the various physical-mathematical formulations derived in the present study, was developed by Uittenbogaard et al. (1996)[1].

In Section B.1 we present the various mathematical-physical formulations of the relevant processes, which are described in Chapters 3, 4 and 5. Section B.2 contains information on the numerical implementation of the equations, and in Section B.3 some numerical accuracy aspects are presented.

B.1 The 1DV-equations for HCMS

the water movement

The 1DV-equation for horizontal momentum reads:

$$\frac{\partial u}{\partial t}+\frac{1}{\rho}\frac{\partial p}{\partial x}=\frac{\partial}{\partial z}\left[(\nu+\nu_T)\frac{\partial u}{\partial z}+\frac{\tau^s_{xz}}{\rho}\right]-\frac{1}{\rho}\frac{2\tau_{sf}}{b} \tag{B.1}$$

where:

b = flow width,
p = pressure,
t = time,
u = horizontal flow velocity, positive in x-direction
x = horizontal co-ordinate,
z = vertical co-ordinate,
ρ = bulk density of water-sediment mixture,
ν = molecular viscosity,
ν_T = eddy viscosity (see (B.12)),
τ^s_{xz} = inter-particle stresses (see (B.36)), and
τ_{sf} = side wall friction.

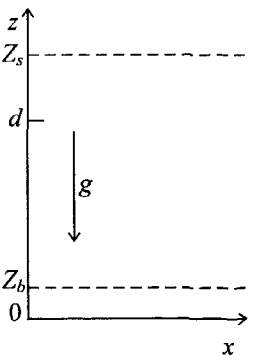

The last term in (B.1) is added to account for side wall friction effects in case of simulating the flow in a confined channel (laboratory flume) of width b. The

[1] Implementation of the various formula developed in the present study has been carried out by several persons of WL|delft hydraulics, i.e. dr. R.E. Uittenbogaard, mrs. H.H. Leepel, mr. J.Th.M. van Kester, mr. J.M. Cornelisse and mrs. P.M.C. Thoolen. The contribution of the author to this implementation has been limited.

orientation of the co-ordinate system is consistent with that of Chapter 3. The bed or lower boundary condition is defined at $z = Z_b$, and the water surface at $z = Z_s(t)$. Hence, the water depth $h = Z_s - Z_b$. Note that in DELFT3D the following convention is used: $Z_s = d + z(t)$; d and Z_b are given with respect to a horizontal reference plane.

We note that by omitting the horizontal advection terms, we implicitly assume that the Froude number of the flow is small, which is generally the case in tidal flow. We have also neglected the vertical velocity component w, which is small with respect to the horizontal component u. However, w may be of the same order of magnitude as the settling velocity in converging or diverging flow, for instance over a spatially varying bed. Hence, we should assume that the bed is flat and horizontal in our applications with the 1DV POINT MODEL. Vertical velocities induced by variations in water level with time, induced by tidal movements, for instance, are accounted for through the application of the σ-transformation (equ. B.38)).

The pressure term in (B.1) is adjusted to maintain a given, time-dependent depth-averaged velocity:

$$\frac{1}{\rho}\frac{\partial p}{\partial x} = \frac{\tau_s - \tau_b}{\rho h} + \frac{U(t) - U_0(t)}{T_{rel}} \quad , \quad U(t) = \frac{1}{h}\int_{z_{bc}}^{Z_s} u(z',t)\,dz' \tag{B.2}$$

where:

T_{rel} = relaxation time (see also Appendix B.3),
U = actual computed depth-averaged flow velocity,
U_0 = desired depth-averaged flow velocity,
z_{bc} = apparent roughness height,
τ_b = bed shear stress, and
τ_s = surface shear stress.

A quadratic friction law, satisfying the log-law, is used:

$$\tau_b = \rho |u_{*b}| u_{*b} \;\; ; \;\; u_{*b} = \frac{\kappa u(z_{bc} + \tfrac{1}{2}\Delta z_b)}{\ln(1 + \tfrac{1}{2}\Delta z_b / z_{bc})} \tag{B.3}$$

where:

κ = von Kármàn constant, and
Δz_b = defined in Appendix B.2.

The boundary conditions to (B.1) read:

$$\tau_b = \left\{ \rho(\nu + \nu_T)\frac{\partial u}{\partial z} + \tau_{xz}^s \right\}\Bigg|_{z=z_{bc}} \quad ; \quad \tau_s = \left\{ \rho(\nu + \nu_T)\frac{\partial u}{\partial z} + \tau_{xz}^s \right\}\Bigg|_{z=Z_s} \tag{B.4}$$

The IDV POINT MODEL is also used to simulate the behaviour of HCMS in an annular flume, in which case also the second part of condition (B.4) is used. The side wall friction is obtained from:

$$\tau_{sf} = \lambda_{sf} \rho |u| u \tag{B.5}$$

where:

λ_{sf} = friction coefficient

The mass balance for suspended sediment

The transport of sediment is modelled with the advection-diffusion equation for various fractions numbered by the superscript *(i)*:

$$\frac{\partial c^{(i)}}{\partial t} - \frac{\partial}{\partial z}\left\{w_s^{(i)} c^{(i)}\right\} - \frac{\partial}{\partial z}\left\{\left(D_s^{(i)} + \Gamma_T^{(i)}\right)\frac{\partial c^{(i)}}{\partial z}\right\} = 0 \,, \quad \text{with}$$
$$w_s^{(i)} = w_{s,r}^{(i)} \frac{(1-\phi_*)(1-\phi_p)}{(1+2.5\phi)} \quad \text{to account for hindered settling} \tag{B.6}$$

where:

$c^{(i)}$ = sediment concentration by mass for fraction (*i*),
D_s = molecular diffusion coefficient for sediment (B.10),
w_s = effective settling velocity for sediment suspension,
$w_{s,r}$ = settling velocity of individual particle (see (B.24)), and
Γ_T = eddy diffusivity (see also (B.13)).

The volumetric concentration of mud flocs ϕ, and the volumetric concentration of their primary particles ϕ_p are related to the mass concentration c and sediment density ρ_s through:

$$\phi = \frac{\sum_{(i)} c^{(i)}}{c_{gel}} \,, \text{ and } \quad \phi_p = \frac{\sum_{(i)} c^{(i)}}{\rho_s} \tag{B.7}$$

where

c_{gel} = gelling concentration (see also (B.23)),
ϕ_* = min $\{1, \phi\}$, and
ρ_s = density of the sediment.

At the water surface and the bed the boundary conditions read:

$$\left\{w_s^{(i)} c^{(i)}\right\}\Big|_{z=Z_s} = 0 \quad ; \quad \left\{\left(D_s + \Gamma_T\right)\frac{\partial c^{(i)}}{\partial z}\right\}\Big|_{z=Z_s} = 0 \text{ and}$$
$$\left\{w_s^{(i)} c^{(i)}\right\}\Big|_{z=Z_b} = E_{b,c} \; ; \quad \left\{\left(D_s + \Gamma_T\right)\frac{\partial c^{(i)}}{\partial z}\right\}\Big|_{z=Z_b} = 0 \tag{B.8}$$

We have split the two boundary conditions (2.14) in four parts, which is allowed as the diffusion term at the bed and at the water surface is zero. At the rigid bed $z = Z_b$ we apply the classical formulae of Partheniades and Krone:

$$E_{b,c} = -w_s^{(i)}\, c^{(i)} \mathrm{S}\left(1 - \theta_d^{(i)}\right) + M^{(i)} \mathrm{S}\left(\theta_e^{(i)} - 1\right) \quad \text{at} \quad z = Z_b \tag{B.9}$$

in which

M = empirical erosion parameter,
θ_d = non-dimensional threshold shear stress for deposition: $\theta_d = \tau_b / \tau_d$,
θ_e = non-dimensional threshold shear stress for deposition: $\theta_e = \tau_b / \tau_e$,
τ_d = threshold shear stress for deposition,

τ_e = threshold shear stress for erosion, and
$S(x)$ = ramp function: $S = x$ for $x > 0$ and $S = 0$ for $x \leq 0$.

The molecular diffusion term D_s is given by:

$$D_s = \frac{kT}{6\pi\mu D} \tag{B.10}$$

in which
D = particle size,
k = Boltzman constant (= $1.38 \cdot 10^{-23}$ J/K), and
T = absolute water temperature.

The influence of the suspended sediment concentration on the bulk fluid density is given by the equation of state:

$$\rho(S, c^{(i)}) = \rho_w(S) + \sum_{(i)} \left\{ \left(1 - \frac{\rho_w(S)}{\rho_s^{(i)}} \right) c^{(i)} \right\} \tag{B.11}$$

with
$\rho_w(S)$ = density of the water due to salinity only.

The k-ε turbulence model

The k-ε turbulence model consists of transport equations for the turbulent kinetic energy k and the turbulent dissipation ε, neglecting horizontal transport components:

$$\frac{\partial k}{\partial t} = \frac{\partial}{\partial z} \left\{ (\nu + \nu_T) \frac{\partial k}{\partial z} \right\} + \nu_T \left(\frac{\partial u}{\partial z} \right)^2 + \frac{g}{\rho} \Gamma_T \frac{\partial \rho}{\partial z} - \varepsilon \tag{B.12}$$

and

$$\frac{\partial \varepsilon}{\partial t} = \frac{\partial}{\partial z} \left\{ \left(\nu + \frac{\nu_T}{\sigma_\varepsilon} \right) \frac{\partial \varepsilon}{\partial z} \right\} + c_{1\varepsilon} \frac{\varepsilon}{k} \nu_T \left(\frac{\partial u}{\partial z} \right)^2 + (1 - c_{3\varepsilon}) \frac{g}{\rho} \Gamma_T \frac{\varepsilon}{k} \frac{\partial \rho}{\partial z} - c_{2\varepsilon} \frac{\varepsilon^2}{k} \tag{B.13}$$

where
ν_T = eddy viscosity; $\nu_T = c_\mu k^2/\varepsilon$,
Γ_T = eddy diffusivity; $\Gamma_T = \nu_T/\sigma_T$, and
σ_T = turbulent Prandtl-Schmidt number.

We have carried out a few simulations for confined flows in laboratory flumes with an additional side-wall-friction induced turbulence production term (i.e. $\tau_{sf}\partial u/\partial z$ and $c_{1\varepsilon}\varepsilon/k\,\tau_{sf}\partial u/\partial z$ are added to the right hand side of (B.12) and (B.13) respectively.

The various coefficients in the standard k-ε turbulence model are summarised in Table B.1:

						stable	unstable
c_μ	$c_{1\varepsilon}$	$c_{2\varepsilon}$	σ_T	σ_ε	κ	$c_{3\varepsilon}$	$c_{3\varepsilon}$
0.09	1.44	1.92	0.7	1.3	0.41	1	0

Table B.1: Coefficients in standard k-ε turbulence model.

The model is subject to the following set of boundary conditions:

$$k|_{x_3=Z_b} = \frac{u_*^2}{\sqrt{c_\mu}}, \quad \varepsilon|_{x_3=Z_b} = \frac{u_*^3}{\kappa z_{wc}}, \quad k|_{x_3=Z_s} = \frac{u_{*,s}^2}{\sqrt{c_\mu}}, \quad \varepsilon|_{x_3=Z_s} = \frac{u_{*,s}^3}{\kappa z_{wc}} \tag{B.14}$$

in which the effects of waves may be included in the shear velocity u_* and where the roughness length z_{wc} for current and waves is given by (B.20); when no waves are present $z_{wc} = z_0$, which is the well-known roughness length for flow only.

The effect of surface waves

The effect of surface waves is modelled through the approach of Grant and Madsen. The rms-value of the wave-induced bed shear stress is defined by:

$$\tau_w = \left\langle \tilde{\tau}_w^2 \right\rangle^{1/2} = \rho u_{*w}^2 \; ; \quad u_{*w}^2 = \frac{1}{2} f_w \hat{u}_{orb}^2 \tag{B.15}$$

in which the near-bed horizontal orbital velocity amplitude $\hat{u}_{orb}$ is determined from the rms wave height H_{rms}. The friction coefficient f_w follows from Swart's formula:

$$\text{for } \frac{A}{k_s} > \frac{\pi}{2}: \; f_w = 0.00251 \cdot \exp\left\{ 5.21 \left(\frac{A}{k_s} \right)^{-0.19} \right\}, \text{ and}$$
$$\text{for } \frac{A}{k_s} \le \frac{\pi}{2}: \; f_w = 0.3 \tag{B.16}$$

where k_s is the Nikuradse roughness height related to the roughness length z_0 through $k_s \approx z_0/30$ and $A \equiv \hat{u}_{orb}/\omega$, with ω = wave frequency. The wave-affected boundary layer thickness δ_w is given by:

$$\delta_w = \frac{2\kappa}{\omega} |u_{*fw}| = \frac{2\kappa}{\omega} \sqrt{u_{*f}^2 + u_{*w}^2} \tag{B.17}$$

where the subscript $._w$ reflects wave-related parameters, $._f$ flow-related parameters and $._{fw}$ the effects of current-wave interaction. Within the turbulent wave-boundary layer the eddy viscosity ν_T reads:

$$z_0 \le z - Z_b \le \delta_w : \quad \nu_T = \kappa |u_{*fw}| (z - Z_b) = \kappa \sqrt{u_{*f}^2 + u_{*w}^2} (z - Z_b) \tag{B.18}$$

Note that the near-bed shear stress $\tau_b = \rho_w u_{*f}^2$ is constant, but as yet unknown, throughout the wave-boundary and yields a logarithmic velocity profile based on $|u_{*fw}|$. Above the wave-boundary layer, wave-induced turbulence is not notable and Grant and Madsen assume:

$$z - Z_b > \delta_w : \quad \nu_T = \kappa |u_{*f}| (z - Z_b) \tag{B.19}$$

which yields the usual logarithmic velocity profile with $|u_{*f}|$ as a parameter. The two velocity profiles are matched at $z - Z_b = \delta_w$. The wave-induced turbulence is assumed to contribute to the mean flow above the wave-boundary through an increase in effective roughness z_{wc}:

$$\delta_w \geq z_0 : \quad \frac{z_{wc}}{z_0} = \left(\frac{\delta_w}{z_0}\right)^{\beta} \; ; \quad \beta = 1 - \left(1 + \left(\frac{u_{*w}}{u_{*f}}\right)^2\right)^{-1/2} \tag{B.20}$$

The effective bed shear stress τ_b and shear velocity u_*, as applied in the preceding sections, follow from applying the logarithmic law of the wall using z_{wc} in stead of z_0. No other effects of wave-current interactions are accounted for at present.

The flocculation model

In the flocculation model (4.35) the geometric relation (4.23) is substituted, yielding an equation for the number and mass concentration N and c, but not for the floc diameter D. The flocculation model, as implemented in the 1DV POINT MODEL, contains the following set of equations:

$$\frac{\partial N}{\partial t} + \frac{\partial}{\partial z}\left(\frac{(1-\phi_*)(1-\phi_p)}{(1+2.5\phi)} w_{s,r} N\right) - \frac{\partial}{\partial z}\left(\Gamma_t \frac{\partial N}{\partial z}\right) = \\ - k_A' k_N^3 (1-\phi_*) G c^{\frac{3}{n_f}} N^{\frac{2n_f-3}{n_f}} + k_B' k_N^{2q} G^{q+1} \left(k_N c^{\frac{1}{n_f}} N^{\frac{-1}{n_f}} - D_p\right)^p c^{\frac{2q}{n_f}} N^{\frac{n_f-2q}{n_f}} \tag{B.21}$$

where

ae_b = breakup efficiency parameter,
D = diameter of mud flocs,
D_p = diameter of primary particles,
D_s = molecular diffusion coefficient for sediment,
$e_c e_d$ = flocculation efficiency parameter,
F_y = yield strength of flocs,
G = dissipation parameter; $G = \sqrt{(\varepsilon/\nu)}$
k_A' = flocculation parameter; $k_A' = 1.5 e_c \pi e_d$
k_B' = floc breakup parameter; $k_B = ae_b D_p^{-p} \left(\mu / F_y\right)^q$
k_N = $\left(D_p^{n_f-3} / f_s \rho_s\right)^{\frac{1}{n_f}}$
N = number concentration of the mud flocs,
n_f = fractal dimension,
p = empirical coefficient; $p = 3 - n_f$,
q = empirical coefficient; $q = 0.5$, and
μ = dynamic viscosity of sediment suspension.

The relation between the number concentration N, the mass concentration c and the floc diameter D, and between the volumetric and mass concentration ϕ and c is given by simple algebraic relations:

$$N = \frac{1}{f_s} \frac{c}{\rho_s} D_p^{n_f-3} D^{-n_f} \tag{B.22}$$

$$\phi = \left(\frac{\rho_s - \rho_w}{\rho_f - \rho_w}\right)\frac{c}{\rho_s} = \frac{c}{\rho_s}\left[\frac{D}{D_p}\right]^{3-n_f} \tag{B.23}$$

where

f_s = shape factor, and

ρ_f = floc density.

Note that the gelling concentration c_{gel} is obtained for unit volumetric concentration, i.e. $\phi = 1$, yielding:

$$c_{gel} = \rho_s\left[\frac{D_p}{D}\right]^{3-n_f} \tag{B.24}$$

The relation between the floc size D and the settling velocity $w_{s,r}$ for a single particle in still water is given by:

$$w_{s,r} = \frac{\alpha}{18\beta}\frac{(\rho_s - \rho_w)g}{\mu} D_p^{3-n_f}\frac{D^{n_f-1}}{1+0.15Re^{0.687}} \tag{B.25}$$

where

Re ≡ particle Reynolds number; $Re = w_{s,r}D/\nu$.

The evolution of the settling velocity in the 1DV POINT MODEL is obtained by a simultaneous solution of (B.21) and (B.5), whereafter the floc diameter D and the settling velocity $w_{s,r}$ are obtained from (B.22) and (B.25), using (B.23) to establish the fractal dimension n_f, together with the following boundary conditions, split again in 2×2 equations:

$$\begin{aligned} &\{w_s N\}\big|_{z=Z_s} = 0 \quad ; \quad \left\{(D_s + \Gamma_T)\frac{\partial N}{\partial z}\right\}\Big|_{z=Z_s} = 0 \text{ and} \\ &\{w_s N\}\big|_{z=Z_b} = E_{b,N} \; ; \quad \left\{(D_s + \Gamma_T)\frac{\partial N}{\partial z}\right\}\Big|_{z=Z_b} = 0 \end{aligned} \tag{B.26}$$

and

$$E_{b,N} = -\frac{(1-\phi_*)(1-\phi_p)}{(1+2.5\phi)} w_{s,r} N \mathrm{S}(1-\theta_d) + \frac{M}{f_s D_e^3 \rho_{f,e}} \mathrm{S}(\theta_e - 1) \quad \text{at} \quad z = Z_b \tag{B.27}$$

where the equilibrium floc diameter D_e and the equilibrium floc density $\rho_{f,e}$ are given by:

$$D_e = D_p + \frac{k_A c}{k_B\sqrt{G}} \text{ and} \tag{B.28}$$

$$\rho_{f,e} = \rho_w + (\rho_s - \rho_w)\left[\frac{D_p}{D_e}\right]^{3-n_f} \tag{B.29}$$

with:

k_A = $0.75 e_c \pi e_d / f_s \rho_s D_p$ and

$k_B = k'_B / n_f$

The model contains the following empirical parameters: ae_b, $e_c e_d$, D_p, F_y, f_s, n_{f1}, n_{f2}, p, q, α and β, which have to be specified by the user through the input to the model.

The consolidation model

The consolidation model, as implemented in the 1DV POINT MODEL, contains the following set of equations:

$$\frac{\partial c}{\partial t} - \frac{\partial}{\partial z}(\Xi_s c) - \frac{\partial}{\partial z}\left(\left(D_s + \Gamma_T + \phi_*^2 \Gamma_c\right)\frac{\partial c}{\partial z}\right) = 0 \tag{B.30}$$

where:

$$\Xi_s = f_{hs} + \frac{f_c}{1+\eta f_c}, \quad \text{with:}$$

$$f_{hs} = w_{s,r}\frac{(1-\phi_*)(1-\phi_p)}{1+2.5\phi}, \quad \text{and} \tag{B.31}$$

$$f_c = k\frac{\rho_s - \rho_w}{\rho_w}\phi_p$$

$$\Gamma_c \equiv \frac{2K_k K_\sigma}{(3-n_f)g\rho_w} \tag{B.32}$$

$$k = K_k \phi_p^{\left(\frac{-2}{3-n_f}\right)} \tag{B.33}$$

$$p^s = K_p \phi_p^{\left(\frac{2}{3-n_f}\right)} \tag{B.34}$$

At the water surface and the bed, the boundary conditions read:

$$\left\{\Xi_s c\right\}\Big|_{z=Z_s} = 0 \;;\; \left\{\left(D_s + \Gamma_T + \phi_*^2 \Gamma_c\right)\frac{\partial c}{\partial z}\right\}\Big|_{z=Z_s} = 0 \text{ and}$$
$$\left\{\Xi_s c\right\}\Big|_{z=Z_b} = 0 \;;\; \left\{\left(D_s + \Gamma_T + \phi_*^2 \Gamma_c\right)\frac{\partial c}{\partial z}\right\}\Big|_{z=Z_b} = 0 \tag{B.35}$$

Again, the boundary conditions (5.16) and (5.17) may be split because the diffusion term is zero at the water surface and k is zero (for single-drained conditions) at the base of the consolidating bed.

The stress tensor τ_{xz}^s for consolidating fluid mud in (B.1) is given by the following rheological model:

$$\tau_{xz}^s = \mu_{mud}\frac{\partial u}{\partial z} \quad \text{with} \quad \mu_{mud} = \frac{a_y \tau_y}{1 + a_y\left|\partial u/\partial z\right|} + \mu^s \tag{B.36}$$

in which:

a_y = coefficient ($a_y = 0.02$ implies $\tau^s_{xz} = 0.95\tau_y$ for $\partial u/\partial z = 10^{-3}$ s^{-1}).

$\mu^s = K_\mu \phi_p^n$

$\tau_y = K_y \phi_p^{\frac{2}{3-\eta}}$

The empirical parameters K_k, K_p, K_y, K_μ, n and η have to be specified by the user through the model input; n can vary between about 2 and 6 for various muds. Through the formulation of (B.36) for μ_{mud} we ascertain that τ^s_{xz} is defined for all values of the shear rate.

The eddy diffusivity at the water-mud interface is set to zero when the yield strength of the mud exceeds the turbulent stress:

$$\Gamma_T = 0 \quad \text{if} \quad \tau_y > \tau_T \equiv \rho \nu_T \frac{\partial u}{\partial z} \tag{B.37}$$

B.2 The numerical implementation of the 1DV-equations

In the 1DV POINT MODEL we apply a simplified version of the so-called σ-co-ordinate transformation:

$$\frac{\partial}{\partial z} = \frac{1}{h}\frac{\partial}{\partial \sigma} \quad \text{with} \quad \sigma \equiv \frac{z - Z_s(t)}{h} \; ; \; h = Z_s(t) - Z_b \tag{B.38}$$

This implies that for a conserved constituent, like suspended sediment, the depth-mean sediment concentration remains constant with varying water level. However, the total mass, integrated over the water column, is not conserved.

The equations are solved on a staggered grid. The vertical grid size distribution does not have to be uniform. The sketch below shows where the various parameters are defined.

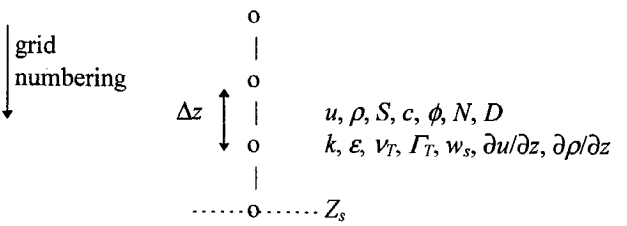

The time discretisation in the numerical solution technique is based on the θ-method; all simulations are carried out with $\theta = 1$, i.e. Euler-implicit time integration. In the vertical direction a first-order upwind scheme is used, together with a central difference scheme for the diffusion operator.

All source terms are modelled explicitly. The sink terms are modelled such that the relevant variables, i.e. k, ε, S, c, N and D never become negative; for details the reader is referred to Uittenbogaard et al. (1997).

A sub-time step can be set by the parameter n_{sub} through which the advection-diffusion equation for flocculation can be solved efficiently with a smaller effective time step than that for the overall process.

The communication between the various modules is given in the sketch below.

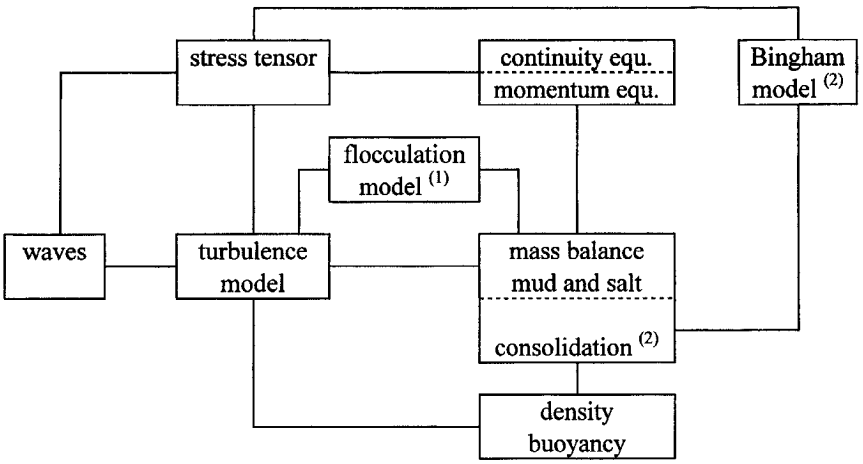

Fig. B.1: Set-up of and communication between modules; (1) only if floc evolution is simulated, (2) only if consolidation is simulated - (1) and (2) not together.

B.3 Requirements for numerical accuracy

Due to the implicit solvers and conservative form of the equations, the numerical scheme is stable and mass conserving for all numerical parameters. However, because of accuracy, we have the following requirements:

1. The grid-size may be chosen non-equidistant. However, it is recommended that the sizes of two neighbouring grid cells do not differ by more than a factor 1.5,
2. The size of the lowest grid cell should be smaller than the thickness of the fluid mud layer, that is when all sediment in the water column has settled, as explained in Section 6.4,
3. From numerical experiments it appears that an optimal choice for the relaxation time is $T_{rel} = 2\times\Delta t$,
4. The time step Δt should be small enough to accommodate for advective effects properly: $\Delta t < \Delta z/w_s$,
5. The numerical diffusivity D_{num} for the upwind scheme used amounts to $D_{num} = w_s\Delta z/2$,
6. The parameter η in (B.31) is set at 10^5 s/m to obtain a smooth transition between consolidation and hindered settling.

Curriculum vitae Johan Christian Winterwerp

Han Winterwerp was born on June 30, 1951 in The Hague, The Netherlands, where he grew up with his parents and his one year younger brother. After finalising his HBS-B examination in 1968 he studied at Delft University of Technology, Department of Aeronautical Engineering, from which he graduated in 1976 on an empirical/numerical study of the boundary layer development in transonic flows. This study was a continuation of his work in 1974-1975 at the Von Kármàn Institute for Fluid Dynamics in Belgium on flow separation under supersonic and hypersonic conditions. After a short employment at Fokker's aircraft company, where he worked on the off-design characteristics of supercritical airfoils and wings, he joined WL|DELFT HYDRAULICS in 1978.

During the first years at WL|DELFT HYDRAULICS he carried out theoretical and numerical studies on stratified flows (salinity intrusion problems). From 1982 till 1986 he was involved in consultancy work on recirculating studies related to cooling water intakes and outfalls. In 1986 he started to specialise in sediment transport, with emphasis on basic research and consultancy work related to cohesive sediments. From 1991 this basic research was partly carried out with staff from Delft University of Technology, Department of Civil Engineering through a part-time affiliation in the framework of The Netherlands Centre for Coastal Research.

In the years 1987-1990 he was project manager Basic Research in Estuaries of the Estuaries and Seas Division of WL|DELFT HYDRAULICS. A large proportion of this basic research was related to experimental studies in the Delft Tidal Flume and the theoretical analyses of the results. In the years 1991-1997 he was head of the Morphology and Sediment Transport Section of the Marine, Coastal and Estuarine Management Department. In 1997 he became product manager Cohesive Sediment Transport and in 1999 he was appointed as expert on Morphology and Sediment Transport, which is his current position.

Han Winterwerp has executed many hydrodynamic, hydro-thermal and hydro-morphological studies all over the world as project leader and as expert in multi-disciplinary project teams, using the various mathematical models developed by WL|DELFT HYDRAULICS. Amongst these are sediment transport studies for the navigational channels of Rotterdam, The Netherlands; of Cochin Port, India; Neva Bay, St. Petersburg, Russia; the Segara Anakan Lagoon, Java, Indonesia; and the Yangtze estuary, China.

He is the author / co-author of about 30 publications at International Conferences and in Technical Journals or Reference Books. For one of these papers he won the Karl Emil Hilgard Hydraulic Prize of the American Society of Civil Engineers with Dr. C. Kranenburg for their papers in the Journal of Hydraulic Engineering on "The erosion of fluid mud layers", June 1997.

Han Winterwerp married Mary-Ann Thoms in 1976, from which marriage two children were born, their son Peter in 1982 and their daughter Ineke in 1978. In his free time he likes to read, play tennis and bridge, and skate and ski in winter time. Opera, though, is his all-season favourite entertainment.

Acknowledgements

This work could not have been carried out without the help and assistance of many good friends and colleagues. Dr. Cees Kranenburg has been a long-time and very stimulating companion with many good ideas, always forcing me to think straight and formulate accurately. Dr. Rob Uittenbogaard guided me through the complicated world of turbulence and numerical modelling. Cees and Rob were always available for discussions and answering my numerous questions, and I have learned incredibly much from them. Prof. Dr. Jurjen Battjes is gratefully acknowledged for his stimulation, discussions and critical comments.

The 1DV POINT MODEL, which is the major tool used in my studies, was developed initially by Dr. Rob Uittenbogaard, Prof. Dr. Guus Stelling, Mr. Jan van Kester and Mrs. Heleen Leepel. Later, Dr. Rob Uittenbogaard, Mr. John Cornelisse and Mrs. Pauline Thoolen contributed to the implementation of the various formulations derived in this study. I am very indebted to their skills presented and dedication in realising the robust, yet flexible software that resulted from their work.

Dr. Henk van den Boogaard, Dr. Zheng Bing Wang and Dr. Robbert Fokkink were always available to help me with the mathematics. Mr. Rinze Bruinsma produced many of the graphs in this thesis and their lay-out, Mr. Hans Roode made the front cover, based on a photograph which was made available freely by HAECON, Belgium. My struggling with the hardware, trying to run the software in a dedicated mode, has been lightened considerably by the efforts of Mr. Kees Koree and Mr. Roberto IJzerman.

I am very grateful to Mr. Ad van Os who trusted me with specialising in the field of sediment transport, in which I had no background at all at that time, and his encouragement to participate in The Netherlands Centre for Coastal Research. In hindsight, this participation turned out to be the real start of my scientific mud career.

I like to thank the management of WL|DELFT HYDRAULICS in general, and Mr. Tom Schilperoort and Mr. Andries Roelfzema in particular for giving me the opportunity to actually write this thesis. The underlying studies have been financed by Rijkswaterstaat (The Netherlands Ministry of Transport, Public Works and Water Management) through their SILTMAN project, by the European Union in the framework of the 2nd and 3rd MAST-programme (the G8M Morphodynamics project and the COSINUS project), and through WL|DELFT HYDRAULICS' corporate research funds. I like to thank Dr. Johan de Kok and Dr. Wim van Leussen of Rijkswaterstaat for making available and permitting me to use the data of the field measurements in the Maasmond-area (Section 7.4) and in the Ems estuary (Section 7.3).

I like to acknowledge my colleagues of WL|DELFT HYDRAULICS for their interest in my work and their help, not only directly with the study reported herein, but also with the many other tasks that had to be fulfilled during the work on this thesis - had this not been the case, this thesis would not have been finalised. Also the discussions with, and comments and critical questions of my graduate- and PhD-students and of my colleagues within the COSINUS-project have been very helpful and stimulating.

Finally, I like to thank my parents for providing me with the education that enables me to do the work I like, and my dear Mary-Ann, Peter and Ineke for their love and patience; my efforts to write this thesis have not always been easy for them.